Biologically Active Secondary Metabolites from Freshwater and Terrestrial Cyanobacteria

BY

Hahk-Soo Kang
B.S., Chung-Ang University, 2003
M.S., Chung-Ang University, 2005

DISSERTATION

Submitted as partial fulfillment of the requirements
for the degree of Doctor of Philosophy in Pharmacognosy
in the Graduate College of the
University of Illinois at Chicago, 2012

Chicago, Illinois

Defense Committee:

Jimmy Orjala, Chair
Alexander Mankin
Brian Murphy
Duncan Wardrop, Chemistry
Steven Swanson

DEDICATION

My doctoral dissertation is dedicated to my parents, Kyoungdon Kang and Myoungjae Song.

My doctoral dissertation is dedicated to my mother's 60th birthday.

My doctoral dissertation is also dedicated to my elder sister Joohyun Kang, brother-in-law Changil Shin and their two sons Woobin Shin and Dongbin Shin.

EPIGRAPH

I believe there is no philosophical high-road in science, with epistermological singposts. We are in a jungle and find our way by trial and error, building our road behind us as we proceed.

Max Born (1882-1970), Nobel Prize, 1954

Wisdom is not a product of schooling but of the lifelong attempt to acquire it.

Albert Einstein

Try as hard as for perfection, the next result of our labors is an amazing variety of imperfectness. We are surprised at our own versatility in being able to fail in so many different ways.

Samuel McChord Crothers

Firmness of purpose is one of the most necessary sinews of character, and one of the best instruments of success. Without it, genius wastes its efforts in a maze of inconsistencies.

Philip Dormer Chesterfield

ACKNOWLEDGEMENTS

My graduate study and research here at UIC has not been always easy. I have faced lots of difficult problems with regard to my research, preliminary exam and course work for the past four years, and it would not have been possible to overcome those problems without other people's help. Therefore, I would like to thank many people who have made this dissertation possible.

My family: I want to deeply thank my parents for their unfailing support, guidance, and love to me throughout my life. I feel fortunate to have such great parents. My parents have always been role models for me and taught me how to live a life without losing a passion and the importance of a life-long study. Also, every time I came back from vacation, they gave me books about the story of successful people to read on the planes that have influenced my life as a graduate student. I also would like to thank my elder sister and brother-in-law Changil Shin for their kindness and encouragement throughout my Ph.D. study.

Dr. Orjala's LAB: My deepest thank goes to my Ph.D advisor Dr. Jimmy Orjala. He has given me an opportunity to join his LAB, also always been supportive of my research and driven me to the right way throughout my Ph.D study, so that I have been able to concentrate on my research without any difficulty. I am also grateful to Dr. Alec Krunic for his meaningful discussions on my research projects and help with NMR experiments. Without him, my publications and this dissertation would not be possible. I also would like to thank Eddie Lee. He has been such a good friend of mine in the LAB and also taught me how to do micro-isolation and culture cyanobacteria. I really enjoyed the trip to Wisconsin we went together to collect cyanobacterial samples. My thanks also go to Drs. Shunyan Mo and Goerge Chlipala. Shunyan helped me a lot to settle down in the LAB and taught me all the experiments while I was doing a LAB rotation. George set up the dereplication method in our LAB and trained me. I really enjoyed doing dereplication, and this dereplication shaped the early part of Ph.D research. In addition, He has given me a lot of meaningful dissection about cyanobacterial taxonomy. I also would like to thank other LAB

ACKNOWLEDGEMENTS (continued)

members including Dr. Megan Sturdy, Dr. Jiachen Zi, Hyunjung Kim and Shangwen Luo for having been good friends of mine and also good research colleagues, and also for their kindness and help on my journey through a Ph.D. study.

Other LAB: I deeply thank Dr. Steven M. Swanson for his consultation during my course work and writing me a letter of recommendation in support of my postdoc application. I also would like to thank Qi Shen and Jilai Yang in Dr. Swanson's LAB, who have produced most of the cell line assay data for extracts, fractions and pure compounds described in this dissertation. I appreciate Dr. Bernard Santarsiero and Dr. Ben Ramirez for conducting an X-ray crystallography of merocyclophane A for providing me an access to 600 MHz NMR at Center for Structural Biology, respectively. My big thank also goes to Chaitanya Aggarwal in Dr. Federle's LAB for helping me with molecular biology experiments including PCR and gel electrophoresis. I also appreciate Dr. Kirk Hevener and Henry Su in Dr. Jonson's LAB for performing a molecular mechanic study of merocyclophane B.

Preliminary examination and dissertation committee members: I am grateful to Dr. Brian Murphy, Dr. Chun-Tao Che, Dr. Michael Federle and Dr. Steven M. Swanson for being on my preliminary examination committee. I also would like to deeply thank Dr. Alexander Mankin, Dr. Brian Murphy, Dr. Duncan Wardrop, Dr. Jimmy Orjala and Dr. Steven M. Swanson for being on my dissertation committee and also for meaningful comments on my dissertation.

Korean community: Lastly, I would like to deeply thank people in Korean community at UIC College of pharmacy for their great kindness and encouragement throughout my Ph.D. study. Especially, Changwha Hwang, Hyunjung Kim and Jahye Myung have been really good friends of mine during my Ph.D. study, leaving me so many memories that I will never forget for the rest of my life. My deep appreciation goes

ACKNOWLEDGEMENTS (continued)

to Dr. Hyunwoo Lee and Dr. Hyunyeong Jung for having been so kind to me and given me very meaningful consultation on my carrier as a natural products chemist throughout my Ph.D. study.

All of the researches described in this dissertation were conducted as a part of PO1 anticancer project funded by NCI/NIH with the grant No. CA125066.

HSK

TABLE OF CONTENTS

TABLE OF CONTENTS (continued)

LIST of FIGURES

LIST of FIGURES (continued)

LIST of TABLES

ABBREVIATIONS

Abu (2-amino-2-butenoic acid)

Adda (3-amino-9-methoxy-2,6,8-trimethyl-10-phenyldeca-4E, 6E-dienoic acid)

Ahp (3-amino-6-hydroxy-2-piperidone)

Dha (dehydroalanine)

Dhb (dehydrobutyrine)

C. raciborskii (*Cylindrospermum raciborskii*)

CID (collision-induced dissociation)

COSY (correlation spectroscopy)

FDAA (1-fluoro-2,4-dinitrophenyl-5-L-alanine amide)

FDLA (1-fluoro-2,4-dinitrophenyl-5-L-leucine amide)

Hamd (2-hydroxy-3-amino-4-methyldodecanoic acid)

Hamcd (2-hydroxy-3-amino-4-methyl-12-chlorododecanoic acid)

Hamct (2-hydroxy-3-amino-4-methyl-12-chlorotetradecanoic acid)

Hamhh (2-hydroxy-3-amino-4-methyl-14-hydrxyhexadecanoic acid)

Hamho (2-hydroxy-3-amino-4-methyl-15-hydroxyoctadecanoic acid)

Hamoh (2-hydroxy-3-amino-4-methyl-14-oxohexadecanoic acid)

Hamoo (2-hydroxy-3-maino-4-methly-15-oxooctadecanoic acid)

HMBC (heteronuclear multiple bond correlation)

HRESIMS (high-resolution electrospray ionization mass spectrometry)

HSQC (heteronuclear single quantum coherence)

NMR (nuclear magnetic resonance)

NOESY (nuclear overhauser effect spectroscopy)

NRPS (non-ribosomal peptide synthase)

ORF (open reading frame)

ABBREVIATIONS (continued)

ROESY (rotating-frame Overhauser effect spectroscopy)

TE (thioesterase)

TOCSY (total correlation spectroscopy)

PKS (polyketide synthase)

ACP (acyl carrier protein)

CHAPTER 1: INTRODUCTION

1.1 Natural products as a source for drug discovery

Since the initial discovery of penicillin by Alexander Fleming in the early 20th century, many pharmaceutical companies and scientist have extensively explored natural sources, including the kingdom of plants and the microbial world, to find biologically active compounds with therapeutic potential (Beutler, 2009). These efforts led to the discovery of several clinically important drugs, many of which have been used as life-saving drugs including antibiotics, immunosupressants and anti-cancer drugs (Figure 1.1). As evidenced by these examples, it is clear that natural products have played a central role as platform for the discovery of front-line drugs during the past century.

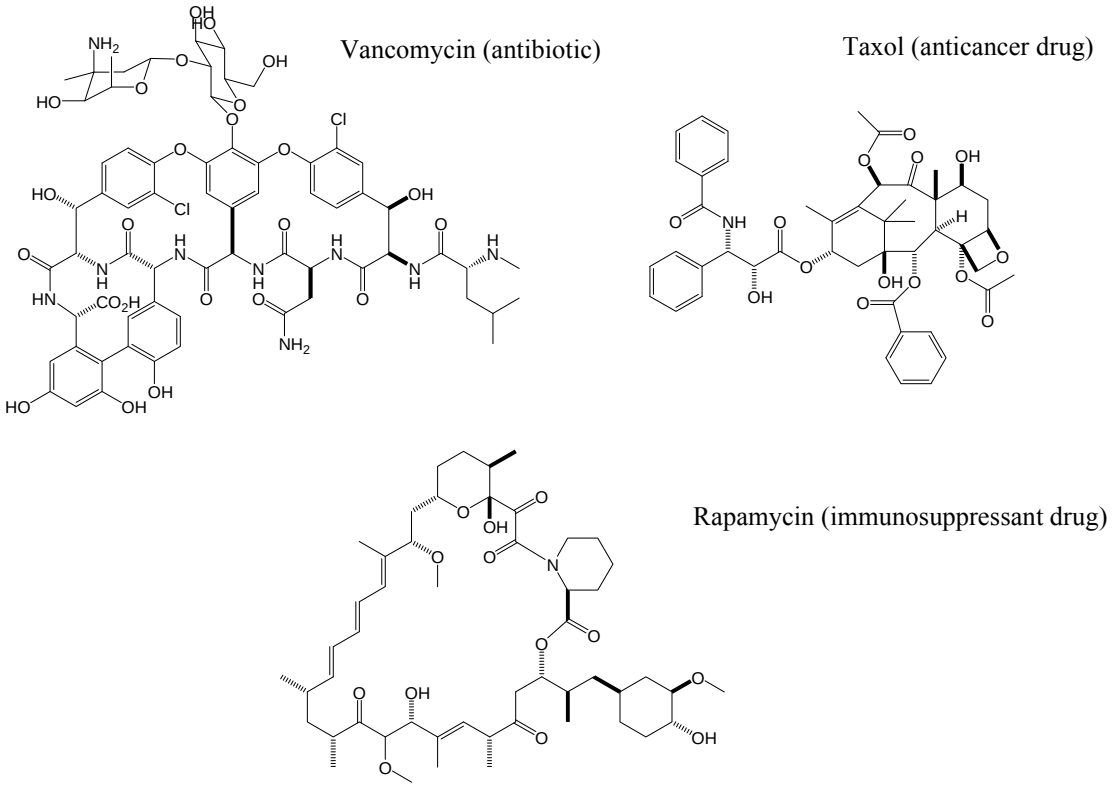

Figure 1.1 Some of the landmark drugs discovered from natural sources

A recent review paper published by Newman and Cragg in 2012 included a statistical analysis of the sources for small molecule drugs, covering the 1,073 new chemical entries approved by FDA from

1981 to 2010 (Newman and Cragg, 2012). This analysis showed that during this time period, 59 drugs (6%) of the new chemical entities were unmodified natural products and 299 drugs (28%) were semisynthetically modified natural products, thus accounting for 34% of the drugs approved during this time frame. However, this percentage significantly increased by further analysis of the 710 drugs (66%) that were of synthetic origin. Of these 177 drugs (16%) were based on a natural product pharmacophore and 146 drugs (14 %) mimicked a natural product inhibitor at the molecular target of interest. Thus, 64% of drugs approved during this time period could be classified as derived or inspired from nautral products. This analysis clearly demonstrated the continuing and valuable contributions of natural products in the drug development process, not only as potential chemotherapeutic agents, but also as lead compounds that provide the basis and inspiration for semi-synthesis or total synthesis of effective new drugs.

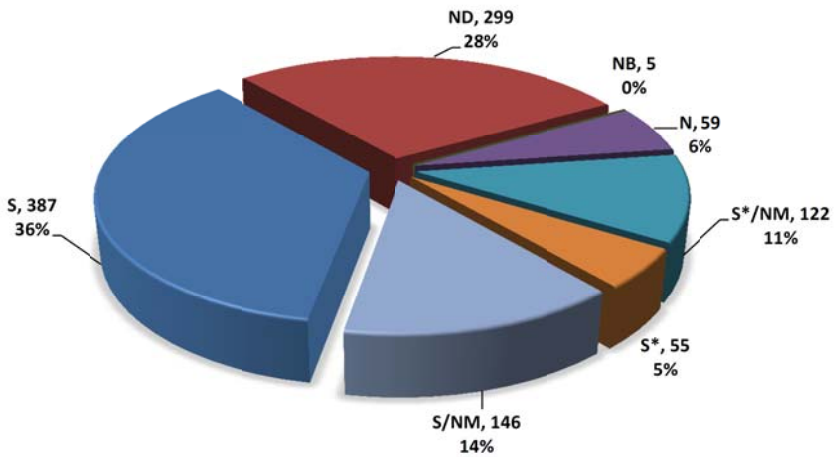

N : a Natural product
NB : a Natural product "Botanical"
ND : Derived from a natural product and is usually a semisyntehtic modification
S : a synthetic compound with no natural product conception
S/NM : a synthetic compound showing competitive inhibition of the natural product substrate
S* : a synthetic compound with a natural product pharmacophore
S*/NM: a synthetic compound with a natural product pharmacophore showing competitive inhibition of the natural product substrate

Chart 1.1 Small Molecule New Chemical Entities 01/1981 – 10/2010 (adapted from Newman and Cragg, 2012).

Natural products are often referred to as privileged structures that are shaped by evolutionary pressures to interact with a variety of biological targets for specific purposes, a view supported by the fact that natural products have become effective drugs for a wide variety of therapeutic indications (Koehn, 2005). As described in details in the two reviews (Clardy and Walsh, 2004; Ganesan, 2008), natural product drugs generally exhibit unique structural features that are significantly different from synthetic drugs. One of the major structural features observed in natural products is their surprisingly high structural complexity. These structures are created from relatively simple building blocks, but often contain multiple stereogenic centers. Natural product drugs are also composed of higher numbers of carbon, hydrogen and oxygen atoms, but less nitrogen and other elements as compared to synthetic drugs. Also, the molecular weights of many natural product drugs exceed 500 Da and display high polarity, thus violating Lipinski's "rule of five" (TABLE I: Ganesan, 2008). The rule is used as a guideline for medicinal chemists to design drugs with oral bioavailability and desired pharmacokinetic properties. Despite their relatively high molecular weights and violation of Lipinski's "rule of five", natural products often display excellent pharmacokinetic properties; for example, half of natural product drugs, listed in TABLE I, are orally available. In addition, natural products often exhibit well-defined 3D conformations. This conformational rigidity, which is established by non-covalent interactions or by the presence of double bonds, allows the molecules to avoid entropy loss and retain sufficient binding energy as molecules bind to biological targets. These distinct structural features observed in natural product drugs clearly demonstrate that natural products not only serve as a source for clinically important therapeutic drugs, but also teach us valuable lessons about how nature designs chemicals to achieve desired biological activities. These lessons can again provide medicinal chemists with starting points to design the large pool of chemical libraries for combinatorial synthesis.

As stated above, it is clear that natural products will continue to provide us unique chemotypes that have been never seen or synthesized before, and will be valuable as drugs as well as chemical probes to study and understand biological systems.

TABLE I: THE LIPINSKI PARAMETER OF SOME OF THE NATURAL PRODUCT LEADS (taken from Ganesan, 2008).

Natural Product	**Formula**	**MW**	**Log P**	**Hd**	**Ha**	**Rot**	**PDA**	**HA**	**ST**
Validamycin	$C_{20}H_{35}NO_{13}$	498	-5.2	12	14	7	253	34	14
Midecamycin	$C_{41}H_{67}NO_{15}$	814	2.1	3	16	14	206	57	9
Pseudomonic acid	$C_{26}H_{44}O_9$	501	2.5	4	9	17	146	35	8
Taxol	$C_{47}H_{51}NO_{14}$	854	3.0	4	14	14	221	62	11
Echinocandin B	$C_{52}H_{81}N_7O_{16}$	1060	1.8	14	16	20	368	75	15
Rapamycin	$C_{51}H_{79}NO_{13}$	914	4.3	3	13	6	195	65	15
Cyclosporine A	$C_{62}H_{111}N_{11}O_{12}$	1203	5.2	5	12	15	279	85	12
Lipstatin	$C_{29}H_{49}NO_5$	492	7.5	1	5	21	82	35	5
Avermectin B_{1a}	$C_{48}H_{72}O_{14}$	873	2.3	3	14	8	170	62	20
FK506	$C_{44}H_{69}NO_{12}$	804	3.3	3	12	7	178	57	14
Daptomycin	$C_{72}H_{101}N_{17}O_{26}$	1621	-3.7	22	29	35	702	115	13
Calicheamicin $_{\gamma 1}$	$C_{55}H_{74}IN_3O_{21}S_4$	1368	3.2	8	23	24	308	84	19
Average	**$C_{46}H_{70}N_4O_{14}$**	**917**	**2.2**	**7**	**15**	**16**	**259**	**64**	**13**

MW, molecular weight; **Log p**, C logp; **Hd**, H-bond donors; **Ha**, H-bond acceptors; **Rot**, number of rotatable bonds; **PSA**, polar surface area; **HA**, heavy atom count of nonhydrogen atoms; **St**, stereogenic centers.

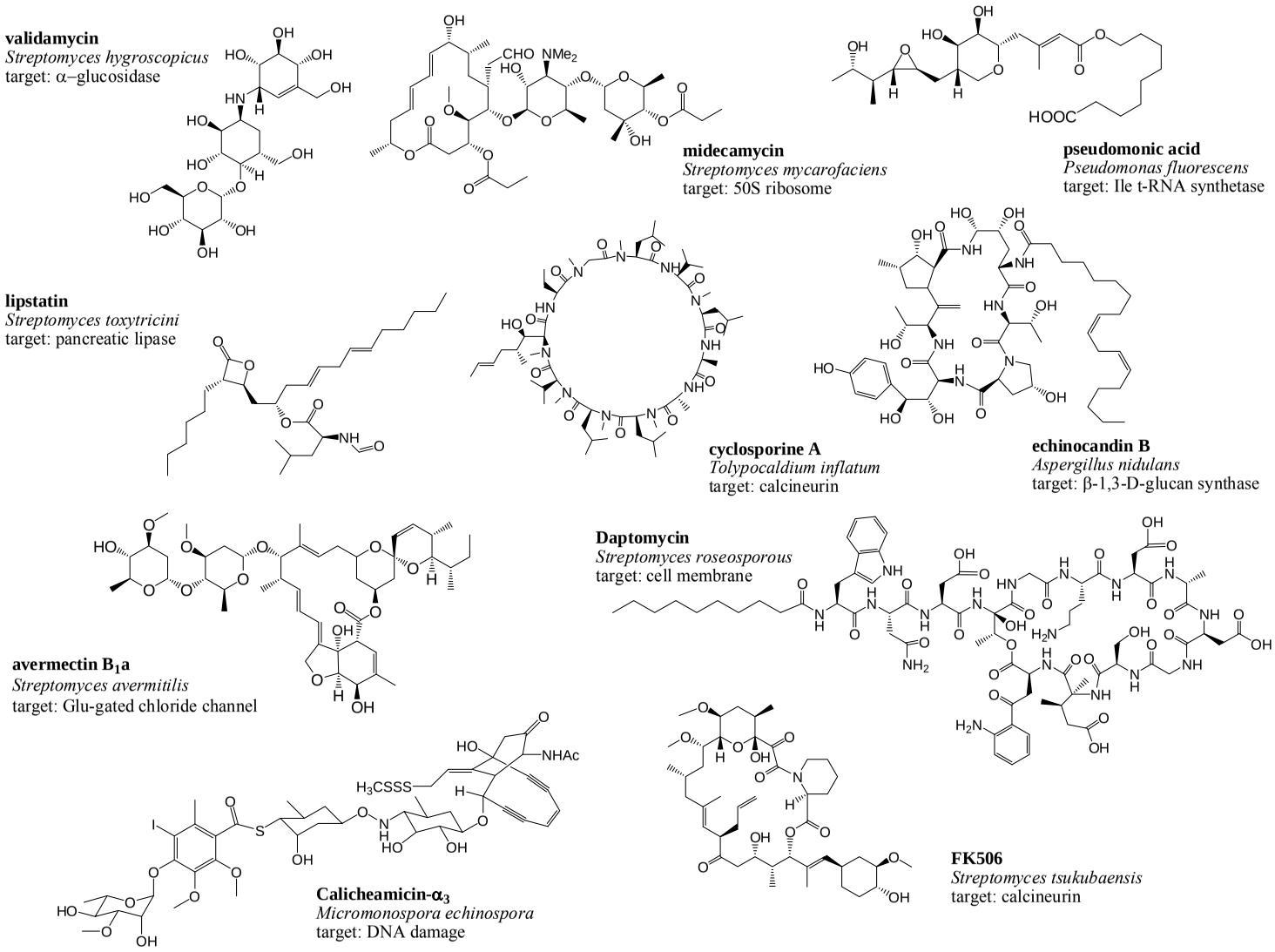

Figure 1.2 Structures of natural products discovered since 1970 that led to an approved drug in 1981-2006 (adapted from Ganesan, 2008).

1.2 Cyanobacteria

Cyanobacteria, also known as blue-green algae, are a phylum of photosynthetic bacteria. These bacteria are found in a wide range of habitats including marine, freshwater and terrestrial environments. Due to their ability to perform oxygenic photosynthesis, it is believed that cyanobacteria changed the early earth's reducing environment into an oxidizing environment, thus shaping the current respiration-based life forms (Badger, 2003; Sleep, 2008). This sub-chapter will cover the general characteristics, current taxonomic system, general habitats and ecology of cyanobacteria with an emphasis on freshwater and terrestrial species.

1.2.1 General characteristics

The name cyanobacteria comes from the presence of a blue-green pigment protein, phycocyanin. The overall ratio between phycocyanin and the red pigment protein, phycoerytherin, determines the characteristic colors of individual cyanobacterial species, which vary from blue-green to purple, red, brown to black. In terms of cell structures, cyanobacteria are classified as gram-negative bacteria, since their cellular structures contain LPS (lipopolysaccharide) layer as well as an outer cell membrane. However, in contrast to other gram-negative bacteria, cyanobacteria have thick peptidoglycan layers, resembling those of gram-positive bacteria, and are also lacking teichoic acids (Hoiczyk, 2000). In addition to this, cyanobacteria cells are surrounded by mucilaginous sheaths, made of polysaccharides (Tease & Walker, 1987). This gelatinous cellular structure provides protection, in addition it allows cyanobacteria to acquire trace elements for metabolism and hold colonies together.

1.2.2 Taxonomic classification

Cyanobacteria are considered to be a relatively shallow-branching phylum compared to other groups of bacteria, since variations in their 16S rRNA sequences are smaller than 20 %. However, cyanobacteria are morphologically very diverse, and these morphological differences have traditionally been

the primary base of the cyanobacterial classification system. The phylum of cyanobacteria is classified into five sub-sections based on morphological characteristics comprising five orders as described in the Bergey's Manual of Systematic Bacteriology (Castenholz 2001).

- Sub-section **I**. Chroococcales: unicellular
- Sub-section **II**. Pleurocapsales: large cells subdividing into smaller baeocysts
- Sub-section **III**. Oscillatoriales: simple filamentous
- Sub-section **IV**. Nostocales: filamentous, non-branching heterocyst-forming
- Sub-section **V**. Stigonematlaes: filamentous, branching, heterocyst-forming

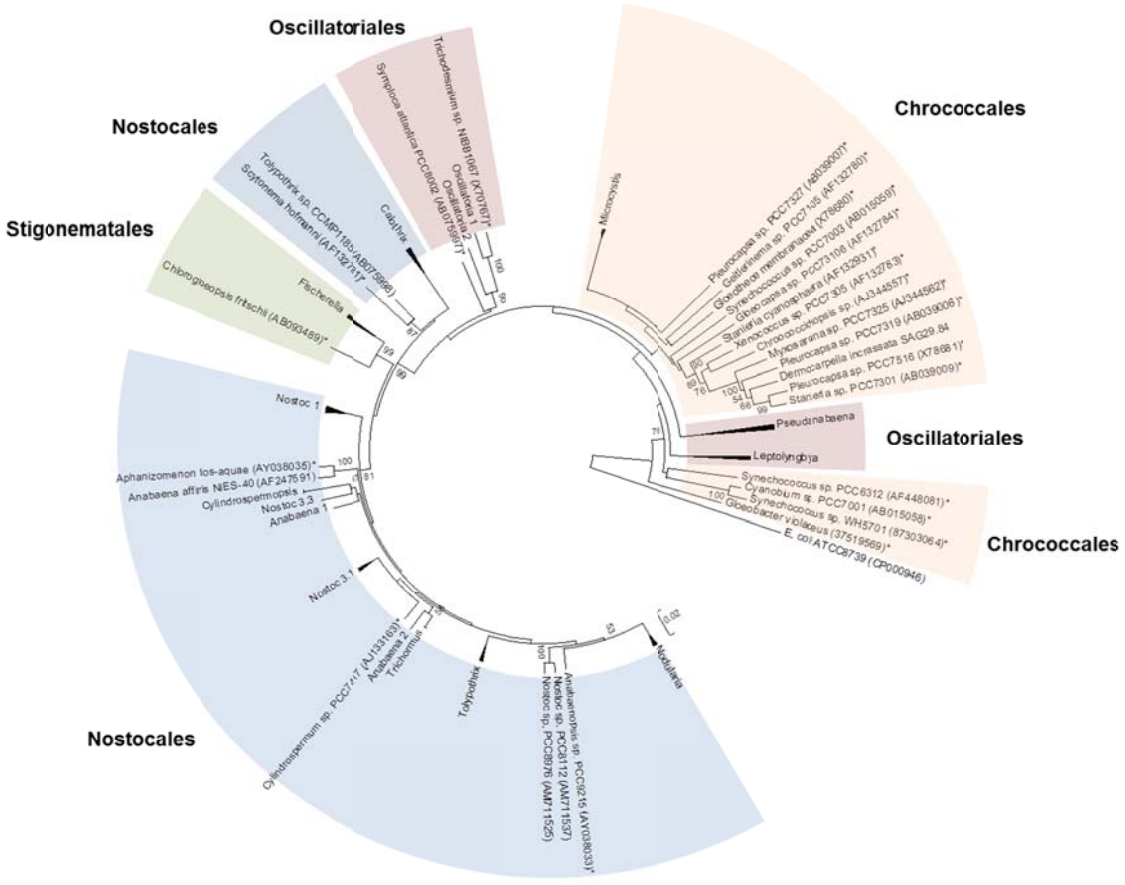

Figure 1.3 Phylogenetic tree constructed using 16S rRNA gene sequences of reference cyanobacteria retrieved from Bergey's manual of systematic bacteriology

The number of cyanobacterial 16S rRNA gene sequences available in public databases has dramatically increased during the past ten years, thus analyses of 16S rRNA gene sequences are now routinely used in combination with morphological analysis for the taxonomic identification of cyanobacteria. However, the results of 16S rRNA gene analyses are not always consistent with the morphological classifications, leading to the paraphyletic nature of most of the genera (Figure 1.3). This has raised a need for revision of the current cyanobacterial taxonomic system (Komárek, 2006).

1.3 Ecotypes of freshwater and terrestrial cyanobacteria and their secondary metabolites

Cyanobacteria are found in a variety of habitats ranging from oceans to soil to freshwater. Due to their ability to convert solar energy and carbon dioxide into organic compounds, termed CO_2 fixation, and nitrogen gas into ammonia, termed nitrogen fixation (figure 1.4), cyanobacteria play a critical role in many ecosystems as a primary source for production of organic compounds (Hess, 2011). Cyanobacteria are also found in many environmental conditions as different ecotypes that adapt to the specific environmental conditions. Therefore, it can be anticipated that different cyanobacterial ecotypes would have a different evolutional history, and thus produce different types of small molecules with distinct biological activities. The most commonly observed ecotypes include microbial mats, freshwater blooms, picoplankton and symbionts. This sub-chapter aims to review the most commonly observed cyanobacterial ecotypes found in freshwater and terrestrial environments, and to evaluate their biosynthetic capacity to produce biologically active small molecules.

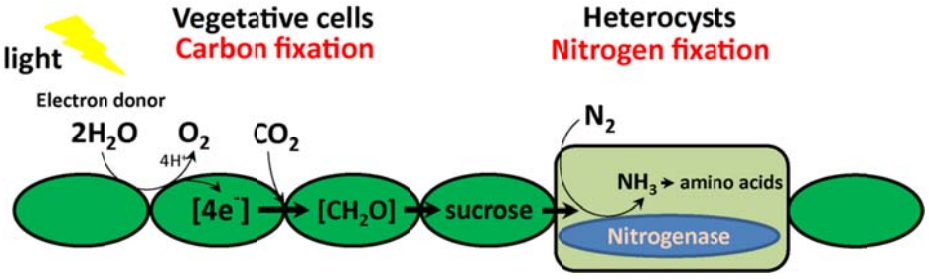

Figure 1.4 Two types of cyanobacterial cells where carbon and nitrogen fixation are performed

1.3.1 Mat-forming Cyanobacteria

Microbial mats are a dense population of microorganisms characterized by the vertical stratification of functionally different microbial groups (Stal & Caumette, 1994). Cyanobacteria-dominated mats are found in a wide range of environments from tropics to Antarctica (Paerl, 2000). It has been proposed that globally distributed microbial mats, which incorporate a range of photosynthetic and anaerobic mi-

croorganisms, contributed to global biogeochemical change by oxygenic photosynthesis, increasing biological productivity (Hoehler et al., 2001). Microbial mats are considered to be closed ecosystems, and their laminated microbial structures are formed by the physicochemical gradients of light, oxygen and sulphide (Stal & Caumette, 1994). In most cases, the formation of these microbial communities is initiated by cyanobacteria, which occupies the top layer of the laminated structures (Figure 1.5). The layer below cyanobacteria is composed of anaerobic phototrophic purple sulfur bacteria, which oxidize sulfide into sulfate, followed by the layer of sulfate-reducing bacteria, which reduce sulfate back to sulfide.

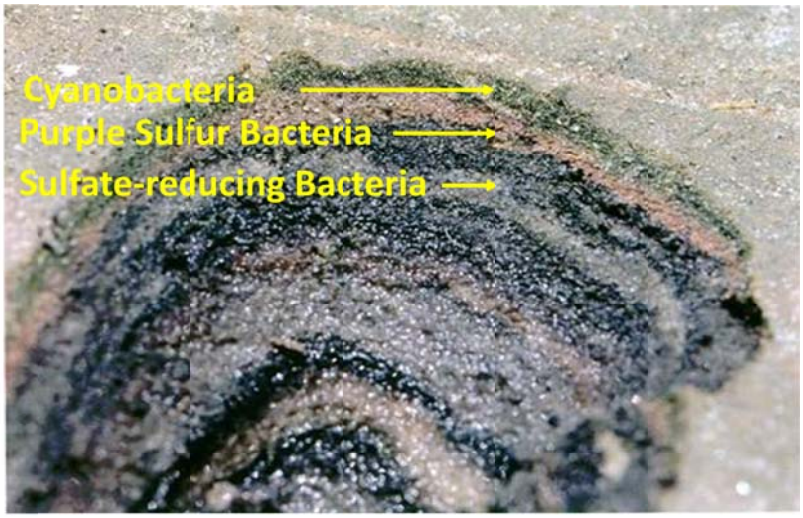

Cyanobacteria from microbial mats (Farbstreifen-Sandwatt)
http://www.icbm.de/~gmb/21184.html

Figure 1.5 Typical laminated structures of cyanobacteria-dominated microbial mats

Cyanobacteria play many roles in these microbial communities, and some of these aspects have attracted the attention of chemical ecologists. First, cyanobacteria produce organic matters by oxygenic photosynthesis and these are the primary products of microbial mat communities. Second, when exposed to high light intensities, cyanobacteria produce sunscreen pigments, thus protecting the underlying community from damages caused by UV irradiation. Scytonemin is one of the representative cyanobacterial sunscreen pigments (Figure 1.6) (Balskus, 2011).

Scytonemin is an indole-based yellow-brown pigment featuring a highly conjugated heterocyclic skeleton (Figure 1.6). It is often found in the upper layers of microbial mats occupied by cyanobacteria. The precursors of scytonemin are *L*-tryptophan and *p*-hydroxyphenylpyruvic acid. *L*-tryptophan is converted to 3-indole pyruvic acid and subsequently coupled with *p*-hydroxyphenylpyruvic acid by a thiamin-dependent enzyme. The monomer synthesis involves decarboxylation, cyclization, and oxidation steps after conjugation, and oxidative dimerization finalizes the biosynthesis of scytonemin (Balskus, 2008). This biosynthesis of scytonemin is initiated in response to UV-A exposure, and it is accumulated within the extracellular sheath of the producing organisms to form a protective layer that absorbs almost 90% of UV irradiation (λ_{max} = 370 nm in vivo, 384 nm in vitro) (Garcia-Pichel & Castenholz, 1991).

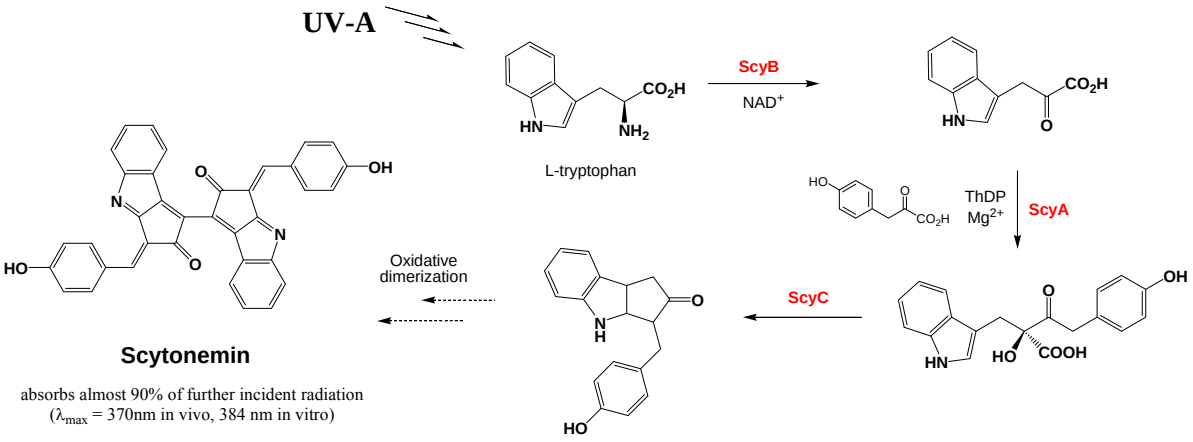

Figure 1.6 The structure and biosynthesis of the cyanobacterial sunscreen pigment scytonemin (adapted from Balskus, 2008)

1.3.2 Bloom-forming cyanobacteria

Cyanobacteria also appear in the freshwater environments in the form of blooms, which are defined by the massive population of certain bacterial species. Planktonic (free-floating) cyanobacteria are the dominant cyanobacterial species found in freshwater blooms. Most of the bloom-forming cyanobacteria produce secondary metabolites, which are often toxic to human. The occurrence of cyanobacterial

blooms can cause environmental problems, particularly by contaminating drinking water supply (Blaha, 2009). For this reason, toxins found in cyanobacterial blooms have been the subject of research for toxicologists rather than chemical ecologists or natural product chemists. Major toxins produced by freshwater bloom-forming cyanobacteria include hepatotoxins, neurotoxins and cytotoxins, and these toxins cause serious human health problems (Blaha, 2009).

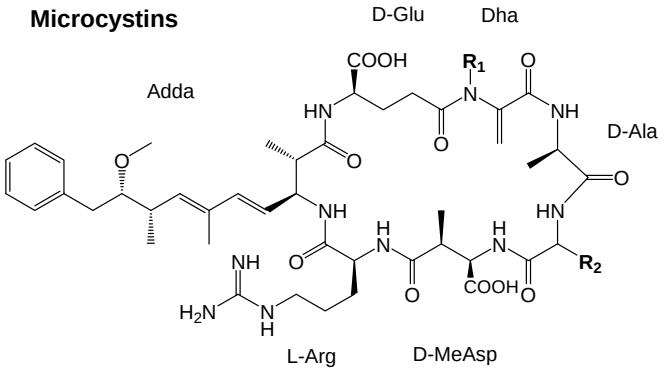

Microcystins	R_1	R_2
MCY-LR	CH_3	L-Leu
MCY-RR	CH_3	L-Arg
MCY-YR	CH_3	L-Tyr
[Dha^7]MCY-LR	H	L-Leu
[Dha^7]MCY-RR	H	L-Arg
[Dha^7]MCY-YR	H	L-Tyr

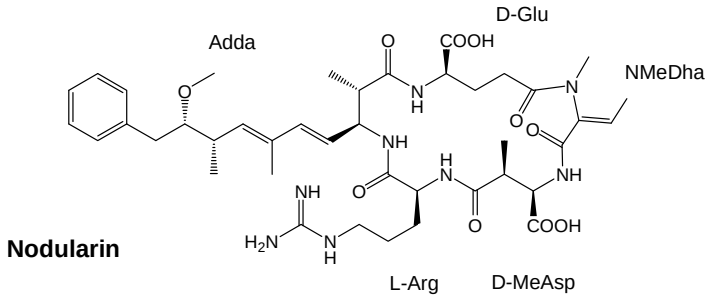

Figure 1.7 The structures of microcystins and nodularin

1) Microcystins and nodularins

Microcystins are cyclic heptapeptides and the major class of cyanobacterial hepatotoxin (Rinehart et al., 1988; Yoshizawa et al., 1990). Their expression is frequently observed in blooms of taxonomically diverse freshwater cyanobacteria, including both unicellular cyanobacteria such as *Microcystis* and *Planktothrix* spp., and heterocystous cyanobacteria such as *Anabaena*, *Aphanizomenon* and *Nostoc* spp. (Matthiensen et al., 2000; Keil et al., 2002) (Figure 1.7). The microcystins possess PK-NRP hybrid archi-

tectures, and more than 70 variants have been identified to date. The most common variant is microcystins-LR, which displays several unique structural features such as a *β*-amino acid Adda (3-amino-9-methoxy-2,6,8-trimethyl-10-phenyl-4,6-decadienoic acid), a *N*-methylated Dha (dehydroalanine) and a *β*-methylated Asp residues. The biosynthesis of microcystin-LR has been well-characterized and featured an integrated PKS and NRPS hybrid biosynthetic pathway, which requires ten genes, mcyA-J, composed of 11 modules, including a precursor-loading module, four PKS modules and six NRPS modules, and three modification enzymes (Figure 1.8) (Tillett, 2000). The four PKS modules are responsible for the synthesis of the *β*-amino acid Adda, whereas the six NRPS modules incorporate Glu, Ser, Ala, Asp and Arg. Of these, Ser, Ala and Asp are further modified by dehydration, epimerization and *N*-methylation, respectively. The final TE domain cyclizes between the amino group of Adda and the carboxyl group of Arg to form a cyclic heptapeptide core structure.

Nodularins are cyclic pentapeptides and comprise another major class of hepatotoxins produced by the bloom-forming heterocystous cyanobacteria *Nodularia* spp (Jonasson et al., 2008). The first structure of nodularin was reported in 1988 (Rinehart et al., 1988), and approximately 50 structural variants have been identified to date. The structures of nodularins closely resemble those of microcystins, and differ by the absence of two amino acid residues (D-Ala and L-Leu from microcystin-LR).

Both microcystins and nodularins cause acute hepatotoxicity upon exposure, and the mechanism involves the irreversible inhibition of protein phosphatases 1 and 2A, two serine/threonine protein phosphatases. These are key regulatory enzymes catalyzing dephosphorylation of serine/threonine residues in various phosphorproteins (Yoshizawa, 1990). Inhibition of protein phosphatases results in the loss of cytoskeletal integrity and subsequent cytolysis or apoptosis, primarily in hepatocytes. The interaction of microcystin-LR with protein phosphatase 1 and 2A follow a two steps mechanism: microcystin-LR first binds to the enzyme and subsequently forms covalent adducts during prolonged reaction time (Campos & Vasconcelos, 2010). X-ray crystallography studies indicated that microcystin-LR binds to the PP-1c α isoform, through interactions at three sites of the enzyme including the hydrophobic groove, C-terminal

groove and catalytic site. The α-carboxyl group of the γ-linked D-Glu residue, the carboxyl group of the D-MeAsp residue and the hydrophobic Adda residue play significant roles for the activity by interacting with the C-terminal groove, the catalytic site and the hydrophobic groove, respectively.

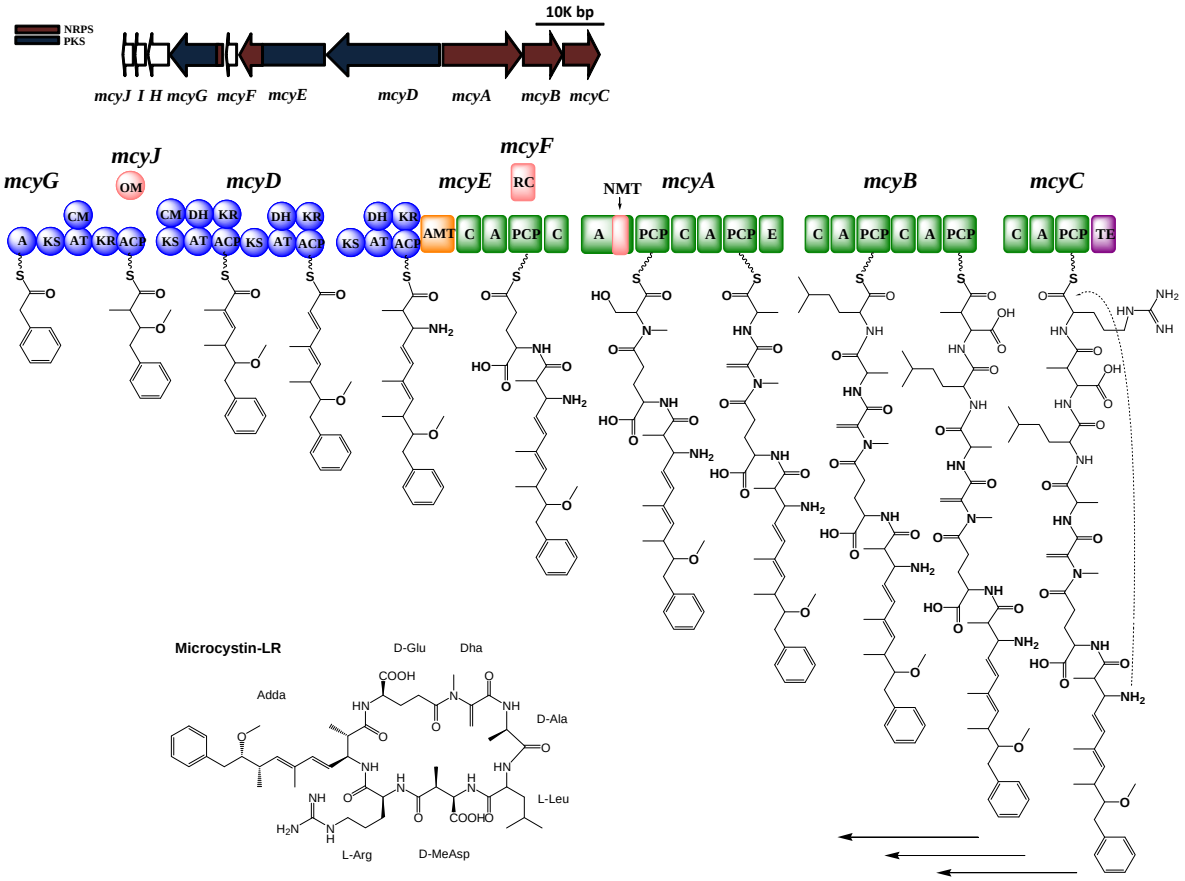

Figure 1.8 The schematic description of the microcystin-LR biosynthetic pathway (adapted from Tillett, 2000)

2) Cylindrospermopsin

In 1979, an outbreak of a hepatitis-like illness, also known as the Palm mystery disease, was observed in Palm Island, Queensland, Australia (Prociv, 2008; Griffiths & Saker, 2003). This outbreak hospitalized 138 people. At the time it was noticed that this outbreak coincided with the occurrence of sever-

al algal blooms in the local drinking water supply. An epidemiological study later suggested that treatment with copper sulfate to control the bloom formation caused lysis of the cyanobacterial cells, releasing a toxin into the water. Animal studies later confirmed that *Cylindrospermopsis raciborskii* was highly toxic out of three cyanobacterial strains that were identified in the algal bloom sample (Hawkins et al., 1985). The compound responsible for toxicity was later isolated from cultures of the toxic strain and named cylindrospermopsin (Figure 1.9) (Ohtani et al., 1992).

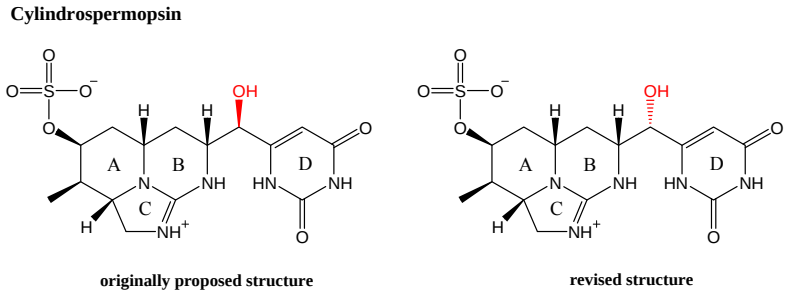

Figure 1.9 The originally proposed and revised structures of cylindrospermopsin

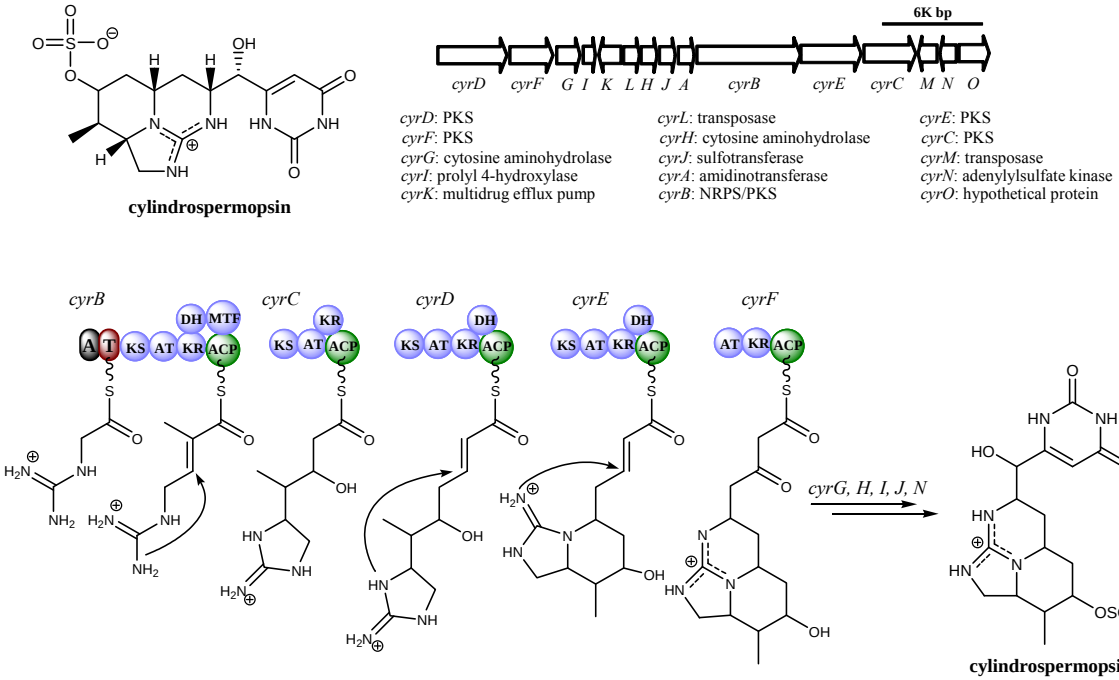

Figure 1.10 The structure and biosynthetic pathway of cylindrospermopsin (adapted from Mihali et al., 2008).

The structure of cylindrospermopsin was fully characterized by Moore's group in 1992 by NMR and MS analyses and featured a tricyclic guanidine (rings A, B and C) and a uracil (ring D) (Ohtani et al., 1992). However, later total synthesis indicated that the absolute configuration of the hydroxy-bearing carbon was misassigned, revising it to *S* (Heintzelman et al., 2001). The biosynthetic gene cluster for production of cylindrospermopsin was cloned and characterized from the strain *C. raciborskii* AWT205 (Mihali et al., 2008). The 45 kb-long gene cluster was comprised of 15 ORFs containing all genes required for biosynthesis, regulation and export of cylindrospermopsin (Figure 1.10). Cyra A, amidinotransferase, initiates the biosynthesis by transferring an amidino group onto Gly, followed by five polyketide extensions with subsequent reductions. The tricyclic guanidine was formed by Michael addition in a stepwise manner. The formation of a uracil ring involves a pyrimidine biosynthesis mechanism and tailoring reactions, including sulfation and hydroxylation, completing the biosynthesis of cylindrospermopsin.

Cylindrospermopsin showed a broad spectrum of toxicity, including hepatotoxicity, cytotoxicity (Runnegar et al., 1994, 1995 & 2002) and neurotoxicity (Kiss et al., 2002). In addition, potential carcinogenic effect has also been reported (Humpage et al., 2000). The mechanisms for these broad toxicities are proposed to be the result of its ability to interact with multiple targets, including glutathione and protein synthesis as well as cytochrome P450.

3) Anatoxin-a

Anatoxin-a is a cyanobacterial neurotoxin, known to be produced by the freshwater bloom-forming cyanobacterium *Anabaena flos-quae* (Smith et al., 1987). Production of anatoxin-a was also reported from the other genera including *Aphanizomenon* (Wood et al., 2007), *Planktothrix* (Viaggiu et al., 2004) and *Oscillatoria* sp. (Edwards et al., 1992). The structure of anatoxin-a features an azabicyclo[4.2.1]non-2-ene ring system, and the biosynthesis of anatoxin-a involves the initial loading of Pro by an adenylation domain (anaC) followed by three polyketide extensions, which were catalyzed by three

putative type I PKS enzymes (*anaE*, *F* and *G*) (Figure 1.11) (Méjean et al., 2009). The unique azabicyclo[4.2.1] nonane ring system is proposed to be formed by Michael addition type cyclization, and involves the nucleophilic addition of the α-carbonyl carbon of the growing polyketide chain to the imine carbon of the 3,4-dihydro-2H-pyrrole ring. Anatoxin-a is a potent antagonist of the nicotinic acetylcholine receptor, leading to severe acute asphyxia (Wonnacott & Gallagher, 2006).

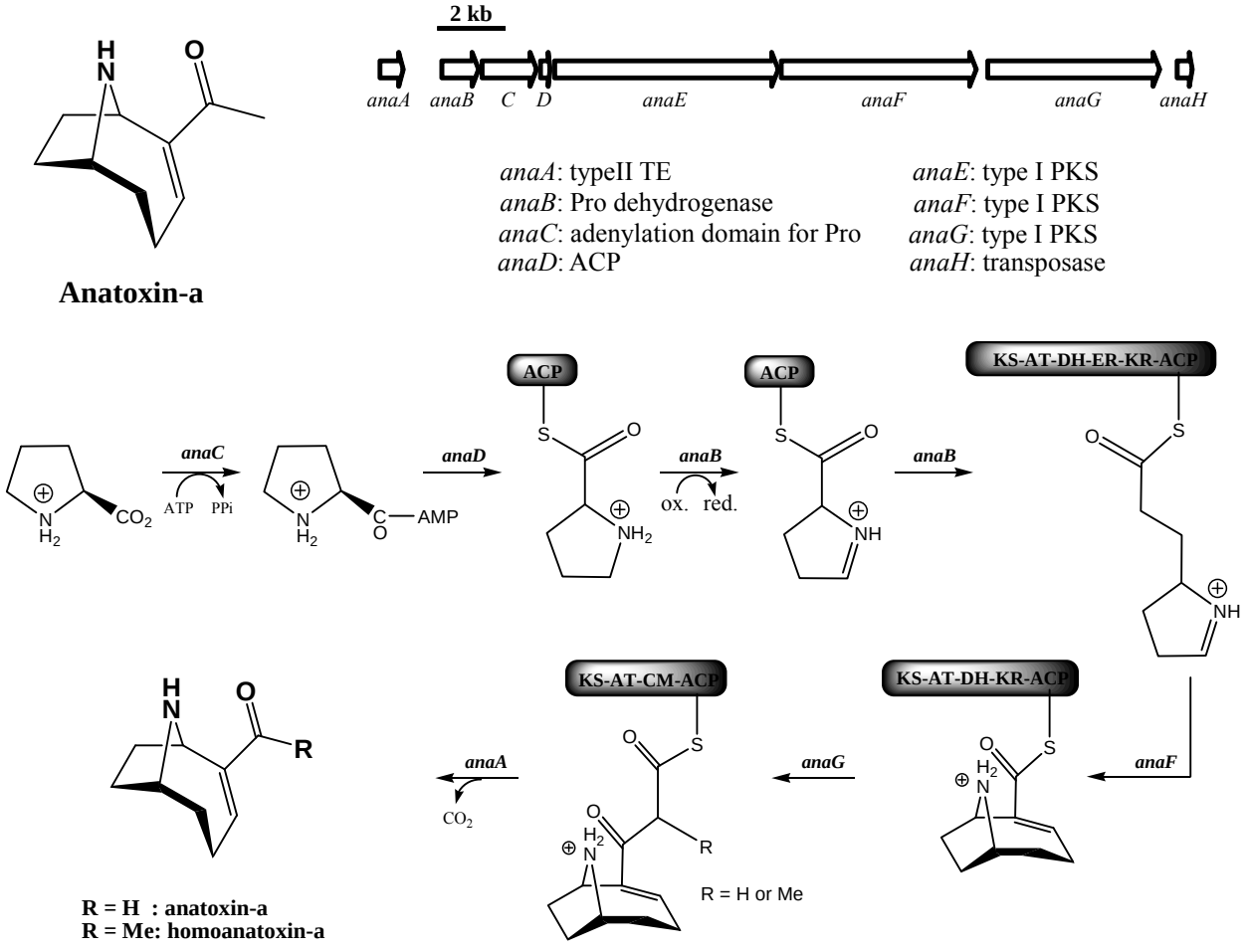

Figure 1.11 The structure and biosynthetic pathway of anatoxin-a (adapted from Méjean et al., 2009).

4) Saxitoxin

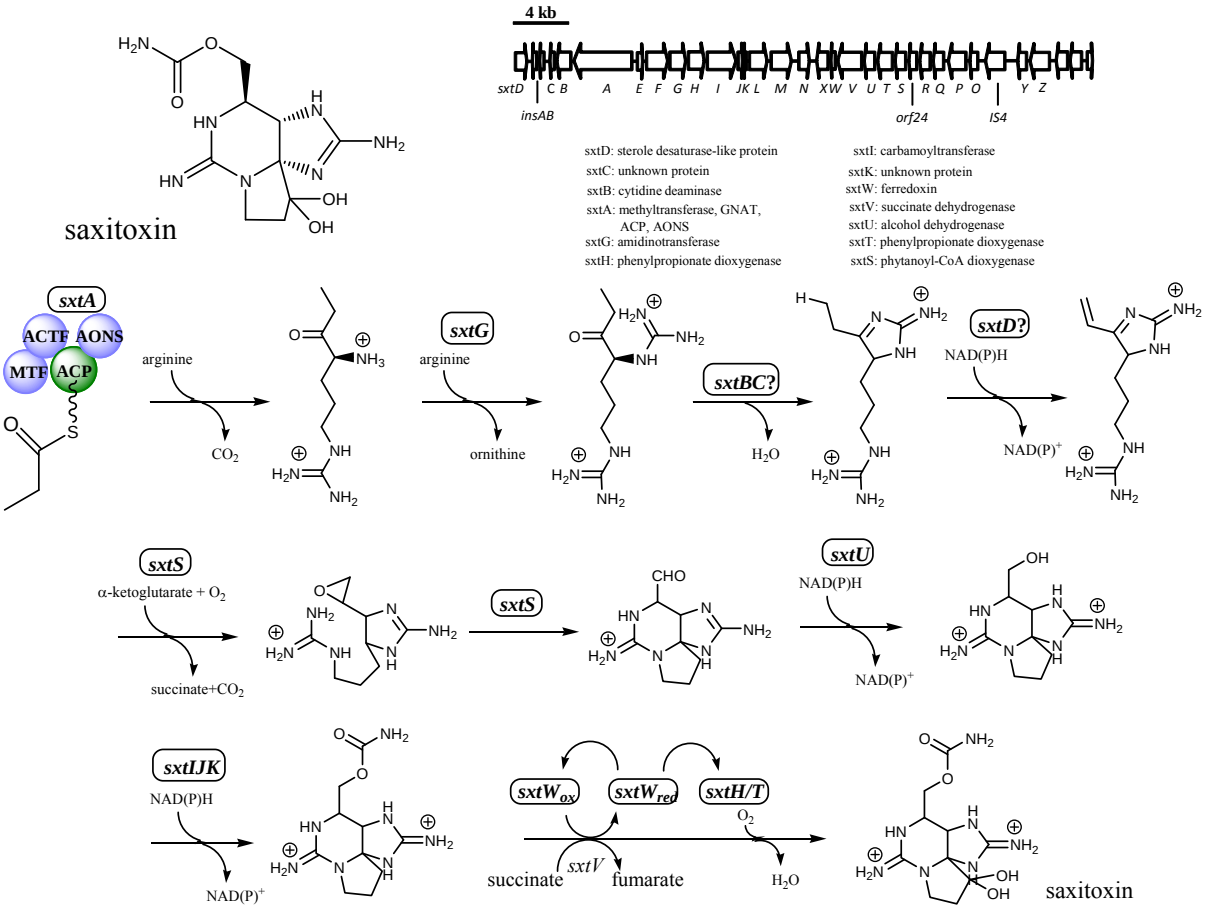

Figure 1.12 The structure and biosynthetic pathway of saxitoxin (adapted from Kellmann et al., 2008)

Another well-characterized cyanobacterial neurotoxin is saxitoxin. Production of saxitoxin has been reported from both freshwater and marine cyanobacteria including *Anabaena*, *Ahpanizomenon*, *Cylindrospermopsis* and *Planktothrix* spp. (Landsberg, 2002). Saxitoxin is known as the causative agent for paralytic shellfish poisoning, which is associated with the consumption of shellfish that have accumulated saxitoxin (Llewellyn, 2006). The tricyclic structure of saxitoxin is characterized by the presence of two guanidines, one carbamate and one diol functionalities. The several analogs of saxitoxin have been identified, which include neosaxitoxin, the gonyautoxins and decarbamoylsaxitoxin. The gene cluster responsible for the biosynthesis of saxitoxin has been characterized from *Cylindrospermopsis raciborskii* T3,

and includes 26 proteins with 30 catalytic functions (Figure 1.12) (Kellmann et al., 2008). The initial step of the saxitoxin biosynthesis involved a Claisen condensation between Arg and propionate, which was derived from methylation of acetate, putatively catalyzed by new type of PKS. The next steps involved several enzymes catalyzing three heterocyclizations and tailoring steps including carbamidation and diolization. Saxitoxin is one of the most potent natural neurotoxin known to date. The potent neurotoxicity of saxitoxin arises from its ability to selectively block the voltage-gated sodium channels of nerve cells, preventing normal cellular function and leading to paralysis (Huot et al., 1989). Due to its potent paralyzing effect without killing nerve cells, an attempt was made to develop saxitoxin as an anesthetic; however, the innate systemic toxicity makes it unlikely for saxitoxin to be developed as a drug.

5) Ahp-containing depsipeptides

Depsipeptides containing an Ahp (3-amino-6-hydroxyl-2-piperidone) residue, likely derived from Glu, is a common class of cyanobacterial metabolites identified in taxonomically diverse bloom-forming cyanobacteria, including both freshwater and marine species (Grach-Pogrebinsky et al., 2003, Gesner-Apter & Carmeli, 2009; Gunasekera et al., 2009). This class of compounds has been reported to be produced at significant levels upon bloom formation. The structures of Ahp-containing depsispeptides obtained directly from bloom samples are shown in Figure 1.13 (Banker & Carmeli, 1999; Gesner-Apter & Carmeli, 2009; Grach-Pogrebinsky et al., 2003; Kodani et al., 1999; Ploutno & Carmeli, 2002; Ploutno et al., 2002; Reshef & Carmeli, 2001; Zafrir & Carmeli, 2009). Additional Ahp-containing depsipeptides have been found in cultured material, comprising over 100 structural variants reported up to date; however all of them share common structural features. All of the Ahp-containing depsipeptides possess cyclic hexapeptide cores with an ester linkage between the side chain hydroxy group of Thr and the carboxyl group of Val or Ile. Structural diversity of Ahp-containing depsipeptides is created by substrate promiscuity observed for several amino acid residues in the depsipeptide core, composition of the amino acid branch stretching out from NH of Thr, and various acylation patterns at the *N*-terminal of the amino acid branch.

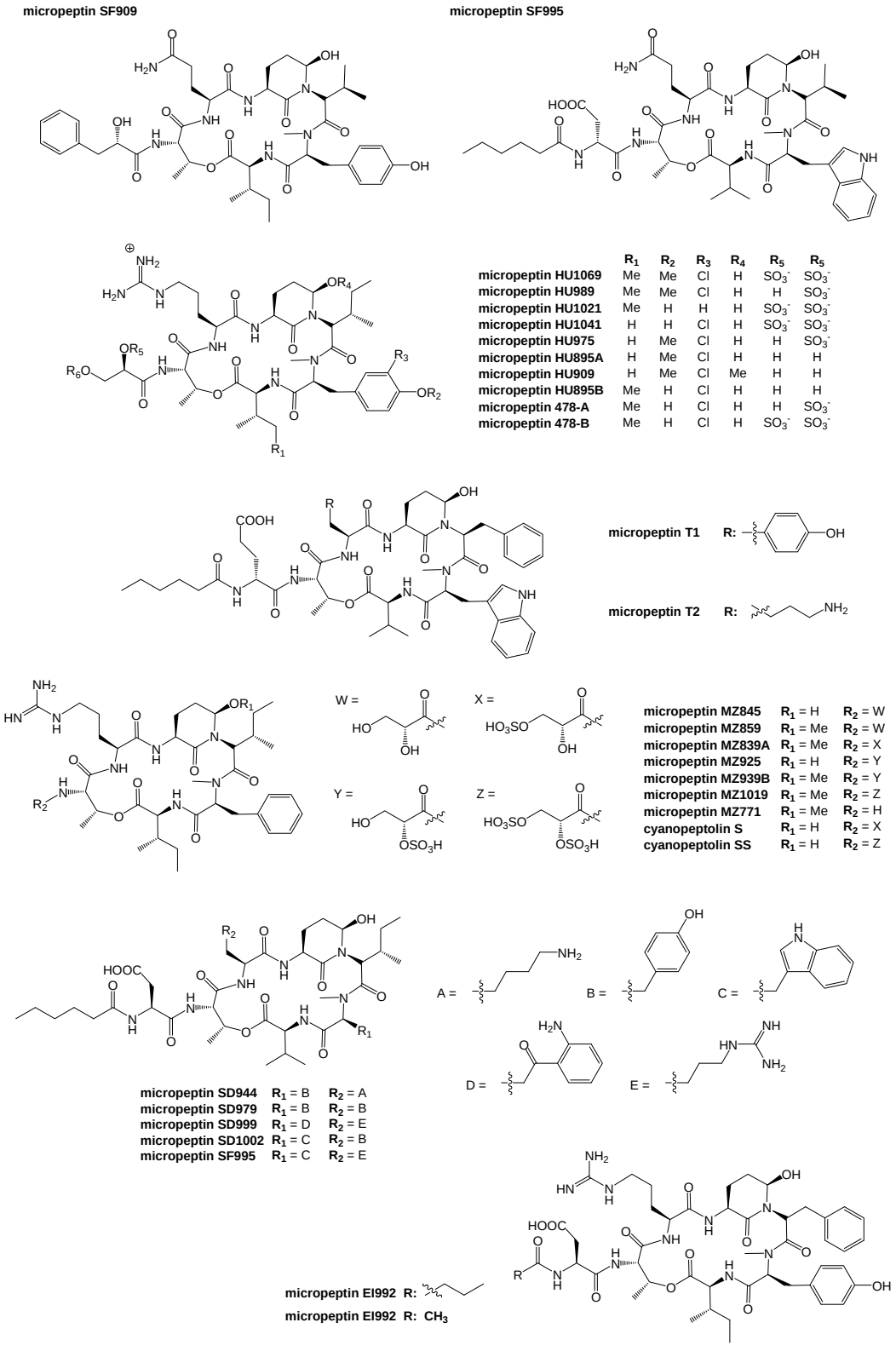

Figure 1.13 Structures of cyanobacterial Ahp-containing depsipeptides isolated from bloom samples of freshwater cyanobacteria

Most of cyanobacterial Ahp-containing depsipeptides are inhibitors of serine-proteases such as trypsin, chymotrypsin and elastase with different selectivity, depending on variations in their structures. Co-crystallographic data of elastase with scyptolin A suggested that the protease selectivity of this class of compound depends on the type of amino acids located between Ahp and Thr, due to different binding preferences to the enzyme's specificity pocket (Matern et al., 2003). Preferences for the inhibition of chymotrypsin and elastase were conferred by a bulky hydrophobic amino acid (Phe, Tyr or Trp) and a small neutral amino acid (Ala, Gly or Val), respectively. On the other hand, a positively charged amino acid (Arg or Lys) was preferred for the inhibition of trypsin. Due to the ability of Ahp-containing depsipeptides to inhibit serine proteases, their ecological role is believed to be as inhibitors of digestive enzymes and a chemical defense against crustacean predators (Berry et al., 2008). However, studies by Sedmak *et al*. showed that the Ahp-containing depsipeptide planktopeptin BL1125 induced cyanobacterial cell lysis, leading to the hypothesis that these protease inhibitors could play an important ecological role by controlling cyanobacterial population density in the natural environment (Sedmak et al., 2008 and 2009).

1.3.3 Symbiotic cyanobacteria

Most of cyanobacteria are free-living, but some cyanobacteria maintain symbiotic relationships with other organisms. In marine environments, cyanobacteria participate in symbiosis with diatoms, sponges, tunicates and dinoflagellates (Carpenter & Foster, 2002; Janson, 2002). In terrestrial ecosystems, cyanobacteria have been found in diverse symbiotic systems with a wide range of hosts, including fungi, bryophytes, *Azolla* (water fern), cycads (gymnosperm) and *Gunnera* (angiosperm) (Rai et al., 2000). The genus *Nostoc*, which is mostly found in terrestrial ecosystems, is the dominating cyanobacterial genus involved in symbiotic associations with fungi and plants. This is due to its capability to fix nitrogen (Adams & Duggan, 2008; Svenning, 2005; Rikkinen et al., 2002). The other genera such as *Scytonema* and *Chroococcus* have also been identified in various symbiotic systems (Lücking et al., 2009). The most well-studied symbiotic cyanobacterial species is *Nostoc punctiforme* that maintain diazotrophic symbiosis

with many organisms such as the bryophytes *Anthocerus punctatus* and *Blasia pusilla*, water ferns from the genus *Azolla*, the cycads *Macrozamia* spp. and the angiosperm *Gunnera* (Meeks et al., 2001 & 2002; Liaimer et al., 2011). Full genome sequencing of the symbiotic strain, *N. punctiforme* ATCC 29133, revealed the presence of an extraordinary large number of secondary metabolite biosynthetic gene clusters. Lichens are symbiotic associations that are composed of fungi as mycobionts and algae as photobionts. Cyanobacteria occur in approximately 10 % of lichens as photobionts, and the representative genera of lichen cyanobacteria include *Nostoc* and *Scytonema* (Svenning et al., 2005; Rikkinen et al., 2002). In lichen symbiotic systems, cyanobacteria play an important role in providing organic matters to their fungal symbiotic partners by oxygenic photosynthesis. Although there have not been many natural products isolated from lichen cyanobacteria, studies have indicated that lichen cyanobacteria would be prolific producers of biologically active secondary metabolites.

The most compelling example of symbiotic cyanobacterial secondary metabolites would be the promising anti-cancer drug leads cryptophycins. Cryptophycin A was first isolated as an antifungal agent from the lichen cyanobacterium *Nostoc* sp. ATCC 53789 by a group from Merck. The structure was proposed by this group; however, no further studies were carried out due to the severe toxicity associated with this compound. A later study by a group at U. of Hawai obtained cryptophycin A from a closely related *Nostoc* sp. GSV 224, and fully characterized the structure of cryptophycin A along with six minor analogues. This group also reported potent anti-tumor activity for these compounds (Trimurtulu, 1994). Since then, several analogues have been described, and over 25 structural variants have been reported to date (Chaganty, 2004; Subbaraju, 1997). Cryptophycin A, the major component, consisted of four residues, including a phenyl-octenoic acid, 3-chloro-*O*-methyl-*D*-tyrosine, methyl *β*-alanine and *L*-leucic acid. All the other cryptophycins differ from cryptophycin A in one or two residues of the molecule.

The high degree of structural variation found among analogues of cryptophycin family indicated flexibility and versatility of the biosynthetic pathway. The gene cluster encoding the biosynthesis of cryptophycins has been identified and characterized from the lichen cyanobacterial symbiont *Nostoc* sp.

ATCC 53789 by Dr. Sherman's group (Magarvey et al., 2006). The cryptophycin-biosynthetic gene cluster (crp A-H) is composed of two PKS enzymes harboring a loading module and three PKS modules, two NRPS enzymes harboring three NRPS modules, and four tailoring enzymes including a CYP450 epoxidase, an inron-containing 2-oxoglutarate dependent oxygenase, an amino acid decarboxylase and a non-heme halogenase (Figure 1.14). The third NRPS module, which incorporates the leucic acid residue, contained a ketoreductase domain to catalyze the reduction of ketone into hydroxyl group after transamination.

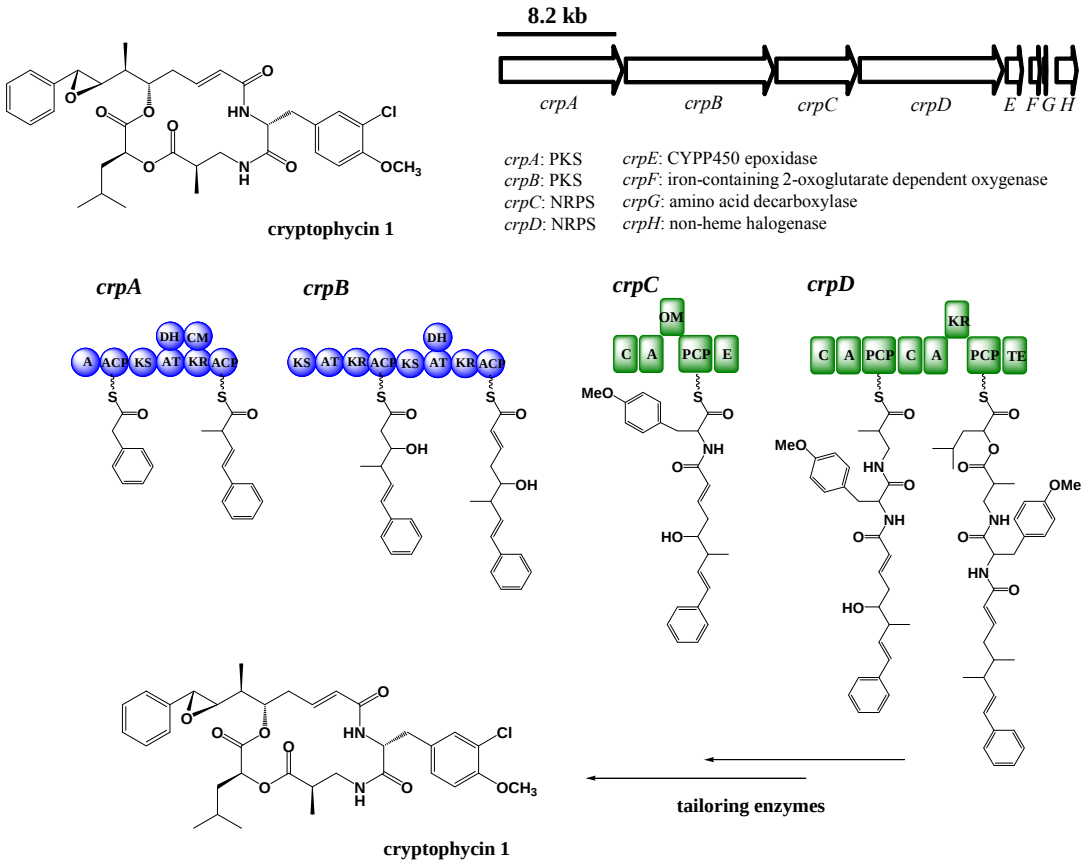

Figure 1.14 The structure of cryptophycin 1 and its biosynthetic pathway (adapted from Magarvey et al., 2006).

Cryptophycins were reported as one of the most potent tubulin destabilizing agents known to date,

and arrested tumor cells at the G1-M phase (Smith et al., 1994). This caused hyper-phosphorylation of Bcl-2, triggering the apoptotic cascades (Lu et al., 2001). In addition, cryptophycins were resistant to p-glycoprotein pumps, thus effective against multidrug-resistant tumor cell lines (Smith et al., 1994). These attractive and promising biological activities lead to the development of a synthetic analogue, cryptophycin 52, that entered the phase II clinical trial. However, the initial result indicated severe toxicity associated with this molecule, preventing further development as an anticancer drug (Edelman et al., 2003).

1.3.4 Other non-bloom forming cyanobacteria in freshwater and terrestrial environments

Most cyanobacteria are non-bloom forming and free-living, and these dominant life form of cyanobacteria can be found in diverse freshwater and terrestrial environments. Some of them, mainly filamentous cyanobacteria, form visible small colonies under favorable growth conditions. To access the secondary metabolites produced by non-bloom forming cyanobacteria, a culture-dependent approach is necessary, since in most cases sufficient biomass required for the chemical investigation cannot be acquired directly by environmental collections. However, it can be difficult to use cultured cyanobacteria for chemical investigations due to their inherent slow-growing properties. Doubling times for most filamentous cyanobacteria usually range from 15 to as long as 48 hrs (Meeks & Elhai, 2002), thus optimizing the culture condition for each strain and culturing a large number of strains for the activity screening is often an extremely time-consuming process. For these reasons, most culture efforts have been focused on bloom-forming cyanobacteria, including the genera Microcystis and Anabaena for the study of their toxin production. The majority of cyanobacterial secondary metabolites reported to date have been isolated from field-collected samples collected either freshwater or marine environments (Harada, 2004; Tan, 2007). Accordingly, there are relatively few examples of cyanobacterial secondary metabolites reported from cultured non-bloom forming cyanobacteria that are originated from freshwater and terrestrial environments.

Studies of biologically active secondary metabolites from cultured non-bloom forming freshwater

and terrestrial cyanobacteria was pioneered by Moore's group at University of Hawaii during in the 1980s and the 1990s. During this period, several novel cyanobacterial secondary metabolites were reported, and representative classes include polyketide-derived macrolides (Ishibashi et al., 1986; Moore et al., 1986), boron-containing compounds, indole alkaloids (Moore et al., 1984), [7.7]paracyclophanes (Moore et al., 1990) and cyclic lipopeptides (Moore et al., 1989), all of which displayed a wide spectrum of biological activities.

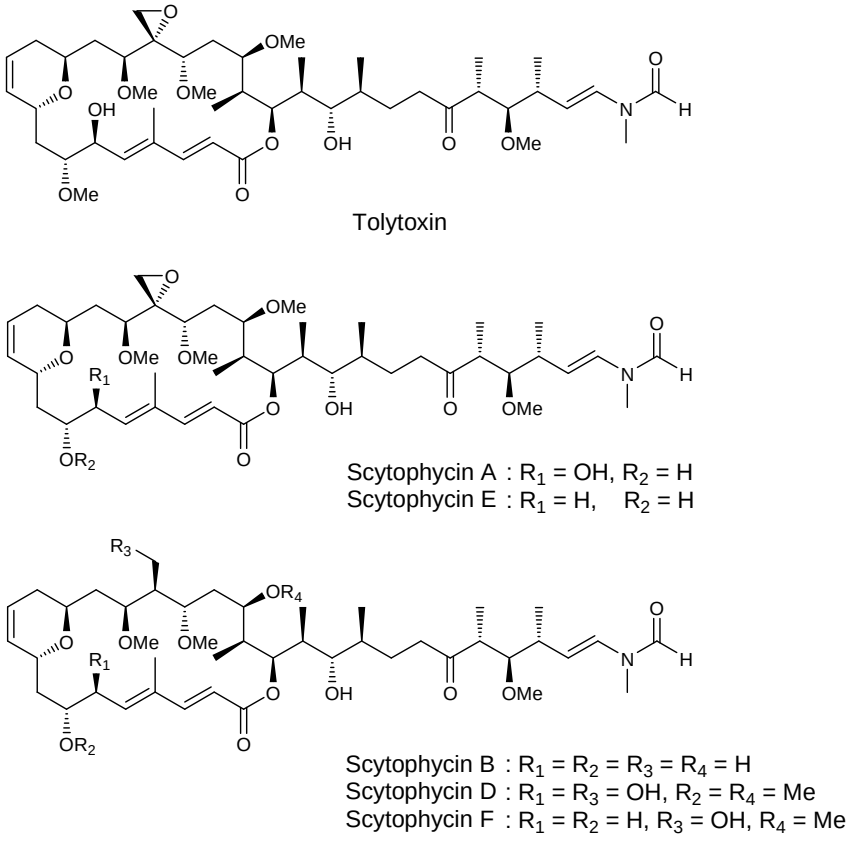

Figure 1.15 The structures of tolytoxin and scytophycins.

Scytophycins and tolytoxin are polyoxygenated 22-membered macrolides produced by terrestrial false-branching cyanobacteria of the genera *Tolypothrix* and *Scytonema* (Figure 1.15) (Ishibashi et al., 1986; Moore et al., 1986). Tolytoxin, a potent cytotoxin and fungicide, was the first compound belonging

to this class and was isolated from a field-collected sample of the terrestrial cyanobacterium *Tolypothrix conglutinata* found at Fanning Island in 1977. Determination of the full structure could not be achieved due to insufficient biomass acquired at that time. In 1986, Moore's group isolated the closely related compounds, scytophycins A-E, from the cultured terrestrial cyanobacterium *Scytonema pseudohofmanni* and fully characterized their structures (Moore et al., 1986; Ishibashi et al., 1986). Later, tolytoxin was re-isolated along with several scytophycin analogues from several cultured *Scytonema* strains, enabling the determination of the tolytoxin structure (Carmeli et al. 1990). Tolytoxin and scytophycins shared a highly oxygenated 22-membered macrolide core structure with an aliphatic branch stretched out from the oxygenated carbon. This aliphatic branch was highly functionalized with methyl, hydroxy and methoxy groups, and also contained an acid labile enamide system. All of the compounds belonging to this class possessed the same carbon skeleton, and the structure diversity originated from the various degrees of hydroxylation and methoxylation of the macrolide core structures. Tolytoxin and the scytophycins were microfilament-depolymerizing agents, thus exhibited potent cytotoxicity against various cancer cell lines (Smith et al., 1993). These compounds were also resistant to a P-glycoprotein-mediated efflux system, therefore considered to be effective against multi-drug resistant cancer cells.

Indole alkaloids are a group of cyanobacterial secondary metabolites produced by terrestrial true-branching cyanobacteria of the order Stigonematales. These alkaloids can be divided into several sub-groups based on their ring structures, including hapalindoles (Moore et al., 1984 & 1987), hapalonamides (Moore et al., 1987), welwitindolinones (Stratmann et al., 1994), fischerindoles (Park et al., 1992) and ambiguine isonitriles (Smitka et al., 1992) (Figure 1.16). This family of compounds shared common structural features, represented by an indole heterocycle with a monoterpene unit appended at C-3 and the presence of either isonitrile or isothiocyanate. This core structure further diversified through oxidation, chlorination, dehydrogenation, ring formation and rearrangement, and nearly 70 structural analogues have been reported to date (Richter et al., 2008). This family of compounds displayed a broad range of biological activities. For examples, both antibacterial and antimycotic activities were reported for hapalindoles

(Moore et al., 1987), and ambiguine isonitriles showed fungicidal activity (Smitka et al., 1992). Welwitindolinones were found to be responsible for the multidrug resistance reversing activity of *Hapalosiphon welwitschii* and the insecticidal activity of *Westiella intricata* (Stratmann et al., 1994).

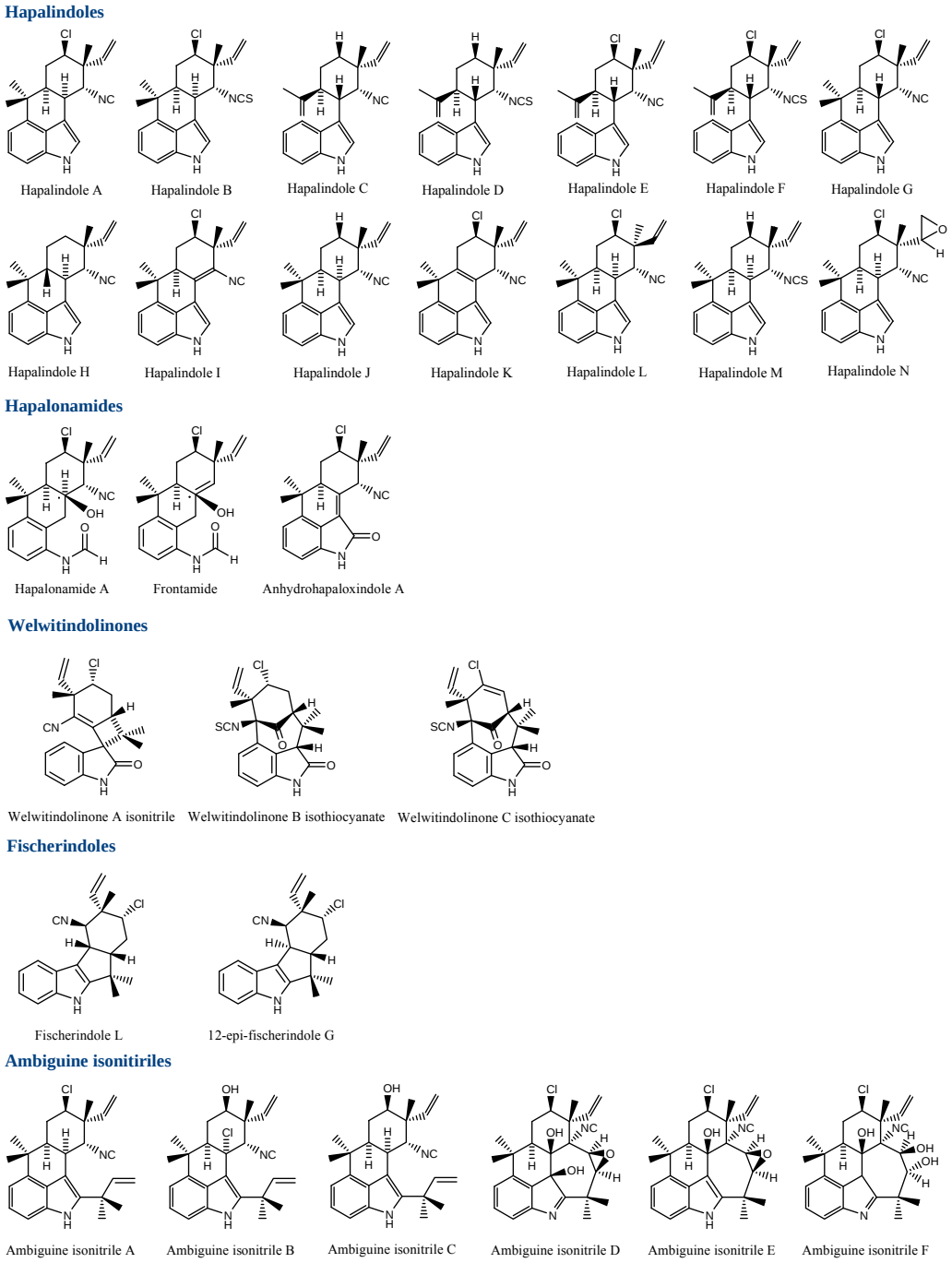

Figure 1.16 The structures of cyanobacterial indole alkaloids reported from Moore's group.

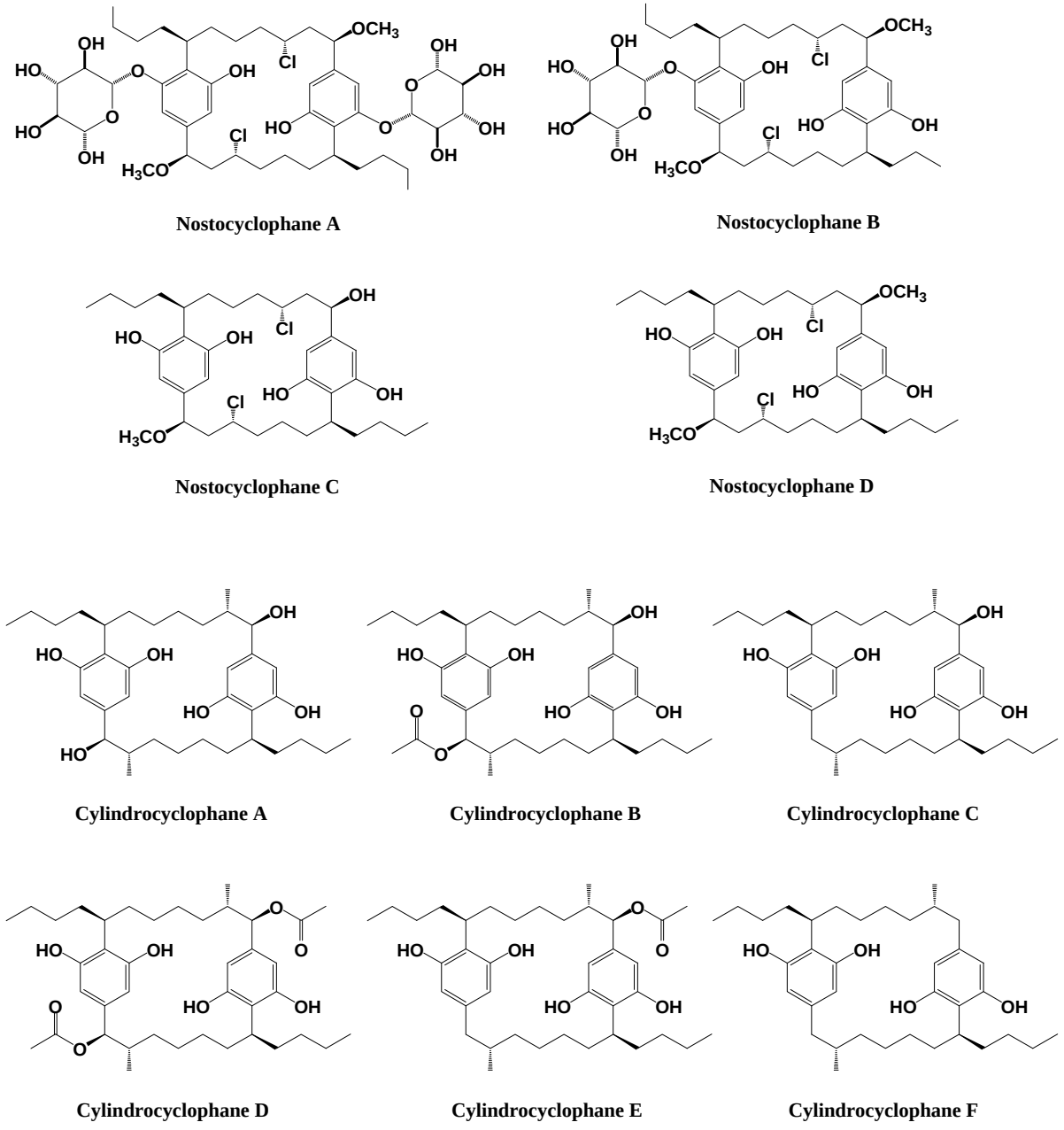

Figure 1.17 The structures of naturally occurring [7.7]paracyclophanes isolated from terrestrial cyanobacteria by Moore's group during the early 1990s.

Another group of secondary metabolites isolated from cultured terrestrial cyanobacteria was [7.7]paracyclophanes. This group of compounds was produced by heterocyst-forming filamentous cyanobacteria of the genera *Cylindrospermum* and *Nostoc*, both belonging to the order Nostocales. The first

compounds belonging to this class were reported in 1990 by Moore's group, and included cylindrocyclophane A and nostocyclophane D (Moore et al., 1990). Since then, several analogues have been reported with the same basic carbon skeletons, comprising the cylindrocyclophanes and nostocyclophanes as the two classes of cyanobacterial [7.7]paracyclophanes (Figure 1.17) (Chen et al., 1991; Moore et al., 1992). These two classes of cyclophanes shared common structural features. First, two benzene rings containing a resorcinol moiety are connected in *para* positions by seven carbons. Second, the benzylic carbons were further branched out at C-7/14 by four carbons-long aliphatic chain, conferring a C_2 axis of symmetry to the cyclophane core structures.

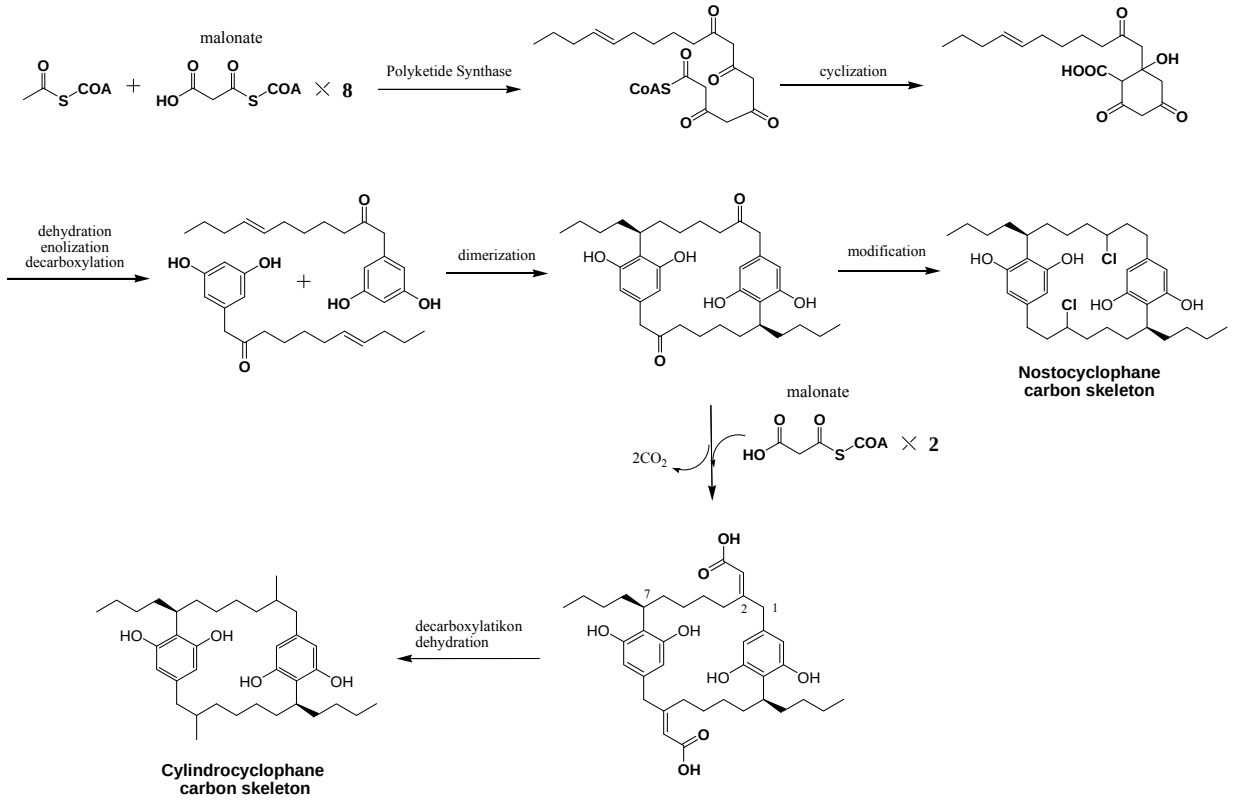

Figure 1.18 Proposed biosynthetic pathways for cyclindrocyclophane D by ^{13}C feeding experiments (adapted from Bobzin & Moore, 1993)

Isotope-feeding experiments for cylindrocyclophane D indicated the polyketide origin of these

molecules (Bobzin & Moore, 1993). The presence of a C_2 axis of symmetry in the cyanobacterial cyclophanes led to the hypothesis that the biosynthetic pathway of these molecules would involve the dimerization of two nonaketides (Figure 1.18). This cyclophane core structure was further diversified by methylation at C-2/15 (β-position) and chlorination at C-3/17 (α-position) to complete the cylindrocyclophane and nostocyclophane core structures. However, whether these modifications occur before or after dimerization is still not clearly understood. The nostocyclophanes were further modified by hydroxylation or methoxylation at C-1/14 and/or glycosylation on the phenolic hydroxyl groups. For the cylindrocyclophanes, structural analogues with various modifications at C-1/14 by hydroxylation, acetylation or carbamidation as well as chlorination at C-30/34 have been reported, creating further diversity of this compound family (Moore et al., 1992; Bui et al., 2007; Chlipala et al., 2010). These diverse cyanobacterial [7.7]paracyclophanes exhibited a broad spectrum of biological activities, including antibacterial, antifungal and cytotoxic activities.

Several structurally related cyclic lipodecapeptides, calophycin and puwainaphycins A-E, were reported by Moore's group in early 1990s from two cultured terrestrial cyanobacteria of the genera *Calothrix* and *Anabaena* (Moore et al., 1989; Gregson et al., 1992; Moon et al., 1992). These cyanobacterial cyclic lipodecapeptides shared common features represented by the presence of one lipophilic β-amino acid with a 2-hydroxy-3-amino-4-methyl functionality and the conserved amino acid sequence of Val-β-amino acid-Pro-*N*MeAsn. The structure diversity of these molecules derived from differences in β-amino acid chain lengths, β-amino acid modifications, and amino acid compositions of the variable region (Figure 1.19). The calophycin showed a broad-spectrum fungicidal activity, while puwainaphycins showed cardiotonic activity (Moore et al., 1989; Gregson et al., 1992; Moon et al., 1992).

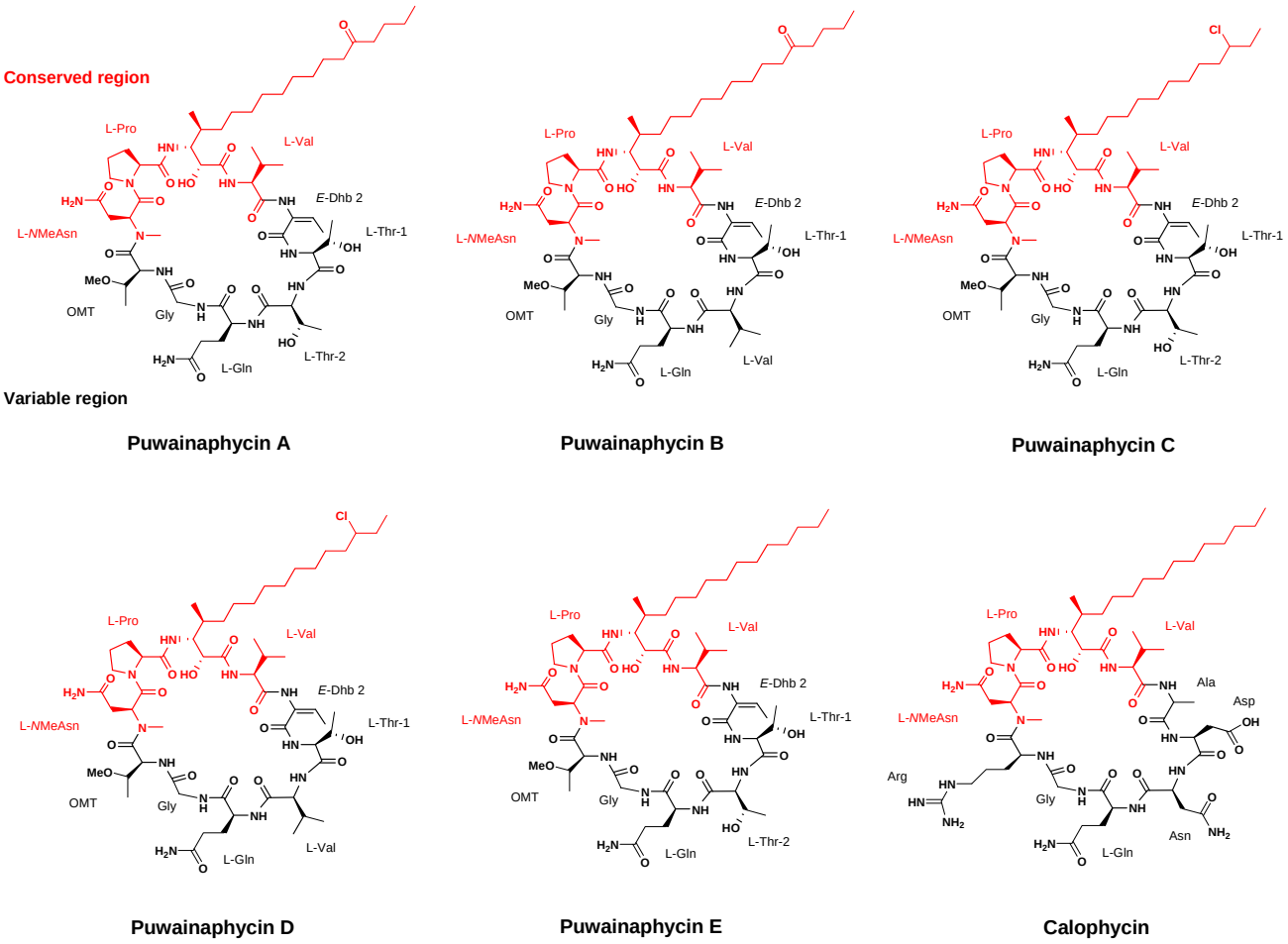

Figure 1.19 Structures of cyclic lipodecapeptides isolated from terrestrial *Anabaena* spp.by Moore's goup. (**Red**: conserved amino acids, **Black**: variable amino acids)

1.4 Rationalization and objective of the study

Cyanobacteria are one of the oldest organisms, and their existence dates back 3.5 billion years ago. This long evolutionary history, combined their important ecological roles, implies that their biosynthetic capabilities to produce biologically active secondary metabolites have evolved to create a large pool of active compounds with diverse structures. As shown above, in freshwater and terrestrial environments, cyanobacteria are present as diverse ecotypes, including microbial mats, blooms, symbionts and small colonies (non-bloom forming). Most of the studies on cyanobacterial secondary metabolites to date have been biased to bloom-forming cyanobacteria, mainly due to the environmental significances associated with the production of toxic substances. These studies however showed that freshwater and terrestrial cyanobacteria have a high capacity to produce biologically active secondary metabolites of diverse biosynthetic origins, comparable to that of their more studied marine counterparts.

The majorities of cyanobacteria in freshwater and terrestrial environments are non-bloom forming and appear as only small colonies even under favorable growth conditions. Previous studies on secondary metabolites, produced by this cyanobacterial ecotype, proved that their chemical structures occupy a distinct chemical space divergent from those of well-studied bloom-forming cyanobacteria, probably due to their distinct evolutionary paths. For example, the cyclophane scaffold is only found in terrestrial non-bloom forming cyanobacteria belonging to the order nostocales. Therefore, it can be rationalized that studying the chemistries of small-colony forming cyanobacteria, which are widespread all over the globe in freshwater and terrestrial environments, would provide not only new classes of molecules with new scaffolds, but also new structural analogs of known scaffolds that might result in improved biological activities.

Cyanobacteria are phototrophs and therefore use carbon dioxide as their major carbon source while most of other bacteria are chemotrophs that use glucose as a carbon source. Due to this reason, it could be rationalized that cyanobacteria do not need to compete with other bacteria to acquire nutrients necessarily for their growth in the environments. Instead, most of cyanobacteria appear as visible colo-

nies in the environments where cyanobacterial cells are held together by mucopolysaccharides produced as the result of photosynthesis. These polysaccharides-rich cyanobacterial colonies would be a good source of nutrients for small animals such as crustacean species. Based on this ecological assumption, it would be reasonable to conclude that cyanobacteria have evolved to produce diverse toxic compounds as a chemical defense mechanism, and cytotoxicity would comprise one of the major toxicity mechanisms as shown in above examples. Therefore, the scope of this study is to isolate cytotoxic compounds from relatively under-explored non-bloom forming cyanobacteria found in freshwater and terrestrial environments and to evaluate the potential of those compounds as anticancer drug leads.

To this end, we employed culture-dependent approach to explore chemistries of non-bloom forming cyanobacteria in freshwater and terrestrial environments. The culture collection has been established on the basis of strains isolated from field-collected samples (UIC strains) and strains acquired from established culture collections (UTEX, SAG and CCALA strains). Extracts were prepared from a 4L scale culture of each strain and evaluated for antiproliferative activity against cancer cells as well as brine shrimp toxicity. Active extracts were subjected to fractionation followed by dereplication using LC-MS and ^{1}H NMR in combination with HPLC-based activity profiling that associates LC chromatogram with activity. This dereplication method allowed us to classify active strains based on structural groups of active compounds. Based on the result, UTEX 1613, UIC 10035, UIC 10062 and SAG 74.79 were selected for chemical investigation. The following chapters describe the isolation and structure determination of biologically active compounds from these selected strains.

CHAPTER 2:

ANTIPROLIFERATIVE CYCLIC LIPODECAPEPTIDES FROM THE TWO CULTURED CYANOBACTERIA, *Anabaena minutis-sima* (UTEX 1613) and Cf. *Anabaena* sp. (UIC 10035)

2.1 Introduction

Cyclic lipopeptides represent a large subclass of non-ribosomal peptides that often contain non-standard amino acids such as Dhb (*α*, *β*-dehydro-*α*-aminobutyric acid), *β*-hydroxy amino acids, and *N*- and/or *O*-methylated amino acids (Sieber et al., 2005; Strieker et al., 2009). This subset of non-ribosomal peptides has shown a wide spectrum of biological activities, including antibacterial and antifungal as well as cytotoxic activities, and some of these are regarded as promising candidates for clinical evaluation (Baltz et al., 2005; Barrett, 2002). Mode of action studies of the phytotoxin syringomycin from *Pseudomonas syringae* and the antibiotic daptomycin from *Streptomyces roseosporus* revealed that the lipophilic residues played a key role for the biological activities of these molecules (Takemoto et al., 1991; Straus et al., 2006). The presence of lipophilic residues allows these molecules to penetrate into cell membranes and form transmembrane pores, leading to rapid depolarization of cells by the leakage of intracellular ions.

Cyanobacteria (blue-green algae) have been shown to be prolific producers of bioactive secondary metabolites (Tan, 2007; Wagoner et al., 2007; Harada, 2004), and are well-known producers of cyclic lipopeptides (Welker et al., 2006). Numerous cyclic lipopeptides have been isolated from both freshwater and marine cyanobacteria, with a ring size of up to 12 peptide residues. Cyclic deca- and undecapeptides, containing 10 and 11 residues, have been reported to exhibit a wide spectrum of biological activities, including antifungal (MacMillan et al., 2002; Frankmölle et al., 1992), cardiotonic (Moore et al., 1989; Gregson et al., 1992), and cytotoxic (Gerwick et al., 1992; Bonnard et al., 2007) activities. A common structural feature of cyclic deca- and undecapeptides is the occurrence of one lipophilic *β*-amino acid residue (Weler and Von Döhren, 2006). Most of the cyclic lipopeptides in this class also possess non-standard amino acids, such as *N*-methylated *α*-amino acids, *α*- and/or *β*-hydroxy amino acids, and Dhb (*α*, *β*-dehydro-*α*-aminobutyric acids). A recent study done by Hrouzek et al. revealed a possible mode of action of cyanobacterial lipopeptides for cytotoxic activity (Hrouzek et al., in press). An elevated concentration of intracellular Ca^{2+} and subsequent cell necrosis was observed after addition of the cyanobacterial cyclic lipodecapeptides, puwainaphycins F/G, indicating that these molecules interacted with cell mem-

brane, causing rapid membrane depolarization similar to other well-known pore-forming lipoeptides such as daptomycin and syringomycin.

In our continuing search for biologically active secondary metabolites from laboratory-cultured cyanobacteria, we evaluated the cell extracts of *Anabaena minutissima* (UTEX 1613) and Cf. *Anabaena* sp. (UIC 10035). In this chapter, we describe the isolation, structure determination and biological activity of twelve structurally related cyclic lipodecapeptides, named minutissamides A-D and homesteadamides A-H, possessing one/two Dhbs, one *N*-methylated Asn and one lipophilic *β*-amino acid residue with 2-hydroxy-3-amino-4-methyl moiety. The planar structures were determined by spectroscopic techniques including HRESIMS, tandem MS, and 1D and 2D NMR (COSY, TOCSY, HSQC, HMBC and ROESY) experiments. The absolute configurations of the *α*-amino acid residues were determined by Marfey's method, whereas the stereoconfiguration of the lipophilic *β*-amino acid residue was solved by a combination of the advanced Marfey's method, *J*-based configurational analysis and ROE correlations.

2.2 Minutissamides A-D, cyclic lipodecapeptides from the cultured cyanobacterium *Anabaena minutissima* (UTEX 1613)

2.2.1 Isolation of minutissamdes A-D (1 – 4)

Anabaena minutissima (UTEX 1613) was grown in Z media (Falch et al., 1995). The freeze-dried cells were extracted with a mixture of CH_2Cl_2 and MeOH (1:1), and dried in vacuo. The cell extract was subsequently fractionated by column chromatography using Diaion HP-20 resin and an increasing amount of iPrOH in water. LC-MS analysis of the fraction eluting at 40% iPrOH indicated the presence of potentially new peptides with molecular weights of 1118, 1152, 1188 and 1190. Subsequent Sephadex LH-20 column chromatography followed by reversed-phase HPLC yielded minutissamides A – D (**1** – **4**).

2.2.2 Structure determination of minutissamides A-D

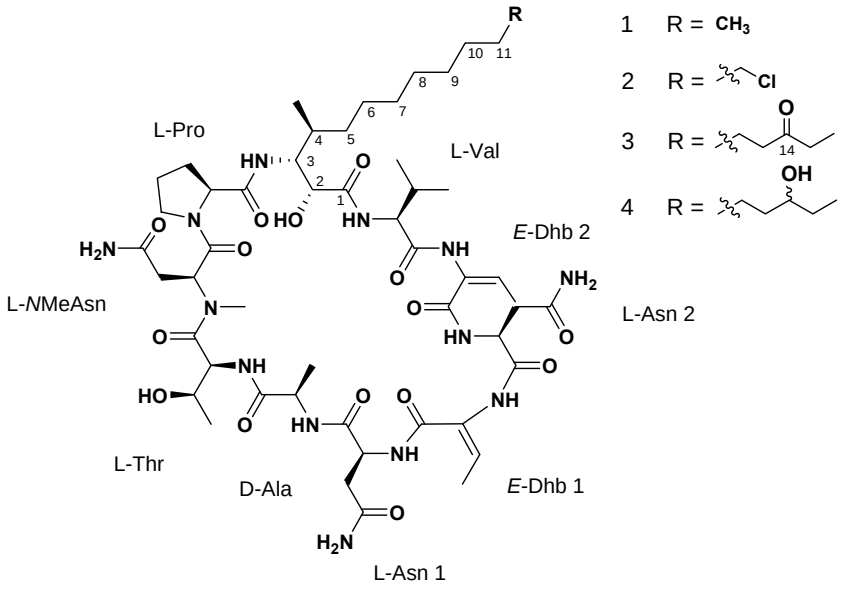

Minutissamide A (**1**) was obtained as a colorless amorphous powder. The molecular formula of **1** was determined as $C_{51}H_{83}N_{13}O_{15}$ by HRESIMS analysis (*m/z* 1140.6049 $[M+Na]^+$). The ^1H NMR spectrum in DMSO-d_6 showed a signal distribution typical for a lipopeptide, including several exchangeable amide NH signals (6.5 – 10.5 ppm), signals in α-proton region (4 – 6 ppm), methylene signals (1.2 – 1.3 ppm), and numerous aliphatic doublet and triplet methyl signals (0.5 – 2.0 ppm). The structures of the amino acid residues were elucidated by interpretation of the COSY and TOCSY spectra (Figure 2.1 and TABLE II), and indicated the presence of ten residues, including nine α-amino acid residues and one lipophilic β-amino acid residue. Six of the α-amino acid residues were identified as the common amino acids: proline (Pro), threonine (Thr), alanine (Ala), valine (Val) and two asparagines (Asn). In addition, the structures of three non-standard amino acid residues were determined by analysis of the COSY, HSQC and HMBC spectra (Figure 2.1). A HMBC correlation from the *N*-Methyl singlet (δ_H 2.96) to the C-2_{NMeAsn} (δ_C 49.4) in combination with a COSY correlation between *N*MeAsn H-2 (δ_H 5.53) and *N*MeAsn H_2-3 (δ_H 2.00 and 3.02) identified the structure of *N*-methyl asparagine (*N*MeAsn). The presence of two

Dhb residues was deduced from a COSY correlation observed between the methyl protons (H_3-4_{Dhb1}, δ_H 1.90 and H_3-4_{Dhb2}, δ_H 1.66) and the corresponding olefinic proton (H-3_{Dhb1}, δ_H 5.71 and H-3_{Dhb2}, δ_H 5.30), combined with a HMBC correlation from the methyl protons (H_3-4_{Dhb1} and H_3-4_{Dhb2}) to the corresponding olefinic carbon (C-$2_{Dhb1,}$ δ_C 130.1 and C-$2_{Dhb2,}$ δ_C 133.0). The 2-hydroxy-3-amino-4-methyl portion of Hamd (2-hydroxy-3-amino-4-methyldodecanoic acid) was identified by sequential COSY correlations between H-2 (δ_H 4.18)/H-3 (δ_H 3.93)/H-4 (δ_H 1.65), as well as the COSY correlations between H-3 (δ_H 3.93) and 3-NH (δ_H 6.85) and between H-4 (δ_H 1.65) and 4-Me (δ_H 0.58). Further COSY correlations from H-4 (δ_H 1.65) to H_2-5 (δ_H 1.17 and 1.61), H_2-5 to H_2-6 (δ_H 1.18 and 1.24), and H_2-6 to the region of highly overlapped methylene signals (H_2-7-11, δ_H 1.26-1.27), which corresponded with five carbons in the HSQC spectrum (δ_C 30.1, 29.2, 29.7, 31.8 and 22.6) and finally to the methyl triplet proton H_3-12 (δ_H 0.87), completed the structure of Hamd.

The sequence of the 10 residues was established by analysis of the ROESY and selective HMBC spectra (Figures 2.1 and 2.2, and TABLE II). The selective HMBC spectrum of the carbonyl region was used to resolve the largely overlapped amide carbonyl signals (Claridge et al., 2003). Starting from the Dhb_2 residue, ROE correlations between Dhb_2-NH (δ_H 9.17) and Val H-2 (δ_H 4.29), between Val-NH (δ_H 6.85) and Hamd H-2 (δ_H 4.18), and between Hamd-NH (δ_H 6.85) and Pro H-2 (δ_H 4.19) suggested a partial sequence of Dhb_2-Val-Hamd-Pro. HMBC correlations from Dhb_2-NH (δ_H 9.17) to Val C-1 (δ_C 169.2), from Val H-2 (δ_H 4.29) to Hamd C-1 (δ_C 170.1) and from Hamd H-3 (δ_H 3.93) to Pro C-1 (δ_C 171.9) confirmed this partial sequence. HMBC correlations from Pro H-2 (δ_H 4.19) to *N*MeAsn C-1 (δ_C 168.3) and from *N*MeAsn N-Me (δ_H 2.96) to Thr C-1 (δ_C 170.4), together with ROE correlations between Pro H_2-5 (δ_H 4.10) and *N*MeAsn H-2 (δ_H 5.53) and between *N*MeAsn N-Me (δ_H 2.96) and Thr H-2 (δ_H 4.63), further expanded the sequence to Dhb_2-Val-Hamd-Pro-*N*MeAsn-Thr. ROE correlations between Thr-NH (δ_H 7.30) and Ala H-2 (δ_H 4.29), and between Ala-NH (δ_H 8.27) and Asn_1 H-2 (δ_H 4.40), combined with HMBC correlations from Thr NH (δ_H 7.30) to Ala C-1 (δ_C 172.5) and from Ala NH (δ_H 8.27) to Asn1 C-1 (δ_C 171.2) established the sequence of Dhb_2-Val-Hamd-Pro-*N*MeAsn-Thr-Ala-Asn_1, leaving

two residues (Dhb_1 and Asn_2) unassigned. The complete sequence of Dhb_2-Val-Hamd-Pro-*N*MeAsn-Thr-Ala-Asn_1-Dhb_1-Asn_2 was deduced by a HMBC correlation from Asn_1-NH (δ_H 8.45) to Dhb_1 C-1 (δ_C 163.4) and a ROE correlation between Dhb_1-NH (δ_H 10.18) and Asn_2 H-2 (δ_H 4.92). Lastly, HMBC correlations from Asn_2 H-2 (δ_H 4.92) and NH (δ_H 8.73) to Dhb_2 C-1 (δ_C 163.6) closed the ring, completing the planar structure of minutissamide A (**1**).

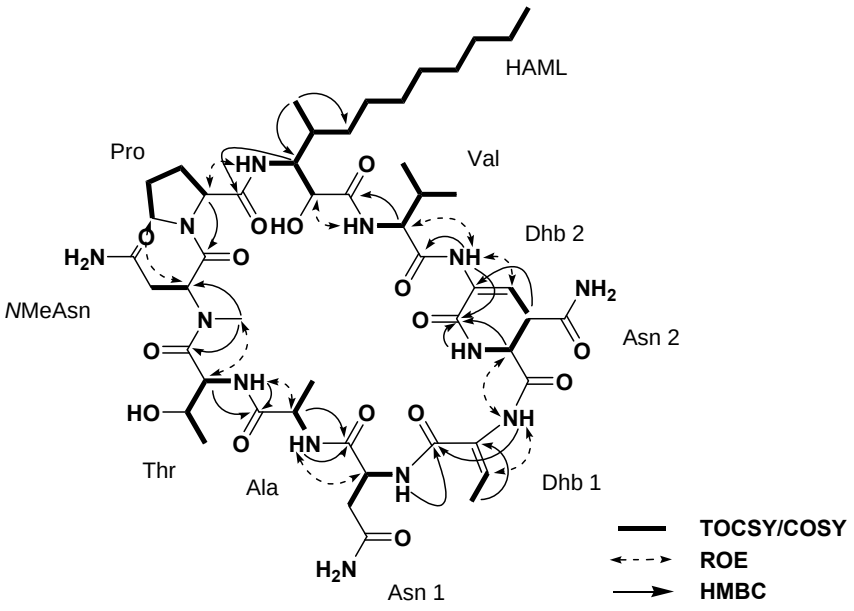

Figure 2.1 Key 2D correlations used for the determination of the planar structure of minutissamide A (**1**).

Mass fragmentation analysis was performed to further verify the 2D structure of minutissamide A (**1**) (Eckart et al., 1985). The ESI-MS/MS analysis of the CID fragmentation acquired using a quadrupole-time of flight (Q-TOF) tandem mass spectrometer supported the proposed planar structure of **1**. The parent peak was observed at *m/z* $[M+H]^+$ 1118.6. The ring opening occurred between Pro and *N*MeAsn, forming an acylium ion. The continuous fragmentation yielded the fragment ions at *m/z* 990.6 (B_8) $[M + H - N\text{MeAsn}]^+$, 889.5 ($B_7$) $[M + H - N\text{MeAsn} - Thr]^+$, 704.4 ($B_6$) $[M + H - N\text{MeAsn} - Thr - Ala - Asn_1]^+$, 621.4 ($B_5$) $[M + H - N\text{MeAsn} - Thr - Ala - Asn_1 - Dhb_1]^+$, 507.4 ($B_4$) $[M + H - N\text{MeAsn} - Thr - Ala - Asn_1 - Dhb_1 - Asn_2]^+$ and 396.3 (A_3) $[M + H - N\text{MeAsn} - Thr - Ala - Asn_1 - Dhb_1 - Asn_2 -$

$Dhb_2]^+$ (Figure 2.3). This fragmentation pattern was in complete agreement with the structure determined by 2D NMR analysis.

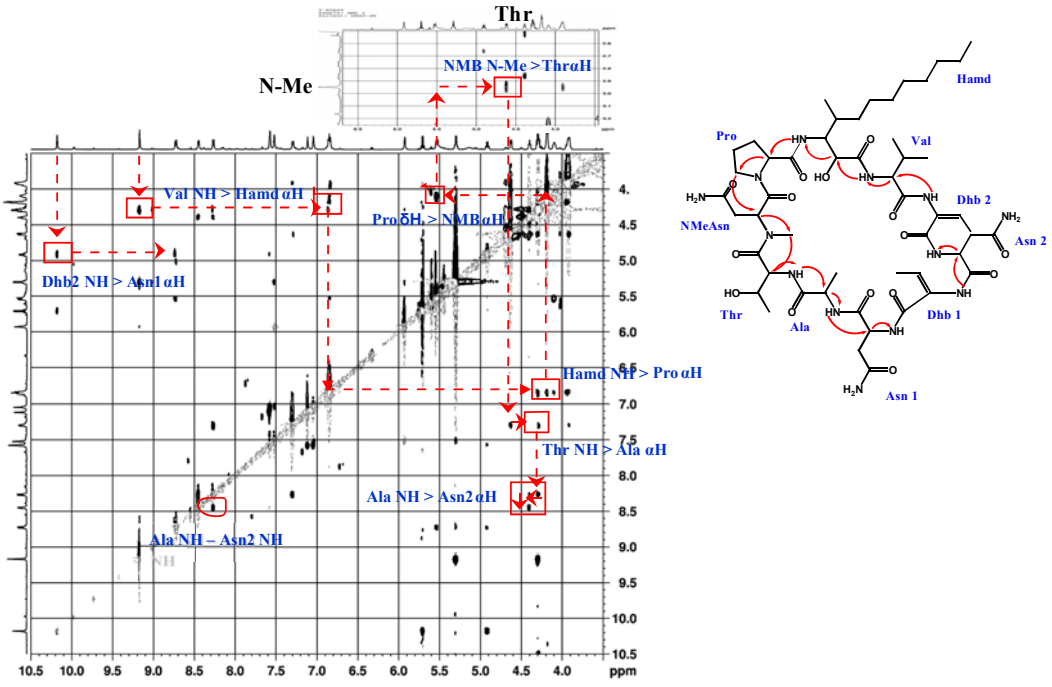

Figure 2.2 Sequential ROE correlations for the determination of amino acid sequence of minutissamide A (**1**) (600 MHz, DMSO-d_6): Mixing time was set to 200 ms.

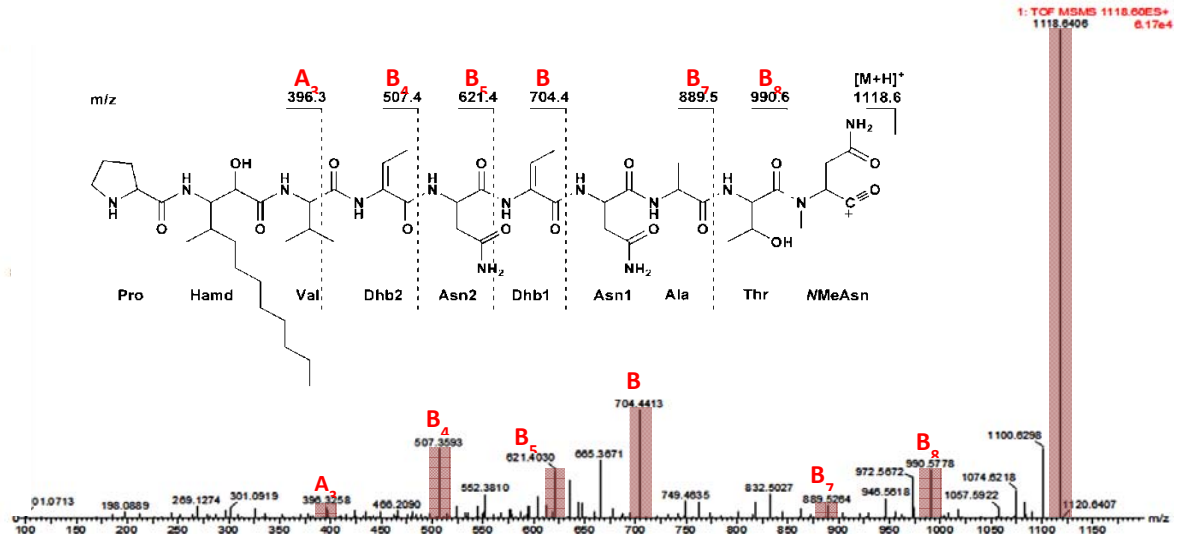

Figure 2.3 ESI-MS/MS data of minutissamide A (**1**) acquired using CID fragmentation method.

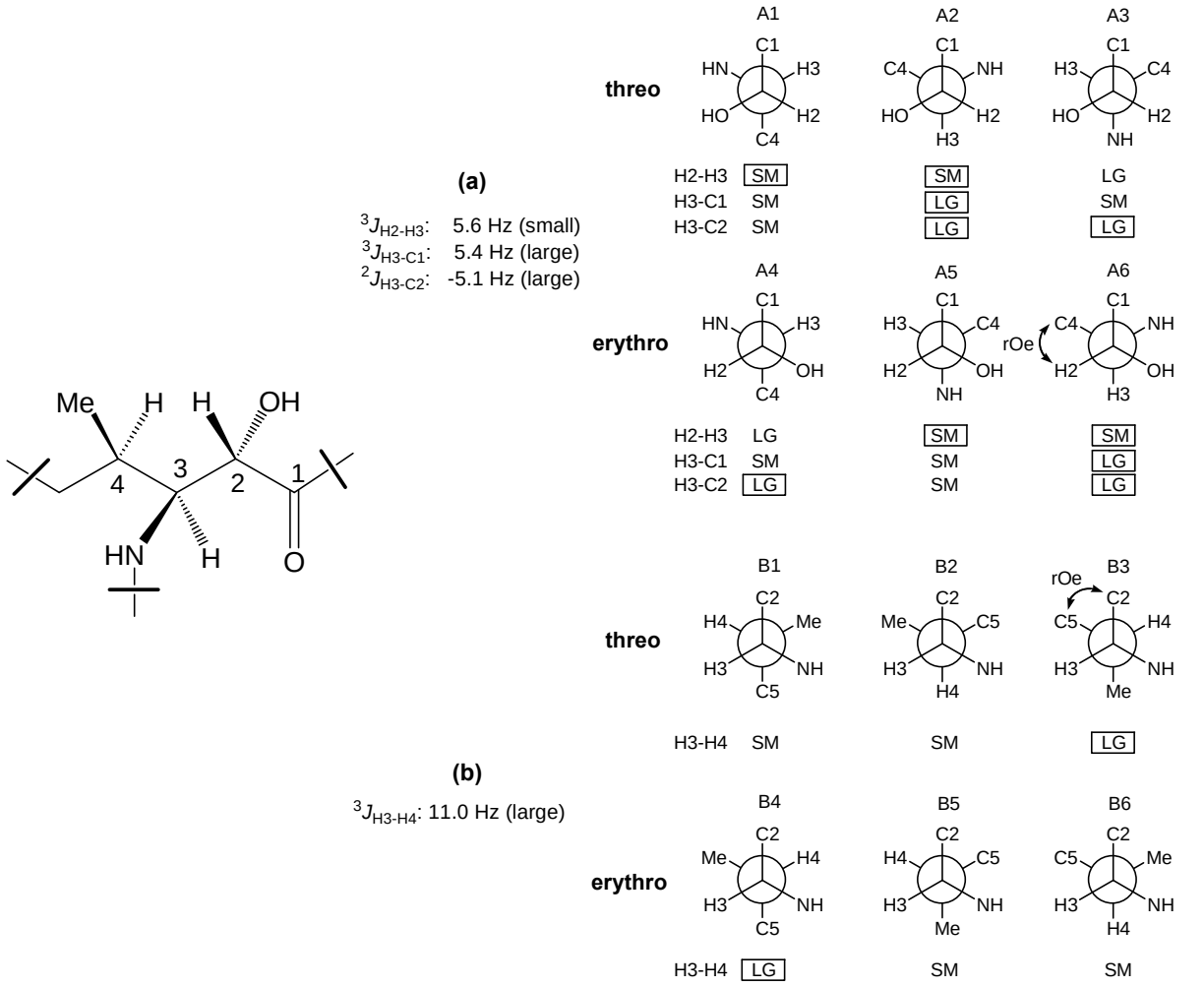

Figure 2.4 Newman projections for (a) C-2/C-3 and (b) C-3/C-4. All the possible relative conformations are shown. The DQF-COSY and phase-sensitive HMBC spectra were used for the calculation of homo- and hetero nuclear coupling constants. Labels below projections denote the predicted size of coupling constants. The predicted values that are consistent with observed values are highlighted by a box. Observed rOe correlations are presented as arched lines: (a) H-2/H-4 and (b) H-2/H_2-5.

Minutissamide A (**1**) contained three different types of stereogenic centers, the geometric configuration of Dhbs, the configurations of the α-amino acid residues and the configurations of the three consecutive chiral centers in the Hamd residue. A number of techniques were used for the assignment of stereoconfiguration of **1**, including Marfey's method and the advanced Marfey's method, *J*-based configurational analysis and ROE correlations. A strong ROESY cross-peak between the respective NH (δ_H 10.18

or δ_H 9.17) and the corresponding olefinic proton (H-3, δ_H 5.71 or δ_H 5.30) was observed for both Dhb_1 and Dhb_2, assigning the geometric configuration of both double bonds as *E* (Figure 2.1). The absolute configurations of the common amino acids and *N*MeAsn were assigned as L-Pro, L-Thr, L-Asn_1, L-Asn_2, L-Val, D-Ala and L-*N*MeAsn by chromatographic comparison of Marfey's derivatives between the acid hydrolysate of **1** and appropriate amino acid standards (Bhushan et al., 2004).

The *β*-amino acid residue Hamd of **1** contained three asymmetric centers, C-2, C-3 and C-4. Since these three asymmetric centers were consecutively located, the relative configuration was first determined by *J*-based configurational analysis, and the advanced Marfey's method was then used to determine the absolute configuration at C-3. The relative configuration of the Hamd residue was established by combination of *J*-based configurational analysis and ROE correlations as shown in Figure 2.4. Homonuclear ($^3J_{H\text{-}H}$) coupling constants were acquired from the DQF-COSY spectrum, and the phase-sensitive HMBC spectrum was used for the calculation of heteronuclear ($^2J_{CH}$ and $^3J_{CH}$) coupling constants (Ding, 2000). The small $^3J_{HH}$ (5.6 Hz) between H-2 and H-3, the large $^3J_{CH}$ (5.4 Hz) between H-3 and C-1, and the large $^2J_{CH}$ (-5.1 Hz) between H-3 and C-2 allowed for two possible conformations (A2 and A6) out of the six conformations shown in Figure 2.4a. The conformation A6 was found to be the correct conformation based on a ROE correlation observed between H-2 and H-4, assigning the relative configuration between C-2 and C-3 as *erythro*. The same method was applied for the assignment of the relative configuration between C-3 and C-4. On the basis of the large $^3J_{HH}$ (11.0 Hz) measured between H-3 and H-4, only two conformations (B3 and B4) were possible as shown in Figure 2.4b. A ROE correlation observed between H-2 and H_2-5 confirmed B3 as the correct confirmation assigning the relative configuration between C-3 and C-4 as *threo*. The nearly identical carbon chemical shifts of C-1, C-2, C-3 and C-4 (δ_C 170.1, 70.0, 56.6 and 32.6) of Hamd to those (δ_C 169.8, 69.9, 56.2 and 32.4) of HAMP in puwainaphycin E provided further evidence for these relative configurations (Gregson et al, 1992). Since the relative configurations of C2-C3 and C3-C4 were *erythro* and *threo*, respectively, the absolute configurations of the three chiral centers (C-2, C-3 and C-4) in the Hamd residue could be either *RRS* or *SSR*. Lastly, the

advanced Marfey's method was applied to assign the absolute configuration of the Hamd residue (Figure 2.5) (Fujii et al., 1997; Harada et al., 1996). The acid hydrolysate of **1** was derivatized with L- and DL-FDLA, respectively. These L- and D-FDLA derivatives of the HAML residue adopt well-defined 3D conformations due to hydrogen bonds formed between amino acid NHs and nitro groups of the benzene ring. Two hydrophobic side chains from the amino acid leucine and the *β*-amino acid Hamd could be arranged in *cis* or *trans* conformation, and *cis* conformation is considered to be more hydrophobic (Fujii et al., 1998). Therefore, chromatographic method can be used to compare hydrophobicity of L- and D-FDLA derivatives of the Hamd residue in **1**. LC-MS analysis of DL-FDLA derivatives identified two peaks (*m/z* 538 $[M-H]^-$) at 43.3 and 48.8 min that corresponded to the molecular weight of the FDLA derivatives of Hamd, while the L-FDLA derivative of Hamd gave one peak at 48.8 min, indicating that the L-FDLA derivative is more hydrophobic than the D-FDLA derivative. Thus, the absolute configuration of C-3 was assigned as R configuration. Previous application of this method for the determination of the absolute configuration of Ahda (amino-2-hydroxy decanoic acid) also showed that the R-L and S-D derivatives are more hydrophobic than the R-D and S-L derivatives (Fujii et al., 1998). As a result, the absolute configuration of the Hamd residue in **1** was assigned as 2*R*,3*R*,4*S*.

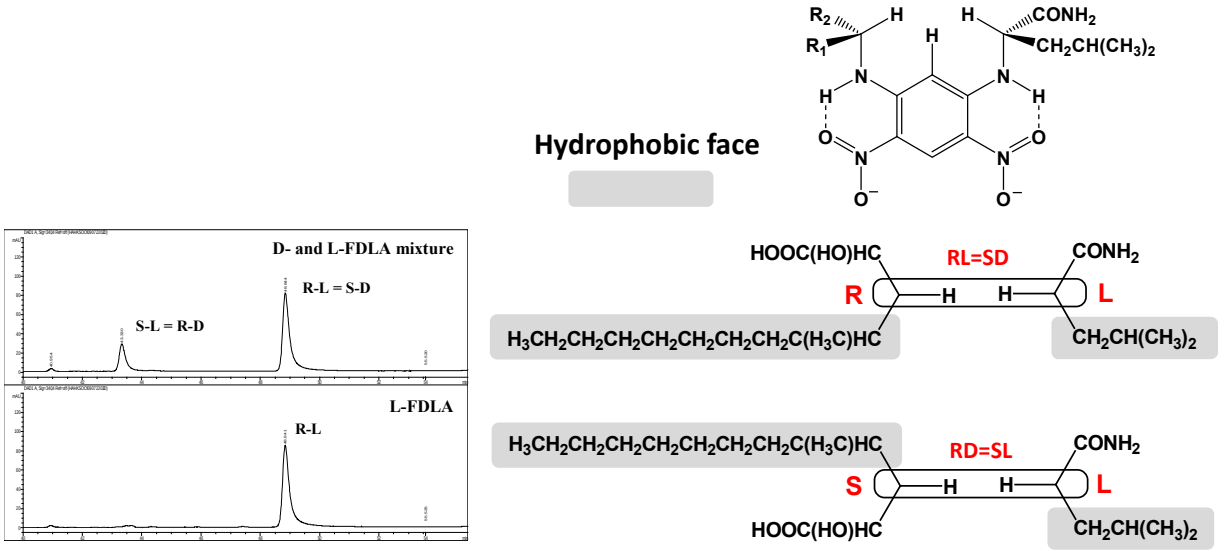

Figure 2.5 The advanced Marfey's method used to determine the absolute configuration of the *β*-amino acid residue at C-3.

Minutissamide B (**2**) was obtained as colorless, amorphous powder. The molecular formula of **2** was deduced as $C_{51}H_{82}ClN_{13}O_{15}$ on the basis of HRESIMS analysis (*m/z* 1174.5790 $[M+Na]^+$). The M+2 isotope peak found at 1176.6 verified the presence of chlorine in **2**. The ^1H and ^{13}C NMR spectra of **2** were almost identical to those of **1** except for in the Hamd residue, where the terminal methyl proton signal had been replaced by a new triplet methylene resonance at 3.62 ppm. This indicated that chlorine was positioned on the terminal methyl carbon of Hamd, thus re-naming it Hamcd (2-hydroxy-3-amino-4-methyl-12-chlorododecanoic acid). The sequential COSY correlation network of H_2-12/H_2-11/H_2-10 and the slightly down-fielded chemical shifts of H_2-11 (δ_H 1.70) and H_2-10 (δ_H 1.37) further supported the structure of **2**. The stereoconfiguration of **2** was determined by comparison of proton and carbon chemical shifts as well as optical rotation to those of **1**. The carbon chemical shifts of all the stereogenic centers in **2** were similar to those observed for **1** (deviation, < 0.2 ppm), suggesting the same relative configurations. The specific rotations of both **1** and **2** displayed positive values (**1**, $[\alpha]_D$ +4; **2**, $[\alpha]_D$ +5). On the basis of these data, we submit that the absolute configurations of all the stereogenic centers in **2** are the same as those found in **1**.

Minutissamide C (**3**) was obtained as colorless amorphous powder. The HRESIMS analysis (*m/z* 1210.6610 $[M+Na]^+$) suggested the molecular formula of **3** to be $C_{55}H_{89}N_{13}O_{16}$. Detailed comparison of ^1H and ^{13}C NMR spectra indicated that compounds **1** and **3** share the same cyclic decapeptide core structure. The only difference was the replacement of the dodecanoic acid residue found in **1** with an oxidized hexadecanoic acid residue in **3** (TABLE III). The ^1H NMR spectrum of **3** displayed three additional methylene protons, H_2-12 (δ_H 1.44), H_2-13 (δ_H 2.38) and H_2-15 (δ_H 2.40), as compared to **1**. In addition to the three methylene carbon signals (δ_C 23.6, δ_C 41.9 and δ_C 35.4), a signal characteristic of a ketone (δ_C 211.5) was also apparent in the ^{13}C NMR spectrum. The molecular weight difference of 70 between **1** and **3** corresponded to three methylenes and one ketone, indicating the presence of Hamoh (2-hydroxy-3-amino-4-methyl-14-oxohexadecanoic acid) in **3**. The location of ketone group at C-14 in Hamoh was determined by the proton chemical shifts of H_2-13 (δ_H 2.38) and H_2-15 (δ_H 2.40), and the TOCSY correla-

tion observed between H_2-15 (δ_H 2.40) and H_3-16 (δ_H 0.90). A three bond HMBC correlation from the terminal methyl protons (H_3-16, δ_H 0.90) to the ketone carbon (C-14, δ_C 211.5) further confirmed this location. The stereoconfiguration of **3** was assigned by comparison of spectroscopic data to those of **1**. No significant difference (deviation, < 0.1ppm) was found for ^{13}C chemical shifts of all the stereogenic centers in **3** when compared to **1**. Also, compound **3** displayed the positive specific rotation ($[\alpha]_D$ +3). Together, these data suggested the absolute configurations of the stereogenic centers in **3** to be identical to those of **1**.

Minutissamide D (**4**) was also obtained as colorless amorphous powder. The HRESIMS spectrum of **4** displayed a major ion peak at 1212.6740 $[M+Na]^+$, suggesting a molecular formula of $C_{55}H_{91}N_{13}O_{16}$. The ^1H and ^{13}C NMR spectra of **4** were almost identical to those of **3**, except that the ketone in Hamoh had been replaced by resonances for a carbinol moiety (δ_H 3.28 and δ_C 71.5). This, together with the molecular weight difference of 2 between **3** and **4**, suggested that the ketone in Hamoh of **3** had been reduced to a hydroxyl group in **4**, forming a Hamhh residue (2-hydroxy-3-amino-4-methyl-14-hydroxyhexadecaonic acid). The structure of Hamhh was further supported by analysis of the COSY and HMBC spectra. Sequential COSY correlations between H_3-16 (δ_H 0.83)/H_2-15 (δ_H 1.16 and 1.35)/H-14 (δ_H 3.28) and a HMBC correlation from H_3-16 (δ_H 0.83) to C-14 (δ_C 71.5) placed the hydroxyl group at C-14. The absolute configurations of the amino acid residues and the three chiral centers in the Hamhh residue appeared to be the same as those found for **1** by comparison of ^{13}C chemical shifts and optical rotation ($[\alpha]_D$ +2). Compound **4** possessed one more stereogenic hydroxyl-bearing carbinol carbon (C-14) in the Hamhh residue. Mosher ester analysis was attempted in an effort to assign the absolute configuration of this carbinol stereogenic center. However, the presence of three hydroxyl groups (one in Thr and two in Hamhh) resulted in a mixture of products and a very complex ^1H NMR spectrum of Mosher ester product of **4**. Hydrolysis of **4** followed by isolation of the Hamhh residue would be necessary for Mosher ester analysis, but was not attempted due to the limited amount of sample available. Thus, the absolute configuration of C-13 carbinol carbon in Hamhh could not be assigned conclusively.

The structure of minutissamides A – D (**1** – **4**) was characterized by the presence of a lipophilic *β*-amino acid residue, a 2-hydroxy-3-amino-4-methyl dodecanoic or hexadecanoic acid, and three nonstandard amino acids (*N*MeAsn and two Dhbs). The *β*-amino acid residue was further modified by chlorination in **2**, by oxidation to ketone in **3** or by hydroxylation in **4**. The structures of minutissamides A – D (**1** – **4**) revealed some similarities to the cyclic decapeptides, puwainaphycins A – E, isolated from a Hawaiian terrestrial *Anabaena* sp (Gregson et al., 1992). The sequence of five residues in the puwainaphycins, including Dhb, Val, *β*-amino acid unit, Pro and *N*MeAsn, was conserved in the minutissamides. The other five amino acid residues, OMT (O-methyl-Thr), Gly, Gln, Thr-2 (or Val-2) and Thr-1 found in the puwainaphycins, were replaced by Thr, Ala, Asn1, Dhb1 and Asn2 in the minutissamides. The core structure of the lipophilic *β*-amino acid residues, characterized by 2-hydroxy-3-amino-4-methyl substitution, and the modification pattern of this residue by chlorination and oxidation were also similar to those observed in the puwainaphycins.

TABLE II: NMR SPECTROSCOPIC DATA FOR MINUTISSAMIDES A AND B IN DMSO-d_6

		Minutissamide A (**1**)						Minutissamide B (**2**)		
		δ_C[a]	δ_H[b]	mult. (J in Hz)	**COSY**	**HMBC**	**ROESY**	δ_C[e]	δ_H[c]	mult. (J in Hz)
Hamd or Hamcd	1	170.1						170.0		
	2	70.0	4.18	d (4.8)	3	3		70.0	4.18	overlapped
	3	56.6	3.93	m	2, 4	1[e], 2, 1_{Pro}[e]		56.6	3.92	M
	4	32.6	1.65	m	3, 5, 4-Me			32.6	1.65	m
	5	33.8	1.17 1.61	m m	4, 6			33.7	1.17 1.61	m m
	6	25.9	1.18 1.24	m m	5, 6			25.9	1.16 1.23	m m
	7	30.1	1.26	m	6, 8			30.1	1.23	m
	8	29.2	1.26	m	7, 9			29.7	1.23	m
	9	29.7	1.26	m	8, 10			29.1	1.26	m
	10	31.8	1.26	m	10, 11			26.6	1.37	m
	11	22.6	1.27	m	11, 12			32.4	1.70	m
	12	14.5	0.87	t (7.2)	11	10, 11		45.8	3.62	t (6.6)
	2-OH		5.51	br s	2					nd[c]
	3-NH		6.85	partly over-lapped	3	1_{Pro}[e]	3, 2_{Pro}		6.88	partly over-lapped
	4-Me	16.3	0.58	d (6.6)	4	3, 4, 5	3	16.4	0.57	d (6.6)
Pro	1	171.9						171.9		
	2	60.5	4.19	m	3	3, 4, 1_{NMeAsn}		60.4	4.18	m
	3	30.7	1.91	m	2, 4	1		30.7	1.92	m
	4	24.2	1.85 1.92	m m	3, 5			24.2	1.83 1.92	m m
	5	47.3	3.26 4.10	m m	4	2	2_{NMeAsn}	47.3	3.25 4.09	m m
*N*MeAsn	1	168.3						168.3		
	2	49.4	5.53	dd (12.0, 3.0)	3	1[e], 3, 4[e]	5_{Pro}, 3, N-Me	49.3	5.53	brd (12.0)
	3	34.4	2.00 3.02	m dd (15.6, 12.0)	2, 4	1[e], 2[e], 4[e]		34.4	2.00 3.01	m m
	4	172.1						172.1		
	N-Me	30.7	2.96	s		2, 1_{Thr}[e]	2_{Thr}, 3_{Thr}	30.7	2.95	s
	NH_2		5.92 7.52	s s		3			6.03 7.52	m m
Thr	1	170.4						170.4		
	2	55.3	4.63	dd (8.4, 3.6)	2-NH, 3	1[e], 3, 1_{Ala}[e]	N-Me, 3, 4	55.3	4.62	m
	3	66.8	3.92	m	2, 4			66.8	3.92	m
	4	20.0	1.00	d (6.0)	3	2, 3		19.9	0.99	d (6.6)
	3-OH		5.13	br s						nd[d]
	NH		7.30	d (7.8)	2	1_{Ala}	2, 3		7.30	d (8.4)
Ala	1	172.5						172.5		
	2	48.9	4.29	q (7.2)	2-NH, 3	1[e], 1_{Asn1}[e]		48.7	4.28	m
	3	17.3	1.23	d (7.2)	2	1[e], 2		17.3	1.22	d (7.2)
	NH		8.27	d (8.4)	2	2, 1_{Asn1}	2, 2_{Asn1}, NH_{Thr}, NH_{Asn1}			
Asn1	1	171.2						171.2		
	2	50.5	4.40	m	2-NH, 3	3	3	50.3	4.39	m
	3	36.2	2.56 2.87	m dd (18.6, 7.2)	2	1[e], 2, 4[e]		36.2	2.53 2.88	m dd (16.8, 7.2)
	4	173.2						173.2		
	NH		8.45	d (7.2)	2	1_{Dhb1}	2		8.45	d (7.2)
	NH_2		7.04 7.58	s s		3			7.04 7.59	s s
Dhb1	1	163.4						163.4		
	2	130.1						130.1		
	3	125.6	5.71	q (7.2)	4	1, 2, 4	NH	125.6	5.71	q (7.2)
	4	13.7	1.90	d (7.2)	3	2, 3		13.6	1.89	d (7.2)
	NH		10.18	s		1, 1_{Asn2}[e]	3, 2_{Asn2}		10.20	s

Asn2	1	172.4						172.4		
	2	49.4	4.92	q (7.2)	2-NH, 3	1[e], 3, 1_{Dhb2}[e]	3	49.4	4.91	q (7.8)
	3	39.1	2.67 2.77	dd (15.0, 7.2) dd (15.0, 7.8)	2	1[e], 2, 4[e]		39.2	2.67 2.77	dd (15.0, 7.2) dd (15.0, 7.8)
	4	172.6						172.7		
	NH		8.73	d (7.8)	2	1_{Dhb2}			8.74	d (7.8)
	NH_2		7.11 7.58	s s		3			7.12 7.59	s s
Dhb2	1	163.6						163.6		
	2	133.0						133.0		
	3	116.5	5.30	q (7.2)	4	1, 2, 4	NH	116.4	5.29	q (7.2)
	4	13.5	1.66	d (7.2)	3	2, 3		13.3	1.65	d (7.2)
	NH		9.17	s		1[e], 3, 1_{Val}[e]	3, 2_{Val}		9.21	s
Val	1	169.2						169.2		
	2	56.2	4.29	d (10.8)	2-NH, 3	1[e], 1_{HAML}[e]		56.2	4.28	m
	3	33.1	1.75	m	2, 4	1[e]		33.1	1.74	m
	4	19.4	0.83	d (6.6)	3	2, 3, 4’		19.3	0.82	d (6.6)
	4’	19.1	0.90	d (6.6)	3	2, 3, 4		19.0	0.89	d (6.6)
	NH		6.85	partly over-lapped	2		2_{HAML}		6.88	partly over-lapped

[a] carbon chemical shifts were assigned from DEPT-Q spectrum measured at 226 MHz, [b] measured at 600 MHz, [c] nd: not detected, [d] assigned from the selective HMBC spectrum, [e] assigned from the HSQC and HMBC spectra.

TABLE III: ^{1}H AND ^{13}C NMR DATA FOR MINUTISSAMIDES C AND D IN DMSO-d_6

		Minutissamide C (**3**)			Minutissamide D (**4**)		
		δ_C[a]	δ_H[b]	mult. (*J* in Hz)	δ_C[a]	δ_H[b]	mult. (*J* in Hz)
	1	170.0			170.1		
	2	70.0	4.17	d (4.8)	70.0	4.18	d (4.2)
Hamoh	3	56.5	3.92	m	56.6	3.92	m
or	4	32.6	1.65	m	32.6	1.65	m
Hamhh	5	33.8	1.17 1.62	m m	33.9	1.17 1.61	m m
	6	25.9	1.16 1.23	m m	25.9	1.16 1.23	m m
	7	30.1	1.23	m	30.1	1.25	m
	8	29.1	1.23	m	29.1	1.25	m
	9	29.7	1.23	m	29.7	1.25	m
	10	29.4	1.23	m	29.4	1.25	m
	11	29.4	1.23	m	29.4	1.25	m
	12	23.6	1.44	q (7.2)	25.8	1.16 1.35	m m
	13	41.9	2.38	t (7.2)	35.4	1.26 1.32	m m
	14	211.5			71.5	3.28	m
	15	35.4	2.40	q (7.8)	30.1	1.16 1.35	m m
	16	8.2	0.90	t (7.8)	10.6	0.83	t (7.2)
	2-OH			nd[c]			nd[c]
	3-NH		6.84	partly overlapped		6.87	partly overlapped
	4-CH_3	16.4	0.57	d (6.6)	16.5	0.57	d (6.6)
Pro	1	171.9			172.0		
	2	60.6	4.18	m	60.6	4.18	m
	3	30.8	1.92	m	30.8	1.92	m
	4	24.2	1.84 1.91	m m	24.3	1.83 1.91	m m
	5	47.3	3.26 4.10	m m	47.3	3.25 4.09	m m
*N*MeAsn	1	168.2			168.3		
	2	49.4	5.52	dd (12.0, 3.0)	49.1	5.53	dd (12.0, 3.0)

	3	34.4	2.00 3.01	m dd (16.2, 12.6)	34.4	1.99 3.01	m dd (15.6, 12.6)
	4	172.1			172.1		
	N-Me	30.8	2.95	s	30.8	2.95	s
	NH_2		5.95 7.52	s s		6.01 7.52	s s
Thr	1	170.4			170.4		
	2	55.3	4.62	dd (9.0, 3.6)	55.3	4.62	dd (8.4, 3.6)
	3	66.8	3.93	m	66.8	3.91	m
	4	20.0	0.99	d (6.0)	20.0	0.98	d (7.8)
	3-OH			nd[d]			nd[d]
	NH		7.29	d (9.0)		7.30	d (7.8)
Ala	1	172.6			172.6		
	2	48.9	4.28	m	49.0	4.28	m
	3	17.3	1.22	d (7.2)	17.4	1.22	d (7.2)
	NH		8.26	d (8.4)		8.26	d (8.4)
Asn1	1	171.2			171.2		
	2	50.5	4.39	td (7.2, 3.0)	50.5	4.39	td (7.2, 3.0)
	3	36.2	2.53 2.87	m dd (16.8, 7.2)	36.2	2.52 2.87	m dd (16.8, 7.2)
	4	173.2			173.2		
	NH		8.45	d (7.2)		8.44	d (7.2)
	NH_2		7.04 7.58	s s		7.04 7.59	s s
Dhb1	1	163.4			163.4		
	2	130.1			130.1		
	3	125.6	5.70	q (7.2)	125.8	5.70	q (7.8)
	4	13.7	1.89	d (7.2)	13.7	1.89	d (7.8)
	NH		10.18	s		10.19	s
Asn2	1	172.4			172.4		
	2	49.4	4.90	q (7.2)	49.5	4.91	q (7.2)
	3	39.0	2.66 2.76	dd (15.0, 7.2) dd (15.0, 7.8)	39.2	2.67 2.76	dd (15.0, 7.2) dd (15.0, 7.8)
	4	172.6			172.7		
	NH		8.73	d (7.8)		8.73	d (7.8)
	NH_2		7.12 7.59	s s		7.12 7.59	s s
Dhb2	1	163.6			163.7		
	2	133.0			133.0		
	3	116.4	5.29	q (7.2)	116.5	5.29	q (7.2)
	4	13.5	1.65	d (7.2)	13.5	1.64	d (7.2)
	NH		9.18	s		9.19	s
Val	1	169.2			169.3		
	2	56.2	4.28	m	56.3	4.28	m
	3	33.1	1.74	m	33.1	1.74	m
	4	19.4	0.82	d (6.6)	19.4	0.82	d (6.6)
	4’	19.1	0.89	d (6.6)	19.1	0.89	d (6.6)
	NH		6.84	partly overlapped		6.86	partly overlapped

[a]carbon chemical shifts were assigned from DEPT-Q spectrum measured at 226 MHz, [b] measured at 600 MHz, [c] nd: not detected

2.3 Homesteadamides A-H, cyclic lipodecapeptides from the cultured cyanobacterium Cf. *Anabaena* sp. (UIC 10035)

2.3.1 Isolation of homesteadamides A – H (5 – 12)

Cf. *Anabaena* sp. UIC 10035 was isolated from the sample collected in the town of Homestead, South Florida, 2007. The isolated strain was maintained and cultured in inorganic Z medium (Falch et al., 1995). For chemical investigation, the freeze-dried cells (7.5 g) were extracted with the mixture of CH_2Cl_2 and MeOH (1:1), and dried in vacuo. The resulting extract (0.5 g) was fractionated using Diaion HP-20 resin with an increasing amount of iPrOH in H_2O. Fractions eluting at 40 and 60 % aqueous iPrOH exhibited antiproliferative activity against MD-MB-435 cells (95 % and 100 % at 25 μg/ml, respectively). LC-MS analysis of these fractions indicated the presence of a series of nitrogen-containing compounds with molecular weights ranging between 1150 and 1250 Da. These fractions were combined and subjected to HPLC purification using reversed-phase columns to yield eight cyclic lipodecapeptides, named homesteadamides A – H (**5** – **12**).

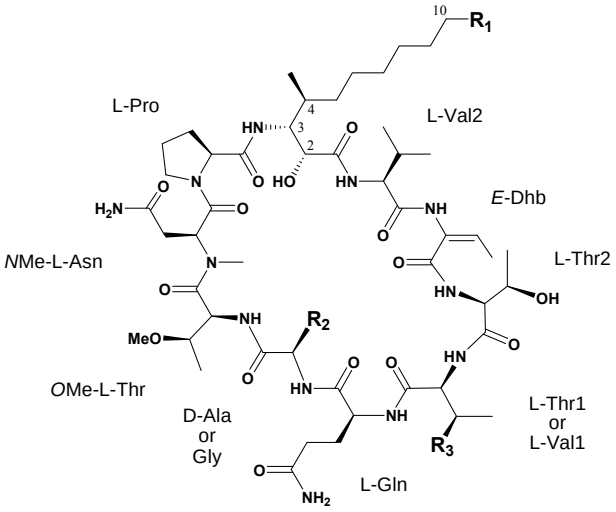

	R_1		R_2		R_3	
5		Hamoo	CH_3	D-Ala	OH	L-Thr1
6		Hamct	CH_3	D-Ala	OH	L-Thr1
7		Hamho	CH_3	D-Ala	OH	L-Thr1
8		Hamoo	CH_3	D-Ala	CH_3	L-Val1
9		Hamoo	H	Gly	OH	L-Thr1
10		Hamct	H	Gly	OH	L-Thr1
11		Hamho	H	Gly	OH	L-Thr1
12		Hamoo	H	Gly	CH_3	L-Val1

2.3.2. Structure determination of homesteadamides A-H

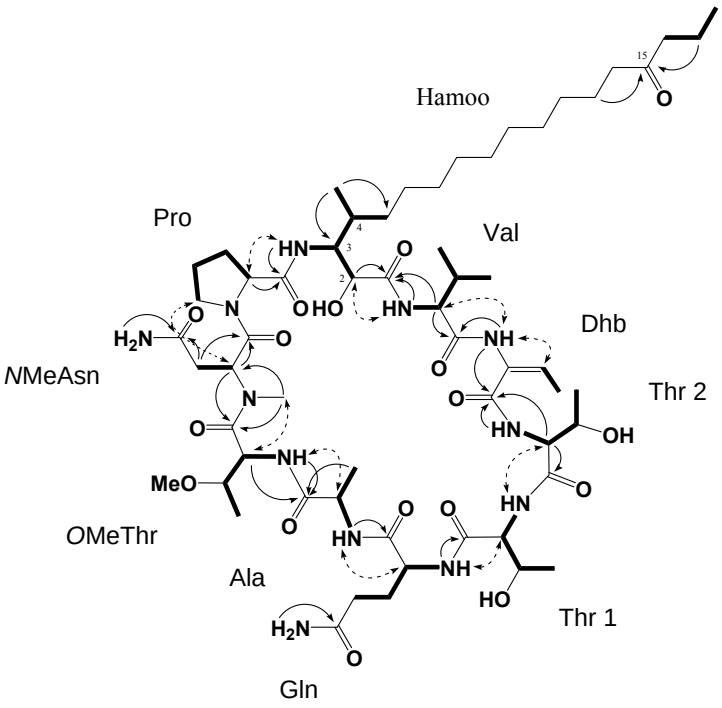

Figure 2.6 Key 2D correlations used for the determination of the planar structure of homesteadamide A (**5**).

Homesteadamide A (**5**) was obtained as a colorless, amorphous powder. The molecular formula of **5** was determined as $C_{59}H_{101}N_{12}O_{17}$ by HRESIMS analysis. The signal distribution pattern observed in the ^{1}H NMR spectrum (DMSO-d_6) suggested this compound to be a lipopeptide by the presence of largely overlapped aliphatic methylene proton signals (δ_H 1.25) along with amide NH (δ_H 6.0 – 10.0), amino acid αH (δ_H 3.5 – 5.5) and aliphatic doublet methyl (δ_H 0.5 – 2.0) proton signals. Analysis of the COSY and TOCSY spectra identified ten amino acids including six standard amino acids (Pro, Ala, Gln, two Thrs and Val). The structures of three non-standard amino acids (*N*MeAsn, *O*MeThr and Dhb) were determined by 2D NMR analysis including COSY, HSQC and HMBC. The structure of the β-amino acid residue was determined as Hamoo (2-hydroxy-3-amino-4-methyl-15-oxooctadecanoic acid) by analysis of 2D NMR data (Figure 2.6). COSY correlations between NH (δ_H 6.77) and H-3 (δ_H 3.92), and between a doublet methyl (δ_H 0.57) and H-4 (δ_H 1.68), as well as sequential COSY correlations from H-2 (δ_H 4.17) to H_2-5 (δ_H 1.17 and 1.62), which in turn further coupled with the overlapped methylene signals (δ_H 1.25),

indicated the presence of the 2-hydroxy-3-amino-4-methyl moiety in the *β*-amino acid residue. The isolated TOCSY correlation fragment of H_2-16/H_2-17/H_3-18 and HMBC correlations from H_2-13 (δ_H 1.44) and H_2-17 (δ_H 1.47) to a ketone carbon (δ_C 210.6) indicated that the ketone was positioned at C-15, determining the structure of the Hamoo residue.

The ten amino acid residues were connected by analysis of the HMBC and ROESY spectra (Figure 2.6). Starting from the Hamoo residue, HMBC correlations from Hamoo NH to Pro C-1 (δ_C 171.2) and from *N*-Me (δ_H 2.93) to *N*MeAsn C-2 (δ_C 49.7) and *O*MeThr C-1 (δ_C 169.6), along with ROE correlations between Hamoo NH (δ_H 6.77) and Pro H-2 (δ_H 4.25), between Pro H_2-5 (δ_H 3.11 and 4.21) and *N*MeAsn H-2 (δ_H 5.52), established a partial sequence of Hamoo-Pro-*N*MeAsn-*O*MeThr. This partial sequence was further expanded into Hamoo-Pro-*N*MeAsn-*O*MeThr-Ala-Gln-Thr_1 by HMBC correlations from *O*MeThr NH (δ_H 6.74) to Ala C-1 (δ_C 171.9), from Ala NH (δ_H 7.58) to Gln C-1 (δ_C 171.1) and from Gln NH (δ_H 7.25) to Thr_1 C-1 (δ_C 170.4), as well as ROE correlations between *O*MeThr NH (δ_H 6.74) and Ala H-2 (δ_H 4.19), between Ala NH (δ_H 7.58) and Gln H-2 (δ_H 4.08), and between Gln NH (δ_H 7.25) and Thr_1 H-2 (δ_H 3.90). The complete sequence of Hamoo-Pro-*N*MeAsn-*O*MeThr-Ala-Gln-Thr_1-Thr_2-Dhb-Val was determined by HMBC correlations from Thr_2 NH (δ_H 8.37) to Dhb C-1 (δ_H 163.9) and from Dhb NH to Val C-1 (δ_C 168.8), together with ROE correlations between Thr_1 NH (δ_H 8.84) and Thr_2 H-2 (δ_H 5.02), and between Dhb NH (δ_H 9.08) and Val H-2 (δ_H 4.31). Lastly, HMBC correlations from Val NH (δ_H 6.85) and Val H-2 (δ_H 4.31) to Hamoo C-1 (δ_C 169.6), and a ROE correlation observed between Val NH and Hamoo H-2 indicated homesteadamide A (**5**) to be a cyclic peptide, completing the planar structure of **5**.

To confirm the amino acid sequence of **5**, fragmentation analysis was carried out using quadrupole ion trap CID MS/MS data (Figure 2.7). In the MS^1 analysis, the most intense peak corresponded to the sodium adduct ion of **5** (*m/z* 1271.7 $[M+Na]^+$). CID fragmentation of this sodiated precursor ion generated a set of y-type fragment ions instead of b-type, which are commonly observed in CID fragmentation of protonated precursor ions. This predominant formation of y-type fragments by CID of sodiated

precursor ions has been previously reported (Sabareesh and Balaram, 2006). The two most intense ions at *m/z* 1227.7 and 1183.7 corresponded to $[M+Na-CONH_2]^+$ and $[M+Na-2CONH_2]^+$, and resulted from the sequential loss of the side chain amides from *N*MeAsn and Gln. Ring-opening at two different sites yielded two sets of y-type fragment ions. Ring-opening between Dhb and Thr yielded ions at *m/z* 755.5, 870.5, 941.6 and 1069.6, corresponding to y_5, y_6, y_7 and y_8 fragments, respectively (Figure 2.7A). The second set of fragment ions, resulted from ring-opening between *N*MeAsn and Pro, included m/z 465.2, 667.3, 750.3, 849.4 and 1174.7, corresponding to y_4, y_6, y_7, y_8 and y_9 (Figure 2.7B). This fragmentation pattern agreed well with the sequence determined by 2D NMR analysis, thus further supporting the planar structure of **5**.

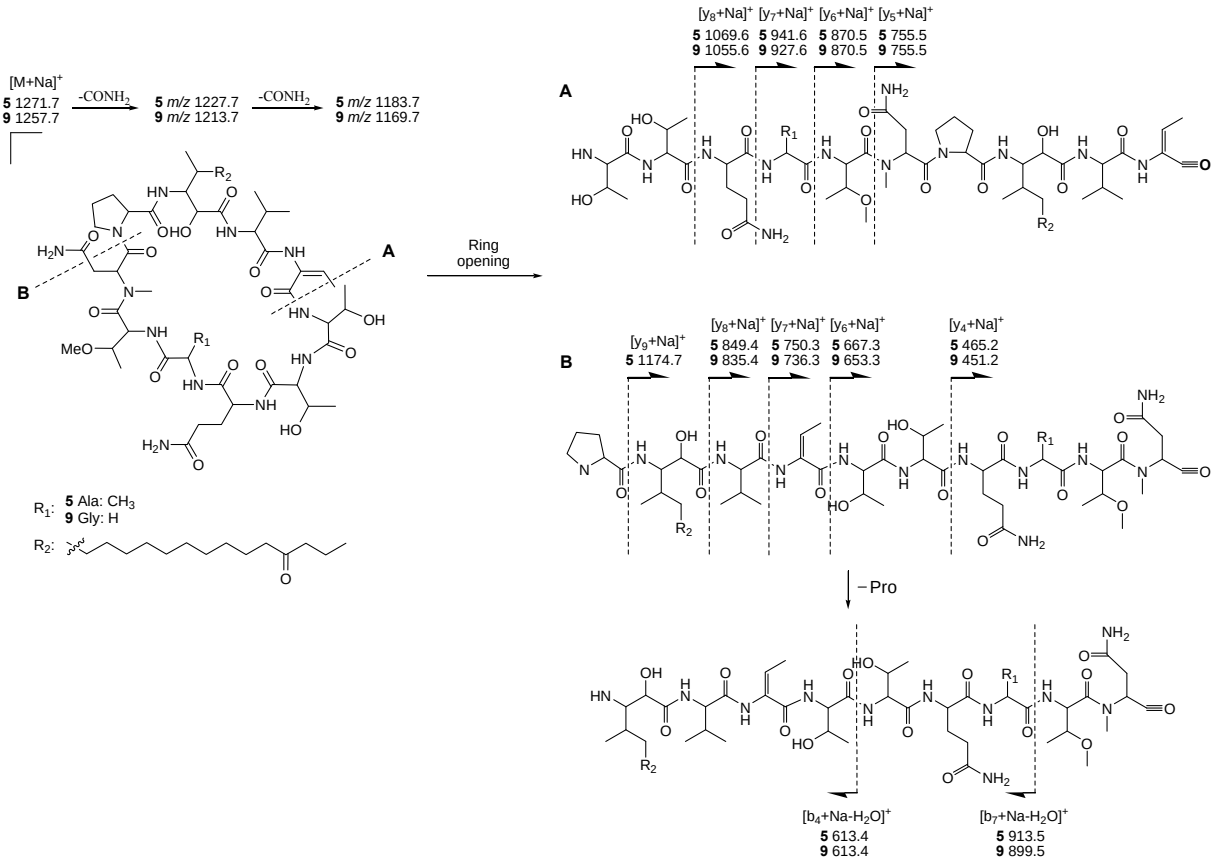

Figure 2.7 ESI-MS/MS fragmentation of homesteadamides A (**5**) and E (**9**).

The stereoconfiguration of **5**, including the geometric configuration of Dhb and the absolute configurations of α- and β-amino acids, was determined on the basis of ROE correlations and the advanced Marfey's method as well as comparison of ^{1}H and ^{13}C NMR chemical shifts. A strong ROE correlation observed between Dhb NH and Dhb H-3 assigned the *E* configuration to the Dhb residue. For the assignment of amino acid configurations, advance Marfey's analysis was carried out as previously described (Fujii et al., 1997, 1998; Harada et al., 1996). LC-MS comparison between L-FDLA and DL-FDLA derivatives of the acid hydrolysate of **5** assigned L-configuration to Pro, Gln, and Val, and D-configuration to Ala. The L-FDLA derivative of the acid hydrolysate of **5** was further compared with those of authentic standards of Thr (L-Thr, D-Thr, L-*allo*-Thr and D-*allo*-Thr), *N*MeAsn (*N*Me-L-Asn and *N*Me-D-Asn) and *O*MeThr (*O*Me-L-Thr, *O*Me-DlThr, *O*Me-L-*allo*-Thr, *O*Me-D-*allo*-Thr), assigning L configuration to these amino acids. Homesteadamide A (**5**) shares the same asymmetric centers, 2-hydroxy-3-amino-4-methyl, in the β-amino acid residue as the puwainaphycins and minutissamides (Gregson et al., 1992). These three consecutive asymmetric centers in Hamoo showed nearly identical ^{1}H (< 0.1 ppm) and ^{13}C (< 1 ppm) NMR chemical shifts to those of the puwainaphycins and minutissamides, suggesting the same relative configuration. In LC-MS analysis, the DL-FDLA derivative of the acid hydrolysate of **5** exhibited two peaks at 67.0 and 72.2 min, corresponding to the molecular weight of the FDLA derivative of Hamoo (*m/z* 638.3 $[M+H]^{+}$), while the L-FDLA derivative resulted in one peak at 72.2 min. This result was consistent with those reported for the β-amino acids Ahda (3-amino-2-hydroxydecanoic acid) in microginin (Fujii et al., 1998) and Hamd (2-hydroxy-3-amino-4-methyldodecanoic acid) in minutissamide A, suggesting the same absolute configuration (*R* at C-3) in Hamoo. Taken together, the absolute configuration of the three consecutive asymmetric carbons (C-2, C-3 and C-4) in Hamoo was assigned as *RRS*, completing the stereoconfiguration of **5**.

Homesteadamide B (**6**) was obtained as a colorless, amorphous powder. The molecular formula was determined as $C_{55}H_{93}ClN_{12}O_{16}$ based on HRESIMS, which exhibited the molecular ion peak at *m/z* 1213.6645 ($[M+H]^{+}$) and M+2 isotope peak. Comparison of the 1D and 2D NMR spectra of **6** and **5** re-

vealed that compound **6** shared the same amino acid sequence with **5** and differed only in the *β*-amino acid residue. The four carbon differences in the molecular formula suggested that the *β*-amino acid residue of **6** was composed of 14 carbons (tetradecanoic acid) instead of 18 carbons. The down-fielded proton signal of H-12 (δ_H 3.99), as well as sequential COSY correlations from the terminal methyl H_3-14 (δ_H 0.96) to this down-fielded proton H-12 via one diastereotopic methylene H_2-13 (δ_H 1.64 and 1.78), positioned the chlorine at C-12, establishing Hamct (2-hydroxy-3-amino-4-methyl-12-chlorotetradecanoic acid) as the the *β*-amino acid residue. An HMBC correlation from the terminal methyl H_3-14 to the chlorinated C-12 (δ_C 66.4) further confirmed the structure of Hamct. Compound **6** showed nearly identical ^1H and ^{13}C NMR chemical shifts to those of **5** at all of the stereogenic centers and the negative specific rotation ($[\alpha]_D$ -19) similar to that of **5** ($[\alpha]_D$ -29), thus indicated the stereoconfiguration of **6** to be the same as that of **5**. The absolute configuration for the additional chlorine-bearing stereocenter (C-12), located distant from other stereocenters in Hamct, could not be assigned.

Homesteadamide C (**7**) was also obtained as a colorless, amorphous powder. The HRESIMS spectrum of **7** displayed a molecular ion at m/z 1251.7564 ($[M+H]^+$), suggesting the molecular formula as $C_{59}H_{102}N_{12}O_{17}$, which is two mass units higher than that of **5**. The ^1H NMR spectrum of **7** also closely resembled that of **5** except for the *β*-amino acid residue. The notable difference was the up-fielded chemical shifts of H_2-14 (δ_H 1.26 and 1.30) and H_2-16 (δ_H 1.28) as compared to those of **5**, both of which were connected by the oxygenated methine proton H-15 (δ_H 3.35) in the COSY spectrum, indicating the presence of Hamho (2-hydroxy-3-amino-4-methyl-15-hydrxyoctadecanoic acid) in **7**. The stereoconfiguration of **7** was suggested to be the same as that of **5** based on the nearly identical NMR chemical shifts, except for the terminal region of Hamho combined with the negative specific rotation ($[\alpha]_D$ -22), which was similar to that of **5** ($[\alpha]_D$ -29). The assignment of the absolute configuration for the additional hydroxyl-bearing carbinol carbon (C-15) in Hamho was not attempted due to the limited amount of sample available.

Homesteadamide D (**8**) was obtained as a colorless, amorphous powder. The molecular formula of **8** was deduced as $C_{60}H_{102}N_{12}O_{16}$ on the basis of HRESIMS analysis (m/z 1247.7622 $[M+H]^+$). The detailed analysis of the COSY and TOCSY spectra of **8** revealed that it was similar to that of **5**, but differed by one amino acid in the cyclic peptide core. In the TOCSY spectra, a new spin system, corresponding to the amino acid Val, had replaced the spin system of Thr1, indicating the presence of Val1 instead of Thr1. The absolute configuration of this Val residue was determined by advanced Marfey's analysis in the same way as described for **5**. LC-MS comparison between the L- and DL-FDLA derivatives of the acid hydrolysate of **8** assigned the L-configuration to Val. The result of advanced Marfey's analysis, together with comparison of ^1H and ^{13}C NMR chemical shifts between **8** and **5**, also suggested that the absolute configurations of all of the other amino acids found in **8** are the same as those found for **5**.

Homesteadamide E (**9**), a colorless, amorphous powder, displayed a molecular ion peak at m/z 1235.7328 ($[M+H]^+$) in HRESIMS analysis, indicating a molecular formula of $C_{58}H_{99}N_{12}O_{17}$. The molecular weight of **9** was smaller than that of **5** by 14 mass units and identical to that of the previously reported cyclic lipodecapeptide, puwainaphycin A (Gregson et al., 1992). Detailed analysis of the 2D NMR spectra revealed that the structure of **9** differed from that of **5** by the presence of Gly instead of Ala, thus sharing the same cyclicpeptide core as puwainaphycin A. The only difference found between **9** and puwainaphycin A was the position of a ketone in the β-amino acid residue. An isolated spin system, composed of the three proton signals H_3-18 (δ_H 0.83), H_2-17 (δ_H 1.46) and H_2-16 (δ_H 2.36), was found in the TOCSY spectrum. This, together with HMBC correlations from H_3-18 and H_2-17 to C-15, indicated a ketone to be positioned at C-15 in **9** instead of at C-16 as found for puwainaphycin A. The amino acid sequence of **9** was further confirmed by analysis of tandem MS data, which showed a nearly identical fragmentation pattern to that of **5** (Figure 2.7). Lastly, advanced Marfey's analysis of the acid hydrolysate of **9**, as well as ^1H and ^{13}C NMR data, suggested that the absolute configurations of all of the amino acids to be the same as those reported for puwainaphycin A.

Homesteadamide F (**10**) was also obtained as a colorless, amorphous powder. The HRESIMS spectrum of **10** displayed a molecular ion peak at m/z 1199.6477 ($[M+H]^+$) as well as a M+2 isotope peak, indicating the presence of a chlorine, thus the molecular formula of **10** was deduced as $C_{54}H_{91}ClN_{12}O_{16}$. Analysis of 1D and 2D NMR data of **10** revealed that the structure of **10** is similar to that of **9** except for the *β*-amino acid residue. Considering the 36 Da mass difference between **10** and **9** and the presence of a chlorine, the *β*-amino acid residue of **10** was suggested to be Hamct, the same as found in **6**. The chlorine was placed at C-12 by an HMBC correlation from the terminal methyl protons H_3-14 (δ_H 0.96) to the chlorinated carbon C-12 (δ_C 66.4). The stereoconfiguration of **10** was considered to be the same as that found for **9** based on the nearly identical ^1H and ^{13}C NMR chemical shifts at all of the stereogenic centers and the negative specific rotation ($[\alpha]_D$ -19) similar to that of **9** ($[\alpha]_D$ -26). The absolute configuration of the additional chlorine-bearing stereocenter (C-12) in Hamct of **10** could not be assigned.

The last two compounds, homesteadamides G (**11**) and H (**12**), were not separable in reversed-phase HPLC, thus obtained as a mixture in a ratio of 3:5 as determined by ^1H NMR analysis. The HRESIMS spectrum of the mixture showed the two molecular ion peaks at and m/z 1237.7381 (**11**, $[M+H]^+$) and m/z 1233.7482 (**12**, $[M+H]^+$), suggesting the molecular formulas as $C_{58}H_{100}N_{12}O_{17}$ and $C_{59}H_{100}N_{12}O_{16}$, respectively. Attempts to separate **11** and **12** using reversed-phase HPLC failed due to complete overlap of the two peaks, thus structure determination was carried out using the mixture. The majority of signals in the ^1H NMR spectrum appeared to be identical between **11** and **12**, except for one amino acid and the *β*-amino acid residue. In the TOCSY spectrum, two doubled NH (δ_H 9.03 and δ_H 8.67) and *α*-H (δ_H 3.80 and δ_H 3.82) signals, the sum of which showed the same integration as other signals, indicating them to belong to different spin systems (Thr1 and Val1). In addition, COSY and HMBC analysis identified the presence of two *β*-amino acids, Hamho and Hamoo. The molecular weight and the integration ratio suggested the presence of Thr1 and Hamho in **11**, and Val1 and Hamoo in **12**. Advanced Marfey's analysis of the acid hydrolysate of the mixture assigned the L-configuration to all of the amino acids present in **11** and **12**. Nearly identical ^1H and ^{13}C NMR data of stereogenic centers (C2, C3 and C4)

in the *β*-amino acid residue to those of other compounds (**5** – **10**) as well as the minutissamides and puwainaphycins suggested the absolute configuration of the *β*-amino acid residue for both **11** and **12** to be *RRS*. The determination of the absolute configuration at C-15 in Hamho was not attempted in this study due to the limited amount of sample.

Cf. *Anabaena* sp. UIC 10035 produced a range of cyclic lipodecapeptides in a laboratory culture that are structurally related to the previously reported cyclic lipodecapeptides, puwainaphycins A – E isolated from *Anabaena* sp. BQ-16-1 (Gregson et al, 1992). The homesteadamides showed higher structural diversity than the puwainaphycins and minutissamides. This high structural diversity of cylic lipodecapeptides produced by the strain UIC 10035 could be attributed to its biosynthetic flexibility to incorporate two different amino acids (Ala/Gly and Thr1/Val1) by adenylation domains in two NRPS modules, and two different fatty acids by an acyl ligase in a PKS module followed by variable modifications including oxidation, chlorination and hydroxylation. Thus, homesteadamides A – H (**5** – **12**) produced by the strain UIC 10035 represents a good example of nature's strategy to diversify their products using substrate promiscuity.

TABLE IV: ^{1}H AND ^{13}C NMR DATA FOR HOMESTEADAMIDES A-D IN DMSO-d_6

		homesteadamide A (**5**)			homesteadamide B (**6**)			homesteadamide C (**7**)			homesteadamide D (**8**)		
		δ_C[a]	δ_H[b]	mult. (*J* in Hz)	δ_C[a]	δ_H[b]	mult. (*J* in Hz)	δ_C[d]	δ_H[c]	mult. (*J* in Hz)	δ_C[d]	δ_H[c]	mult. (*J* in Hz)
	1	169.6			169.6			169.6			169.5		
	2	69.6	4.17	d (4.8)	69.6	4.17	d (4.8)	69.6	4.17	d (4.8)	69.6	4.16	d (4.8)
Hamoo,	3	56.0	3.92	td (10.8, 4.8)	55.9	3.94	td (10.8, 4.8)	56.0	3.94	td (10.8, 4.8)	56.0	3.94	td (10.8, 4.8)
Hamct	4	32.2	1.68	m	32.2	1.68	m	32.2	1.68	m	32.2	1.68	m
or	5	33.4	1.17	m	33.4	1.17	m	33.4	1.17	m	33.4	1.17	m
Hamho			1.62	m		1.62	m		1.61	m		1.62	m
	6	25.5	1.17	m	25.5	1.17	m	25.5	1.17	m	25.5	1.17	m
			1.25	m		1.26	m		1.25	m		1.25	m
	7	29.7	1.25	m	29.7	1.25	m	29.7	1.25	m	29.7	1.25	m
	8	29.3	1.25	m	29.1	1.25	m	29.3	1.25	m	29.3	1.25	m
	9	29.1	1.25	m	28.6	1.25	m	29.1	1.25	m	29.1	1.25	m
	10	29.0	1.25	m	26.1	1.36	m	29.0	1.25	m	29.0	1.25	m
						1.46	m						
	11	28.9	1.25	m	37.5	1.63	m	28.9	1.25	m	28.9	1.25	m
						1.73	m						
	12	28.6	1.25	m	66.4	3.99	m	28.6	1.25	m	28.6	1.25	m
	13	23.3	1.44	m	30.9	1.64	m	30.8	1.25	m	23.3	1.44	m
						1.78	m						
	14	41.9	2.37	t (7.2)	10.8	0.96	t (7.2)	37.7	1.26	m	41.9	2.37	t (7.2)
									1.30	m			
	15	210.6						69.2	3.35	m	210.6		
	16	43.8	2.36	t (7.2)				39.9	1.28	m	43.8	2.36	t (7.2)
	17	16.7	1.47	s (7.2)				18.9	1.26	m	16.7	1.47	s (7.2)
									1.38	m			
	18	13.6	0.83	t (7.2)				14.5	0.86	t (7.2)	13.6	0.83	t (7.2)
	3-NH		6.77	d (10.8)		6.77	d (10.8)		6.78	d (10.2)		6.76	d (10.7)
	4-Me	16.0	0.57	d (6.6)	16.0	0.58	d (6.6)	16.0	0.58	d (6.6)	16.0	0.57	d (6.6)
Pro	1	171.2			171.2			171.2			171.2		
	2	59.9	4.25	dd (8.4, 2.4)	56.0	4.25	dd (8.4, 2.4)	56.0	4.26	dd (7.8, 2.4)	59.8	4.26	dd (7.8)
	3	30.1	1.94	m	30.1	1.94	m	30.1	1.94	m	30.1	1.94	m
			1.99	m		1.99	m		1.99	m		1.99	m
	4	23.4	1.71	m	23.4	1.71	m	23.4	1.71	m	23.3	1.70	m
			1.84	m		1.84	m		1.84	m		1.85	m
	5	46.7	3.11	m	46.7	3.10	m	46.7	3.11	m	46.7	3.10	m
			4.21	m		4.20	m		4.21	m		4.21	m
*N*MeAsn	1	167.4			167.5			167.4			167.4		
	2	49.7	5.52	dd (11.4, 3.6)	49.7	5.52	dd (12.0, 3.0)	49.7	5.53	dd (12.0, 3.0)	49.7	5.52	dd (11.4, 3.6)
			1.97	overlapped		1.97	overlapped		1.97	overlapped		1.97	overlapped
	3	33.7	3.00	dd (15.6, 12.0)	33.7	3.00	dd (15.6, 12.0)	33.7	3.00	dd (5.6. 12.0)	33.7	2.99	dd (16.0, 11.9)
	4	171.5			171.5			171.5			171.5		
	N-Me	30.5	2.93	s	30.5	2.93	s	30.5	2.93	s	30.5	2.92	s
	NH_2		5.99	s		6.00	s		6.01	s		6.02	s
			7.49	s		7.49	s		7.50	s		7.49	s
*O*MeThr	1	169.6			169.6			169.6			169.5		
	2	52.6	4.79	dd (9.0, 1.8)	52.6	4.79	dd (9.6, 2.4)	52.6	4.80	dd (9.6, 1.8)	52.6	4.80	dd (9.2, 1.4)
	3	75.1	3.71	qd (6.0, 1.8)	75.1	3.71	qd (6.0, 2.4)	75.1	3.72	qd (6.0, 1.8)	75.0	3.72	qd (6.0, 1.4)
	4	14.7	0.95	d (6.0)	14.7	0.95	d (6.0)	14.7	0.96	d (6.0)	14.6	0.95	d (6.0)
	O-Me	55.6	3.13	s	55.6	3.13	s	55.6	3.14	s	55.6	3.13	s
	NH		6.74	d (9.0)		6.74	d (9.6)		6.75	d (9.6)		6.78	overlapped
Ala	1	171.9			171.9			171.9			171.8		
	2	49.1	4.19	p (7.8)	49.1	4.19	p (7.8)	49.1	4.20	p (7.8)	49.1	4.20	p (7.8)
	3	16.3	1.29	d (7.8)	16.3	1.29	d (7.8)	16.3	1.29	d (7.8)	16.3	1.29	d (7.8)
	NH		7.58	d (7.8)		7.58	d (7.8)		7.59	d (7.8)		7.64	d (7.8)
Gln	1	171.1			171.1			171.1			170.6		
	2	52.9	4.08	m	52.9	4.08	m	52.9	4.08	m	53.2	4.07	m
	3	26.5	1.78	m	26.5	1.77	m	26.5	1.78	m	26.1	1.81	m
			2.03	m		2.03	m		2.03	m		2.02	m

	4	31.8	2.15	m	31.8	2.14	m	31.8	2.15	m	31.7	2.15 2.19	m m
	5	173.9			173.9			173.9			173.6		
	NH		7.25	d (9.0)		7.24			7.26	d (7.8)		7.41	d (8.0)
	NH_2		6.80	s		6.79	s		6.80	s		6.77	s
			7.27	s		7.27	s		7.28	s		7.34	s
Thr1	1	170.4			170.5			170.4			NA[d]		
or	2	61.3	3.90	m	61.3	3.90	dd (4.2, 3.0)	61.3	3.91	m	60.5	3.91	t (3.9)
Val1	3	65.2	4.17	overlapped	65.2	4.18	overlapped	65.2	4.17	overlapped	28.8	2.20	m
	4	20.6	1.25	overlapped	20.6	1.25	d (6.0)	20.6	1.25	overlapped	17.6	0.98	d (6.8)
	4’										19.0	1.03	d (6.8)
	NH		8.84	brs		8.96	brs		8.83	brs		8.54	brs
Thr2	1	174.2			174.2			174.2			174.4		
	2	56.6	5.02	dd (10.2, 2.4)	56.6	5.02	dd (9.6, 2.4)	56.6	5.03	brd (11.4)	56.6	4.99	dd (9.7, 1.9)
	3	70.3	4.57	brm	70.3	4.58	brm	70.3	4.58	brm	70.2	4.55	brm
	4	19.0	1.25	overlapped	19.0	1.25	d (6.0)	19.0	1.25	overlapped	19.1	1.25	overlapped
	NH		8.37	d (10.2)		8.37	d (9.6)		8.38	d (10.2)		8.42	d (9.7)
Dhb	1	163.9			163.9			163.9			163.9		
	2	132.4			132.4			132.4			132.4		
	3	117.3	5.38	q (7.2)	117.4	5.38	q (7.8)	117.4	5.39	q (7.2)	117.3	5.39	q (7.2)
	4	13.2	1.75	d (7.2)	13.2	1.75	d (7.8)	13.2	1.75	d (7.2)	13.2	1.74	d (7.2)
	NH		9.08	s		9.08	s		9.09	s		9.10	s
Val2	1	168.8			168.8			168.8			168.6		
	2	55.5	4.31	dd (9.0, 6.0)	55.5	4.31	dd (9.0, 6.6)	55.5	4.32	dd (9.0, 6.6)	55.5	4.32	dd (9.0, 6.3)
	3	32.7	1.81	m	32.7	1.81	m	32.7	1.81	m	32.5	1.81	m
	4	18.4	0.83	d (6.0)	18.4	0.83	d (6.6)	18.4	0.83	d (6.6)	18.3	0.82	d (6.8)
	4’	19.0	0.89	d (6.0)	19.0	0.89	d (6.6)	19.0	0.89	d (6.6)	19.0	0.87	d (6.8)
	NH		6.85	d (9.0)		6.85	d (9.0)		6.86	d (9.6)		6.87	d (9.2)

[a] assigned from the DEPT-Q spectrum recorded at 226 MHz, [b] measured at 600 MHz, [c] assigned from the HSQC and HMBC spectra. [d] NA: not assigned due to the signal missing

TABLE V: ^{1}H AND ^{13}C NMR DATA FOR HOMESTEADAMIDES E-H IN DMSO-d_6

		homesteadamide E (**9**)			homesteadamide F (**10**)			mixture homesteadamide G (**11**)			mixture homesteadamide H (**12**)		
		δ_C[a]	δ_H[b]	mult. (*J* in Hz)	δ_C[c]	δ_H[b]	mult. (*J* in Hz)	δ_C[c]	δ_H[b]	mult. (*J* in Hz)	δ_C[c]	δ_H[b]	mult. (*J* in Hz)
	1	169.8			169.9			169.8			169.8		
	2	69.6	4.16	d (5.1)	69.7	4.16	d (5.1)	69.5	4.16	d (4.7)	69.5	4.16	d (4.7)
Hamoo,	3	56.2	3.93	td (10.6, 5.1)	56.0	3.93	td (10.3, 5.1)	56.2	3.92	brt (10.6)	56.2	3.92	brt (10.6)
Hamct	4	32.3	1.70	m	32.3	1.69	m	32.3	1.68	m	32.3	1.68	m
or	5	33.5	1.17	m	33.4	1.17	m	33.5	1.16	m	33.5	1.16	m
Hamho			1.60	m		1.61	m		1.61	m		1.61	m
	6	25.6	1.17	m	25.5	1.16	m	25.6	1.16	m	25.6	1.16	m
			1.25	m		1.25	m		1.23	m		1.23	m
	7	29.8	1.25	m	29.7	1.25	m	29.7	1.25	m	29.7	1.25	m
	8	29.3	1.25	m	29.1	1.25	m	29.3	1.25	m	29.3	1.25	m
	9	29.1	1.25	m	28.6	1.25	m	29.1	1.25	m	29.1	1.25	m
	10	29.1	1.25	m	26.1	1.35	m	29.0	1.25	m	29.0	1.25	m
						1.45	m						
	11	29.0	1.25	m	37.5	1.63	m	28.9	1.25	m	28.9	1.25	m
						1.72	m						
	12	28.7	1.25	m	66.4	3.98	m	28.6	1.25	m	28.6	1.25	m
	13	23.4	1.44	m	30.8	1.63	m	30.8	1.25	m	23.3	1.43	m
						1.78	m						
	14	42.0	2.37	t (7.2)	10.7	0.96	t (7.2)	37.3	1.26	m	42.2	2.37	t (7.2)
									1.30	m			
	15	210.9						69.2	3.35	m	211.0		
	16	43.8	2.36	t (7.2)				39.7	1.26	m	43.7	2.36	t (7.2)
	17	16.8	1.46	s (7.2)				18.9	1.26	m	16.7	1.45	s (7.2)
									1.38	m			
	18	13.7	0.83	t (7.2)				14.2	0.84	overlapped	13.7	0.82	t (7.2)
	3-NH		6.83	d (10.3)		6.83	d (10.5)		6.86	overlapped		6.86	overlapped
	4-Me	16.1	0.57	d (6.7)	16.1	0.57	d (6.7)	16.1	0.56	d (6.7)	16.1	0.56	d (6.7)

Pro	1	171.3			171.3			171.3			171.3		
	2	59.9	4.26	dd (8.0, 1.8)	60.0	4.26	dd (8.0, 1.8)	60.0	4.26	dd (8.0, 1.8)	60.0	4.26	dd (8.0, 1.8)
	3	30.2	1.92 1.99	m m	30.1	1.92 1.98	m m	30.2	1.92 1.99	m m	30.2	1.92 1.99	m m
	4	23.4	1.69 1.84	m m	23.4	1.68 1.83	m m	23.4	1.68 1.83	m m	23.4	1.68 1.83	m m
	5	47.0	3.15 4.18	m m	47.0	3.15 4.18	m m	47.0	3.16 4.18	m m	47.0	3.16 4.18	m m
*N*MeAsn	1	167.7			167.8			167.7			167.7		
	2	49.6	5.56 1.96	dd (11.5, 2.7) overlapped	49.7	5.56 1.96	dd (11.5, 2.7) overlapped	49.7	5.55 1.95	dd (11.5, 2.7) overlapped	49.7	5.55 1.95	dd (11.5, 2.7) overlapped
	3	34.0	3.02	dd (15.5, 11.5)	34.0	3.02	dd (15.5, 11.5)	33.9	3.01	dd (15.5, 11.5)	33.9	3.01	dd (15.5, 11.5)
	4	171.7			171.7			171.7			171.7		
	N-Me	30.4	2.94	s	30.4	2.94	s	30.6	2.93	brs	30.6	2.93	brs
	NH_2		5.99 7.52	s s		5.98 7.52	s s		6.11 7.53	s s		6.11 7.53	s s
*O*MeThr	1	169.8			169.9			169.9			169.9		
	2	53.2	4.71	dd (9.2, 2.7)	53.2	4.71	dd (9.2, 3.2)	53.1	4.71	brd (9.2)	53.1	4.72	brd (9.2)
	3	74.9	3.72	qd (6.3, 2.7)	74.9	3.72	qd (6.3, 3.2)	75.0	3.72	qd (6.6, 2.4)	75.0	3.72	qd (6.6, 2.4)
	4	15.2	0.99	d (6.3)	15.2	0.99	d (6.3)	15.2	0.98	d (6.6)	15.2	0.98	d (6.6)
	O-Me	55.9	3.16	s	55.9	3.16	s	55.8	3.15	s	55.8	3.15	s
	NH		6.80	overlapped		6.80	overlapped		6.80	overlapped		6.80	overlapped
Gly	1	169.0			169.0			169.1			169.1		
	2 2’	42.6	3.21 3.98	dd (17.1, 5.1) dd (17.1, 7.4)	42.5	3.21 3.98	dd (17.1, 5.1) dd (17.1, 7.4)	42.6	3.20 3.97	dd (17.1, 5.1) dd (17.1, 7.3)	42.6	3.20 3.97	dd (17.1, 5.1) dd (17.1, 7.3)
	NH		7.95	brt (6.0)		7.95	brt (6.0)		7.97	overlapped		7.97	overlapped
Gln	1	172.0			172.0			172.0			171.6		
	2	53.1	4.09	m	53.0	4.09	m	53.1	4.08	m	53.4	4.08	m
	3	26.5	1.81 2.03	m m	26.4	1.81 2.03	m m	26.3	1.83 2.00	m m	26.5	1.83 2.00	m m
	4	31.8	2.17	m	31.9	2.17	m	31.9	2.16	m	31.9	2.16	m
	5	174.2			174.1			174.2			174.2		
	NH		7.36	brd		7.37	brd		7.35	brd		7.51	brd
	NH_2		6.80 7.29	s s		6.81 7.29	s s		6.86 7.33	s s		6.83 7.39	s s
Thr1	1	170.8			170.8			170.8			171.2		
or	2	62.1	3.81	t (3.8)	62.1	3.82	t (4.0)	62.0	3.80	t (3.8)	61.4	3.82	t (4.0)
Val1	3	65.5	4.11	m	65.5	4.11	M	65.5	4.10	m	28.6	2.14	m
	4	20.7	1.23	overlapped	20.8	1.23	overlapped	20.7	1.23	overlapped	18.1	0.99	d (7.0)
	4’										19.2	1.01	d (7.0)
	NH		8.97	brs		8.84	brs		9.03	brs		8.67	brs
Thr2	1	174.2			174.2			174.2			173.6		
	2	56.9	4.88	dd (9.1, 2.3)	56.9	4.88	dd (9.4, 2.5)	57.0	4.87	brd (9.4)	57.0	4.83	brd (9.1)
	3	70.0	4.60	brm	70.0	4.60	brm	70.0	4.60	brm	70.0	4.60	brm
	4	19.0	1.24	overlapped	19.0	1.24	overlapped	19.0	1.23	overlapped	19.1	1.23	overlapped
	NH		8.35	d (9.3)		8.35	d (9.3)		8.39	d (9.1)		8.42	d (9.6)
Dhb	1	164.2			164.2			164.2			164.6		
	2	132.4			132.5			132.5			132.5		
	3	117.4	5.35	q (7.3)	117.3	5.35	q (7.3)	117.7	5.35	q (7.3)	117.7	5.35	q (7.3)
	4	12.4	1.73	d (7.3)	12.4	1.73	d (7.3)	12.5	1.72	d (7.3)	12.5	1.72	d (7.3)
	NH		9.08	s		9.08	s		9.14	s		9.14	s
Val2	1	168.9			168.8			168.9			168.9		
	2	55.9	4.29	dd (8.8, 6.5)	55.8	4.29	dd (8.8, 6.5)	55.9	4.28	dd (8.8, 6.1)	55.9	4.28	dd (8.8, 6.1)
	3	32.8	1.81	m	32.7	1.80	m	32.7	1.79	m	32.7	1.79	m
	4	18.5	0.82	d (6.8)	18.5	0.82	d (6.8)	18.5	0.81	brd	18.5	0.81	brd
	4’	18.1	0.88	d (6.8)	19.1	0.88	d (6.8)	19.1	0.87	brd	19.1	0.87	brd
	NH		6.87	d (8.9)		6.87	d (9.2)		6.89	overlapped		6.89	overlapped

[a] assigned from the DEPT-Q spectrum recorded at 226 MHz, [b] measured at 600 MHz, [c] assigned from the HSQC and HMBC spectra.

2.4 Antiproliferative activity of minutissamides A-D and homestedamides A-H against cancer cells

Minutissamides A – D (**1** – **4**) were evaluated for their antiproliferative activity against the HT-29 human colon cancer cell line. Minutissamide A (**1**) displayed antiproliferative activity with an IC_{50} value of 2.0 μM, whereas lower activity was observed for minutissamides B – D (**2** – **4**) with IC_{50} values of 20.0, 11.8, and 22.7 μM, respectively. All four minutissamides share an identical cyclic peptide core and only differ in the lipophilic *β*-amino acid residue. For example, the only structural difference between minutissamides A (**1**) and B (**2**) was the presence of a chlorine atom at C-12 of this residue, but minutissamide A (**1**) was found to be 10-fold more active in the HT-29 assay. This suggests that the *β*-amino acid residue plays an important role in the antiproliferative activity of these compounds, and modification of the *β*-amino acid residue might decrease the activity by reducing their lipophilicity.

Homestedamides A – H (**5** – **12**) were also evaluated for their antiproliferative activity against the MDA-MB-435 human melanoma cancer cell line. All of the compounds exhibited the similar level of activity with IC_{50} values ranging between 1 and 10 μM (**5**, 2.9 μM; **6**, 1.2 μM; **7**, 9.9 μM; **8**, 1.1 μM; **9**, 2.9 μM; **10**, 2.6 μM; the mixture of **11** and **12**, 2.9 μg/ml). Since different cell lines were used (HT-29 and MDA-MB-435) for the antiproliferative activity evaluation of the minutissamides and homesteadamides, the amino acid change in the cyclic peptide core could not be correlated with antiproliferative activity for the structure-activity relationship study. Considering the fact that compounds **5** – **12** all showed the similar level of activity, it was suggested that a methyl group of Ala and the change from Thr to Val do not significantly affect the antiproliferative activity of the cyclic lipodecapeptides.

2.5 Morphological and phylogenetic analyses for taxonomic identification of the strain UIC 10035

Taxonomic identification of the UIC 10035 strain was established on the basis of morphological observation and phylogenetic analysis using a partial 16S rRNA gene sequence (1.2 Kb). The strain UIC 10035 was filamentous and developed heterocysts in nitrogen-deficient media, indicating it belonging to the order Nostocales. Long straight and yellow-green colored trichomes and the lack of mucilage indicated UIC 10035 potentially being of the genus *Anabaena* (Figure 2.8). However, the partial 16S rRNA gene sequence of UIC 10035 showed the highest sequence homology to those of *Nostoc* sp. PCC8112 (99.9 %), *Nostoc* sp. PCC8976 (98.5 %) and *Nostoc elgonense* TH3S05 (97.8 %). In the phylogenetic tree constructed using cyanobacterial 16S rRNA gene sequences (Figure 2.9), the monophyletic clade, containing the UIC 10035 strain and three *Nostoc* spp., was not clustered with any of the genus reference strains for either *Nostoc* or *Anabaena*, complicating the taxonomic assignment of the UIC 10035 strain. Pairwise distance analysis between clades indicated that this clade is the most closely related with the clade containing the minutissamides-producing strain *Anabaena minutissima* UTEX 1613 (0.03) and the clade of the genus *Anabaenopsis* (0.03). Based on the morphological similarity and close phylogenetic relationship to the minutissamides-producing strain *Anabaena minutissima* UTEX 1613, the UIC 10035 strain was designated as a cf. *Anabaena* sp.

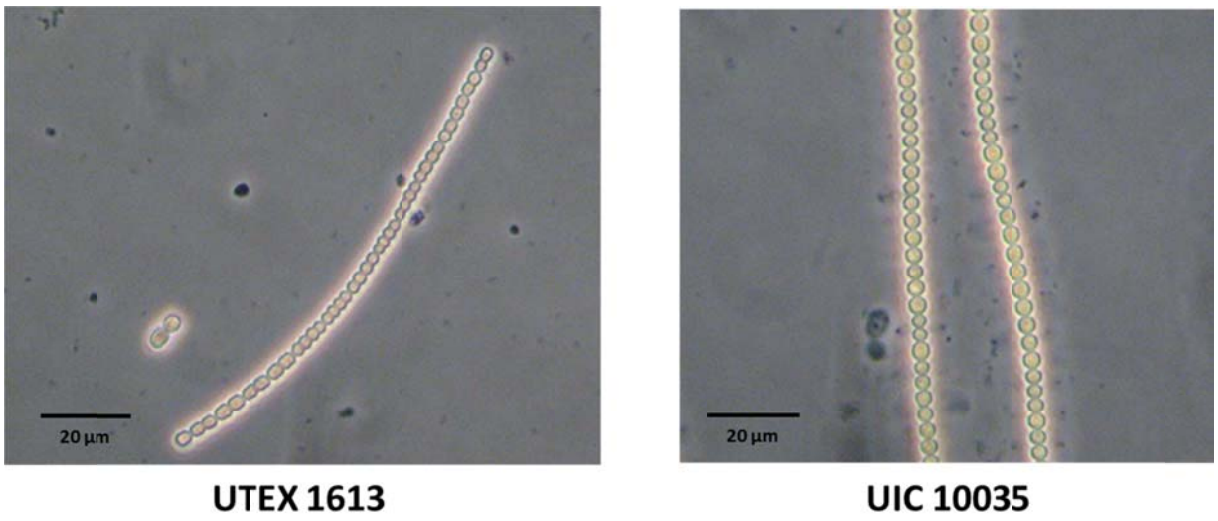

Figure 2.8 Morphological comparison between *Anabaena minutissima* UTEX 1613 and Cf. *Anabaena* sp. UIC 10035

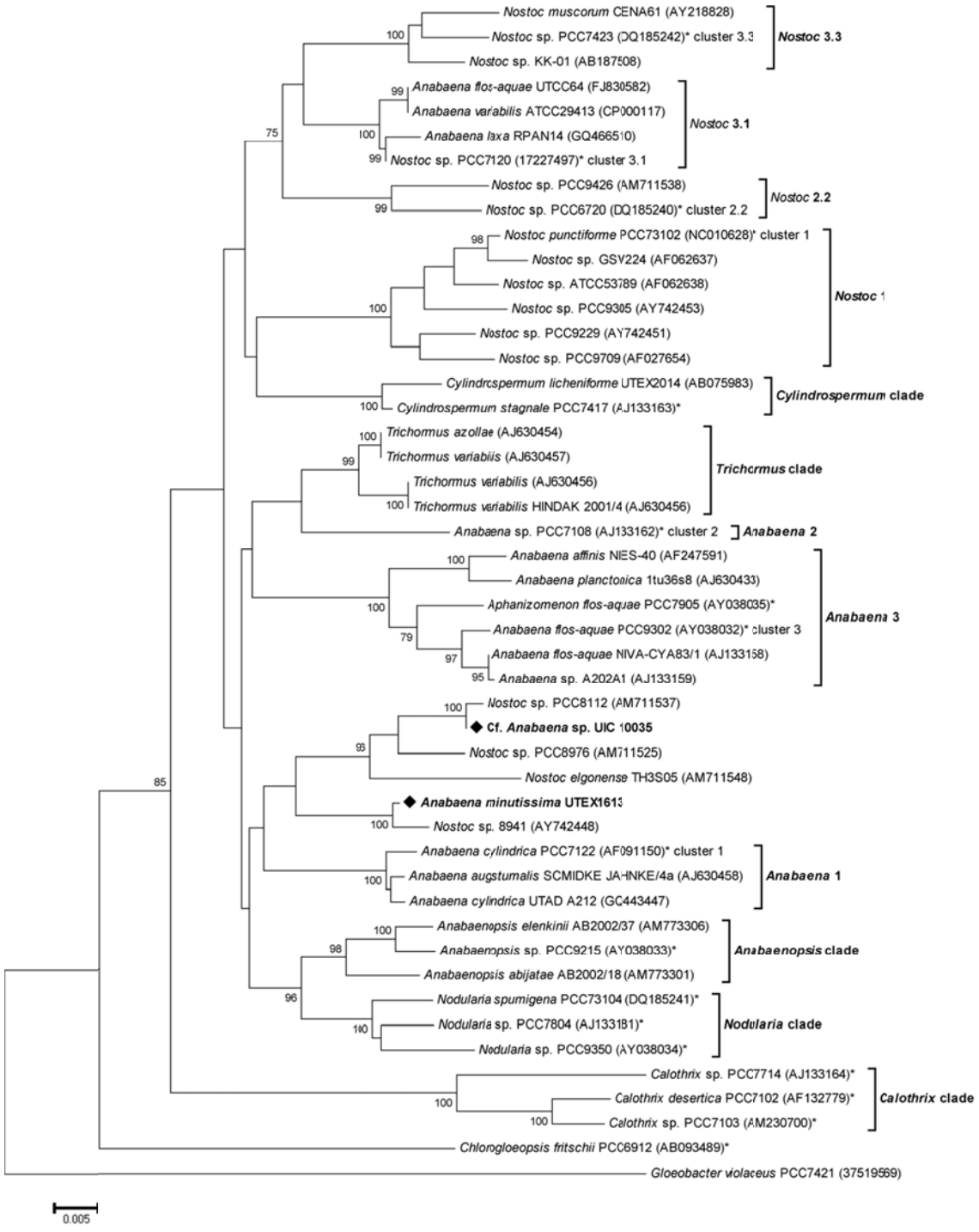

Figure 2.9 Evolutionary distances were determined using the minimum evolution method with 1,000 replicate boots trap re-sampling to construct the phylogenetic tree. Strains denoted with an asterisk (*) are "Bergey's" reference strains. Strains were obtained from NCBI with the accession number given in parentheses. Only bootstrap values greater than or equal to 75% are displayed.

2.6 Experimental

2.6.1 General Experimental Procedures

Optical rotations were measured using a Perkin-Elmer 241 polarimeter. UV spectra were recorded on a Shimadzu UV spectrometer UV2401 and scanned from 190 to 360 nm. 1D and 2D NMR spectra were obtained on a Bruker Avance DRX 600 MHz NMR spectrometer with a 5 mm CPTXI Z-gradient probe and a Bruker Avance II 900MHz NMR spectrometer with a 5 mm ATM CPTCI Z-gradient probe. ^{1}H and ^{13}C NMR chemical shifts were referenced to the solvent signals (DMSO-d_6). A mixing time of 60 ms was set for the TOCSY experiments and 200 ms for the T-ROESY experiments. The HMBC spectra were recorded with the $^{3}J_{C\text{-}H}$ set to 8 Hz, and the HSQC spectra were collected with the $^{1}J_{C\text{-}H}$ set to140 Hz. High-resolution ESI mass spectra were obtained using a Shimadzu IT-TOF LC mass spectrometer. Tandem mass analysis was performed using a Micromass Q-TOF LC, Shimadzu IT-TOF and Thermo Finnigan LTQ-FT mass spectrometers.

2.6.2 Biological Material

2.6.2.1 *Anabaena minutissima* (UTEX 1613)

Anabaena minutissima was acquired from the Culture Collection of Algae at the University of Texas at Austin (UTEX 1613). The cyanobacterium was grown in 20 L flasks containing 18 L inorganic media (Z media) (Falch et al., 1995). Cultures were illuminated with fluorescent lamps at 1.03 klx. The temperature of the culture room was maintained at 22 ºC. After 6-8 weeks, the biomass of cyanobacteria was harvested by centrifugation and freeze-dried.

2.6.2.2 Cf. *Anabaena* sp. (UIC 10035)

Cf. *Anabaena* sp. UIC 10035 was isolated from a sample collected in the town of Homestead, South Florida, in 2007 (N 25°24.2', W 80°33.4'). The strain was cultured in two 22 L glass flasks each containing 13 L of Z media (Falche et al., 1995) under sterile aeration. Cultures were illuminated with

fluorescent lamps at 1.03 klx with 18/6 light/dark cycle. The temperature of the culture was maintained at 22 ºC. After 6 weeks, the biomass of cyanobacteria was harvested by centrifugation and freeze-dried.

2.6.3 Morphological and phylogenetic analyses for taxonomic identification

Morphological studies were performed using the cultivated cyanobacterium UIC 10035. Taxonomic identification of the cyanobacterial specimen was made in accordance with the modern taxonomic system (Komárek et al.). Genomic DNA of the strain UIC 1035 was extracted using the Wizard Genomic DNA purification kit (Promega) according to the manufacturer's protocol. PCR amplification and sequencing of the partial 16S rRNA gene sequence was carried out as previously described (Chlipala et al., 2010) using the cyanobacterial specific primers 106F and 1509R (Nübel et al., 1997). The resulting sequence was deposited in the NCBI GenBank under the accession number JX023442. Phylogenetic analysis was conducted using MEGA 5.0 (Tamura et al., 2011). The sequence of UIC 10035 was aligned with those of other cyanobacteria belonging to the order Nostocales using ClustalW with standard gap opening and extension penalties. The evolutionary history was inferred using the neighbor-joining, minimum evolution and maximum parsimony methods, which showed nearly identical topology with similar bootstrap values.

2.6.4 Extraction and isolation

2.6.4.1 Minutissamides A-D

The freeze-dried biomass (5.2 g) from the total 54 L (3×18 L) culture was harvested and extracted with the solvent of CH_2Cl_2-MeOH (1:1) and concentrated in vacuo to yield 1.1 g of the extract. The extract was fractionated using Diaion HP-20 resin with increasing amounts of iPrOH in H_2O to generate 8 sub-fractions (0, 20, 40, 60, 70, 80, 90, 100 % aqueous iPrOH). The faction eluting at 40 % iPrOH indicated the presence of four new peptides by LC-MS. This fraction was further purified by Sephadex LH-20 column chromatography in MeOH. Fractions 7-9 were found to contain new peptides, thus subjected to reversed phase HPLC (Varian C_8 semi-preparative column, 10 mm × 250 mm, 3 mL/min) eluting with

a linear gradient from 60 to 80% aqueous MeOH for 45 min. Minutissamaides A – D (**1** – **4**) were eluted at 37.9 min (**1**, 1.4 mg), 31.6 min (**2**, 0.4 mg), 30.0 min (**3**, 1.0 mg) and 33.5 min (**4**, 0.7 mg), respectively.

Minutissamide A (1): colorless amorphous powder; $[\alpha]^{25}_{D}$ +4° (*c* 0.06, MeOH); UV (MeOH) λ_{max} (log ε) 243 (3.45) nm; IR (neat) 3317 (br), 2925, 2861, 1681, 1635 (br), 1561, 1541 cm^{-1}; ^{1}H and ^{13}C NMR (see TABLE II); HRESIMS *m/z* 1140.6049 $[M+Na]^+$ (calcd for $C_{51}H_{83}N_{13}O_{15}Na$, 1140.6029)

Minutissamide B (2): colorless amorphous powder; $[\alpha]^{25}_{D}$ +5° (*c* 0.02, MeOH); UV (MeOH) λ_{max} (log ε) 230 (4.24) nm; IR (neat) 3315 (br), 2926, 2852, 1670, 1647 (br), 1545, 1516, 1459, 1402 cm^{-1}; ^{1}H and ^{13}C NMR (see TABLE II); HRESIMS *m/z* 1174.5790 $[M+Na]^+$ (calcd for $C_{51}H_{83}ClN_{13}O_{15}Na$, 1174.5640)

Minutissamide C (3): colorless amorphous powder; $[\alpha]^{25}_{D}$ +3° (*c* 0.07, MeOH); UV (MeOH) λ_{max} (log ε) 242 (2.62) nm; IR (neat) 3315 (br), 2926, 2857, 1664, 1630 (br), 1533, 1447, 1402 cm^{-1}; ^{1}H and ^{13}C NMR (see TABLE III); HRESIMS *m/z* 1210.6610 $[M+Na]^+$ (calcd for $C_{55}H_{89}N_{13}O_{16}Na$, 1210.6448)

Minutissamide D (4): colorless amorphous powder; $[\alpha]^{25}_{D}$ +2° (*c* 0.05, MeOH); UV (MeOH) λ_{max} (log ε) 240 (3.94) nm; IR (neat) 3320 (br), 2926, 2852, 1664, 1636 (br), 1539, 1453, 1379 cm^{-1}; ^{1}H and ^{13}C NMR (see TABLE III); HRESIMS *m/z* 1212.6740 $[M+Na]^+$ (calcd for $C_{55}H_{91}N_{13}O_{16}Na$, 1212.6604)

2.6.4.2 Homesteadamides A – H

The freeze-dried biomass (7.5 g) from the total 26 L (2×13 L) culture was harvested and extracted with CH_2Cl_2-MeOH (1:1) to yield the extract (458.7 mg). The resulting extract was fractionated using Diaion HP-20 resin with increasing amounts of iPrOH in H_2O to generate eight sub-fractions (0, 20, 40, 60, 70, 80, 90, 100 % iPrOH in H_2O). Fractions eluting at 40 and 60 % iPrOH exhibited antiproliferative activity against MDA-MB-435 cells (95 % and 100% at 25 μg/ml, respectively). LC-MS dereplication of these fractions indicated the presence of a series of nitrogen-containing compounds with molecular weights, ranging between 1,150 and 1,250 Da. Reversed-phase HPLC of these fractions using C_8 column (Varian 10 mm × 250 mm, 3 mL/min) with a linear gradient from 60 to 80% aqueous MeOH for 50 min

yielded three sub-fractions, and homesteadamides B (**6**, 1.1 mg) and E (**9**, 1.7 mg). The resulting sub-fractions were re-purified by reversed-phase HPLC using C_{18} column with the same gradient condition as described above to yield homesteadamides A (**5**, 1.3 mg), C (**7**, 0.5 mg), D (**8**, 0.6 mg) and F (**10**, 0.7 mg), and the mixture (1.1 mg) of homesteadamides F (**11**) and G (**12**).

Homesteadamide A (5): colorless, amorphous powder; $[\alpha]^{25}_{D}$ -29 (*c* 0.09, MeOH); UV (MeOH) λ_{max} (log ε) 203 (4.52), 234 (3.88) nm; IR (neat) 3325 (br), 2930, 2855, 1662 (br), 1535 cm^{-1}; ^{1}H and ^{13}C NMR (see TABLE IV); HRESIMS *m/z* 1249.7411 $[M+H]^+$ (calcd for $C_{59}H_{101}N_{12}O_{17}$, 1249.7408)

Homesteadamide B (6): colorless, amorphous powder; $[\alpha]^{25}_{D}$ - 19 (*c* 0.05, MeOH); UV (MeOH) λ_{max} (log ε) 202 (4.39), 233 (3.69) nm; IR (neat) 3324 (br), 2926, 2855, 1630 (br), 1539 cm^{-1}; ^{1}H and ^{13}C NMR (see TABLE IV); HRESIMS *m/z* 1213.6645 $[M+H]^+$ (calcd for $C_{55}H_{94}ClN_{12}O_{16}$, 1213.6599)

Homesteadamide C (7): colorless, amorphous powder; $[\alpha]^{25}_{D}$ - 22 (*c* 0.02, MeOH); UV (MeOH) λ_{max} (log ε) 202 (4.24), 233 (3.54) nm; IR (neat) 3338 (br), 2928, 2852, 1676 (br), 1540 cm^{-1}; ^{1}H and ^{13}C NMR (see TABLE IV); HRESIMS *m/z* 1251.7608 $[M+H]^+$ (calcd for $C_{59}H_{103}N_{12}O_{17}$, 1251.7564)

Homesteadamide D (8): colorless, amorphous powder; $[\alpha]^{25}_{D}$ - 30 (*c* 0.02, MeOH); UV (MeOH) λ_{max} (log ε) 201 (4.16), 233 (3.42) nm; IR (neat) 3320, 2920, 2851, 1634 (br), 1535 cm^{-1}; ^{1}H and ^{13}C NMR (see TABLE IV); HRESIMS *m/z* 1247.7622 $[M+H]^+$ (calcd for $C_{60}H_{103}N_{12}O_{16}$, 1247.7615)

Homesteadamide E (9): colorless, amorphous powder; $[\alpha]^{25}_{D}$ - 26 (*c* 0.13, MeOH); UV (MeOH) λ_{max} (log ε) 203 (4.46), 233 (3.81) nm; IR (neat) 3322 (br), 2929, 2855, 1658 (br), 1643 (br), 1537 cm^{-1}; ^{1}H and ^{13}C NMR (see TABLE V); HRESIMS *m/z* 1235.7238 $[M+H]^+$ (calcd for $C_{58}H_{99}N_{12}O_{17}$, 1235.7251)

Homesteadamide F (10): colorless, amorphous powder; $[\alpha]^{25}_{D}$ - 19 (*c* 0.05, MeOH); UV (MeOH) λ_{max} (log ε) 202 (4.29), 233 (3.62) nm; IR (neat) 3294 (br), 2931, 2857, 1674 (br), 1540 cm^{-1}; ^{1}H and ^{13}C NMR (see TABLE V); HRESIMS *m/z* 1199.6477 $[M+H]^+$ (calcd for $C_{54}H_{92}ClN_{12}O_{16}$, 1199.6443)

Homesteadamides G (11) and H (12): colorless, amorphous powder; $[\alpha]^{25}_{D}$ - 26 (*c* 0.04, MeOH); UV (MeOH) λ_{max} (log ε) 202 (4.28), 233 (3.59) nm; IR (neat) 3291 (br), 2932, 2855, 1679 (br), 1541 cm^{-1}; ^{1}H and ^{13}C NMR (see TABLE V); HRESIMS for **7** *m/z* 1237.7381 $[M+H]^{+}$ (calcd for $C_{58}H_{101}N_{12}O_{17}$, 1237.7408); HRESIMS for **8** *m/z* 1233.7482 $[M+H]^{+}$ (calcd for $C_{59}H_{101}N_{12}O_{16}$, 1233.7459)

2.6.5 Marfey's analysis

2.6.5.1 Amino acid configurations of minutissamides A - D

Approximately 0.3 mg of minutissamide A (**1**) was hydrolyzed using 6 N HCl (500 μL) in a high-pressure tube for 16 h at 110 ºC. The hydrolysate was dried under vacuum and re-dissolved in H_2O. This procedure was repeated three times to completely remove the remaining HCl. For the derivatization with Marfey's reagent (FDAA), the hydrolysate (0.1 mg) or amino acid standards was dissolved in H_2O (50 μL), and 1N $NaHCO_3$ (20 μL) and acetone (110 μL) were added. The reaction was initiated by adding FDAA solution (20 μL, 1-fluoro-2,4-dinitrophenyl-5-L-alanine amide, 10 mg/mL w/v in acetone), proceeded for 1h at 40 ºC and quenched by adding 1N HCl (20 μL). The reactant was dried under vacuum and re-dissolved in CH_3CN for HPLC analysis. Chromatographic analysis of the FDAA derivatives was performed on an Altech C_{18} reversed phase column (5 μm, 250 × 4.6 mm) with the flow rate of 1.0 mL/min. Aqueous CH_3CN containing 0.1% formic acid (FA) was used as a mobile phase eluting with a linear gradient from 10 % to 100 % (A: H_2O containing 0.1 % FA and B: CH_3CN containing 0.1 % FA, gradient condition: 0 min-10%B, 5min-10%B, 35 min-20%B, 65 min-30%B, 70 min-60%B, 72 min-100%B and 80 min-100%B). The absolute configurations of the amino acids were assigned by comparing the retention times with those of the corresponding amino acid standards. The retention times of the FDAA derivatives of the authentic amino acid standards were identified at 30.70 (L-Thr and *N*-Me-D-Asp), 32.30 (L-Asp), 36.17 (*N*-Me-L-Asp), 36.94 (D-Asp), 41.06 (L-Ala), 42.54 (D-Thr), 44.57 (L-Pro), 49.84 (D-Pro), 51.76 (D-Ala), 59.09 (L-Val) and 71.45 (D-Val) min. The FDAA derivatives of the amino acids from the hydrolysate of **1** showed peaks at 32.30, 36.17, 44.57, 51.76 and 59.09 min corresponding

to L-Asp, N-Me-L-Asp, L-Pro and L-Val, respectively. The peak at 30.70 min was identified as L-Thr by LC-MS analysis (*m/z* 372, $[M + H]^+$).

2.6.6 Advanced Marfey's Analysis

2.6.6.1 The absolute configuration of the *β*-amino acid residue in minutissamide A

A total of 0.2 mg of the acid hydrolysate of minutissamide A (**1**), separated into 0.1 mg each for L-FDLA and DL-FDLA derivatization, were dissolved in H_2O (50 μL) and then mixed with 1N $NaHCO_3$ (20 μL) and acetone (110 μL). Finally, L-FDLA or DL-FDLA (20 μL, 10 mg/mL w/v in acetone) was added, and then the mixtures were heated to 40 ºC for 1h. The reaction mixtures were cooled down to room temp., and 1N HCl (20 μL) was added to quench the reaction. After dryness, the FDLA derivatives were dissolved in CH_3CN for LC-MS analysis. The chromatograms of L-FDLA and DL-FDLA derivatives were compared for the assignment of the absolute configuration of Hamd. LC-MS analysis was performed using a Varian reverse-phased C_{18} column (250 × 2.0 mm) at the flow rate of 0.4 mL/min. The linear gradient eluting from 20 % to 75 % aqueous CH_3CN (0.1% FA) for 50 min was used as a mobile phase, and ESI was used as an ionization method. Two peaks corresponding to the L- and D-FDLA derivatives of Hamd were observed at 43.33 and 48.84 min (*m/z* 538, $[M–H]^–$), respectively. The L-FDLA derivative of Hamd gave one peak at 48.84 min.

2.6.6.2 Amino acid configurations of homesteadamides A-H

Approximately 0.3 mg of homesteadamide A (**5**) was hydrolyzed with 6 N HCl (500 μL) for 16 h at 110 °C. The resulting acid hydrolysate was separated into two equal portions for derivatization with either L-FDLA or DL-FDLA. Each portion was dissolved in H_2O (50 μL), and mixed with 1N $NaHCO_3$ (20 μL) and L-FDLA or DL-FDLA (20 μL, 10 mg/mL in acetone). Then, acetone was added to a final volume of 200 μL, and the reaction mixtures were heated to 40 ºC and stirred for 1 h. After cooling to rt, 1N HCl (20 μL) was added, and the resulting reaction mixtures were air-dried and re-dissolved in CH_3CN (300 μL). LC-MS analysis was carried out using a reversed-phase column (Alltima C_{18}, 250 × 4.6 mm, 5 μm, 1.0 mL/min) with a linear gradient from 20 % to 65 % aqueous CH_3CN containing 0.1% formic acid

for 50 min. The selective ion chromatograms of L-FDLA and DL-FDLA for each amino acid were compared for the assignment of amino acid configurations. The DL-FDLA derivative exhibited two peaks corresponding to the L- and D-FDLA derivatives of each amino acid: Hamoo 67.0 (*S*, C-3) and 72.4 (*R*, C-3) min; Pro 30.4 (L) and 34.1 (D) min; *N*MeAsn 24.0 (D) and 26.1 (L) min; Ala 30.9 (L) and 35.4 (D) min; Gln 27.2 (L) and 28.7 (D) min; Thr 24.5 (L) and 30.6 (D) min; Val 35.8 (L) and 43.8 (D) min. The L-FDLA derivative gave one peak for each amino acid at 72.4 (Hamoo), 30.5 (Pro), 26.3 (*N*MeAsn), 35.6 (Ala), 27.4 (Gln), 24.7 (Thr) and 35.9 (Val) min, confirming the *R* configuration at C-3 for Hamoo, the D-configuration for Ala and the L-configuration for Pro, Ala, Gln and Val. The presence of *N*Me-L-Asn and L-Thr was confirmed by chromatographic comparison of the L-FDLA derivative with those of the amino acid standards *N*Me-L-Asn (26.1 min), *N*Me-D-Asn (24.1 min), L-Thr (24.5), D-Thr (30.6 min), L-*allo*-Thr (25.7 min) and D-*allo*-Thr (27.9 min). Advanced Marfey's analysis of **8**, **10** and the mixture of **11** and **12** was carried out as described above.

2.6.7 Preparation of OMeThr standards of the homesteadamides

Prior to methylation, the amino group of L-Thr was protected according to the previously described protocol (Shendage et al., 2004). Briefly, a 2M Bac_2O solution in THF (2.5 eq) and $NaHCO_3$ (3 eq) were added to a solution of L-Thr (200 mg) in H_2O (3 mL), and stirred overnight at rt. The turbid solution was extracted with Et_2O twice, and the aqueous layer was carefully acidified to pH 3 at 0 °C using saturated citric acid. The resulting acidic solution was extracted with CH_2Cl_2 three times. The CH_2Cl_2 layer was dried using Na_2SO_4 and evaporated to yield *N*Boc-L-Thr (143 mg). For methylation, 2,6-di-tert-butylpyridine (0.5 mL) and methyl trifluoromethansulfonate (methyl triflate, 1 mL) were sequentially added to a solution of *N*Boc-L-Thr (50 mg) in CH_2Cl_2 (2 mL) at 0 °C. The mixture was warmed to rt and stirred overnight. The resulting yellowish solution was cooled to 0 °C, and saturated $NaHCO_3$ was added. The organic phase was washed with water and purified by silica gel column chromatography eluting with n-hexane:EtOAc (99:1) and EtOAc. The EtOAc fraction was dried in vacuo to give *N*Boc-L-Thr methyl ester (40 mg) as light yellowish oil. *N*Boc-L-Thr methyl ester (5 mg) was hy-

drolyzed using 6 N HCl (1 mL) for 16 h at 110 °C to yield the final product *O*Me-L-Thr. *O*Me-D-Thr, *O*Me-L-*allo*-Thr and *O*Me-D-*allo*-Thr standards were prepared in the same say. The prepared *O*MeThr standards were derivatized with L-FDLA as described above and analyzed by LC-MS using a reversed-phase column (Alltima C_{18}, 250 × 4.6 mm, 5 μm, 1.0 mL/min) with a linear gradient from 30 % to 50 % aqueous CH_3CN (0.1% formic acid) for 50 min. L-FDLA derivatives of *O*Me-L-Thr, *O*Me-L-allo-Thr, *O*Me-D-Thr and *O*Me-D-allo-Thr standards were eluted at 33.0, 32.6, 44.1 and 47.6 min, respectively. The L-FDLA derivative of the acid hydrolysate of **5** gave a peak at 33.0 min corresponding to *O*MeThr, indicating the presence of *O*Me-L-Thr. The L-FDLA peak was used as an internal standard to calibrate the retention time difference.

2.6.8 Antiproliferative Assay

Antiproliferative activity against the HT-29 cancer cell line was performed according to established protocols (Seo et al., 2001). Human melanoma MDA-MB-435 cells (Rae et al., 2007) were purchased from the American Type Culture Collection, (Manassas, VA). The cells were propagated at 37 °C in 5% CO_2 in RPMI 1640 medium supplemented with fetal bovine serum (10%), penicillin (100 units/ml) and streptomycin (100 μg/ml). Cells in log phase growth were harvested by trypsinization. A total of 5,000 cells were seeded per well of a 96-well plate and incubated overnight at 37 °C in 5% CO_2. Samples dissolved in DMSO were then sequentially diluted and added to the appropriate wells (total volume 100 μL). Each compound was tested at the following concentrations (µg/ml): 25, 5.0, 1.0, 0.2 and 0.04. The cells were incubated in the presence of test substance for ninety-six hours at 37 °C and evaluated for viability with a commercial absorbance assay (CellTiter 96® AQ_{ueous} One Solution Cell Proliferation Assay, Promega Corp, Madison, WI). Activity was expressed as the percentage of viable cells present relative to the negative (solvent) control. The positive control was vinblastine tested at 1 ng/mL, which had 49% viable cells after treatment.

CHAPTER 3:

MEROCYCLOPHANES A AND B, ANTIPROLIFERATIVE CYCLOPHANES FROM THE CULTURED TERRESTRIAL CYANOBACTERIUM *Nostoc* sp. (UIC 10062)

3.1 Introduction

Several terrestrial cyanobacterial species belonging to the order *Nostocales* have been reported to produce naturally occurring paracyclophanes. Of these, nostocyclyne A, an acetylenic [14]paracyclophane, was isolated from the natural bloom of *Nostoc* sp. and displayed antimicrobial activity against Gram-positive bacteria *S. aureus* and *B. subtilis* (Ploutno et al., 2000). Additionally, cylindrocyclophanes and nostocyclophanes, the two classes of cyanobacterial [7.7]paracyclophanes isolated from the cultured *Nostoc* sp. and *Cylindrospermum* sp., have exhibited a broad spectrum of biological activities, including antibacterial, antifungal and cytotoxic activities (Moore et al., 1990; Chen et al., 1991; Moore et al., 1992; Bui et al., 2007; Chlipala et al., 2010). As regards their formation, the polyketide biosynthetic pathway to these naturally occurring [7.7]paracyclophanes was determined by an isotope precursor feeding experiment, and involves dimerization of two acetate-derived nonaketides and subsequent modifications by chlorination, oxidation and/or methylation, resulting in diverse chemical structures (Bobzin et al., 1993).

Recently, several cyclindrocyclophanes were reported from a terrestrial *Nostoc* sp. (UIC 10022A) obtained from the material collected in the city of Chicago. These compounds displayed inhibitory activity against the 20S proteasome and were also found to be cytotoxic against cancer cell lines, including HT-29, NCI-H460, SF268 and MCF7 cells (Chlipala et al., 2010). In this chapter, we describe the isolation, structure determination and biological activity of two additional cyclophanes, named merocyclophanes A and B (**1** and **2**), isolated from a second *Nostoc* sp. (UIC 10062). The UIC 10062 strain was obtained from a sample collected at Grand Mere State Park in Michigan, and the merocyclophanes were named in recognition of the collection site. Their structures were determined using various spectroscopic methods including HRESIMS, and 1D and 2D NMR analyses. The stereoconfiguration was assigned by a combination of X-ray crystallographic and CD analyses, and the structures of merocyclophanes A and B (**1** and **2**) established a new [7.7]paracyclophane carbon skeleton as characterized by the presence of α-branched methyls at C-1/14.

3.2 Merocyclophanes A and B, antiproliferative cyclophanes from the cultured terrestrial cyanobacterium *Nostoc* sp. (UIC 10062)

3.2.1 Isolation of merocyclophanes A (1) and B (2)

Nostoc sp. (UIC 10062) was isolated from a sample collected at Grand Mere State Park in Michigan. The strain was maintained and cultured in Z media (Falch et al., 1995). The freeze-dried cells were extracted with a mixture of CH_2Cl_2 and MeOH (1:1, v/v) three times and dried *in vacuo* with the resulting extract (156.6 mg) subjected to bioassay-guided fractionation. This cell extract showed antiproliferative activity against the HT-29 human colon cancer cell line (IC_{50} 13.1 μg/mL), thus was fractionated using Diaion HP-20 resin and an increasing amount of iPrOH in H_2O. Fractions eluting at 70 (5.0 mg) and 80 (6.5 mg) % iPrOH were found to be active, with IC_{50} values of 0.9 and 1.2 μg/ml, respectively. LC-MS and UV analyses of the active fractions also indicated the presence of two cyclophanes with molecular weights of 552 and 566 Da along with four previously described indolocarbazoles. Reversed-phase HPLC of these fractions yielded merocyclophanes A (**1**, 2.4 mg, 0.11%) and B (**2**, 0.9 mg, 0.04%).

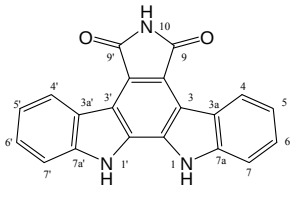

arcyriaflavin A

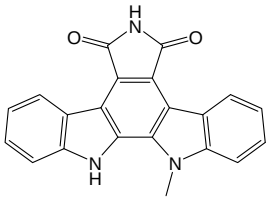

1-methyl arcyriaflavin A

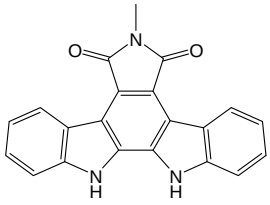

10-methyl arcyriaflavin A

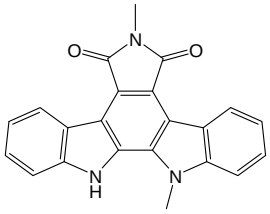

1,10-dimethyl arcyriaflavin A

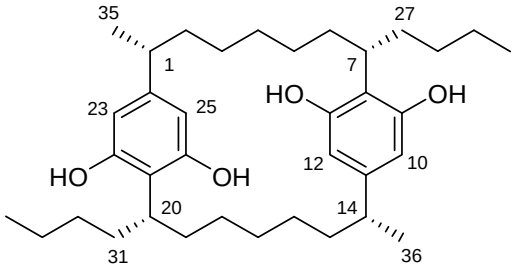

merocyclophane A (**1**)

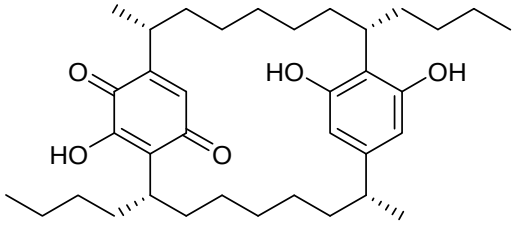

merocyclophane B (**2**)

3.2.2 Structure determination of merocyclophanes A and B

Merocyclophane A (**1**) was obtained as white amorphous powder, and the molecular formula was determined as $C_{36}H_{56}O_4$ by HRESIMS analysis (*m/z* 551.4170 $[M-H]^-$). The total numbers of proton and carbon signals, determined by analysis of ^1H and 2D NMR spectra, were only half of those required by the molecular formula, thus indicating the presence of C_2 axis of symmetry in **1**. The structure of **1** was elucidated by analysis of the 2D NMR spectra including COSY, HSQC and HMBC (Figure 3.1, TABLE VI). The appearance of only two aromatic singlets (H-10/23, δ_H 6.04 and H-12/25, δ_H 6.00) indicated the presence of two tetrasubstituted aromatic rings. The carbon chemical shifts of C-9/22 (δ_C 158.5) and C-13/26 (δ_C 156.9), together with HMBC correlations from H-7/20 (δ_H 3.10) to C-9/22 (δ_C 158.5) and C-13/26 (δ_C 156.9), identified these partial structures as two 2,5-dialkylresorcinol moieties. Sequential COSY correlations from H1/14 to H7/20 combined with HMBC correlations from H-10/23 (δ_H 6.04) and H-12/25 (δ_H 6.00) to C-1/14 (δ_C 41.8) and from H-7/20 (δ_H 3.10) to C-9/22 (δ_C 158.5) and C-13/26 (δ_C 156.9) completed the [7.7]paracyclophane core. Additional sequential COSY correlations from the H-7/20 to the triplet methyls H_3-30/34 via three methylenes (H_2-27/31, H_2-28/32 and H_2-29/33) further expanded the carbon chains. Structure determination was completed by an HMBC correlation from the doublet methyl (H_3-35/36, δ_H 1.15) to the aromatic carbon (C-11/24, δ_C 146.6) combined with a COSY correlation between H-1/14 (δ_H 2.30) and H-35/36 (δ_H 1.15), placing methyl groups at C-1/14.

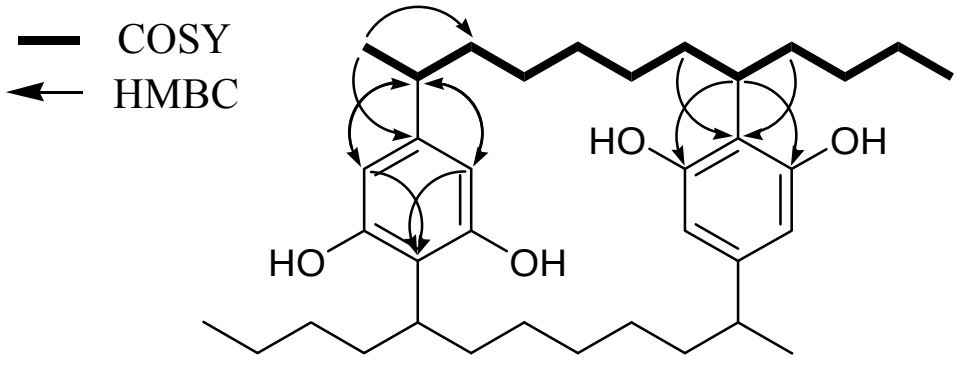

Figure 3.1 Key 2D correlations used for structure determination of **1**

The structure of **1** possessed four stereogenic centers, whose stereoconfiguration was determined by a combination of X-ray crystallographic and CD spectral analyses. Merocyclophane A (**1**) was crystallized from acetonitrile by slow evaporation. Single-crystal X-ray analysis established the relative configuration of **1** as shown in Figure 3.2. The absolute configurations at C-1/14 and C-7/20 were established by comparison of the CD spectrum of **1** with those reported for the nostocyclophanes (Chen et al., 1991). Cotton effects observed between 220 ~ 230 nm and between 270 ~ 280 nm arise from π- π* transitions of a benzene chromophore. According to the benzene sector rule, the chlorine-bearing stereogenic carbons in the nostocyclophanes, three carbons away from the benzene chromophore, should not affect Cotton effects in these regions (Smith, 1998). The CD spectrum of **1** exhibited negative Cotton effects at 227 ($\Delta\varepsilon$, -4.35) and 277 ($\Delta\varepsilon$, -2.73), similar to those observed for the nostocyclophanes, suggesting the same absolute configuration. Therefore, the absolute configurations of the four stereogenic carbons C-1/14 and C-7/20 in **1** were assigned as "*R*" and "*S*", respectively.

Merocyclophane B (**2**) was obtained as purple amorphous powder, and the HRESIMS data (*m/z* 565.3954 $[M-H]^-$) established the molecular formula as $C_{36}H_{54}O_5$. The ^1H NMR spectrum of **2** closely resembled that of **1**, except for one of the two aromatic rings. This resulted in an unsymmetric structure. The presence of a hydroxyquinone in **2** was suggested by analysis of the UV spectrum. A chromophore corresponding to the quinone absorption was observed at 521 nm, which shifted to 413 nm in the presence of acid (0.04 v/v % TFA in MeOH). This was consistent with the observed color change from deep purple to yellow upon addition of TFA. The appearance of the down-fielded carbon chemical shift of C-23 (δ_C 132.6 compared to δ_C 104.5 in **1**) further supported the presence of the hydroxyquinone moiety in **2**. However, significant line broadening of NMR signals was observed in the hydroxyquinone moiety, causing a number of expected correlations to be absent in the HMBC spectrum, even at the elevated temperature (343 K). Thus, the carbon chemical shifts of C-21, C-22, C-25 and C-26 could not be detected. The presence of the unsymmetrical hydroxyquinone moiety in **2** raised the possibility of two conformations arising from hindered rotation around the C1-C24 and C20-C21 bonds, resulting in the formation of two

diastereotopic atropisomers. A torsion energy scan carried out using MM3 force-field calculation showed high rotational energy barriers between the two possible atropisomers (Figure 3.3). However, a slow conversion of **1** into **2** was observed during prolonged storage, indicating **2** to be an oxidation artifact of **1**. This non-enzymatic oxidation suggests that both atropisomers are present in a nearly equal amount, which is supported by the identical CD spectrum observed between **1** and **2**. The stereoconfiguration of **2** (C-1/14, C-7/20) was determined by comparison of the CD spectrum with that of **1**. Negative Cotton effects observed at 227 ($\Delta\varepsilon$, -2.22) and 274 ($\Delta\varepsilon$, -2.03) nm indicated the same absolute configuration of **2** as determined for **1**.

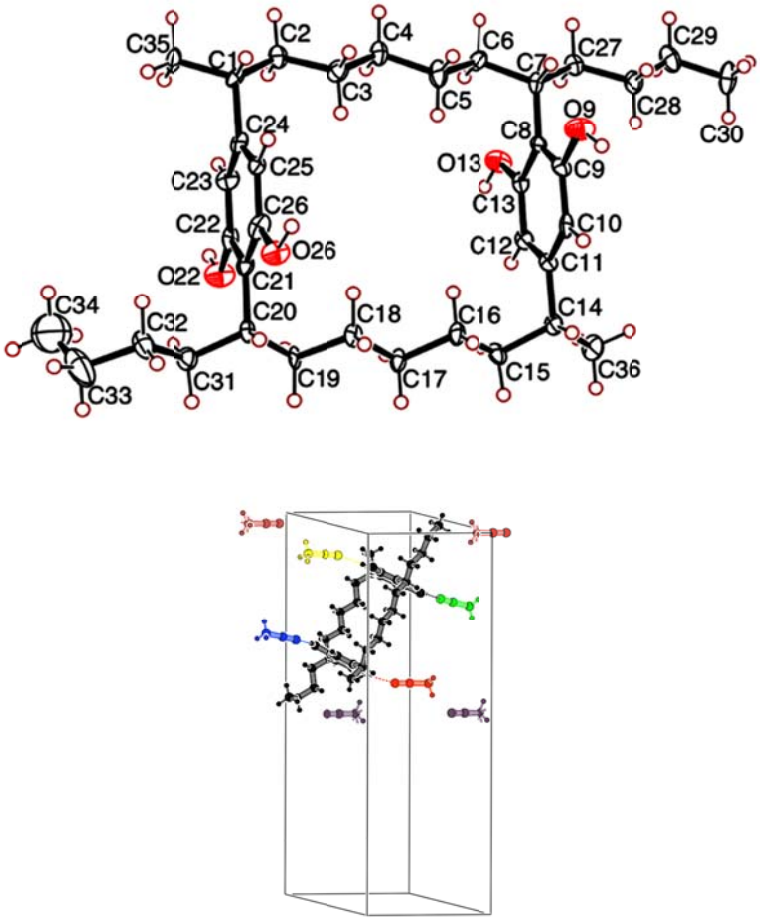

Figure 3.2 ORTEP drawing of merocyclophane A (**1**)

The structures of merocyclophanes A (**1**) and B (**2**) differ from the previously described cylindrocyclophanes and nostocyclophanes by the presence of *α*-branched methyls at C-1/14 as shown in Figure 3.4, whereas cylindrocyclophanes have branched methyls at C-2/15 (*β*-branching). Isotope precursor administration experiments performed by Bobzin et al. indicated the acetate origin of these *β*-branched methyl groups (Bobzin et al., 1993). However, the *C*-methylation in the merocyclophanes occurred at *α*-position, suggesting that these methyl groups are likely derived from SAM (*S*-adenosyl methionine) (Jones et al, 2010).

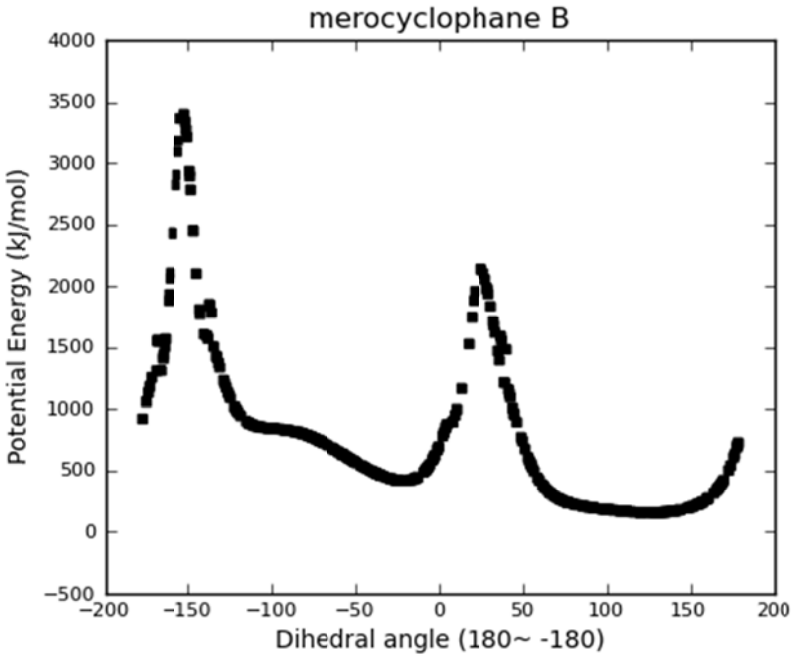

Figure 3.3 Torsion energy profile of the hydroxyquinone ring in merocyclophane B (**2**). The hydroxyquinone ring was rotated 360 degree with 1 degree increment while freezing the remaining atoms. The total energy was calculated *in vacuo* at each degree increment using Maestro 9.2 with the MM3 force field.

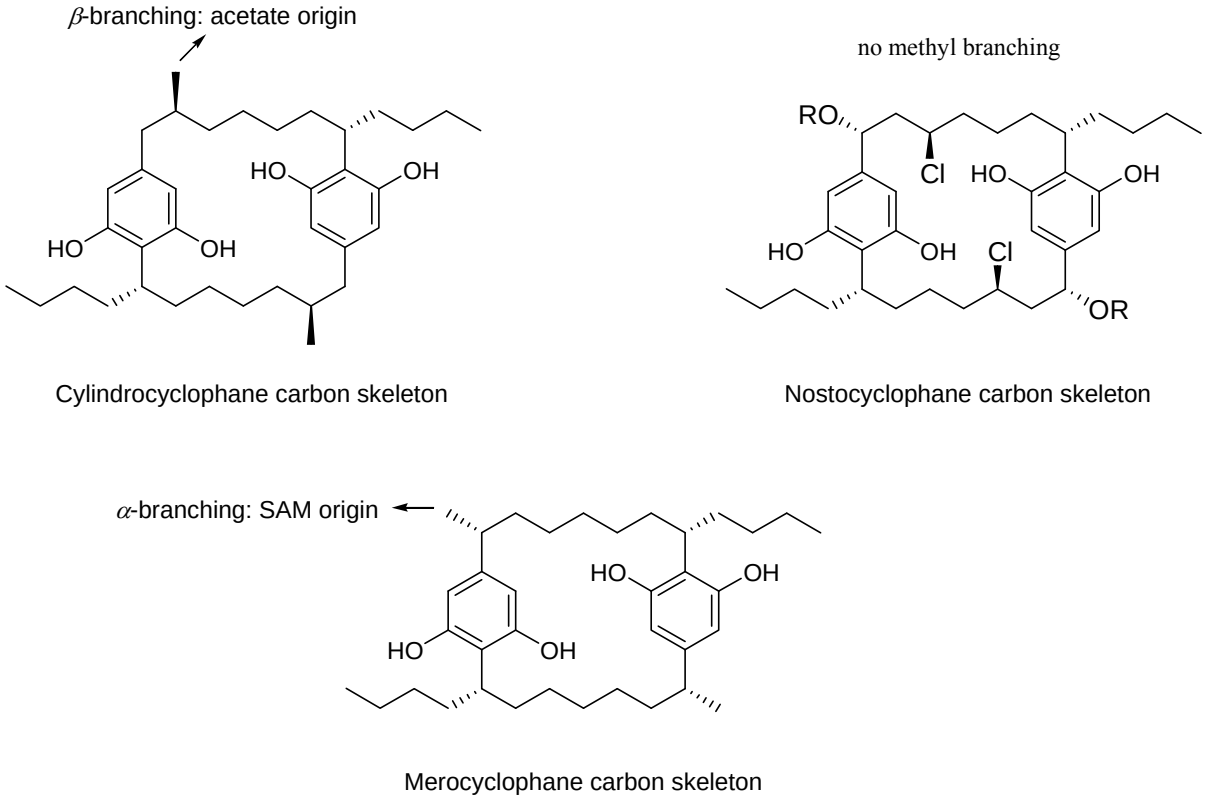

Figure 3.4 Comparison of carbon skeletons between the cylindrocyclophanes, the nostocyclophanes and merocyclophane A

TABLE VI: NMR SPECTROSCOPIC DATA FOR MEROCYCLOPHANE A IN MeOH-d_4

NO.	Merocyclophane A (**1**)				
	δ_C[a]	δ_H	mult. (*J* in Hz)	COSY	HMBC
1 / 14	41.8	2.30	dqd (10.8, 6.9, 3.8)	2/15, 35/36	35/36, 10/23, 12/25, 11/24
2 / 15	40.5	1.32 1.45	m m	1/14, 3/16	1/14, 3/16, 11/24, 35/36
3 / 16	30.7	0.65 0.93	m m	2/15, 4/17	1/14, 2/15, 5/18
4 / 17	32.4	0.88 1.27	m m	3/16, 5/18	
5 / 18	30.6	0.67 0.98	m m	4/17, 6/19	
6 / 19	35.1	1.31 1.97	m qd (12.4, 4.0)	5/18, 7/20	7/20
7 / 20	36.7	3.10	m	6/19, 27/31	5/18, 6/19, 8/21, 9/22, 13/26, 27/31, 28/32
8 / 21	116.1				
9 / 22	158.5				
10 / 23	104.5	6.04	s		14/1, 8/21, 12/25, 9/22
11 / 24	146.6				
12 / 25	109.1	6.00	s		14/1, 8/21, 10/23, 13/26
13 / 26	156.9				
27 / 31	34.7	1.49 1.92	m m	7/20, 28/32	28/32, 29/33, 7/20
28 / 32	31.6	1.11 1.19	m m	27/31, 29/33	
29 / 33	23.8	1.25 1.29	m m	28/32, 30/34	
30 / 34	14.4	0.83	t (7.1)	29 / 33	28/32, 29/33
35 / 36	23.5	1.15	d (6.9)	1 / 7	1/14, 2/15, 11/24

[a]assigned from the HSQC and HMBC spectra

TABLE VII: NMR SPECTROSCOPIC DATA FOR MEROCYCLOPHANE B IN DMSO-d_6

No.	Merocyclophane B (**2**)		
	δ_C[a]	δ_H	mult. (*J* in Hz)
1	28.7	2.86	m
2	37.6	1.22	m
		1.44	m
3	29.0	0.62	m
		0.94	m
4	30.3	0.84	m
		1.24	m
5	28.9	0.66	m
		0.94	m
6	33.0	1.27	m
		1.89	m
7	34.3	3.06	m
8	113.8		
9	155.4		
10	102.5	5.97	s
11	144.3		
12	107.3	5.95	s
13	156.7		
14	39.6	2.26	
15	38.6	1.21	m
		1.40	m
16	29.0	0.62	m
		0.94	m
17	30.3	0.84	m
		1.24	m
18	28.9	0.69	m
		0.95	m
19	33.1	1.32	m
		1.63	m
20	35.5	2.80	br m
21	nd[b]		
22	nd[b]		
23	132.6	6.30	br s
24	149.1		
25	nd[b]		
26	nd[b]		
27	32.8	1.45	m
		1.80	m
28	29.7	1.05	m
		1.12	m
29	21.9	1.19	m
30	13.8	0.79	t (7.3)
31	32.9	1.40	m
		1.70	m
32	29.7	1.05	m
		1.12	m
33	21.9	1.19	m
34	13.8	0.79	t (7.3)
35	20.0	1.01	br d
36	22.4	1.08	d (6.9)
9-OH		8.53	br s
13-OH		8.54	br s
26-OH		10.24	br s

[a]assigned from the HSQC and HMBC spectra, nd[b]: no signals observed at 25°C presumably due to signal broadening

3.3 Antiproliferative activity of merocyclophanes A and B

Merocyclophanes A and B (**1** and **2**) were tested for their antiproliferative activity against the HT-29 human colon cancer cell line. Both **1** and **2** displayed antiproliferative activity with IC_{50} values of 3.3 μM and 1.7 μM, respectively. Merocyclophanes A and B (**1** and **2**) possessed similar levels of antiproliferative activity as those reported for cylindrocyclophanes A –F against various cell lines (0.5 – 5 μg/mL). A SAR study on cyclindrocyclophane A suggested that the 2,5-dialkylresorcinol moiety was the pharmacophore needed for the antiproliferative activity of cylindrocyclophanes, and that the activity was significantly enhanced by the presence of [7.7]paracyclophane core structure (Yamakoshi et al, 2009). The structure of merocyclophane A (**1**) differs from that of cyclindrocyclophane A by the position of methyl groups and the lack of alkyl hydroxy groups; however, both compounds showed a similar level of activity. This indicates that replacement of the hydroxyl groups at C-1/14 or C-2/15 by methyl groups does not significantly change the antiproliferative activity of natural [7.7]paracyclophanes.

3.4 Taxonomic identification of the UIC 10062 strain

Taxonomic identification of the strain UIC 10062 was conducted on the basis of microscopic examination and phylogenetic analysis using a 16S rRNA gene sequence. Microscopic observation of the cultured UIC 10062 suggested this strain to be a *Nostoc* sp. (see Supplementary data) (Wehr et al., 2003; Castenholz et al., 2001). For phylogenetic analysis, a nearly 1.3 kb sequence of the partial PCR-amplified 16S rRNA gene of UIC 10062 was aligned with the 16S rRNA gene sequences of *Bergey's* reference strains and other related species retrieved from GenBank. Phylogenetic trees were constructed using three different methods (neighbor-joining, minimum evolution and maximum parsimony) and showed nearly identical topology, particularly in the clade that includes UIC 10062, with very similar bootstrap values (the neighbor-joining tree shown in Figure 3.6). The resulting phylogenetic tree indicated that UIC 10062 formed a monophyletic clade with *Nostoc* sp. GSV224, *Nostoc* sp. ATCC53789, *Nostoc* sp. PCC9305 and *Nostoc punctiforme* PCC73102 (the *Bergey's* reference strain for *Nostoc* cluster 1), and

thus UIC 10062 was designated within this cluster. The comparison of 16S rRNA gene sequences among three [7.7]paracyclophane-producing cyanobacteria (*Nostoc* sp. UIC 10062, *Nostoc* sp. UIC 10022A and *Cylindrospermum licheniforme* UTEX 2014) showed that variation in 16S rRNA gene sequences did not correlate with chemical variability. The two genetically quite distant strains of *Nostoc* sp. UIC 10022A and *C. licheniforme* UTEX 2014 (5% sequence divergence) have been identified to produce cylindrocyclophanes. However, the 16S rRNA gene sequence of *C. licheniforme* UTEX 2014 showed a higher sequence homology to *Nostoc* sp. UIC 10062 (96%) than to UIC 10022A (95%). Merocyclophanes produced by *Nostoc* sp. UIC 10062 have α-branched methyls at C-1/14, which are biosynthetically distinct from the β-branched methyls found in the cyclindrocyclophanes. Also, among these three strains, only *Nostoc* sp. UIC 10022A is known to produce chlorinated cyclophanes. Considering the quite distant phylogenetic relationships of 16S rRNA genes among cyclophane-producing species, it can be hypothesized that there has been a potential horizontal gene transfer between species, and these genes have evolved to have different modification patterns.

Figure 3.5 Morphological description of *Nostoc* sp. UIC10062: The thalli occurred as macroscopic, irregular mats in clusters. The filaments were isopolar with solitary, intercalary heterocysts, intermittent akinetes, and cylindrical with cells organized in trichomes. The trichomes were long, straight or irregularly waved, and covered with a thin, barely visible, muscilageous sheath. The cells were barrel-shaped with a cell length (2-3 µm) to width (1.5-2 µm). Constrictions at the cell cross-walls were observed in which cells were divided perpendicularly to the trichome axis.

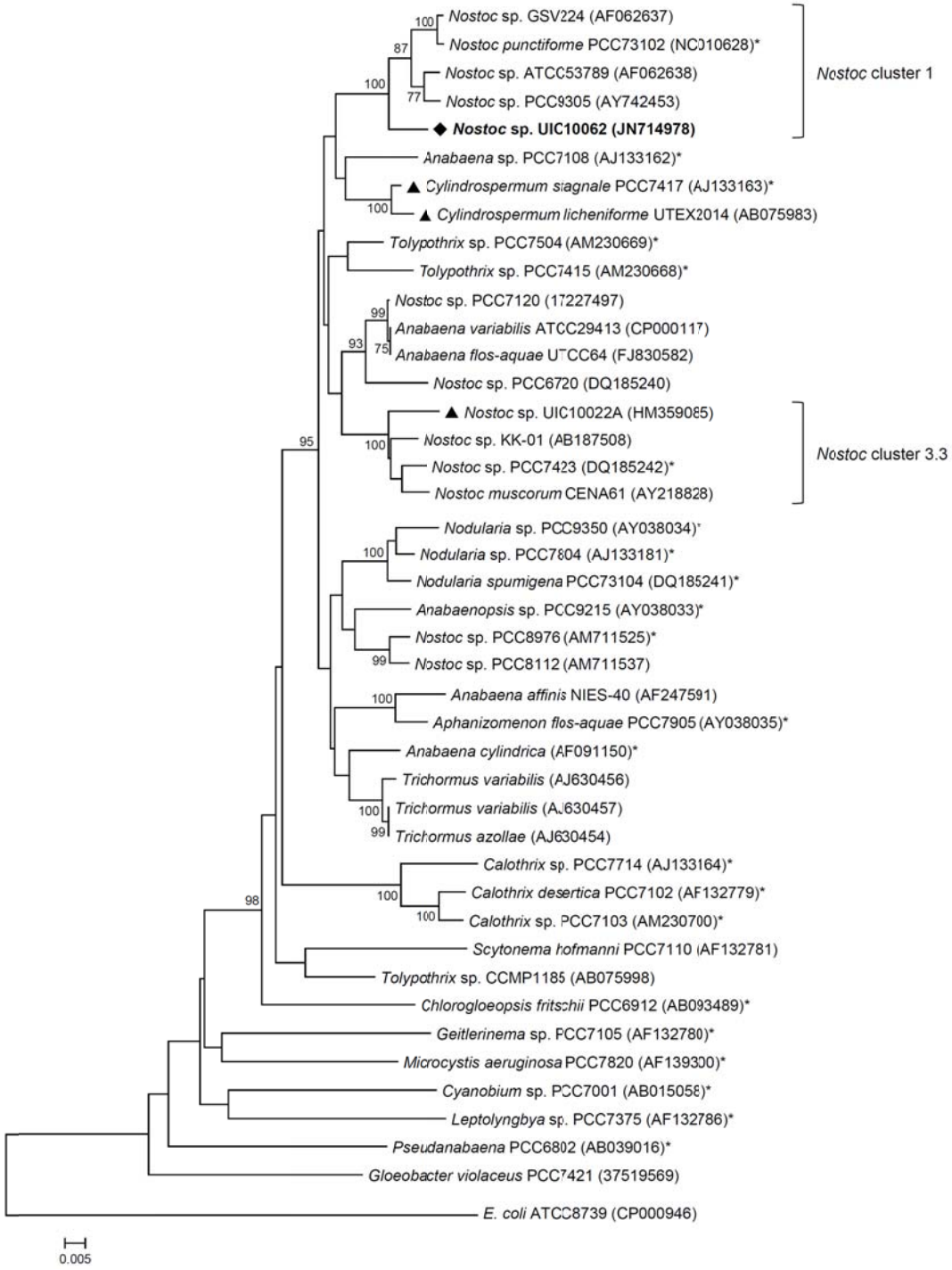

Figure 3.6 Phylogenetic relationships of 16S rRNA genes from cyanobacteria. Evolutionary distances were determined using the neighbor-joining method with 1000 replicate bootstrap resampling to construct the phylogenetic tree. Strains were obtained from NCBI with the accession number given in parentheses. Strains marked with a (*) were obtained as Bergey's reference strains. Cyanobacterial strains previously reported to produce cylindrocyclophanes are denoted by a triangle (▲). Only bootstrap values greater than or equal to 75% are displayed.

3.5 Experimental

3.5.1 General experimental procedures

Optical rotations were measured using a Perkin-Elmer 241 polarimeter. UV spectra were measured on a Shimadzu UV spectrometer UV2401 and scanned from 190 to 360 nm. CD spectra were recorded on a JASCO J-710 CD spectrometer. IR spectra were acquired using a Jasco FTIR-410 Fourier transform infrared spectrometer. 1D and 2D NMR spectra were obtained on a Bruker Avance DRX 600 MHz NMR spectrometer with a 5 mm CPTXI Z-gradient. ^{1}H and ^{13}C NMR chemical shifts were referenced to the solvent signals (MeOH-d_4 and DMSO-d_6). The HMBC spectrum was recorded with the average $^{3}J_{CH}$ of 8 Hz and the HSQC spectrum was measured with the average $^{1}J_{CH}$ of 140 Hz. Low- and high-resolution ESI mass spectra were obtained using a Shimadzu IT-TOF LC mass spectrometer.

3.5.2 Biological material

Nostoc sp. (UIC 10062) was isolated from a sample collected at the north pond of Grand Mere State Park in Michigan in 2007 (N 42°00.679′, W 86°32.417′). The unialgal strain (UIC 10062) was produced through micropipette isolation techniques (Chlipala et al., 2009). The strain was cultured in a 22 L glass flask containing Z media (18 L) with sterile aeration (Falch et al., 1995). Cultures were illuminated with fluorescent lamps at 1.03 klx with an 18/6 h light/dark cycle. The temperature of the culture room was maintained at 22 ºC. After 6 weeks, the biomass of cyanobacteria was harvested by centrifugation and then freeze-dried.

3.5.3 Strain identification

Morphological studies were performed using a cultivated cyanobacterium UIC 10062 with microscopic observation for morphological characterization conducted using a Zeiss Axiostar Plus light microscope equipped with a Canon PowerShot A620 camera. The following parameters were selected to characterize its morphology: thallus morphology, shape of trichome, morphology of terminal cells, shape and arrangement of vegetative cells, presence and arrangement of heterocystes and akinetes (Figure 3.5).

Taxonomic identification of the cyanobacterial specimen was made in accordance with the modern taxonomic system (Komárek et al., 2003).

3.5.4 DNA extraction, PCR amplification and sequencing

Cell mass (258 mg), obtained from a static culture of *Nostoc* sp. (UIC 10062), was centrifuged at 14,000 × *g* for 5 min, and pretreated with lysozyme and proteinase K as follows prior to using the Wizard Genomic DNA purification kit. The cell pellet was re-suspended in lysis buffer (2.5 mL, 10 mM Tris, 0.1M EDTA, 0.5% w/v SDS, 20 μg/mL pancreatic RNase, pH 8.0) containing lysozyme (1 mg/mL) and incubated at 37˚C for 1 hr. To this mixture, proteinase K was added to a final concentration of 100 μg/mL, and incubated at 50˚C for 1 h. After incubation, the cell material was recovered by centrifugation at 14,000 × *g* for 3 min. DNA was extracted from this pretreated cell material using the Wizard Genomic DNA purification kit (Promega), where the protocol was slightly modified to include mechanical disruption after the addition of the nuclei lysis solution (step 6). A portion of the 16S rRNA gene was PCR-amplified using the cyanobacteria-specific primers 106F and 1509R (Martínez-Murcia et al., 1995). For a total volume of 50 μL, the reaction mixture contained DNA (5 μL, approximately 90 ng), Phusion HF Buffer (10 μL, 5x), dNTP mix (1 μL, 10 mM), each primer (1 μL, 10 μM), Phusion high-fidelity DNA polymerase (0.5 μL), and H_2O (31.5 μL). The reaction was performed in a Bio-Rad C1000 thermal cycler as following reaction program: initial denaturation for 30 s at 98˚C, 35 amplification cycles of 10 s at 98˚C, 30 s at 53˚C and 30s at 72˚C, and a final extension for 10 min at 72˚C. PCR products were purified using a MinElute PCR purification kit (Qiagen) and sequenced using the cyanobacteria-specific primers 106F and 1509R as well as the internal primers, 359F and 781R (Nübel et al., 1997). The resulting 16S rRNA gene sequence was deposited in the NCBI GenBank under the accession number JN714978.

3.5.5 Phylogenetic analysis

Phylogenetic and molecular evolutionary analyses were conducted using MEGA 5.0 (Tamura et al., 2011). The resulting sequence chromatograms were visually inspected, and the total sequence of

1,290 nucleotides was aligned with 40 cyanobacterial species retrieved from GenBank as well as *Gloeobacter violaceus* PCC7421 as an outgroup. Cyanobacterial reference strains were firstly selected from *Bergey's Manual* (Castenholz, 2001), and only sequences of at least 1 kb were retrieved from GenBank. Multiple sequence alignment was performed with ClustalW in MEGA 5.0 with standard gap opening and extension penalties. The evolutionary history was inferred using the neighbor-joining (NJ), minimum evolution (ME) and maximum parsimony (MP) methods. One thousand replicates were used to evaluate the robustness of branches in the inferred trees generated. Subgroups with greater than 75% consistency in the tree are labeled at the respective nodes.

3.5.6 Extraction and isolation

Freeze-dried biomass (2.2 g) from 18 L of culture was harvested and extracted with CH_2Cl_2-MeOH (250 mL, 1:1) three times and concentrated *in vacuo* to yield an extract (0.2 g), which was fractionated using Diaion HP-20 resin with iPrOH-H_2O (50 mL) to generate 8 sub-fractions (0:10, 2:8, 4:6, 6:4, 7:3, 8:2, 9:1 and 10:0 v/v). Fractions eluted with iPrOH-H_2O (7:3 v/v, 5.0 mg; 8: 2 v/v, 6.5 mg) were found to be active in the antiproliferative assay against HT-29 cells with IC_{50} values of 0.9 and 1.2 μg/ml, respectively. LC-MS analysis of these fractions indicated the presence of new compounds, and they were subjected to reversed-phase HPLC (Varian C_8 semi-preparative column, 10 mm × 250 mm, 3 mL/min) eluting with gradient of MeOH-H_2O (7:3 to 9:1 v/v for 45 min). Merocyclophanes A and B (**1** and **2**) were eluted at 37.9 min (**1**, 2.4 mg, 0.11%) and 31.6 min (**2**, 0.9 mg, 0.04%), respectively.

Merocyclophane A (1). White amorphous powder; $[\alpha]^{25}_D$ −29 (*c* 0.024, MeOH); UV (MeOH) λ_{max} (log ε) 207 (4.55), 221 (4.02), 272 (3.24) nm; CD (MeOH) λ_{max} ($\Delta\varepsilon$) 213 (-6.40), 227 (-4.35), 277 (-2.73); IR (neat) ν_{max} 2954, 2920, 2851, 1650, 1541, 1507 cm^{-1}; for ^1H and ^{13}C NMR spectroscopic data, see TABLE VI; HRESIMS *m/z* 551.4170 $[M-H]^-$ (cacld for $C_{36}H_{55}O_4$, 551.4100)

Merocyclophane B (2). Purple amorphous powder; $[\alpha]^{25}_D$ – 19 (*c* 0.070, MeOH); UV (MeOH) λ_{max} (log ε) 207 (4.25), 221 (3.98), 273 (3.57), 324 (2.76), 521 (2.59) nm; CD (MeOH) λ_{max} ($\Delta\varepsilon$) 211 (-3.66), 227 (-

2.22), 274 (-2.03) nm; IR (neat) ν_{max} 2955, 2924, 2855, 1664, 1635, 1595, 1527 cm^{-1}; for ^{1}H and ^{13}C NMR spectroscopic data, see TABLE VII; HRESIMS *m/z* 565.3954 $[M-H]^-$ (cacld for $C_{36}H_{54}O_5$, 565.3893)

3.5.7 X-ray crystallographic analysis of merocyclophane A (1)

Crystals for X-ray analysis were grown from CH_3CN. A small single crystal, roughly 30 × 30 × 30 μm, was selected for data collection at sector-22-BM, and encased in Paratone-N oil and cooled to 100K to minimize crystal degradation and X-ray radiation damage. The MAR 225 CCD detector was set at a distance of 85 mm from the crystal using a wavelength of 0.80Å to collect data near a resolution of 0.86 Å. 36 images were collected, each with a rotation sweep of 10°. The images were indexed, and the intensities were integrated and scaled with XDS (Kabsch, 1993). The WinGX package was used for structure solution and refinement. The space group was identified as C2 with one molecule in the asymmetric unit (Farrugia, 1999). SHELX was used for structure solution and refinement on F2. Six CH_3CN molecules were found in the asymmetric unit, with two of them sitting on 2-fold axes. Four CH_3CN molecules are each involved in hydrogen bonding with the four aromatic hydroxyl groups; the remaining two CH_3CN molecules reside in channels formed at the interface of the larger macrocycles as they pack together in the unit cell. Crystal data: $C_{36}H_{56}O_4 \cdot 5CH_3CN$, MW = 758.1, monoclinic, space group C2 (5); *a* = 14.735 (2) Å, *b* = 10.840 (5) Å, *c* = 29.842 (3) Å, β = 95.226 (4)°, *V* = 4747 (2) $Å^3$; Z = 4, D_c = 0.057 mg/m^3; μ = 0.057 mm^{-1}; *F*000 = 1656. Reflections collected / unique = 13719 / 5724 (R_{int} = 0.0815); final R1 = 0.0882, wR2 = 0.2285 for reflections with I > 2σ(I); R1 = 0.1311, wR2 = 0.2572 for all unique data. Crystallographic data (ID No. 818958) have been deposited with the Cambridge crystallographic Data Centre. Copies of the data can be obtained, free of charge, on application to the Director, CCDC, 12 Union Road, Cambridge CB2 1EZ, UK (e-mail: deposit@ccdc.cam.ac.uk).

3.5.8 HT-29 antiproliferative assay

The antiproliferative activity of merocyclophanes A (**1**) and (**2**) against the HT-29 cancer cell line was evaluated according to a previously established protocol (Seo et al., 2001).

CHAPTER 4:

SANCTOLIDE A, A 14-MEMBERED PK-NRP HYBRID MACROLIDE FROM THE CULTURED CYANOBACTERIUM *Oscillatoria Sancta* (SAG 74.79)

4.1 Introduction

Polyketide-nonribosomal peptide (PK-NRP) hybrids represent a major class of cyanobacterial secondary metabolites (Singh, et al., 2005). Diverse cyanobacterial metabolites belonging to this class have been isolated from both freshwater and marine cyanobacteria. A major group of cyanobacterial PK-NRP hybrid metabolites is lipopeptides, where linear or cyclic peptides contain one lipophilic residue of polyketide origin such as *β*-amino acid and *N*-acyl residues (Van Wagoner et al., 2007). Another subclass of cyanobacterial PK-NRP hybrid metabolites is comprised of macrolides whose building blocks are mainly acetates with one or two amino acids incorporated into their macrolide ring structures. These compounds are less commonly found in cyanobacteria. Examples include laingolide, laingolides A and B, madangolide and palmyrolide A, all of which have 15-membered macrolide rings containing a rare *N*-methyl enamide functionality (Klein et al., 1996, 1999; Pereira et al., 2010; Matthew et al., 2010). These metabolites were all obtained from marine cyanobacteria belonging to the order Oscillatoriales.

In our continuing search for biologically active secondary metabolites from cultured cyanobacteria, the cell extract of *Oscillatoria sancta* (SAG 74.79) was initially evaluated for its activity in a brine shrimp toxicity assay and found to be active. This chapter describes the isolation and structure determination of a 14-membered PK-NRP hybrid macrolide, named sanctolide A (**1**). The planar structure was determined using spectroscopic techniques including HRESIMS, and 1D and 2D NMR analyses. The relative configuration of sanctolide A (**1**) was solved by *J*-based configurational analysis along with NOE correlations, and Mosher ester and chiral HPLC analyses were carried out for the assignment of the absolute configuration.

4.2 Isolation of sanctolide A (1)

Oscillatoria sancta was obtained from the SAG (Sammlung von Algenkulturen Göttingen) culture collection of algae (strain ID: 74.79), and grown in inorganic media (BG-12) (Falch et al., 1995).

The freeze-dried cells were extracted with a mixture of CH_2Cl_2-MeOH (1:1 v/v). This organic extract was fractionated using Diaion HP-20 resin with an increasing amount of iPrOH in water. The fractions eluting at 70%, 80% and 90% iPrOH displayed toxicity against brine shrimp. HPLC-based activity profiling of these fractions using reversed-phase column identified one minor peak as the active component (Figure 4.1). Dereplication by LC-MS and ^{1}H NMR indicated this peak to be a potentially new metabolite with a molecular weight of 439 Da. Scale-up culture (4 × 2L) and re-isolation was performed using the method described above followed by reversed-phase HPLC to yield sanctolide A (**1**, 2.6 mg).

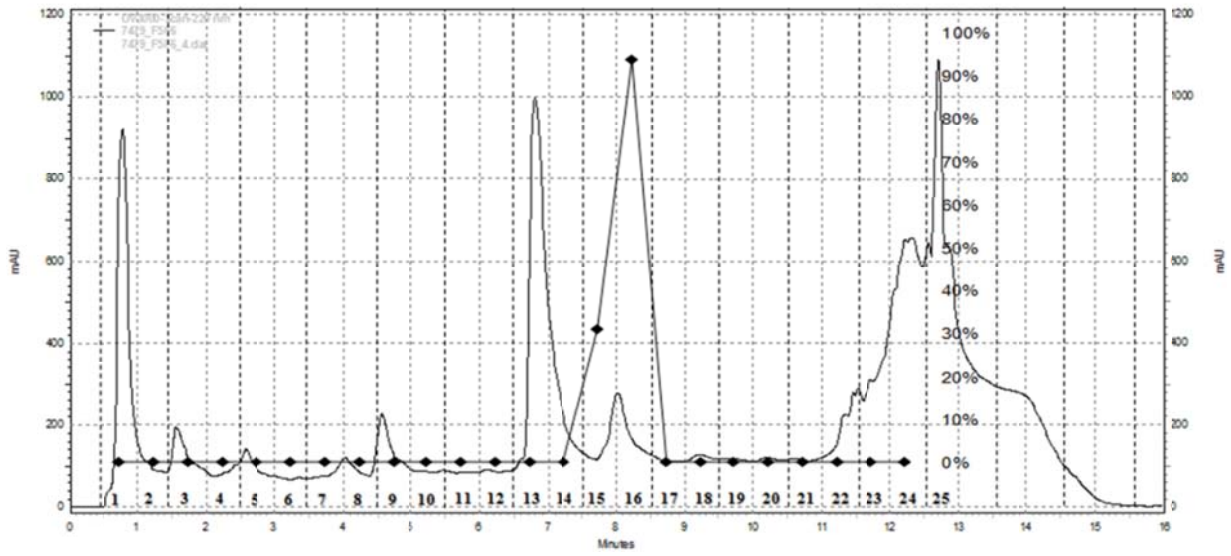

Figure 4.1 HPLC-based activity profiling (UV: 230 nm); ♦ Brine shrimp toxicity (% lethality) **Method**: 50%~70% aqueous MeOH for 10 min; column: onyx C_{18} 4.6×100 mm; flow rate: 4 ml/min; total 24 fractions were collected (0.5 min for one fraction) in a 96-well plate using a fraction collector.

4.3 Structure determination of sanctolide A

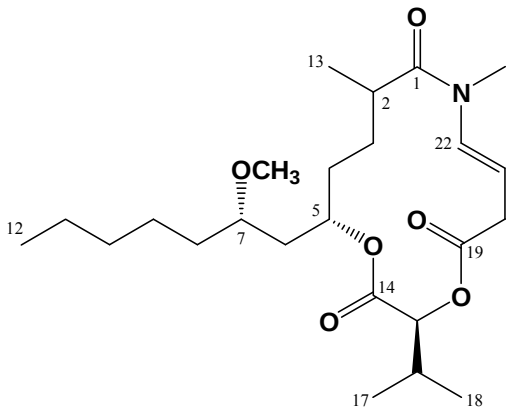

Sanctolide A (**1**)

Sanctolide A (**1**) was obtained as colorless oil. The molecular formula of **1** was established as $C_{24}H_{41}NO_6$ by HRESIMS analysis. Analysis of the ^{1}H NMR spectrum of **1** in combination with the DEPT-Q and HSQC spectra indicated the presence of two olefinic protons (δ_H 6.70 and 5.12), three oxygenated methines (δ_H 5.11, 5.00 and 3.12), one *O*-methyl (δ_H 3.28), one *N*-methyl (δ_H 3.06), two methines (δ_H 2.56 and 2.31), five diastereotopic methylenes (δ_H 2.0 – 1.0), three homotopic methylenes (δ_H 1.28 and 1.24), as well as three dolublet (δ_H 1.13, 0.94 and 0.90) and one triplet methyl (δ_H 0.87) protons. Analysis of the COSY spectrum established three partial structures **1a**, **1b** and **1c** (Figure 4.2). The first partial structure (**1a**) was assembled by sequential COSY correlations from H-2 (δ_H 2.56) to H_3-12 (δ_H 0.87) along with a COSY correlation between H-2 and H_3-13 methyl (δ_H 1.13). Down-field chemical shifts of H-5 (δ_H 5.00) and H-7 (δ_H 3.12) indicated that C-5 and C-7 were oxygenated. The second partial structure (**1b**) was established from COSY correlations between H-15 (δ_H 5.11) and H-16 (δ_H 2.31), and between H-16 and H_3-17/H_3-18 methyl protons (δ_H 0.94/0.90). A downfield chemical shift of H-15 (δ_H 5.11) and the absence of a NH signal indicated this partial structure to be a 2-hydroxyisovaleric acid. COSY correlations between H-20 (δ_H 3.20 and 3.15)/H-21 (δ_H 5.12)/H-22 (δ_H 6.70) determined the last

partial structure as a 1, 3-functionalized propylene (**1c**) possessing the *trans* geometry due to the large $^{3}J_{HH}$ (14.0 Hz) observed between H-21 and H-22.

The three partial structures (**1a**, **1b** and **1c**) were assembled through HMBC correlations (Figure 4.2). An HMBC correlation from the *O*-methyl singlet (δ_H 3.28) to C-7 methine (δ_C 77.7) placed a methoxy group at C-7. The chemical shift of C-14 (δ_C 170.0) combined with HMBC correlations from H-5 (δ_H 5.00) and H-16 (δ_H 2.31) to C-14 allowed the assembly of partial structures **1a** and **1b** via an ester linkage. The connection between substructures **1b** and **1c** was established by HMBC correlations from H-15 (δ_H 5.11) and H-21 (δ_H 5.12) to C-19 (δ_C 168.7), positioning the 2-hydroxyisovaleric acid between **1a** and **1c** via two ester linkages. HMBC correlations from an *N*-methyl singlet (δ_H 3.06) to C-22 (δ_C 132.4) and C-1 (δ_C 174.5), and from H_3-13 (δ_H 1.13) to C-1 linked **1a** and **1c** through the *N*-methyl enamide bridge, completing the assembly of a 14-membered macrolide ring scaffold.

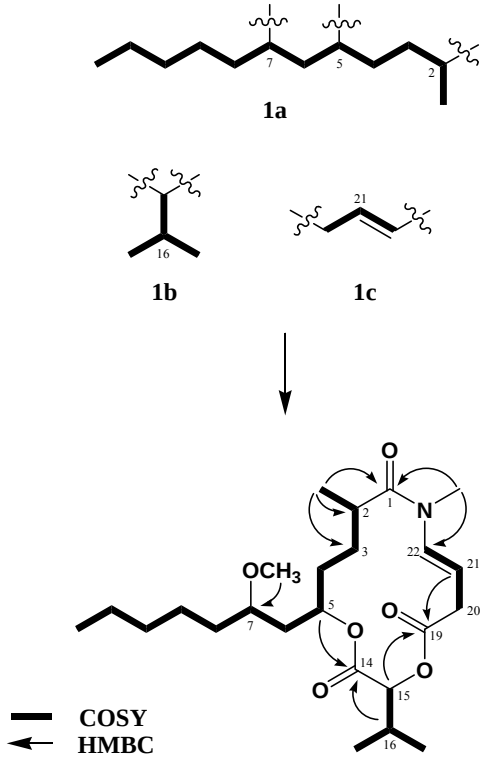

Figure 4.2 Key 2D NMR correlations used for the determination of the planar structure of sanctolide A(**1**).

The relative configuration between C5 and C7 was determined by *J*-based configurational analysis in combination with NOE correlations (Matsumori et al., 1999) (Figure 4.3). Homonuclear ($^3J_{HH}$) and heteronuclear ($^2J_{CH}$ and $^3J_{CH}$) coupling constants were obtained from the DQF-COSY and GBIRD-HSQMBC spectra, respectively (Rance et al., 1983; Williamson et al., 2000). A small $^3J_{H5H6a}$ (3.8 Hz) and a large $^3J_{H5H6b}$ (8.1 Hz) indicated the *gauche* conformation between H-5 and H-6a and the *anti* conformation between H-5 and H-6b, respectively, leaving A3 and A4 as two possible conformations (Figure S4.9: the list of all the possible conformations). An NOE correlation observed between H_2-4 and H-6a indicated A4 to be the only possible conformation, allowing the stereospecific assignments of the diastereotopic protons H-6a/b (Figure 4.3). For the C6-C7 bond, only two conformations B1 and B5 were possible based on a large $^3J_{H6aH7}$ (9.0 Hz) and a small $^3J_{H6bH7}$ (2.9 Hz) (Figure S4.9: the list of all the possible rotamer conformations). An NOE correlation observed between H-6b and H_2-8 and between H-5 and OMe left B1 as the only possible conformation, thus allowing the assignment of the *anti* configuration for the 1,3-methine system at C5-C7.

The relative configuration between C5 and C7 was determined by *J*-based configurational analysis in combination with NOE correlations (Matsumori et al., 1999) (Figure 4.3). Homonuclear ($^3J_{HH}$) and heteronuclear ($^2J_{CH}$ and $^3J_{CH}$) coupling constants were obtained from the DQF-COSY and GBIRD-HSQMBC spectra, respectively (Rance et al., 1983; Williamson et al., 2000). A small $^3J_{H5H6a}$ (3.8 Hz) and a large $^3J_{H5H6b}$ (8.1 Hz) indicated the *gauche* conformation between H-5 and H-6a and the *anti* conformation between H-5 and H-6b, respectively, leaving A3 and A4 as two possible conformations (Figure S4.9: the list of all the possible conformations). An NOE correlation observed between H_2-4 and H-6a indicated A4 to be the only possible conformation, allowing the stereospecific assignments of the diastereotopic protons H-6a/b (Figure 4.3). For the C6-C7 bond, only two conformations B1 and B5 were possible based on a large $^3J_{H6aH7}$ (9.0 Hz) and a small $^3J_{H6bH7}$ (2.9 Hz) (Figure S4.9: the list of all the possible rotamer conformations). An NOE correlation observed between H-6b and H_2-8 and between H-5 and OMe left B1 as the only possible conformation, thus allowing the assignment of the *anti* configuration for the 1,3-methine system at C5-C7.

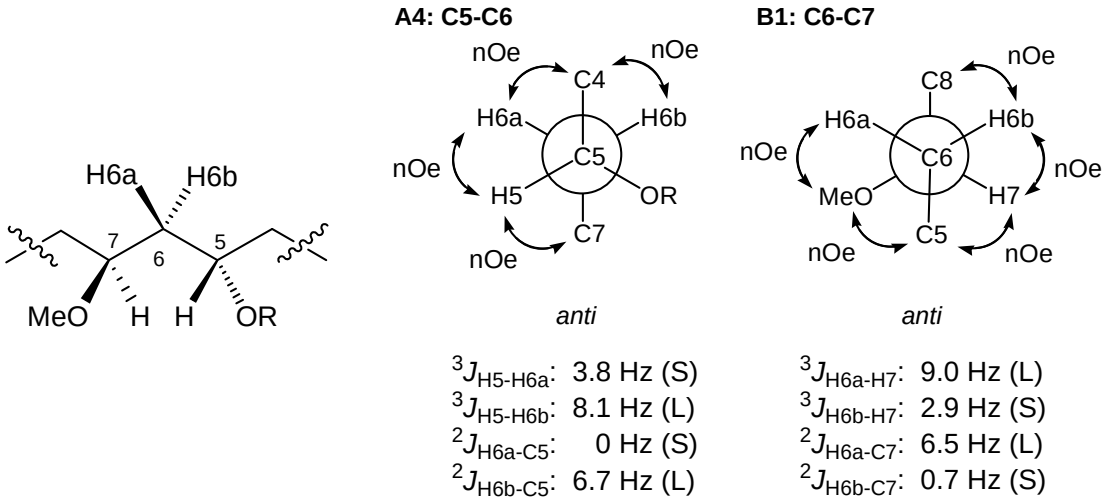

Figure 4.3 Newman projections for A4: C5-C6 and B1: C6-C7. The DQF-COSY and GBIRD-HSQMBC spectra were used for the measurement of homo- and hetero-nuclear coupling constants. Labels in parentheses denote the predicted size of coupling constants: S-small, M-medium and L-large. No correlation observed in the HSQMBC spectrum was assigned as a coupling of 0 Hz. Observed nOe correlations are presented as arched arrows. The list of all the possible rotamer conformations can be found in the appendices.

Determination of the relative configuration for the 1,4-methine system between C-2 and C-5 using NMR methods was complicated as analysis of the NOE spectrum indicated the presence of multiple conformations for the macrolide ring in **1**. The stereogenic proton H-5 showed NOE correlations with all of four diastereotopic protons including H-3a/b and H-4a/b, and a NOESY experiment recorded with a short mixing time (200 ms) verified these cross-peaks to be real NOE correlations as opposed to artifacts arising from spin diffusion. Therefore, the possible relative configuration for the 1,4-methine system at C2-C5 was suggested by NOE correlations in combination with *J*-coupling analysis (Figure 4.4). The methine proton H-2 showed NOE correlations with H-3b/H-4a, suggesting the spatial proximity between these protons, whereas NOE correlations observed between H_3-13 and H-3a/H-4b indicated these protons to be in the same plane, enabling the stereospecific assignments of these two diastereotopic proton pairs. However, the stereogenic methine proton H-5 showed NOE correlations with all four protons of H_2-3a/b and H_2-4a/b. A large $^3J_{H5H4a}$ (7.6 Hz) and a small $^3J_{H5H4b}$ (2.1 Hz) indicated the *anti* conformation between H-4a and H-5, and the *gauche* conformation between H-4b and H-5, respectively, leaving C1 and

C6 as two possible conformations. The observed heteronuclear coupling constants, including a large $^{2}J_{H4a\text{-}C5}$ (5.4 Hz), a small $^{2}J_{H4b\text{-}C5}$ (0 Hz) and a small $^{3}J_{H5\text{-}C3}$ (1.9 Hz) corresponded with the C1 conformation (Figure 4.4). Thus, the *erythro* configuration was suggested for the 1,4-methine system C2-C5: however the opposite configuration could not be completely excluded. The NOE correlation observed between H-5 and H-4a, as well as the value of $^{3}J_{H4aH5}$ (7.6 Hz) close to the reported boundary between large and medium values, are likely due to the minor contribution from the C2 conformation as shown in Figure 4.4.

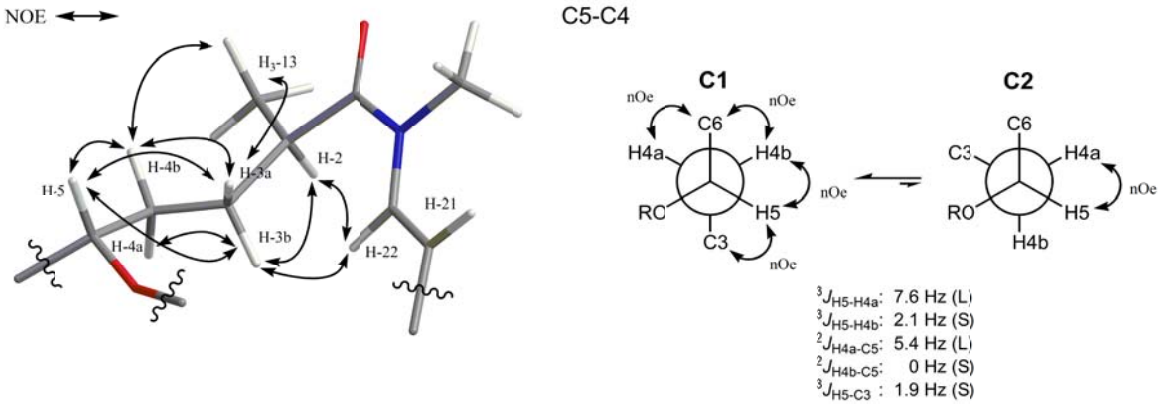

Figure 4.4 Key nOe correlations and a possible conformation of the C5-C4 fragment supporting the *erythro* configuration between C-2 and C-5 in **1**. Labels in parentheses denote the predicted size of coupling constants: S-small; L-large. No correlation observed in the HSQMBC spectrum was assigned as a coupling of 0 Hz. All the possible rotamers are listed in the appendices.

The absolute configuration at C-5, C-7 and C-15 was established by Mosher ester and chiral HPLC analyses (Figure 4.5). ^{1}H NMR and LC-MS analyses indicated that acid hydrolysis of sanctolide A (**1**) resulted in the formation of **2** due to the labile nature of an enamide moiety under acidic conditions, similar as reported for palmyrolide A (Pereira et al., 2010). The isolation of **2** from the acid hydrolysate was necessary for Mosher ester analysis, but challenging due to the lack of a chromophore. Alternatively, solvolysis of **1** was carried out using sodium methoxide in MeOH, and the resulting product was dried *in vacuo* for 24 hrs. ^{1}H NMR and LC-MS analyses identified the presence of **2** as a sole product probably due to volatile nature of the other methyl ester products. The resulting solvolysis product was then sub-

jected to Mosher ester analysis. Two equal portions of **2** were derivatized with (*R*)- and (*S*)-MTPA chlorides at C-5 to yield (*S*)- and (*R*)-MTPA esters (**2S** and **2R**), respectively. Interpretation of the ^{1}H NMR chemical shift differences ($\Delta\delta_{S\text{-}R}$) between **2S** and **2R** assigned the *S* configuration to C-5, thereby leading to the assignment of the absolute configuration as 5*S*,7*S*. The absolute configuration of the remaining 2-hydroxyisovaleric acid residue (**3**) was assigned by chiral HPLC analysis of the acid hydrolysate. Comparison of the retention times between the acid hydrolysate of **1** and two authentic standards *L*- and *D*-2-hydroxyisovaleric acids allowed the absolute configuration of **3** to be assigned as *L*.

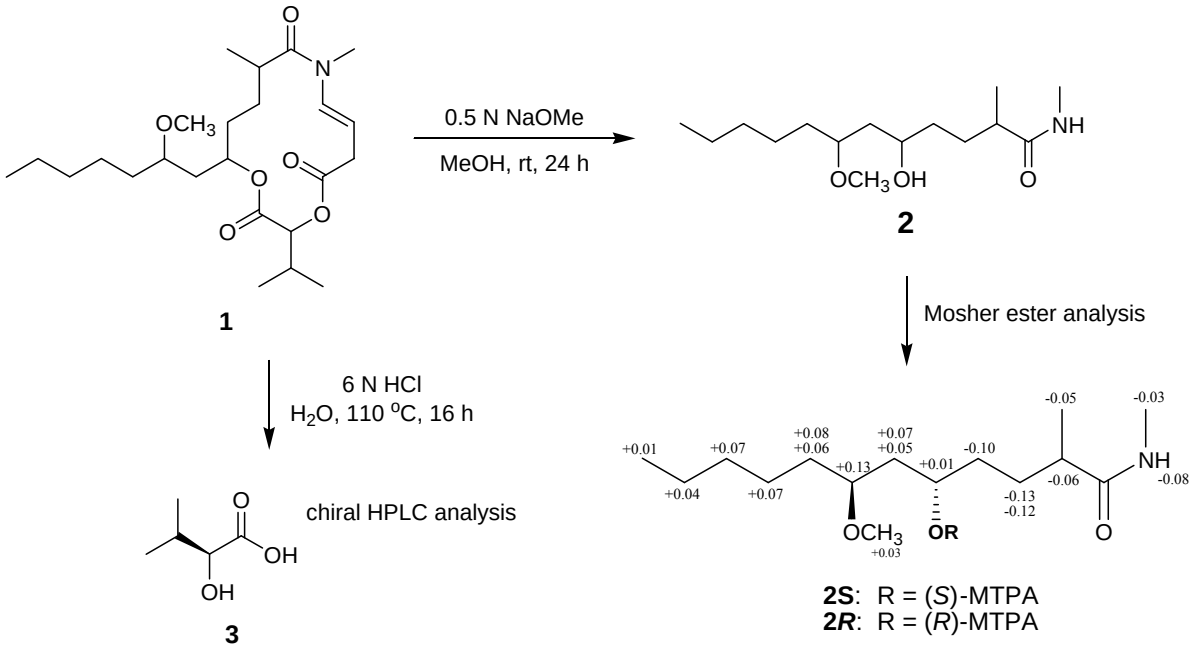

Figure 4.5 Methanolysis and acid hydrolysis for the absolute configuration of sanctolide A (**1**) at C-5 and C-15; $\Delta\delta_{S\text{-}R}$ values ($\Delta\delta_{S\text{-}R} = \delta_S - \delta_R$) for the MTPA esters **2S** and **2R**.

4.4 Biological activity of sanctolide A (1)

Sanctolide A (**1**) exhibited moderate toxicity to brine shrimp with an LD_{50} value of 23.5 μM. Sanctolide A (**1**) was also tested for its cytotoxicity against the HT-29 and MDA-MB-435 cell lines as well as antibacterial activity against *E. coli* and *S. aureus*, but no activity was found in either assay at the

highest concentration tested (25 μg/mL). As observed for other enamide-containing natural products (Klein et al., 1996, 1999; Pereira et al., 2010; Matthew et al., 2010), sanctolide A (**1**) was highly labile and underwent rapid enamide hydrolysis in the presence of water or acid, resulting in an opening of the macrolide ring (Figure 4.6). Pereira et al. proposed the mechanism of enamide hydrolysis in acidic conditions (Pereira et al., 2010). This enamide hydrolysis can also occur in neutral pH in a similar manner and involves the reversible conversion of the eneamide moiety into an iminium ion, which undergoes addition by water followed by proton transfer, leading to the formation of a secondary amide and an aldehyde (Figure 4.7). A degradation experiment indicated that the enamide of sanctolide A (**1**) was completely hydrolyzed in 48 hrs at rt upon addition of water at similar concentrations used in our biological assay systems, indicating that the macrolide ring structure would be degraded during biological evaluation. This labile nature of the enamide moiety in **1** could be explained by the conformational strain of a macrolide ring structure. In linear molecules, the enamide functional group is present as a conjugated system between an amide and a double bond, adopting a flat conformation. However, the flat conformation of the enamide moiety would cause the ring strain of a conformationally flexible 14-membered macrolide, thus would trigger hydrolysis of the enamide moiety into a secondary amide and an aldehyde. The molecular mechanic study of **1** would be required to prove this hypothesis.

Sanctolide A (**1**) features a new class of cyanobacterial macrolides where two amino acid precursors Gly and Val are incorporated into a polyketide chain to form a 14-membered macrolide ring structure. The biosynthesis of sanctolide A (**1**) was proposed as follows: The first step of biosynthesis involves the formation of a hexaketide (C1 – C12) chain by six PKS modules with α-branched methyl (C-13), which is likely originated from *S*-adenosyl-*L*-methionine (SAM) (Jones et al., 2010). This hexaketide chain is further expanded with *N*-methyl glycine by a NRPS module followed by ketide extension by one acetate unit, reduction, dehydration and double bond isomerization, resulting in the formation of the C21-C22 enamide functionality as proposed for the palmyrolide A (Pereira et al., 2010). The 2-hydroxyisovaleric acid linked to the hydroxyl group at C-5 is likely formed by transamination of Val followed by reduction

(Jones et al., 2010). The cyclization between C-15 hydroxyl and C-19 carboxyl group is likely to occur in a final step, thus completing the proposed biosynthesis of sanctolide A (**1**).

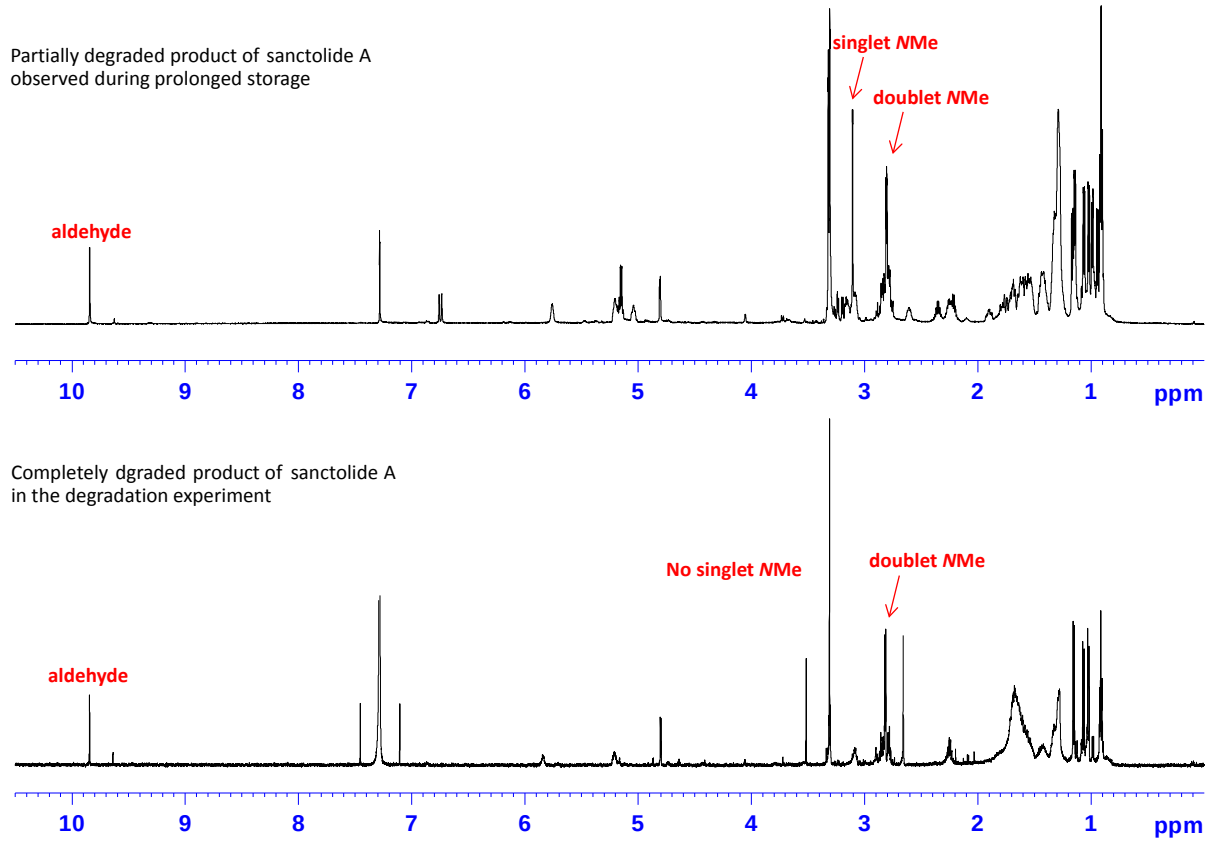

Figure 4.6 ^{1}H NMR spectra (600 MHz, $CDCl_3$) of the partially and completely degraded products of sanc tolide A (**1**).

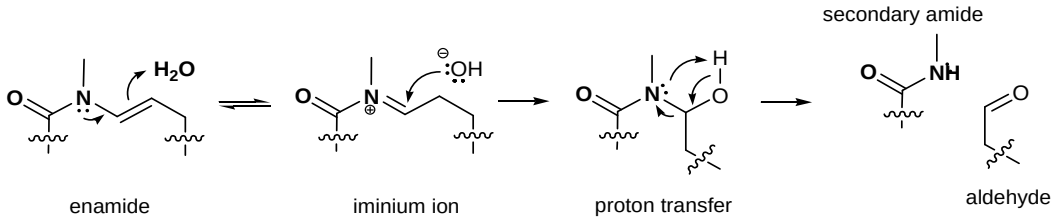

Figure 4.7 Proposed enamide hydrolysis of sanctolide A (**1**) in neutral pH that leads to ring-opening of th e macrolide ring structure.

TABLE VIII: NMR SPECTROSCOPIC DATA FOR SANCTOLIDE A IN $CDCl_3$

		sanctolide A (**1**)					
		δ_C [a, c]	δ_H [b,c]	mult.(*J* in Hz)	COSY[b]	HMBC[b]	NOESY[b,d]
1		174.5					
2		38.1	2.56	m	3, 13	1, 3, 4, 13	3b, 4a, 13, 22
3	a	29.2	1.21	m	2, 4	1, 2, 4, 5, 13	3b, 4b, 13
	b		1.68	m			2, 3a, 4a, 5
4	a	34.1	1.42	m	3, 5	2, 3	3b, 4b, 13
	b		1.86	m			3a, 4a, 5, 13
5		73.3	5.00	m	4, 6	3, 4, 6, 7, 14	3a, 3b, 4a, 4b, 6a, 6b, 7, *O*Me
6	a	40.3	1.59	ddd (14.4, 9.0, 4.2)	5, 7	4, 5, 7, 8	4a, 4b, 6b, 7, *O*Me
	b		1.74	ddd (14.4, 7.8, 3.0)			6a, 5, 7, 8a, 8b
7		77.7	3.12	m	6, 8	5, 6, *O*-Me	5, 6a, 6b, 7, 8a, 8b
8	a	33.2	1.37	m	7, 9	6, 7, 9, 10	6a, 6b, 8b
	b		1.50	m			6b, 7, 8a, OMe
9		32.0	1.24	m	8, 10	7, 8, 10, 11	
10		24.3	1.24	m	9, 11	8, 9, 11, 12	
11		22.6	1.28	m	10, 12	9, 10, 12	
12		14.2	0.87	t (7.1)	11	10, 11	
13		14.9	1.13	d (6.9)	2	1, 2, 3	2, 3a, 4a, 4b
14		170.0					
15		77.0	5.11	d (6.4)	16	14, 16, 17, 18, 19	16, 17, 18
16		29.6	2.31	sd (6.8, 6.4)	15, 17, 18	14, 15, 17, 18	15, 17, 18
17		18.6	0.94	d (6.8)	16, 18	15, 16, 18	
18		17.2	0.90	d (6.8)	16, 17	15, 16, 17	
19		168.7					
20		34.5	3.15	dd (6.5, 1.3)	21	19, 21, 22	21, 22
			3.20	d (6.9)			
21		102.7	5.12	m	20	19, 20, 22	20, 22, *N*Me
22		132.4	6.70	d (14.0)	21	1, 20, N-Me	2, 3b, 20, 21, *N*Me
O-Me		56.6	3.28	s		7	5, 6a, 8a, 8b, 17
N-Me		30.6	3.06	s		1, 22	21, 22

[a] assigned using the DEPT-Q spectrum recorded at 226 MHz, [b] recorded at 600 MHz, [c] chemical shifts were referenced to the $CDCl_3$ solvent signals (δ_H 7.24 and δ_C 77.2). [d] mixing time: 600 ms

4.5 Experimental

4.5.1 General Experimental Procedures

Optical rotations were measured using a Perkin-Elmer 241 polarimeter. UV spectra were measured on a Shimadzu UV spectrometer UV2401 and scanned from 190 to 360 nm. CD spectra were recorded on a JASCO J-710 CD spectrometer. IR spectra were acquired using a Jasco FTIR-410 Fourier transform infrared spectrometer. 1D and 2D NMR spectra were obtained on a Bruker Avance DRX 600 MHz NMR spectrometer with a 5 mm CPTXI Z-gradient. ^{1}H and ^{13}C NMR chemical shifts were referenced to the solvent signals (MeOH-d_4 and DMSO-d_6). The HMBC spectrum was recorded with the average $^{3}J_{CH}$ of 8 Hz and the HSQC spectrum was measured with the average $^{1}J_{CH}$ of 140 Hz. Low- and high-resolution ESI mass spectra were obtained using a Shimadzu IT-TOF LC mass spectrometer.

4.5.2 Biological material

Oscillatoria sancta was acquired from the SAG Culture Collection of Algae at the University of Göttingen (strain ID: SAG 74.79). The cyanobacterium was grown in four 2.8 L Fernbach flasks each containing 2 L of inorganic media (BG-12) (Falch et al., 1995). Cultures were static and illuminated with fluorescent lamps at 1.03 klx with an 18/6 h light/dark cycle. The temperature of the culture room was maintained at 22 ºC. After 6-8 weeks, the biomass was harvested by centrifugation and freeze-dried.

4.5.3 Extraction and isolation

The freeze-dried biomass (1.4 g) from the total 4 L culture was harvested and extracted with CH_2Cl_2-MeOH (1:1) and concentrated in vacuo to yield 91.12 mg of extract. The extract was fractionated using Diaion HP-20 resin with an increasing amount of iPrOH in H_2O to generate 8 sub-fractions (0, 20, 40, 60, 70, 80, 90, 100 % aqueous iPrOH). The brine shrimp toxicity was traced to fractions 5 and 6. These active fractions were further fractionated on an Onyx ODS column (4.6 × 100 mm, 4 ml/min) eluting with MeOH gradient in water from 50% to 70% for 10 min to give 24 sub-fractions, which were tested on the brine shrimp toxicity assay. Activity profiling associated the HPLC chromatogram with the

brine shrimp toxicity and identified the presence of a minor active peak. LC-MS and ^{1}H NMR analyses indicated this peak to be a potentially new compound. For the structure determination, a scale-up culture was performed under static conditions, and re-isolation was achieved using the method described above. The fractions containing the active peak were combined and subjected to reversed-phase HPLC (Varian C_8 semi-preparative column, 10 mm × 250 mm, 3 mL/min) eluting with gradient using aqueous MeOH from 70 to 90 % for 45 min. Sanctolide A (**1**) was eluted at 34.2 min (**1**, 2.6 mg).

Sanctolide A (1). colorless oil; $[\alpha]^{25}_{D}$ - 41 (*c* 0.1, MeOH); UV (MeOH) λ_{max} (log ε) 234 (3.77) nm; IR (neat) ν_{max} 2964, 2928, 1736, 1678, 1638 cm^{-1}; 1D and 2D NMR data, see TABLE VIII; HRESIMS *m/z* 440.3005 $[M+H]^+$ (calcd for $C_{24}H_{41}NO_6$, 440.3012)

4.5.4 Methanolysis of sanctolide A (1)

A portion of **1** (1.2 mg) was treated with 1 mL of 0.5 N NaOMe in MeOH and stirred for 24 h at 25°C. The resulting mixture was extracted with CH_2Cl_2 two times and dried *in vacuo* overnight to give 0.8 mg of **2** as a sole product. **Compound 2:** colorless oil; ^{1}H NMR data (600 MHz, $CDCl_3$) δ 5.58 (1H, m, NH), 3.87 (1H, m, H-5), 3.44 (1H, m, H-7), 3.34 (3H, s, OCH_3), 2.78 (3H, d, J = 4.6 Hz, NCH_3), 2.23 (1H, m, H-2), 1.73 (1H, m, H-3b), 1.67 (1H, ddd, J = 14.6, 8.9 and 2.9 Hz, H-6b), 1.60 (1H, m, H-8a), 1.52 (1H, ddd, J = 14.6, 6.4 and 1.4 Hz, H-6a), 1.44 (1H, m, H-3a), 1.43 (2H, m, H_2-4), 1.42 (1H, m, H-8a), 1.28 (2H, m, H_2-11), 1.27 (2H, m, H_2-9), 1.27 (2H, m, H_2-10), 1.13 (3H, d, J = 6.9 Hz, H_3-13), 0.87 (3H, t, J = 7.0 Hz, H_3-12); HRESIMS *m/z* 274.2386 $[M+H]^+$ (calcd for $C_{15}H_{32}NO_3$, 274.2382)

4.5.5 Mosher ester analysis of 2

(*S*)-MTPA ester of 2 (2S): Compound **2** (0.4 mg) was dissolved in 200 μL of dry CH_2Cl_2. Then, 5 μL of (*R*)-MTPA chloride and catalytic amount of DMAP were added into the solution. After standing overnight at room temperature, the reaction mixture was concentrated *in vacuo* and re-dissolved in MeOH. The product was purified by reversed-phase ODS HPLC using a gradient from 75 to 95 % aqueous MeOH for 40 min to yield 0.3 mg of **2S**. (*S*)-MTPA ester (**2S**): colorless oil; ^{1}H NMR data (600 MHz,

$CDCl_3$) δ 7.48 – 7.56 (2H, m, Ar-H), 7.39 – 7.41 (3H, m, Ar-H), 5.31 (1H, m, NH), 5.30 (1H, m, H-5), 3.60 (3H, s, OCH_3), 3.26 (3H, s, OCH_3), 3.06 (1H, m, H-7), 2.74 (3H, d, J = 4.9 Hz, NCH_3), 2.07 (1H, m, H-2), 1.73 (1H, ddd, J = 14.7, 9.3 and 2.8 Hz, H-6b), 1.58 (1H, m, H-6a), 1.53 (2H, m, H_2-4), 1.52 (1H, m, H-3b), 1.49 (1H, m, H-8b), 1.35 (1H, m, H-8a), 1.28 (2H, m, H_2-11), 1.24(1H, m, H-3a), 1.24 (2H, m, H_2-9), 1.24 (2H, m, H_2-10), 1.03 (3H, d, J = 6.9 Hz, H_3-13), 0.86 (3H, t, J = 7.3 Hz, H_3-12); HRESIMS *m/z* 512.2592 $[M+Na]^+$ (calcd for $C_{25}H_{38}NO_5Na$, 512.2600)

(*R*)-MTPA ester of 2 (2R): Compound **2R** was prepared from **2** and (*S*)-MTPA chloride in the same manner as described for **2S.** (*R*)-MTPA ester (**2R**): colorless oil; ^{1}H NMR data (600 MHz, $CDCl_3$) δ 7.48 – 7.56 (2H, m, Ar-H), 7.39 – 7.41 (3H, m, Ar-H), 5.39 (1H, m, NH), 5.29 (1H, m, H-5), 3.60 (3H, s, OCH_3), 3.23 (3H, s, OCH_3), 2.93 (1H, m, H-7), 2.77 (3H, d, J = 4.9 Hz, NCH_3), 2.13 (1H, m, H-2), 1.66 (1H, ddd, J = 14.6, 9.5 and 2.5 Hz, H-6b), 1.64 (1H, m, H-3b), 1.63 (2H, m, H_2-4), 1.53 (1H, m, H-6a), 1.43 (1H, m, H-8b), 1.37 (1H, m, H-3a), 1.27 (1H, m, H-8a), 1.24 (2H, m, H_2-11), 1.17 (2H, m, H_2-9), 1.17 (2H, m, H_2-10), 1.08 (3H, d, J = 6.9 Hz, H_3-13), 0.85 (3H, t, J = 7.2 Hz, H_3-12); HRESIMS *m/z* 512.2595 $[M+Na]^+$ (calcd for $C_{25}H_{38}NO_5Na$, 512.2600)

4.5.6 Chiral HPLC analysis of 2-hydroxyisovaleric acid (3)

Absolute configuration of the 2-hydroxyisovaleric acid residue (**3**): A portion of **1** (200 μg) was hydrolyzed in 6 N HCl (1 mL) at 110^{o}C for 16 h. The acid hydrolysate of **1** was evaporated to dryness and then re-dissolved in 200 μL of water. HPLC analysis was carried out on a chiral column by comparing the retention times of the components of the hydrolysate with those of authentic standards. Condition: 15% CH_3CN in 2 mM $CuSO_4$, 1 ml/min, Phenomenex Chirex phase 3126 (4.6 × 250 mm) column; elution times (t_R, min) for standards: *L*-2-hydroxyisovaleric acid (34.2 min), *D*-2-hydroxyisovaleric acid (53.3 min). The acid hydrolysate of **1** exhibited a peak at 34.3 min, corresponding to *L*-2-hydroxyisovaleric acid.

CHAPTER 5:

STIGONEMAPEPTIN, AN AHP-CONTAINING DEPSIPEPTIDE WITH ELASTASE-INHIBITORY ACTIVITY FROM THE BLOOM-FORMING FRESHWATER CYANOBACTERIUM *Stigonema* sp.

5.1 Introduction

A major class of cyanobacterial secondary metabolites is cyclic depsipeptides (Tan, 2007; Van Wagoner et al., 2007; Chlipala et al., 2011). This class of compounds commonly contains modified and unusual amino acid residues. One such example is Ahp (3-amino-6-hydroxy-2-piperidone)-containing depsipeptides, which have been isolated from taxonomically diverse cyanobacteria (Pettit et al., 1989; Matern et al., 2001; Fujii et al., 2002; Kisugi and Okino, 2009; Linington et al., 2007). Production of Ahp-containing depsipeptides has frequently been observed in bloom samples from both marine and freshwater cyanobacteria (Grach-Pogrebinsky et al., 2003; Gesner-Apter et al., 2009; Gunasekera et al., 2009). Due to the ability of Ahp-containing depsipeptides to inhibit serine proteases, their ecological role is believed to be as inhibitors of digestive enzymes and a chemical defense against crustacean predators (Berry et al., 2008). However, studies done by Sedmak *et al*. showed that the Ahp-containing depsipeptide, planktopeptin BL1125, induced cyanobacterial cell lysis, leading to the hypothesis that these protease inhibitors could play an important ecological role by controlling cyanobacterial population density in the natural environment (Sedmak et al., 2008 and 2009).

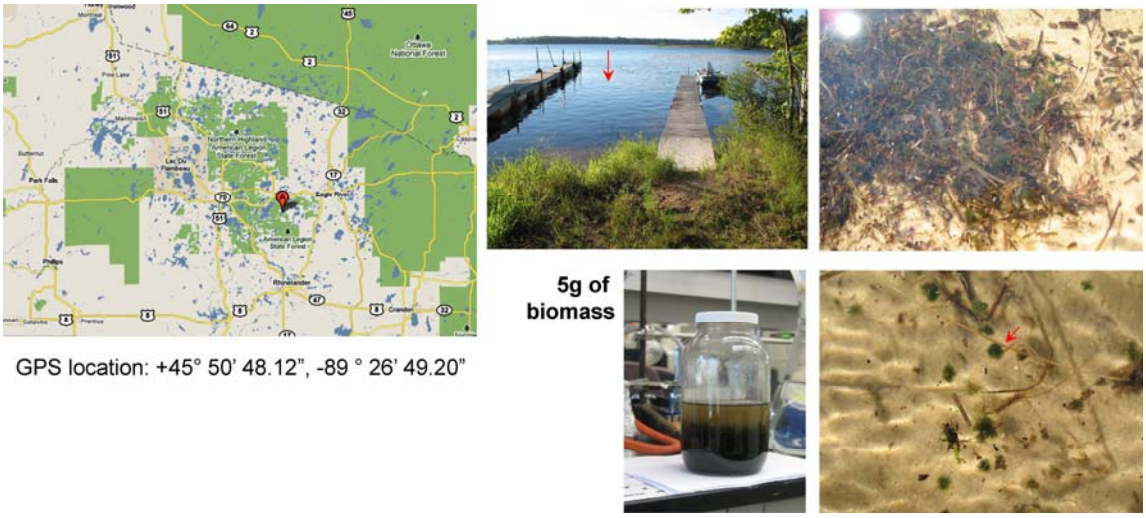

Figure 5.1 The location and photos of the collection site of the sample WI53

Most of the Ahp-containing depsipeptides have shown inhibitory activity against serine proteases such as trypsin, chymotrypsin and elastase with different selectivity depending on variation in their amino acid compositions. Ahp-containing depsipeptides with an Abu (2-amino-2-butenoic acid) residue neighboring the Ahp residue have been found to selectively inhibit elastase as compared to other serine proteases (Matthew et al., 2007; Taori et al., 2007; Kwan et al., 2009). In this chapter, we describe the isolation, structure determination and serine protease inhibitory activity of a new Ahp-containing depsipeptide, named stigonemapeptin (**1**).

5.2 Sample collection and isolation of stigonemapeptin (1)

The sample of the freshwater cyanobacterium (collection ID: WI53) was collected from North Nokomis Lake in the Highland Lake District of northern Wisconsin in August, 2010 (Figure 5.1). Taxonomic identification, carried out on the basis of morphological observation and phylogenetic analysis using 16S rRNA gene sequence, indicated this strain to be *Stigonema* sp. The cyanobacterial cells were manually cleaned from debris and freeze-dried. The freeze-dried cells (5 g) were extracted with a mixture of CH_2Cl_2 and MeOH (1:1). LC-MS analysis of the extract indicated the presence of a potentially new nitrogen-containing compound with a molecular weight of 973.5 Da. The cell extract was subsequently fractionated using Diaion HP-20 resin with an increasing amount of iPrOH in H_2O. The fraction eluting at 40% iPrOH was found to contain the nitrogen-containing compound by LC-MS analysis, and was further purified by reversed-phase HPLC to yield stigonemapeptin (**1**, 4.1 mg, 0.08%).

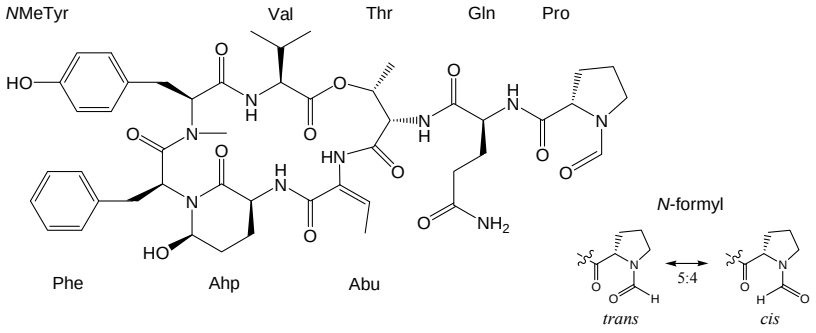

Stigonemapeptin (**1**)

5.3 Structure determination of stigonemapeptin (1)

Stigonemapeptin (**1**) was obtained as a colorless, amorphous powder. The molecular formula of **1** was determined as $C_{48}H_{63}N_9O_{13}$ by HRESIMS analysis. The peptidic nature of **1** was suggested by the signal distribution pattern observed in the ^{1}H NMR spectrum (DMSO-d_6), which included exchangeable amide NH signals (6 - 10 ppm), amino acid α-proton signals (4 - 6 ppm), and aliphatic methylene and methyl signals (0 - 3 ppm). Signal doubling was observed for some of the signals in the ^{1}H NMR spectrum (integration ratio of 5:4), thus implied the presence of two conformers likely arising from one part of the molecule. The structure determination of **1** was carried out using the major conformer. Combined analysis of the COSY and TOCSY spectra identified the structures of six standard amino acids: Val, Tyr, Phe, Thr, Gln and Pro (TABLE IX and Figure 5.2). An HMBC correlation observed from *N*-Me (δ_H 2.76) to Tyr C-2 (δ_C 60.9) indicated that the Tyr residue was *N*-methylated. The presence of an Ahp residue was evident by the appearance of a broad singlet of H-6 (δ_H 5.08) along with sequential COSY correlations from H-6 to NH (δ_H 7.20) and an HMBC correlation from H-6 to C-2 (δ_C 168.9). An amide NH singlet proton signal (δ_H 9.15) and an upfield amide carbonyl carbon signal (δ_C 163.0), as well as a COSY correlation between H-3 (δ_H 5.75) and H-4 (δ_H 1.94), and HMBC correlations from H-3 to C-1 and C-2 (δ_C 128.0), indicated the presence of an Abu residue. An NOE correlation observed between NH and H-3 assigned the *E* geometry to the Abu residue. Lastly, a singlet proton signal (δ_H 8.21), which showed an HSQC correlation with a carbonyl carbon (δ_C 161.2), and HMBC correlations with Pro C-2 (δ_C 57.2) and C-5 (δ_C 46.4), suggested that a formyl group was attached to the amino group of Pro. The complete sequence of eight amino acid residues in **1** was established by combined analysis of the HMBC and ROESY spectra. HMBC correlations from Val NH (δ_H 7.50) and H-2 (δ_H 4.73) to *N*MeTyr C-1 (δ_C 169.4), from *N*-Me (δ_H 2.76) to Phe C-1 (δ_C 170.5), from Phe H-2 (δ_H 4.74) to Ahp C-6 (δ_C 73.8), from Ahp NH (δ_H 7.20) to Abu C-1 (δ_C 163.0) and from Thr H-3 (δ_H 5.38) to Val C-1 (δ_C 172.4), along with a ROESY correlation between Abu NH (δ_H 9.15) and Thr H-2 (δ_H 4.48), established the structure of a cyclic depsipeptide core with an ester linkage formed between the Thr hydroxy and the Val carboxylic acid. This cyclic

depsipeptide core was further branched from Thr NH with the sequence of Gln-Pro-*N*-formyl by HMBC correlations from Thr H-2 (δ_H 4.48) to Gln C-1 (δ_C 172.0) and from Gln NH (δ_H 8.32) to Pro C-1 (δ_C 171.6) along with NOE correlations observed between Thr NH (δ_H 7.74) and Gln H-2 (δ_H 4.29), and between Gln NH and Pro H-2 (δ_H 4.25), completing the planar structure of **1**. The noticeable doubling of NMR signals was observed for the *N*-formylated Pro and Gln residues. These two *N*-formyl proton signals (δ_H 8.21 and 8.08) showed different NOE correlations, one with Pro H_2-5 and the other with Pro H-2, thus indicated that this signal doubling was due to the restricted rotation of the *N*-formyl group between *trans* and *cis* conformations (Figure 5.2). The same phenomenon has been reported for structurally related compounds anabaenopeptilide 202-B and kempopeptin A, possessing *N*-formylated Pro and *N*-acetylated Pro, respectively (Fujii et al., 2002; Taori et al., 2008).

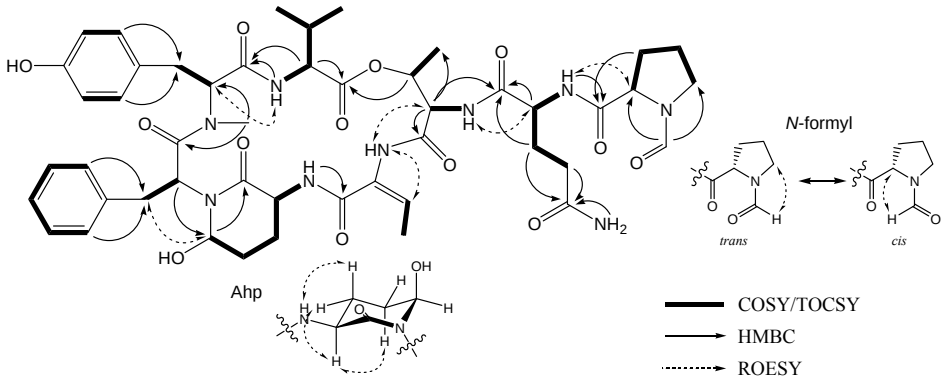

Figure 5.2 Key 2D NMR correlations used for the determination of the planar structure of stigonemapeptin (**1**).

The absolute configurations of the amino acids were assigned using the advanced Marfey's method after acid hydrolysis. Two equal portions of the acid hydrolysate of stigonemapeptin (**1**) were derivatized with L- and DL-FDLA, respectively, and LC-MS comparison between two derivatives assigned an L-configuration for all of the amino acid residues except for the Ahp residue (Figure 5.3). The relative configuration between Ahp C-3 and C-6 was determined by analysis of NOE correlations. A broad singlet proton signal observed for H-6 suggested small coupling constants between H-6 and two diastereo-

topic protons H-5a_{eq} and H-5b_{ax}, indicating H-6 to be in an equatorial position. NOE correlations observed between H-3 and H-5b_{ax}, between NH and H-4b_{ax}, and between H-3 and H-4a_{eq} supported the *chair* conformation of the piperidone ring with the axial hydroxy at C-6 and the equatorial amide NH at C-3 as depicted in Figure 5.2. For the absolute configuration of the Ahp residue, CrO_3 oxidation was carried out prior to acid hydrolysis, and subsequent analysis of the acid hydrolysate by the advanced Marfey's method exclusively identified the presence of L-Glu, thereby assigning the 3*S,6R* configuration to the Ahp residue. This configuration was further supported by nearly identical ^{1}H and ^{13}C NMR chemical shifts of the Ahp residue in stigonemapeptin (**1**) to those reported for the lyngbyastatins and somamides, which shared the same depsipeptide core structure except for the geometry of the Abu residue (Matthew et al., 2007; Taori et al., 2007; Nogle et al., 2001).

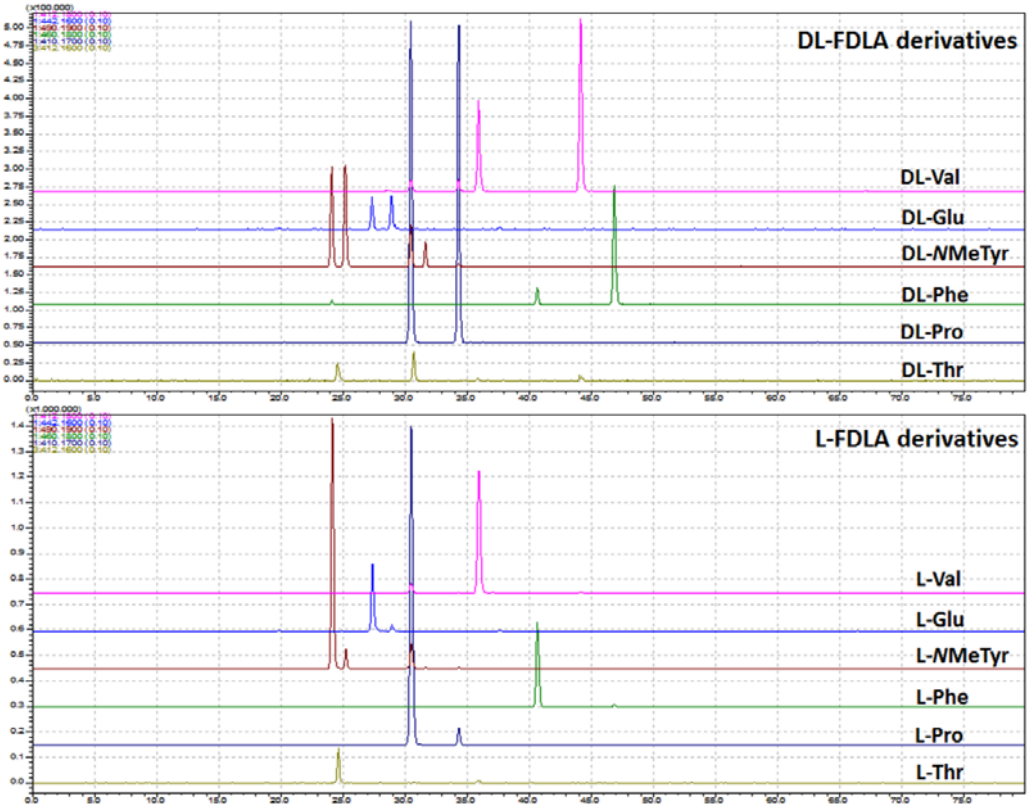

Figure 5.3 Advanced Marfey's analysis of stigonemapeptin (**1**) for the determination of amino acid configurations

TABLE IX: NMR SPECTROSCOPIC DATA FOR STIGONEMAPEPTIN IN DMSO-d_6

		trans conformer			*cis* conformer				
		δ_C[b]	δ_H[a]	mult. (*J* in Hz)	δ_C[b]	δ_H[a]	mult. (*J* in Hz)	HMBC[a]	ROESY[a]
Val	1	172.4			172.4				
	2	56.0	4.73,	overlapped	56.1	4.69,	dd (9.0, 4.2)	1, 1_{NMeTyr}, 3, 4, 5	H-3, H-5, NH
	3	30.8	2.10,	m	30.5	2.09,	m	2, 4, 5	H-2, H-4, H-5
	4	17.2	0.72,	d (6.6)	17.2	0.72,	d (6.6)	2, 3, 5	H-2
	5	19.3	0.86,	d (6.6)	19.3	0.86,	d (6.6)	2, 3, 4	H-2
	NH		7.50,	d (9.6)		7.51,	d (9.0)	1_{NMeTyr}, 2	H-2, H-2_{NMeTyr}
*N*MeTyr	1	169.4			169.4				
	2	60.9	4.86,	dd (11.4, 2.7)	60.9	4.86,	dd (11.4, 2.7)	3, *N*-Me	H-3b, H-5/9, NH_{Val}
	3a	32.8	2.70,	dd (13.2, 11.4)	32.8	2.70,	dd (13.2, 11.4)	2, 4, 5/9	H-2, H-5/9
	3b		3.09,	dd (13.2, 2.7)		3.09,	dd (13.2, 2.7)	2, 4, 5/9	H-2, H-5/9
	4	127.5			127.5				
	5/9	130.4	6.99,	dd (8.4, 1.8)	130.4	6.99,	dd (8.4, 1.8)	3, 5/9, 7	H-2, H-3, H-2_{Phe}
	6/8	115.3	6.77,	d (8.4)	115.3	6.77,	d (8.4)	4, 6/8, 7	
	7	156.3			156.3				
	N-Me	30.5	2.76,	s	30.5	2.76,	s	1_{Phe}, 2	H-2, H-5/9, NH_{Val}
	OH		nd[b]			nd[b]			
Phe	1	170.5			170.5				
	2	50.3	4.74,	overlapped	50.3	4.74,	overlapped	2_{Ahp}, 3, 6_{Ahp}	H-3a, H-3b, H-5/9
	3a	35.3	1.82,	overlapped	35.3	1.82,	overlapped	4, 5/9	H-3b
	3b		2.88,	t (13.8)		2.88,	t (13.8)	2, 4, 5/9	H-2, H-3a, H-5/9, H-6_{Ahp}
	4	136.8			136.8				
	5/9	129.5	6.85,	d (7.8)	129.5	6.85,	d (7.8)	3, 5/9, 7	H-2, H-3, H-$5a_{Ahp}$, H-6_{Ahp}
	6/8	127.8	7.20,	t (7.8)	127.8	7.20,	t (7.8)	4, 6/8	
	7	126.3	7.16,	t (7.8)	126.3	7.16,	t (7.8)	5/9	
Ahp	2	168.9			168.9				
	3	48.0	3.76,	m	48.0	3.76,	m	2, 4	H-4a, NH
	4a	21.8	1.56,	overlapped	21.9	1.56,	overlapped	2, 6	H-3, H-4b
	4b		2.38,	m		2.38,	m		H-4a, NH
	5a	29.2	1.58,	brd (13.2)	29.2	1.58,	brd (13.2)		H-6, H-$5/9_{Phe}$
	5b		1.71,	brd (13.2)		1.71,	brd (13.2)	3, 6	H-3, H-5a, H-6
	6	73.8	5.08,	brs	73.8	5.08,	brs	2, 4	H-5a, H-5b, H-$3b_{Phe}$
	NH		7.20,	overlapped		7.20,	overlapped	1_{Abu}	H-3, H-4b
	OH		nd[b]			nd[b]			
Abu	1	163.0			163.1				
	2	128.0			128.0				
	3	133.4	5.75,	q (7.5)	133.7	5.77,	q (7.5)	1, 2	H-4, NH
	4	13.9	1.94,	d (4.5)	13.9	1.95,	d (7.5)	2, 3	H-3
	NH		9.15,	s		9.29,	s		H-3, H-2_{Thr}, H-3_{Thr}
Thr	1	168.6			168.6				
	2	55.4	4.48,	d (9.0)	55.4	4.50,	d (9.0)	1, 1_{Gln}, 3, 4	H-3, H-4, NH, NH_{Abu}
	3	72.0	5.38,	q (6.5)	72.0	5.41,	q (6.5)	1_{Val}, 4	H-2, H-4
	4	18.3	1.19,	d (6.5)	18.3	1.18,	d (6.5)	2, 3	H-2, H-3
	NH		7.74,	d (9.0)		7.87,	d (9.0)	1_{Gln}	H-2, H-2_{Gln}
Gln	1	172.0			172.1				
	2	52.6	4.29,	m	52.5	4.37,	m	1, 3, 4	H-3b, H-4, NH_{Thr}
	3a	27.0	1.80,	m	27.2	1.80,	m	1, 5	
	3b		1.94,	m		1.96,	m	1, 5	
	4	31.5	2.17,	m	31.6	2.15,	m	2, 3, 5	H-2, H-3b, NH_2
	5	173.9			174.0				
	NH		8.32,	d (7.3)		8.40,	d (7.2)	1_{Pro}	H-2_{Pro}
	NH_2		6.80,	brs		6.79,	brs	5	H-4
			7.27,	brs		7.32,	brs		H-4
Pro	1	171.6			172.1				
	2	57.2	4.25,	dd (8.5, 4.5)	58.9	4.44,	dd (8.2, 3.9)	3, 4	NH_{Gln}, $(H_{N\text{-}formyl})^{cis}$
	3a	29.6	1.85,	m	30.3	1.94,	m		
	3b		2.16,	m		2.14,	m		
	4a	23.7	1.78,	m	22.6	1.81,	m		
	4b		1.89,	m		1.82,	m		
	5a	46.4	3.55,	m	43.8	3.33.	m	2, 3, 4	$(H_{N\text{-}formyl})^{trans}$
	5b		3.61,	m		3.36,	m	2, 3, 4	$(H_{N\text{-}formyl})^{trans}$
N-Formyl	CHO	161.2	8.21,	s	161.5	8.08,	s	2_{Pro}, 5_{Pro}	$(H_2\text{-}5_{Pro})^{trans}$, $(H\text{-}2_{Pro})^{cis}$

[a] Recorded at 600 MHz, [b] Recorded at 226 MHz, [b] nd: not detected probably due to the high content of water in the sample.

5.4 Serine protease inhibitory activity of stigonemapeptin (1)

Many of the Ahp-containing depsipeptides isolated from cyanobacteria have been shown to inhibit serine proteases with different selectivity profiles against trypsin, chymotrypsin and elastase (Figure 5.4). Accordingly, we tested stigonemapeptin (**1**) for its inhibitory activity against these three enzymes. Stigonemapeptin (**1**) showed inhibition of elastase and chymotrypsin with IC_{50} values of 0.26 and 2.93 μM, respectively, whereas no inhibition was found against trypsin at the highest concentration tested (10 μM). This result was in good agreement with activity profiles of known Ahp-containing depsipeptides. Co-crystallographic data of elastase with scyptolin A suggested that the selectivity of this class of compounds for the inhibition of serine proteases varies depending on the type of amino acids located between Ahp and Thr due to different binding preferences to the enzyme's specificity pocket (Matern et al., 2003). Preferences for the inhibition of chymotrypsin and elastase are conferred by a bulky hydrophobic amino acid (Phe, Tyr or Trp) and a small neutral amino acid (Ala, Gly or Val), respectively, whereas a positively charged amino acid (Arg or Lys) is preferred for the inhibition of trypsin. Therefore, the selective inhibitory activity of stigonemapeptin (**1**) against elastase can be attributed to the presence of the Abu residue between Ahp and Thr, as an Abu residue is considered to be relatively small and neutral. Stigonemapeptin (**1**) was also tested for its inhibitory activity against the 20S proteasome and cytotoxicity against HT-29 cancer cells, but showed no activities at the highest concentration tested (25 μM).

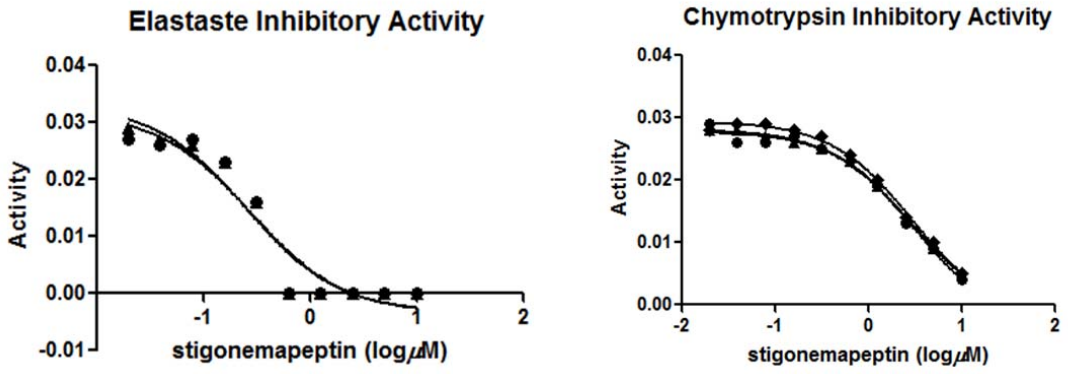

Figure 5.4 Elastase and chymotrypsin inhibitory activity of stigonemapeptin (**1**)

5.5 Taxonomic identification of *Stigonema* sp. WI53

Taxonomic identification of the field-collected sample WI53 was carried out on the basis of morphological observation and phylogenetic analysis using a partial 16S rRNA gene sequence (1.1 Kb) (Figures 5.5 and 5.6). Microscopic observation of the WI53 sample showed the predominance of one filamentous cyanobacterial strain with distinctive true branching pattern, suggesting that this strain belongs to the order Stigonematales. The identity of WI53 was further classified into a *Stigonema* sp. based on the observed morphological similarity to *Stigonema ocellatum* SAG 48.90 represented by the presence of biseriate structures on the true branches as well as on the main trichomes. Phylogenetic analysis of the 16S rRNA gene of WI53 agreed well with the taxonomic identity suggested by morphological analysis. A BLAST search of the partial 16S rRNA gene sequence of WI53 showed the highest sequence homology to that of *Stigonema ocellatum* SAG 48.90 (99%). Due to the lack of the reference strain for the genus *Stigonema*, the 16s rRNA gene sequence of WI53 was aligned with those of other heterocystous cyanobacteria for phylogenetic analysis, most of which were listed in the paper published by Gugger et al (Figure 5.6). The resulting tree revealed that WI53 formed a monophyletic clade with the two *Sigonema ocellatum* strains, SAG 48.90 and SAMA35, which was supported by the high bootstrap value (99 %) and low mean pairwise distance (0.02), clarifying the identity of WI53 as a *Stigonema* sp. The *Stigonema* clade showed quite distant relationships with other clades of the order Stigonematales and showed closer relationships with *Petalonema* sp. and *Nostoc* cluster 1 clade with pairwise distances of 0.04 and 0.05, respectively. As previously recognized, the paraphyletic nature of the order Stigonematales further supports the need for revision of the current cyanobacterial taxonomic system.

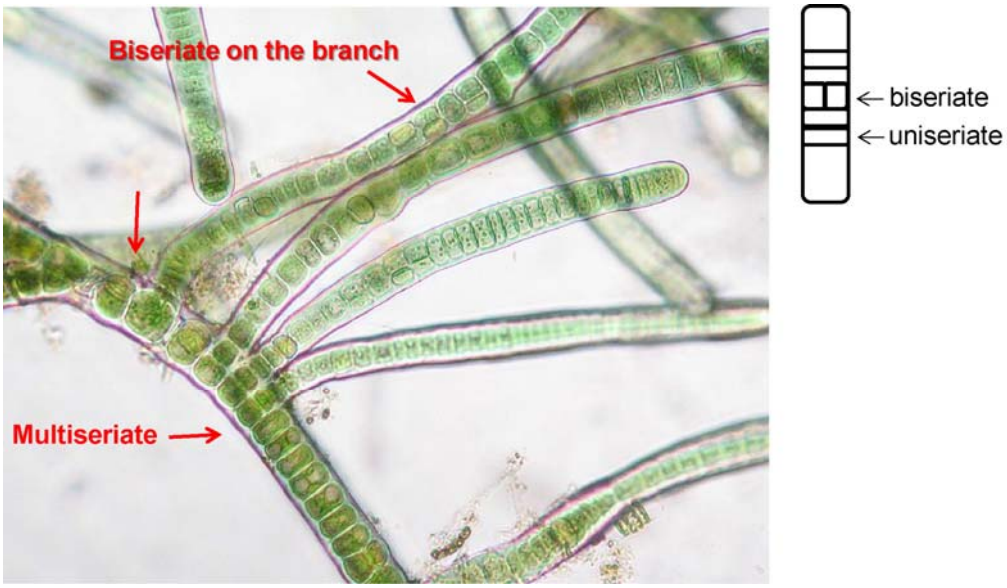

Figure 5.5 Photomicrograph of *Stigonema* sp. (collection ID WI53)

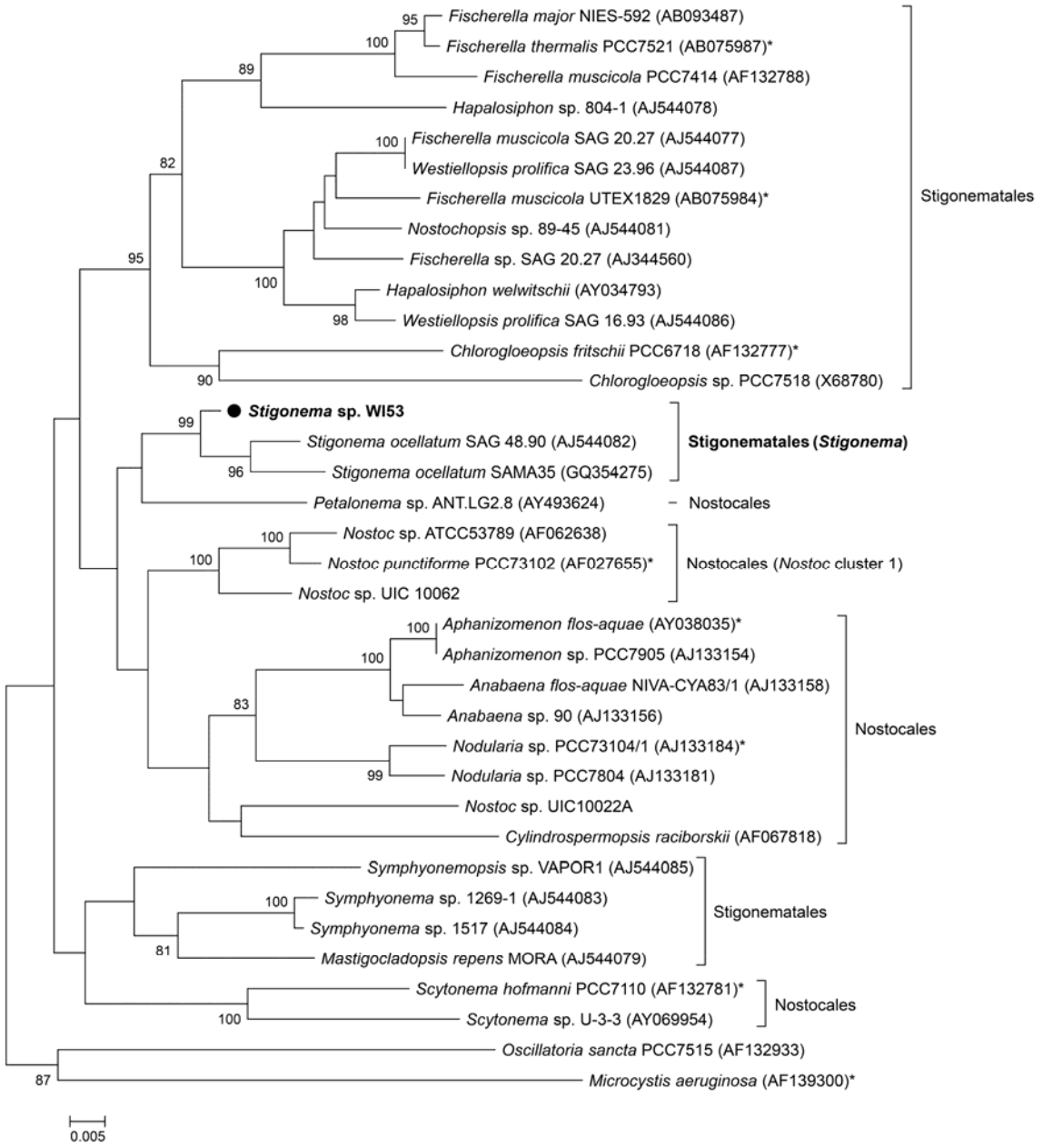

Fgiure 5.6 Phylogenetic relationships of 16S rRNA genes from cyanobacteria. Evolutionary distances w ere determined using the neighbor-joining method with 1,000 replicate bootstrap resampling to construct t he phylogenetic tree. Strains denoted with an asterisk (*) are "Bergey's" reference strains. Only bootstra p values greater than or equal to 75% are displayed. Phylogenetic analysis was conducted using MEGA 5.0.

5.6 Experimental

5.6.1 General experimental procedures

The optical rotation was measured on a Perkin-Elmer 241 polarimeter. UV and IR spectra were recorded on a Shimadzu UV spectrometer UV2401 and a Thermo Nicolet 6700 FT-IR spectrometer, respectively. 1D and 2D NMR spectra including ^{1}H NMR, COSY, TOCSY, HSQC, HMBC and T-ROESY spectra were obtained on a Bruker Avance DRX 600 MHz NMR spectrometer with a 5 mm CPTXI Z-gradient, whereas a Bruker Avance II 900 MHz NMR spectrometer with a 5 mm ATM CPTCLZ-gradient probe was used to acquire the DEPT-Q spectrum. ^{1}H and ^{13}C NMR chemical shifts were referenced to the DMSO-d_6 solvent signals (δ_H 2.50 and δ_C 39.51, respectively). A mixing time of 60 ms was set for the TOCSY experiment and 200 ms for the T-ROESY experiment. The HMBC spectrum was recorded with the average $^{3}J_{CH}$ of 8 Hz and the HSQC spectrum was measured with the average $^{1}J_{CH}$ of 145 Hz. HRESIMS and LC-MS data were obtained on a Shimadzu IT-TOF LC-MS spectrometer.

5.6.2 Sample collection and morphological study

A bloom sample of *Stigonema* sp. (collection ID WI53) was collected from North Nokomis Lake in the Highland Lake District of northern Wisconsin in August, 2010 (N 45°50.4812′, W 89°26.4920). A voucher specimen has been retained at UIC under the collection ID WI53. Morphological analysis was performed using a Zeiss Axiostar Plus light microscope equipped with a Canon PowerShot A620 camera.

5.6.3 DNA extraction and phylogenetic analysis of 16S rRNA gene sequence

For genomic DNA isolation, a sample was re-collected at the same site in August, 2011, and the production of stigonemapeptin (**1**) was confirmed by LC-MS analysis. The kit-based DNA extraction method routinely used in our laboratory (Chlipala et al., 2010) failed to yield genomic DNA in a sufficient quantity and quality for PCR amplification possibly due to the presence of a firm mucilaginous sheath. Therefore, the CTAB-based method was employed as previously described for DNA extraction from cyanobacteria of the genus *Arthrospira* with a slight modification; freeze-thaw cycles were replaced by

grinding in liquid nitrogen (Morin et al., 2010). This extraction method yielded a sufficient amount of the PCR-amplifiable template DNA. The partial 16S rRNA gene was amplified from the isolated genomic DNA using the cyanobacteria-specific primers 106F and 1509R (Nübel et al., 1997). The reaction volume was 26 μL containing 10.5 μL of nuclease free H_2O, 12.5 μL of PCR Master Mix (Promega M7502), 1 μL of each primer (10 μM) and 1 μL of the template DNA. The PCR was performed in a Bio-Rad C1000 thermal cycler as follows: initial denaturation for 30 s at 98 °C, 35 amplification cycles of 10 s at 98 °C, 30 s at 53 °C and 30s at 72 °C, and a final extension for 10 min at 72 °C. PCR products were purified using a MinElute PCR purification kit (Qiagen) and sequenced using the cyanobacteria-specific primers 106F and 1509R as well as the internal primer 359F. The resulting sequence was deposited in the NCBI GenBank under the accession number JQ435860.

5.6.4 Extraction and isolation

The cyanobacterial sample was manually cleaned from debris and freeze-dried. The freeze-dried sample (5 g) was extracted with the solvent mixture of CH_2Cl_2 and MeOH (1:1) and concentrated in vacuo to yield the organic extract (0.5 g). The resulting extract was fractionated using Diaion HP-20 resin and an increasing amount of iPrOH in H_2O. The fraction eluting at 40% iPrOH was found to contain a new nitrogen-containing peptide with a molecular weight of 973.5 Da by LC-MS analysis, and subjected to reversed-phase HPLC (Varian C_8 semi-preparative column, 10 mm × 250 mm, 3 mL/min) to afford stigonemapeptin (**1**, 4.1 mg, 0.08%).

Stigonemapeptin (1): colorless, amorphous powder; $[\alpha]^{25}_D$ - 61 (*c* 0.15, MeOH); UV (MeOH) λ_{max} (log ε) 203 (4.37), 223 (4.08), 272 (3.23) nm; IR (neat) ν_{max} 3276, 2962, 2936, 1734, 1653, 1533, 1517 cm^{-1}; ^1H and ^{13}C NMR, HMBC and ROESY data, see TABLE IX; HRESIMS *m/z* 996.4439 $[M+Na]^+$ (calcd for $C_{48}H_{63}N_9NaO_{13}$, 996.4443)

5.6.5 Absolute configuration of amino acids and Ahp by the advanced Marfey's method

Approximately 0.3 mg of stigonemapeptin (**1**) was hydrolyzed with 6 N HCl (500 μL) for 16 h at 110 °C. The resulting acid hydrolysate was separated into two equal portions for derivatization with either L-FDLA or DL-FDLA. Each portion was dissolved in 50 μL of H_2O, and mixed with 20 μL of 1N $NaHCO_3$ and 20 μL of L-FDLA or DL-FDLA (10 mg/mL in acetone). Then, acetone was added to the final volume of 200 μL, and the reaction mixtures were heated to 40 ºC and stirred for 1 h. After cooling to room temperature, 20 μL of 1N HCl was added, and the resulting reaction mixtures were air-dried and re-dissolved in CH_3CN. LC-MS analysis was performed on a reversed-phase column (Alltima C_{18}, 250 × 4.6 mm, 5 μm, 1.0 mL/min) with a linear gradient from 20% to 65% aqueous CH_3CN containing 0.1% formic acid for 50 min. The selective ion chromatograms of L-FDLA and DL-FDLA for each amino acid derivative were compared for the assignment of amino acid configurations. Two peaks corresponding to the L- and D-FDLA derivatives of each amino acid were observed as follows: Val 35.9 min (L) and 44.2 min (D); Glu 27.4 min (L) and 28.9 min (D); *N*MeTyr 24.1 min (L) and 25.2 min (D); Phe 40.7 min (L) and 46.9 min (D); Pro 30.4 min (L) and 34.3 min (D); Thr 24.6 min (L) and 30.7 min (D). The L-FDLA derivative gave one peak for each amino acid at 35.9, 27.4, 24.1, 40.6, 30.5 and 24.6 min, confirming the L-configuration for Val, Gln, *N*MeTyr, Phe, Pro and Thr. The presence of L-Thr was further confirmed by chromatographic comparison of the L-FDLA derivative of the acid hydrolysate with those of the amino acid standards L-Thr, D-Thr, L-*all*-Thr and D-*allo*-Thr.

For the absolute configuration of the Ahp residue, CrO_3 oxidation was carried out prior to acid hydrolysis as previously described (Matthew et al., 2007; Ishida et al., 1996). Briefly, approximately 0.4 mg of **1** was dissolved in 0.4 mL of glacial AcOH, and CrO_3 (2 mg) was added. The mixture was stirred at rt for 5 h and purified on a C_{18} SPE cartridge eluting with H_2O and MeOH. The resulting oxidized product was hydrolyzed and subjected to advanced Marfey's analysis in the same way as described above. LC-MS analysis exclusively identified the presence of L-Glu, assigning the *S* configuration to Ahp C-3.

5.6.6 Protease Inhibition Assays

The inhibitory activity of stigonemapeptin (**1**) against three serine proteases including elastase, chymotrypsin and trypsin was evaluated according to the previously described method (Gunasekera et al., 2009). Elastase inhibitory activity was tested using elastase from porcine pancreas (Sigma E0258) and *N*-succinyl-Ala-Ala-Ala-p-nitroanilide (Sigma S4760) as a substrate. The assay mixture composed of 79 μL of the assay buffer (1M Tris-HCl, pH 8.0), 5 μL of elastase solution (75 μg/mL in assay buffer) and 1 μL of **1** (various concentrations in DMSO) was pre-incubated in a microtiter plate at rt for 15 min, and then 15 μL of substrate solution (2 mM in assay buffer) was added to each well. The increase in absorbance was measured every 30 s for 30 min at 405 nm using a microplate reader.

For chymotrypsin- and trypsin-inhibition assays, α-chymotrypsin from bovine pancreas (Sigma C4129) and trypsin from porcine pancreas (Sigma T0303) were used with substrates *N*-succinyl-Gly-Gly-Phe-*p*-nitroanilide (Sigma S1899) for chymotrypsin and *N*α-benzoyl-DL-arginine-4-nitroanilide (Sigma B4875) for trypsin. The assay buffer including 50 mM Tris-HCl, 100 mM NaCl and 1 mM $CaCl_2$ (pH 7.8) was used for both assays. To the pre-incubated mixture of 39 μL of assay buffer, 10 μL of enzyme solution (100 μg/mL in assay buffer) and 1 μL of **1** (various concentrations in DMSO) at 37 °C for 15 min, 50 μM of substrate solution (1.5 mM in assay buffer) was added. The absorbance increase was recorded every 30 s for 30 min at 405 nm. Activity was calculated as a percentage inhibition by comparing the slope of an initial linear progress curve of enzyme reactions with **1** at various concentrations to that of the control reaction without compounds.

CHAPTER 6: CONCLUSION AND PERSPECTIVE

6.1 Conclusion and perspective

6.1.1 Chemical investigation of the cultured freshwater and terrestrial cyanobacteria

It is now well established that cyanobacteria produce diverse classes of biologically active secondary metabolites such as non-ribosomal peptides, lipopeptides, polyketides and indole alkaloids. Although numerous studies have been conducted to isolate new biologically active secondary metabolites from cyanobacteria, most of these studies have focused on bloom-forming or large colony-forming cyanobacteria found in either freshwater or marine environments. Cyanobacteria are widespread and found in almost all environments, and the majority of them appear as small colonies. We hypothesized that studying these non-bloom forming cyanobacteria will provide new biologically active secondary metabolites with pharmaceutical potentials.

To study secondary metabolites produced by non-bloom forming cyanobacteria, we employed a culture-dependent approach, since sufficient amounts of biomass for chemical and biological investigation cannot be acquired directly from environmental collections. Our culture collection was established by a combination of strains isolated from samples collected in freshwater and terrestrial environments (UIC strains) and strains acquired from three commercial culture collections (UTEX, SAG and CCALA strains). All strains were cultured at 4L scale, and these cultures were used to establish an extract library. The extract library was then evaluated for cytotoxicity against cancer cells (HT-29 and MDA-MB-435), inhibitory activity against the 20S proteasome and toxicity against brine shrimp. Active extracts were fractionated using Diaion and an increasing amount of iPrOH in H_2O to generate eight fractions. Active Diaion fractions were then subjected to dereplication using LC-MS analysis alone or in combination with HPLC-based activity profiling. HPLC-based activity profiling provided a way to identify active peaks in crude fractions in a semi-high-throughput manner when a number of un-known peaks were found in the active fractions. The active peaks were analyzed by ^{1}H NMR, and dereplication was performed using molecular weights and characteristic ^{1}H NMR signals. This approach conferred two major advantages over traditional bioassay-guided fractionation, which often involves several rounds of fractionation steps:

First, HPLC-based activity profiling significantly reduced the time and labor that took to identify active compounds in fractions, and also enabled simultaneous dereplication of a large number of active strains. Second, this approach allowed us to prioritize active strains for chemical investigation based on the structural classes of active compounds. Using this approach, the strains UTEX 1613, UIC 10035, UIC 10062, SAG 74.79 were found to contain potentially new compounds. The strains UTEX 1613 and UIC 10035 strains were classified as lipopeptides-producing strains. The 10062 strain was classified as a cyclophane-producing strain, and the SAG 74.79 was identified to produce a PK-NRP hybrid compound.

Chemical investigation of the two lipopeptides-producing *Anabaena* spp., UTEX 1613 and UIC 10035, led to the isolation of twelve new antiproliferative cyclic lipodecapeptides (four from UTEX 1613 and eight from UIC 10035), named minutissamides A-D and homesteadamides A-H. The structures of the minutissamides and homesteadamides contained a lipophlic *β*-amino acid residue with a 2-hydroxy-3-amino-4-methyl functionality as well as two non-standard amino acids, *N*-methylated Asn and Dhb. Structural comparison of these twelve structurally related lipopeptides showed that they all shared the same amino acid sequence in the part of the molecules (conserved region: Dhb-Val-*β*-amino acid-Pro-*N*MeAsn), and variations were found in the amino acid composition in the second part of the molecules (variable region). The minutissamides and homesteadamides exhibited antiproliferative activity against the cancer cell line (HT-29 or MDA-MB-435). The isolation of a series of structurally related lipopeptides with a small degree of variation allowed us to analyze structure and activity relationships. This analysis indicated that modifications by oxidation or chlorination in the fatty acid side chain of the lipophilic *β*-amino acid residue significantly decrease the antiproliferative activity, possibly due to reduced lipophilicity of the overall structure. It was also found that some changes in the amino acid composition of the variable region resulted in improved activity. The 10-fold or more reduced activity, observed upon modification of the lipophilic *β*-amino acid residue by hydrophilic functional groups, suggested that the minutissamides and homesteadamides may display antiproliferative activity by interacting with plasma membranes. This is supported by a recent publication by Hrouzek et al. (*in press*,

DOI:10.1021/tx300044t). The authors reported that the treatment of mammalian cells with the structurally related cyanobacterial lipopeptides, puwainaphycins F and G, resulted in the significantly increased concentration of intracellular Ca^{2+} ions, inducing necrotic cell death. Based on this observation, disruption of the membrane potential by interactions with plasma membranes was suggested to be the major mechanism of action for these lipodecapeptides. Most of bacterial lipopeptides are active against Gram-positive bacteria; however, the minutissamides and homesteadamides showed no activity in antibacterial assays (Mycobacterium, and Gram-positive and Gram-negative bacteria). This suggests that the mechanism of membrane interaction would be different from other well-characterized anionic antibacterial lipopeptides such as daptomycin and surfactin that involves micelle formation in the presence of divalent ions (Straus & Hancock, 2006). The well-resolved set of signals, observed in the ^{1}H NMR spectra of the minutissamides and homesteadamides, indicates these lipopeptides to be present in a well-defined conformation in solutions. Therefore, future characterization of the 3D conformations of these lipopeptides in water using 2D NMR techniques would provide an insight into interaction of these lipopeptides with plasma membranes.

Chemical investigation of the cyclophane-producing *Nostoc* sp. (UIC 10062) resulted in the isolation of two new naturally occurring [7.7]paracyclophanes, named merocyclophanes A and B. The structures of merocyclophanes A and B featured a new carbon skeleton, which differed from the previously described cyclindorcyclophane and nostocyclophanes by the presence of α-branched methyls, thus comprising the new family of cyanobacterial [7.7]paracyclophanes. The methyl branching, which occurred at the α-carbon of a ketone of the proposed biosynthetic intermediates suggested that this methyl group may originate from *S*-adenosyl methionine. In merocyclophane B, one of the resorcinol rings in merocyclophane A was replaced by a hydroxyquinone ring, thus creating an unsymmetrical structure. The conversion from the resorcinol ring in merocyclophane A into the hydroxyquinone ring was observed during prolonged storage, thus indicating that merocyclophane B was an oxidative artifact of merocyclphane A. Both merocyclophanes A and B exhibited the same level of antiproliferative activity against the cancer

cell line (HT-29) with low micromolar IC_{50} values. The level of antiproliferative activity of merocyclophanes A and B were also similar to those observed for other cyanobacterial [7.7]paracyclophanes. This suggest that the change in the positions of methyl groups from C-2/15 to C-1/14 does not significantly affect antiproliferative activity of [7.7]paracyclophanes. A structure and activity relationship study done by Yamakoshi et al. showed that the [7.7]paracyclophane core moiety is required for the antiproliferative activity. Modifications occurring at benzylic carbons did not significantly affect the antiproliferative activity of cylindrocyclophanes (Chen et al., 1991). The exact mechanism for the antiproliferative effect of [7.7]paracyclophanes is still unknown. Therefore, attaching fluorescent tags to the benzylic carbons of the cylindrocyclophanes to visualize the molecules inside cells, and subsequent purification of the proteins emitting fluorescence would be a possible strategy to reveal the mode of action of [7.7]paracyclophanes for their antiproliferative activity (Jeffery & Bogyo, 2003).

Chemical investigation of *Oscillatoria sancta* (SAG 74.79) led to the isolation of a new 14-membered PK-NRP hybrid macrolide, named sanctolide A. The structure of sanctolide A featured a rare *N*-methyl enamide and 2-hydroxyisovaleric acid moieties, which are incorporated into a 14-membered macrolide ring. Sanctolide A is the first cyanobacterial 14-membered macrolide of proposed NRPS-PKS hybrid biosynthetic origin. The *N*-methyl enamide and 2-hydroxyisovaleric acid are likely derived from Gly and Val amino acid precursors, respectively. Sanctolide A exhibited the moderate toxicity in the brine shrimp assay. However, it was observed that the *N*-methyl enamide moiety of sanctolide A underwent a rapid hydrolysis in the presence of water, causing opening of the macrolide ring. This labile nature of sanctolide A suggested that the acylic form, formed by enamide hydrolysis, would be the active form giving rise to the toxicity to brine shrimp. Sanctolide A showed no antiproliferative activity against cancer cell lines (HT-29 and MDA-MB-435). This indicates that cytotoxicity is not a major mechanism of brine shrimp toxicity of sanctolide A. The structurally related cyanobacterial metabolite, palmyrolide A, showed neurotoxicity by blocking sodium channel in neuro-2a cells without appreciable cytotoxicity (Pereira et al., 2010). Sanctolide A and palmyrolide A shares a structural similarity represented by a mac-

rolide ring structure containing an *N*-methyl enamide and ester linkages. Based on this, it is highly likely that the brine shrimp toxicity of sanctolide A was due to its neurotoxicity. Therefore, a future study should be directed to evaluating sanctolide A for its ability to modulate ion channels in neurons.

In summary, chemical investigation of the four strains prioritized by our dereplication resulted in the isolation of fifteen new compounds that fall into three distinct structural groups, cyclic lipodecapeptides (the minutissamides and homesteadamides), [7.7]paracyclophanes (the merocyclophanes) and a 14-membered PK-NRP hybrid macrolide (sanctolide A). Among these, the minutissamides, homesteadamides and merocyclophanes displayed cytotoxicity against cancer cells with IC_{50} values in a low micromolar range. This result leaves the possibility that future efforts into finding new metabolites belonging to the same structural classes will result in the discovery of new analogs with better activity. Also, the exact mechanisms of cytotoxicity were not well studied for these classes of compounds, thus this would be an interesting subject for future efforts to develop these molecules as anticancer drug leads that might provide medicinal chemists a strategy to design new derivatives with improved cytotoxicity and selectivity against cancer cells. With the exception of the homesteadamides, all of the compounds isolated in this study showed quite distant structural relationship with previously known compounds belonging to the same structural families. These examples clearly demonstrate that non-bloom forming cyanobacteria are a prolific source of biologically active secondary metabolites that still remain relatively under-explored. Therefore, using a culture-dependent approach to study these widespread non-bloom forming cyanobacteria will continue to provide new biologically active natural products that can serve as leads for future drug discovery efforts.

6.1.2 Chemical investigation of a bloom-forming freshwater cyanobacteria

During a collection trip to Highland Lake District of northern Wisconsin, we observed the occurrence of cyanobacterial bloom in North Nokomis Lake. Microscopic analysis of the bloom sample indicated that the bloom sample contained one major true-branching cyanobacterium belonging to the order Stigonematales. Detailed morphological and 16S rRNA gene sequence analyses of the bloom sample

suggested it to be a *Stigonema* sp. Inspired by the lack of studies of this genus, we conducted a chemical investigation with the bloom sample, which resulted in the isolation of a new Ahp-containing depsipeptide, named stigonemapeptin. In addition to the Ahp residue, stigonemapeptin contained the non-standard amino acids Dab and *N*-formylated Pro. Analog to previously reported Ahp-containing depsipeptides, stigonemapeptin showed potent elastase and chymotrypsin inhibitory activity. Some of the recent researches on the role of cyanobacterial Ahp-containing depsipeptides have revealed that these molecules as protease inhibitors play a very important ecological role controlling cyanobacterial bloom population in the environments (Sedmak et al., 2008). However, proteases are also validated drug targets due to their involvement in a variety of biological pathways, the discovery of new protease inhibitors would be significant leading to the development of new potential therapeutics as antiviral, antibacterial and antiprotozoal drugs (Southan, 2001). Therefore, the future research should be focused on evaluating stigonemapeptin for its inhibitory activity against more diverse protease families to assess its potential as a drug lead.

REFERENCES

Adams, D. G.; Duggan, P. S., Cyanobacteria–bryophyte symbioses. *J. Exp. Bot.* **2008,** 59, 1047-1058.

Badger, M., The roles of carbonic anhydrases in photosynthetic CO_2 concentrating mechanisms. *Photosynth. Res.* **2003,** 77, 83-94.

Balskus, E. P.; Case, R. J.; Walsh, C. T., The biosynthesis of cyanobacterial sunscreen scytonemin in intertidal microbial mat communities. *FEMS Microbiol. Ecol.* **2011**, 77, 322-332.

Balskus, E. P.; Walsh, C. T., Investigating the initial steps in the biosynthesis of cyanobacterial sunscreen scytonemin. *J. Am. Chem. Soc.* **2008**, 130, 15260-15261.

Baltz, R. H.; Miao, V.; Wrigley, S. K., Natural products to drugs: daptomycin and related lipopeptide antibiotics. *Nat. Prod. Rep.* **2005**, *22*, 717-41.

Banker, R.; Carmeli, S., Inhibitors of serine proteases from a waterbloom of the cyanobacterium Microcystis sp. *Tetrahedron* **1999**, 55, 10835-10844.

Barrett, D., From natural products to clinically useful antifungals. *Biochim. Biophys. Acta* **2002**, *1587*, 224-233.

Berry, J.; Gantar, M.; Perez, M.; Berry, G.; Noriega, F., Cyanobacterial Toxins as Allelochemicals with Potential Applications as Algaecides, Herbicides and Insecticides. *Mar. Drugs* **2008**, 6, 117-146.

Beutler, J. A., Natural Products as a Foundation for Drug Discovery. *Current protocols in pharmacology / editorial board, S.J. Enna* **2009,** 46, 9 11 1-9 11 21.

Bhushan, R.; Brückner, H., Marfey's reagent for chiral amino acid analysis: A review. *Amino acids* **2004**, 27, 231-247.

Blaha, L.; Babica, P.; Marsalek, B., Toxins produced in cyanobacterial water blooms - toxicity and risks. *Interdisc. Toxicol.* **2009**, 2, 36-41.

Bobzin, S. C.; Moore, R. E., Biosynthetic origin of [7.7]paracyclophanes from cyanobacteria. *Tetrahedron* **1993**, 49, 7615-7626.

Bonnard, I.; Rolland, M.; Salmon, J. M.; Debiton, E.; Barthomeuf, C.; Banaigs, B., Total structure and inhibition of tumor cell proliferation of laxaphycins. *J. Med. Chem.* **2007**, *50*, 1266-79.

Bui, H. T.; Jansen, R.; Pham, H. T.; Mundt, S., Carbamidocyclophanes A-E, chlorinated paracyclophanes with cytotoxic and antibiotic activity from the Vietnamese cyanobacterium Nostoc sp. *J. Nat. Prod.* **2007**, 70, 499-503.

Burja, A. M.; Banaigs, B.; Abou-Mansour, E.; Grant Burgess, J.; Wright, P. C., Marine cyanobacteria—a prolific source of natural products. *Tetrahedron* **2001**, *57*, 9347-9377.

Campos, A.; Vasconcelos, V., Molecular mechanisms of microcystin toxicity in animal cells. *Int. J. Mol. Sci.* **2010**, 11, 268-287.

Carmeli, S.; Moore, R. E.; Patterson, G. M. L., Tolytoxin and new scytophycins from three species of

REFERENCES (continued)

Scytonema. *J. Nat. Prod.* **1990**, 53, 1533-1542.

Carpenter, E. J. F., R. A., Marine cyanobacterial symbiosis. In: Rai, A. N.; Bergman, B.; Rasmussen, T. (eds) Cyanobacteria in symbioses. Kluwer, Dordrecht, pp 11-19. **2002**.

Castenholz, R. W., Oxygenic photosynthetic bacteria. In: Boone D.R. and Castenholz R.W. (eds), Bergey's Manual of Systematic Bacteriology (2nd ed.), Volumn 1, Springer-Verlag, New York. **2001**, 473-600.

Chaganty, S.; Golakoti, T.; Heltzel, C.; Moore, R. E.; Yoshida, W. Y., Isolation and Structure Determination of Cryptophycins 38, 326, and 327 from the Terrestrial Cyanobacterium *Nostoc* sp. GSV 224†. *J. Nat. Prod.* **2004**, 67, 1403-1406.

Chen, J. L.; Moore, R. E.; Patterson, G. M. L., Structures of nostocyclophanes A-D. .*J. Org. Chem.* **1991**, *56*, 4360-4364.

Chlipala, G.; Mo, S.; de Blanco, E. J. C.; Ito, A.; Bazarek, S.; Orjala, J. Investigation of antimicrobial and protease-inhibitory activity from cultured cyanobacteria. *Pharm. Biol.* **2009**, 47, 53-60.

Chlipala, G. E.; Sturdy, M.; Krunic, A.; Lantvit, D. D.; Shen, Q.; Porter, K.; Swanson, S. M.; Orjala, J., Cylindrocyclophanes with proteasome inhibitory activity from the Cyanobacterium *Nostoc* sp. *J. Nat. Prod.* **2010**, 73, 1529-1537.

Chlipala, G. E.; Mo, S.; Orjala, J., Chemodiversity in freshwater and terrestrial cyanobacteria - a source for drug discovery. *Curr. Drug Targets* **2011,** 12, 1654-1673.

Clardy, J.; Walsh, C., Lessons from natural molecules. *Nature* **2004**, 432, 829-837.

Claridge, T. D. W.; Perez-Victoria, I., Enhanced ^{13}C resolution in semi-selective HMBC: a band-selective, constant-time HMBC for complex organic structure elucidation by NMR. *Org. Biomol. Chem.* **2003**, *1*, 3632-3634.

Ding, K., Direct measurement of heteronuclear long-range coupling constants from phase-sensitive HMBC spectra. *Magn. Reson. Chem.* **2000**, *38*, 321-323.

Edelman, M. J.; Gandara, D. R.; Hausner, P.; Israel, V.; Thornton, D.; DeSanto, J.; Doyle, L. A., Phase 2 study of cryptophycin 52 (LY355703) in patients previously treated with platinum based chemotherapy for advanced non-small cell lung cancer. *Lung cancer* **2003**, 39, 197-199.

Edwards, C.; Beattie, K. A.; Scrimgeour, C. M.; Codd, G. A., Identification of anatoxin-A in benthic cyanobacteria (blue-green algae) and in associated dog poisonings at Loch Insh, Scotland. *Toxicon:* **1992**, 30, 1165-1175.

Eckart, K.; Schwarz, H.; Tomer, K. B.; Gross, M. L., Tandem mass spectrometry methodology for the sequence determination of cyclic peptides. *J. Am. Chem. Soc.* **1985**, *107*, 6765-6769.

Falch, B. S.; König, G. M.; Wright, A. D.; Sticher, O.; Angerhofer, C. K.; Pezzuto, J. M.; Bachmann, H., Biological Activities of Cyanobacteria: Evaluation of Extracts and Pure Compounds. *Planta Med.* **1995**,

REFERENCES (continued)

61, 321-328.

Farrugia, L.J., 'WinGX' suite for small-molecule single-crystal crystallography. *J. Appl. Cryst.* **1999**, 32, 837-838.

Fujii, K.; Ikai, Y.; Oka, H.; Suzuki, M.; Harada, K.-i., A Nonempirical Method Using LC/MS for Determination of the Absolute Configuration of Constituent Amino Acids in a Peptide: Combination of Marfey's Method with Mass Spectrometry and Its Practical Application. *Anal. Chem.* **1997**, 69, 5146-5151.

Fujii, K.; Shimoya, T.; Ikai, Y.; Oka, H.; Harada, K.-i., Further application of advanced Marfey's method for determination of absolute configuration of primary amino compound. *Tetrahedron Lett.* **1998**, 39, 2579-2582.

Fujii, K.; Sivonen, K.; Nakano, T.; Harada, K.-i., Structural elucidation of cyanobacterial peptides encoded by peptide synthetase gene in *Anabaena* species. *Tetrahedron* **2002,** 58, 6863-6871.

Gerwick, W. H.; Jiang, Z. D.; Agarwal, S. K.; Farmer, B. T., Total structure of hormothamnin A, A toxic cyclic undecapeptide from the tropical marine cyanobacterium hormothamnion enteromorphoides. *Tetrahedron* **1992**, 48, 2313-2324.

Ganesan, A., The impact of natural products upon modern drug discovery. *Curr. Opin. Chem. Biol.* **2008**, 12, 306-17.

Garcia-Pichel, F.; Castenholz, R. W., Characterization and biological implications of scytonemin, a cyanobacterial sheath pigment. *J. Phycol.* **1991**, 27, 395-409.

Gesner-Apter, S.; Carmeli, S., Protease Inhibitors from a Water Bloom of the Cyanobacterium *Microcystis aeruginosa*. *J. Nat. Prod.* **2009**, 72, 1429-1436.

Grach-Pogrebinsky, O.; Sedmak, B.; Carmeli, S., Protease inhibitors from a Slovenian Lake Bled toxic waterbloom of the cyanobacterium *Planktothrix rubescens*. *Tetrahedron* **2003**, *59*, 8329-8336.

Gregson, J. M.; Chen, J.-L.; Patterson, G. M. L.; Moore, R. E., Structures of puwainaphycins A–E. *Tetrahedron* **1992**, 48, 3727-3734.

Griffiths, D. J.; Saker, M. L., The Palm Island mystery disease 20 years on: A review of research on the cyanotoxin cylindrospermopsin. *Environ. Toxicology* **2003**, 18, 78-93.

Gunasekera, S. P.; Miller, M. W.; Kwan, J. C.; Luesch, H.; Paul, V. J., Molassamide, a Depsipeptide Serine Protease Inhibitor from the Marine Cyanobacterium *Dichothrix utahensis*. *J. Nat. Prod.* **2009**, 73, 459-462.

Harada, K.-i.; Fujii, K.; Hayashi, K.; Suzuki, M.; Ikai, Y.; Oka, H., Application of d,l-FDLA derivatization to determination of absolute configuration of constituent amino acids in peptide by advanced Marfey's method. *Tetrahedron Lett.* **1996**, 37, 3001-3004.

Harada, K., Production of secondary metabolites by freshwater cyanobacteria. *Chem. Pharm. Bull.* **2004**,

REFERENCES (continued)

52, 889-899.

Hawkins, P. R.; Runnegar, M. T.; Jackson, A. R.; Falconer, I. R., Severe hepatotoxicity caused by the tropical cyanobacterium (blue-green alga) *Cylindrospermopsis raciborskii* (Woloszynska) Seenaya and Subba Raju isolated from a domestic water supply reservoir. *Appl. Environ. Microb.* **1985**, 50, 1292-1295.

Heintzelman, G. R.; Fang, W.-K.; Keen, S. P.; Wallace, G. A.; Weinreb, S. M., Stereoselective Total Synthesis of the Cyanobacterial Hepatotoxin 7-Epicylindrospermopsin: Revision of the Stereochemistry of Cylindrospermopsin. *J. Am. Chem. Soc.* **2001**, 123, 8851-8853.

Hess, W. R., Cyanobacterial genomics for ecology and biotechnology. *Curr. Opin. Microbiol.* **2011**, 14, 608-614.

Hoehler, T. M.; Bebout, B. M.; Des Marais, D. J., The role of microbial mats in the production of reduced gases on the early Earth. *Nature* **2001**, 412, 324-327.

Hoiczyk, E.; Hansel, A., Cyanobacterial cell walls: news from an unusual prokaryotic envelope. *J. Bacteriol.* **2000**, 182, 1191-1199.

Hrouzek, P.; Kuzma, M.; Černý, J.; Novák, P.; Fišer, R.; Šimek, P.; Lukešová, A.; Kopecký, J., The cyanobacterial cyclic lipopeptides puwaianphycins F/G are inducing necrosis via cell membrane permeabilization and subsequent unusual actin relocalization. *Chem. Res. Toxicol.*, 2012 in press (DOI: 10.1021/tx300044t)

Humpage, A. R.; Fenech, M.; Thomas, P.; Falconer, I. R., Micronucleus induction and chromosome loss in transformed human white cells indicate clastogenic and aneugenic action of the cyanobacterial toxin, cylindrospermopsin. *Mutat. Res.* **2000**, 472, 155-161.

Huot, R. I.; Armstrong, D. L.; Chanh, T. C., Protection against nerve toxicity by monoclonal antibodies to the sodium channel blocker tetrodotoxin. *J. Clin. Invest.* **1989**, 83, 1821-1826.

Ishibashi, M.; Moore, R. E.; Patterson, G. M. L., Scytophycins, cytotoxic and antimycotic agents from the cyanophyte *Scytonema pseudohofmanni*. *J. Org. Chem.* **1986**, 51, 5300-5306.

Ishida, K.; Matsuda, H.; Murakami, M.; Yamaguchi, K., The absolute stereochemistry of micropeptin 90. *Tetrahedron Lett.* **1996,** 37, 9225-9226.

Janson, S., Cyanobacteria in symbiosis with diatoms. In: Rai A. N.; Bergman, B.; Rasmussen, U. (eds) Cyanobacteria in symbioses. Kluwer, Dordrecht, pp 1-10. **2002**.

Jeffery, D. A.; Bogyo, M., Chemical proteomics and its application to drug discovery. *Curr. Opin. Biotech.* **2003**, 14, 87-95.

Jonasson, S.; Vintila, S.; Sivonen, K.; El-Shehawy, R., Expression of the nodularin synthetase genes in the Baltic Sea bloom-former cyanobacterium *Nodularia spumigena* strain AV1. *FEMS Microbiol. Ecol.* **2008**, 65, 31-39.

REFERENCES (continued)

Jones, A.C.; Monroe, E. A.; Eisman, E.B.; Gerwick, L.; Sherman, D.H.; Gerwick, W.H., The unique mechanistic transformations involved in the biosynthesis of modular natural products from marine cyanobacteria. *Nat. Prod. Rep.* **2010**, 27, 1048-1065.

Kabsch, W., Automatic processing of rotation diffraction data from crystals of initially unknown symmetry and cell constants. *J. Appl. Cryst.* **1993**, 26, 795-800.

Keil, C.; Forchert, A.; Fastner, J.; Szewzyk, U.; Rotard, W.; Chorus, I.; Kratke, R., Toxicity and microcystin content of extracts from a Planktothrix bloom and two laboratory strains. *Water Res.* **2002**, 36, 2133-2139.

Kellmann, R.; Mihali, T. K.; Jeon, Y. J.; Pickford, R.; Pomati, F.; Neilan, B. A., Biosynthetic intermediate analysis and functional homology reveal a saxitoxin gene cluster in cyanobacteria. *Appl. Environ. Microb.* **2008**, 74, 4044-53.

Kiss, T.; Vehovszky, A.; Hiripi, L.; Kovacs, A.; Voros, L., Membrane effects of toxins isolated from a cyanobacterium, *Cylindrospermopsis raciborskii*, on identified molluscan neurones. *Comp. Biochem. Physiol.* **2002**, 131, 167-176.

Kisugi, T.; Okino, T., Micropeptins from the Freshwater Cyanobacterium Microcystis aeruginosa (NIES-100). *J. Nat. Prod.* **2009,** 72, 777-781.

Klein, D.; Braekman, J. C.; Daloze, D.; Hoffmann, L.; Demoulin, V., Laingolide, a novel 15-membered macrolide from *Lyngbya bouillonii* (cyanophyceae). *Tetrahedron Lett.* **1996**, 37, 7519-7520.

Klein, D.; Braekman, J. C.; Daloze, D.; Hoffmann, L.; Castillo, G.; Demoulin, V., Madangolide and Laingolide A, Two Novel Macrolides from *Lyngbya bouillonii* (Cyanobacteria). *J. Nat. Prod.* **1999**, 62, 934-936.

Kodani, S.; Suzuki, S.; Ishida, K.; Murakami, M., Five new cyanobacterial peptides from water bloom materials of lake Teganuma (Japan). *FEMS Microbiol. Lett.* **1999**, 178, 343-348.

Koehn, F. E.; Carter, G. T., The evolving role of natural products in drug discovery. *Nat. Rev. Drug Discov.* **2005**, 4, 206-220.

Komárek, J., Komárková, J., Kling, H. 2003. Filamentous Cyanobacteria. In Freshwater Algae of North America; Wehr, J. D., Sheath, R. G., Eds.; Academic Press: San Diego, **2003**; pp 117-196.

Komárek, J., Cyanobacterial taxonomy: Current problems and prospects for the integration of traditional and molecular approaches. *Algae* **2006**, 21, 349-357.

Kwan, J.; Taori, K.; Paul, V.; Luesch, H., Lyngbyastatins 8–10, Elastase Inhibitors with Cyclic Depsipeptide Scaffolds Isolated from the Marine Cyanobacterium Lyngbya semiplena. *Mar. Drugs* **2009,** 7, 528-538.

Landsberg, J. H., The Effects of Harmful Algal Blooms on Aquatic Organisms. *Rev. Fish. Sci.* **2002**, 10, 113-390.

REFERENCES (continued)

Liaimer, A.; Jenke-Kodama, H.; Ishida, K.; Hinrichs, K.; Stangeland, J.; Hertweck, C.; Dittmann, E., A polyketide interferes with cellular differentiation in the symbiotic cyanobacterium *Nostoc punctiforme*. *Environ. Microbiol. Rep.* **2011**, 3, 550-558.

Linington, R. G.; Edwards, D. J.; Shuman, C. F.; McPhail, K. L.; Matainaho, T.; Gerwick, W. H., Symplocamide A, a Potent Cytotoxin and Chymotrypsin Inhibitor from the Marine Cyanobacterium *Symploca* sp. *J. Nat. Prod.* **2007,** 71, 22-27.

Llewellyn, L. E., Saxitoxin, a toxic marine natural product that targets a multitude of receptors. *Nat. Prod. Rep.* **2006**, 23, 200-222.

Lu, K.; Dempsey, J.; Schultz, R. M.; Shih, C.; Teicher, B. A., Cryptophycin-induced hyperphosphorylation of Bcl-2, cell cycle arrest and growth inhibition in human H460 NSCLC cells. *Cancer Chemoth. Pharm.* **2001**, 47, 170-178.

Lücking, R.; Lawrey, J. D.; Sikaroodi, M.; Gillevet, P. M.; Chaves, J. L.; Sipman, H. J. M.; Bungartz, F., Do lichens domesticate photobionts like farmers domesticate crops? Evidence from a previously unrecognized lineage of filamentous cyanobacteria. *Am. J. Bot.* **2009**, 96, 1409-1418.

MacMillan, J. B.; Ernst-Russell, M. A.; de Ropp, J. S.; Molinski, T. F., Lobocyclamides A-C, lipopeptides from a cryptic cyanobacterial mat containing Lyngbya confervoides. *J. Org. Chem.* **2002**, 67, 8210-8215.

Magarvey, N. A.; Beck, Z. Q.; Golakoti, T.; Ding, Y.; Huber, U.; Hemscheidt, T. K.; Abelson, D.; Moore, R. E.; Sherman, D. H., Biosynthetic characterization and chemoenzymatic assembly of the cryptophycins. Potent anticancer agents from cyanobionts. *ACS Chem. Biol.* **2006**, 1, 766-779.

Marfey, P., Determination of D-amino acids. II. Use of a bifunctional reagent, 1,5-difluoro-2,4-dinitrobenzene. *Carlsberg Res. Commun.* **1984**, 49, 591-596.

Martínez-Murcia, A.J.; Acinas, S.G.; Rodriguez-Valera, F., Evaluation of prokaryotic diversity by restrictase digestion of 16S rDNA directly amplified from hypersaline environments. *FEMS Microbiol. Ecol.* **1995**, 17, 247-256.

Matern, U.; Oberer, L.; Falchetto, R. A.; Erhard, M.; König, W. A.; Herdman, M.; Weckesser, J., Scyptolin A and B, cyclic depsipeptides from axenic cultures of *Scytonema hofmanni* PCC 7110. *Phytochemistry* **2001,** 58, 1087-1095.

Matern, U.; Schleberger, C.; Jelakovic, S.; Weckesser, J.; Schulz, G. E., Binding Structure of Elastase Inhibitor Scyptolin A. *Chem. Biol.* **2003**, 10, 997-1001.

Matsumori, N.; Kaneno, D.; Murata, M.; Nakamura, H.; Tachibana, K., Stereochemical determination of acyclic structures based on carbon-proton spin-coupling constants. A method of configuration analysis for natural products. *J. Org. Chem.* **1999**, 64, 866-876.

Matthew, S.; Ross, C.; Rocca, J. R.; Paul, V. J.; Luesch, H., Lyngbyastatin 4, a Dolastatin 13 Analogue with Elastase and Chymotrypsin Inhibitory Activity from the Marine Cyanobacterium *Lyngbya confervoides*. *J. Nat. Prod.* **2007,** 70, 124-127.

REFERENCES (continued)

Matthew, S.; Salvador, L. A.; Schupp, P. J.; Paul, V. J.; Luesch, H., Cytotoxic halogenated macrolides and modified peptides from the apratoxin-producing marine cyanobacterium *Lyngbya bouillonii* from Guam. *J. Nat. Prod.* **2010**, 73, 1544-1552.

Matthiensen, A.; Beattie, K. A.; Yunes, J. S.; Kaya, K.; Codd, G. A., [D-Leu1]Microcystin-LR, from the cyanobacterium Microcystis RST 9501 and from a Microcystis bloom in the Patos Lagoon estuary, Brazil. *Phytochemistry* **2000**, 55, 383-387.

Meeks, J.; Campbell, E.; Summers, M.; Wong, F., Cellular differentiation in the cyanobacterium *Nostoc punctiforme*. *Arch. Microbiol.* **2002**, 178, 395-403.

Meeks, J.; Elhai, J.; Thiel, T.; Potts, M.; Larimer, F.; Lamerdin, J.; Predki, P.; Atlas, R., An overview of the genome of *Nostoc punctiforme* , a multicellular, symbiotic cyanobacterium. *Photosynth. Res.* **2001**, 70, 85-106.

Meeks, J. C.; Elhai, J., Regulation of Cellular Differentiation in Filamentous Cyanobacteria in Free-Living and Plant-Associated Symbiotic Growth States. *Microbiol. Mol. Biol. R.* **2002,** *66* (1), 94-121.

Méjean, A.; Mann, S. p.; Maldiney, T.; Vassiliadis, G. l.; Lequin, O.; Ploux, O., Evidence that Biosynthesis of the Neurotoxic Alkaloids Anatoxin-a and Homoanatoxin-a in the Cyanobacterium *Oscillatoria* PCC 6506 Occurs on a Modular Polyketide Synthase Initiated by l-Proline. *J. Am. Chem. Soc.* **2009**, 131, 7512-7513.

Mihali, T. K.; Kellmann, R.; Muenchhoff, J.; Barrow, K. D.; Neilan, B. A., Characterization of the gene cluster responsible for cylindrospermopsin biosynthesis. *Appl. Environ. Microbiol.* **2008**, 74, 716-722.

Moon, S. S.; Chen, J. L.; Moore, R. E.; Patterson, G. M. L., Calophycin, a fungicidal cyclic decapeptide from the terrestrial blue-green alga *Calothrix fusca*. *J. Org, Chem.* **1992**, 57, 1097-1103.

Moore, B. S.; Patterson, G. M. L.; Mynderse, J. S.; Barchi, J., Toxins from cyanophytes belonging to the scytonemataceae. *Pure & Appl. Chem.* **1986**, 58, 263-171.

Moore, R. E.; Bornemann, V.; Niemczura, W. P.; Gregson, J. M.; Chen, J. L.; Norton, T. R.; Patterson, G. M. L.; Helms, G. L., Puwainaphycin C, a cardioactive cyclic peptide from the blue-green alga *Anabaena* BQ-16-1. Use of two-dimensional carbon-13-carbon-13 and carbon-13-nitrogen-15 correlation spectroscopy in sequencing the amino acid units. *J. Am. Chem. Soc.* **1989**, 111, 6128-6132.

Moore, B. S.; Chen, J. L.; Patterson, G. M. L.; Moore, R. E.; Brinen, L. S.; Kato, Y.; Clardy, J., [7.7]Paracyclophanes from blue-green algae. *J. Am. Chem. Soc.* **1990**, 112, 4061-4063.

Moore, B.S.; Chen, J.L.; Patterson, G.M.L.; Moore, R.E., Structures of cylindrocyclophanes A-F. *Tetrahedron* **1992**, 48, 3001-3006.

Moore, R. E.; Bornemann, V.; Niemczura, W. P.; Gregson, J. M.; Chen, J. L.; Norton, T. R.; Patterson, G. M. L.; Helms, G. L., Puwainaphycin C, a cardioactive cyclic peptide from the blue-green alga Anabaena BQ-16-1. Use of two-dimensional carbon-13-carbon-13 and carbon-13-nitrogen-15 correlation spectroscopy in sequencing the amino acid units. *J. Am. Chem. Soc.* **1989,** 111, 6128-6132.

REFERENCES (continued)

Moore, R. E.; Cheuk, C.; Patterson, G. M. L., Hapalindoles: new alkaloids from the blue-green alga *Hapalosiphon fontinalis*. *J. Am. Chem. Soc.* **1984**, 106, 6456-6457.

Moore, R. E.; Cheuk, C.; Yang, X. Q. G.; Patterson, G. M. L.; Bonjouklian, R.; Smitka, T. A.; Mynderse, J. S.; Foster, R. S.; Jones, N. D., Hapalindoles, antibacterial and antimycotic alkaloids from the cyanophyte Hapalosiphon fontinalis. *J. Org. Chem.* **1987**, 52, 1036-1043.

Moore, R. E.; Yang, X. Q. G.; Patterson, G. M. L., Fontonamide and anhydrohapaloxindole A, two new alkaloids from the blue-green alga Hapalosiphon fontinalis. *J. Org. Chem.* **1987**, 52, 3773-3777.

Morin, N.; Vallaeys, T.; Hendrickx, L.; Natalie, L.; Wilmotte, A., An efficient DNA isolation protocol for filamentous cyanobacteria of the genus Arthrospira. *J. Microbiol. Methods* **2010,** 80, 148-154.

Newman, D. J.; Cragg, G. M., Natural products as sources of new drugs over the 30 Years from 1981 to 2010. *J. Nat. Prod.* **2012**, 75, 311-335.

Nogle, L. M.; Williamson, R. T.; Gerwick, W. H., Somamides A and B, Two New Depsipeptide Analogues of Dolastatin 13 from a Fijian Cyanobacterial Assemblage of *Lyngbya majuscula* and *Schizothrix* Species. *J. Nat. Prod.* **2001,** 64, 716-719.

Nübel, U.; GarciaPichel, F.; Muyzer, G., PCR primers to amplify 16S rRNA genes from cyanobacteria. *Appl. Environ. Microbiol.* **1997**, 63, 3327-3332.

Ohtani, I.; Moore, R. E.; Runnegar, M. T. C., Cylindrospermopsin: a potent hepatotoxin from the blue-green alga Cylindrospermopsis raciborskii. *J. Am. Chem. Soc.* **1992**, 114|, 7941-7942.

Paerl, H. W.; Pinckney, J. L.; Steppe, T. F., Cyanobacterial-bacterial mat consortia: examining the functional unit of microbial survival and growth in extreme environments. *Environ. Microbiol.* **2000**, 2, 11-26.

Park, A.; Moore, R. E.; Patterson, G. M. L., Fischerindole L, a new isonitrile from the terrestrial blue-green alga *fischerella muscicola*. *Tetrahedron Lett.* **1992,** 33, 3257-3260.

Pereira, A. R.; Cao, Z.; Engene, N.; Soria-Mercado, I. E.; Murray, T. F.; Gerwick, W. H., Palmyrolide A, an unusually stabilized neuroactive macrolide from Palmyra Atoll cyanobacteria. *Org. Lett.* **2010**, 12, 4490-4493.

Pettit, G. R.; Kamano, Y.; Herald, C. L.; Dufresne, C.; Cerny, R. L.; Herald, D. L.; Schmidt, J. M.; Kizu, H., Antineoplastic agent. 174. Isolation and structure of the cytostatic depsipeptide dolastatin 13 from the sea hare *Dolabella auricularia*. *J. Am. Chem. Soc.* **1989,** 111, 5015-5017.

Plaza, A.; Bewley, C. A., Largamides A-H, unusual cyclic peptides from the marine cyanobacterium Oscillatoria sp. *J. Org. Chem.* **2006**, 71, 6898-6907.

Ploutno, A.; Carmeli, S., Nostocyclyne A, a novel antimicrobial cyclophane from the cyanobacterium *Nostoc* sp. *J. Nat. Prod.* **2000**, 63, 1524-1526.

Ploutno, A.; Carmeli, S., Modified peptides from a water bloom of the cyanobacterium *Nostoc* sp. *Tetrahedron* **2002,** 58, 9949-9957.

REFERENCES (continued)

Ploutno, A.; Shoshan, M.; Carmeli, S., Three Novel Protease Inhibitors from a Natural Bloom of the Cyanobacterium *Microcystis aeruginosa*. *J. Nat. Prod.* **2002,** *65*, 973-978.

Prociv, P., Algal toxins or copper poisoning--revisiting the Palm Island "epidemic". *Med. J. Aust.* **2004,** 181, 344.

Rae, J. M.; Creighton, C. J.; Meck, J. M.; Haddad, B. R.; Johnson, M. D., MDA-MB-435 cells are derived from M14 melanoma cells--a loss for breast cancer, but a boon for melanoma research. *Breast cancer research and treatment* **2007**, 104, 13-19.

Rajaniemi, P.; Hrouzek, P.; Kastovska, K.; Willame, R.; Rantala, A.; Hoffmann, L.; Komarek, J.; Sivonen, K., Phylogenetic and morphological evaluation of the genera Anabaena, Aphanizomenon, Trichormus and Nostoc (Nostocales, Cyanobacteria). *J. Syst. Evol. Microbiol.* **2005**, 55, 11-26.

Rai, A. N. S., E.; Bergman, B., Cyanobacterium-plant symbioses. *Transley review 116. New Phytol.* **2000**, 147, 449-481.

Rance, M.; Sorensen, O. W.; Bodenhausen, G.; Wagner, G.; Ernst, R. R.; Wuthrich, K., Improved spectral resolution in cosy ^{1}H NMR spectra of proteins via double quantum filtering. *Biochem. Biophys. Res. Commun.* **1983**, 117, 479-485.

Reshef, V.; Carmeli, S., Protease inhibitors from a water bloom of the cyanobacterium *Microcystis aeruginosa*. *Tetrahedron* **2001,** 57, 2885-2894.

Richter, J. M.; Ishihara, Y.; Masuda, T.; Whitefield, B. W.; Llamas, T. s.; Pohjakallio, A.; Baran, P. S., Enantiospecific Total Synthesis of the Hapalindoles, Fischerindoles, and Welwitindolinones via a Redox Economic Approach. *J. Am. Chem. Society* **2008,** *130* (52), 17938-17954.

Rikkinen, J.; Oksanen, I.; Lohtander, K., Lichen Guilds Share Related Cyanobacterial Symbionts. *Science* **2002**, 297, 357.

Rinehart, K. L.; Harada, K.; Namikoshi, M.; Chen, C.; Harvis, C. A.; Munro, M. H. G.; Blunt, J. W.; Mulligan, P. E.; Beasley, V. R.; et al., Nodularin, microcystin, and the configuration of Adda. *J. Am. Chem. Soc.* **1988,** 110, 8557-8558.

Runnegar, M. T.; Kong, S. M.; Zhong, Y. Z.; Lu, S. C., Inhibition of reduced glutathione synthesis by cyanobacterial alkaloid cylindrospermopsin in cultured rat hepatocytes. *Biochem. Pharmacol.* **1995,** 49, 219-225.

Runnegar, M. T.; Xie, C.; Snider, B. B.; Wallace, G. A.; Weinreb, S. M.; Kuhlenkamp, J., In vitro hepatotoxicity of the cyanobacterial alkaloid cylindrospermopsin and related synthetic analogues. *Toxicol. Sci.* **2002,** 67, 81-87.

Sabareesh, V.; Balaram, P., Tandem electrospray mass spectrometric studies of proton and sodium ion adducts of neutral peptides with modified N- and C-termini: synthetic model peptides and microheterogeneous peptaibol antibiotics. *Rapid Commun. Mass Spectrom:* **2006**, 20, 618-628.

Sedmak, B.; Carmeli, S.; Eleršek, T., “Non-Toxic” Cyclic peptides induce lysis of cyanobacteria—an Ef-

REFERENCES (continued)

fective Cell Population Density Control Mechanism in Cyanobacterial Blooms. *Microb. Ecol.* **2008,** *56*, 201-209.

Sedmak, B.; Carmeli, S.; Pompe-Novak, M.; Tušek-Žnidarič, M.; Grach-Pogrebinsky, O.; Eleršek, T.; Žužek, M. C.; Bubik, A.; Frangež, R., Cyanobacterial cytoskeleton immunostaining: the detection of cyanobacterial cell lysis induced by planktopeptin BL1125. *J. Plankton Res.* **2009**, 31, 1321-1330.

Seo, E.-K.; Kim, N.-C.; Mi, Q.; Chai, H.; Wall, M. E.; Wani, M. C.; Navarro, H. A.; Burgess, J. P.; Graham, J. G.; Cabieses, F.; Tan, G. T.; Farnsworth, N. R.; Pezzuto, J. M.; Kinghorn, A. D., Macharistol, a New Cytotoxic Cinnamylphenol from the Stems of *Machaerium aristulatum*. *J. Nat. Prod.* **2001**, 64, 1483-1485.

Shendage, D. M.; Frohlich, R.; Haufe, G., Highly efficient stereoconservative amidation and deamidation of alpha-amino acids. *Org. Lett.* **2004**, 6, 3675-8.

Sieber, S. A.; Marahiel, M. A., Molecular mechanisms underlying nonribosomal peptide synthesis: approaches to new antibiotics. *Chem. Rev.* **2005**, 105, 715-738.

Singh, S.; Kate, B. N.; Banerjee, U. C., Bioactive Compounds from Cyanobacteria and Microalgae: An Overview. *Crit. Rev. Biotechnol.* **2005**, 25, 73-95.

Sleep, N. H.; Bird, D. K., Evolutionary ecology during the rise of dioxygen in the Earth's atmosphere. *Phil. Trans. R. Soc. B* **2008,** 363, 2651-2664.

Smith, C. D.; Carmeli, S.; Moore, R. E.; Patterson, G. M. L., Scytophycins, novel microfilament-depolymerizing agents which circumvent P-glycoprotein-mediated multidrug resistance. *Cancer Res.* **1993**, 53, 1343-1347.

Smith, C. D.; Zhang, X.; Mooberry, S. L.; Patterson, G. M.; Moore, R. E., Cryptophycin: a new antimicrotubule agent active against drug-resistant cells. *Cancer Res.* **1994**, 54, 3779-3784.

Smith, H. E., Chiroptical properties of the benzene chromophore. A method for the determination of the absolute configurations of benzene compounds by application of the benzene sector and benzene chirality rules. *Chem. Rev.* **1998**, 98, 1709-1740.

Smith, R. A.; Lewis, D., A rapid analysis of water for anatoxin a, the unstable toxic alkaloid from Anabaena flos-aquae, the stable non-toxic alkaloids left after bioreduction and a related amine which may be nature's precursor to anatoxin a. *Vet. Hum. Toxicol.* **1987,** 29, 153-154.

Smitka, T. A.; Bonjouklian, R.; Doolin, L.; Jones, N. D.; Deeter, J. B.; Yoshida, W. Y.; Prinsep, M. R.; Moore, R. E.; Patterson, G. M. L., Ambiguine isonitriles, fungicidal hapalindole-type alkaloids from three genera of blue-green algae belonging to the Stigonemataceae. *J. Org. Chem.* **1992**, 57, 857-861.

Southan, C. A genomic perspective on human proteases as drug targets. DDT **2001**, 6, 681-688.

Stal, L. J., and Caumette, P., Microbial Mats: Structure, Development and Environmental Significance. NATO ASI Series G: Ecological Sciences, Vol. 35. Berlin: Springer Verlag **1994.**

REFERENCES (continued)

Stockner, J.; Callieri, C.; Cronberg, G., Picoplankton and other non-bloom forming cyanobacteria in lakes. In *The Ecology of Cyanobacteria. Their Diversity in Time and Space*, Whitton, B. A.; Potts, M., Eds. Kluwer academic Publishers: **2000**; pp 195-231.

Stratmann, K.; Moore, R. E.; Bonjouklian, R.; Deeter, J. B.; Patterson, G. M. L.; Shaffer, S.; Smith, C. D.; Smitka, T. A., Welwitindolinones, Unusual Alkaloids from the Blue-Green Algae Hapalosiphon welwitschii and Westiella intricata. Relationship to Fischerindoles and Hapalinodoles. *J. Am. Chem. Soc.* **1994,** 116, 9935-9942.

Straus, S. K.; Hancock, R. E., Mode of action of the new antibiotic for Gram-positive pathogens daptomycin: comparison with cationic antimicrobial peptides and lipopeptides. *Biochim. Biophys. Acta* **2006**, 1758, 1215-1223.

Strieker, M.; Marahiel, M. A., The structural diversity of acidic lipopeptide antibiotics. *Chembiochem* **2009**, 10, 607-616.

Subbaraju, G. V.; Golakoti, T.; Patterson, G. M.; Moore, R. E., Three new cryptophycins from *Nostoc* sp. GSV 224. *J. Nat. Prod.* **1997,** 60, 302-305.

Svenning, M. M.; Eriksson, T.; Rasmussen, U., Phylogeny of symbiotic cyanobacteria within the genus *Nostoc* based on 16S rDNA sequence analyses. *Arch. Microbiol.* **2005**, 183, 19-26.

Tan, L. T., Bioactive natural products from marine cyanobacteria for drug discovery. *Phytochemistry* **2007,** 68, 954-979.

Tamura, K.; Peterson, D.; Peterson, N.; Stecher, G.; Nei, M.; Kumar, S., MEGA5: molecular evolutionary genetics analysis using maximum likelihood, evolutionary distance, and maximum parsimony methods. *Mol. Biol. Evol.* **2011**, 28, 2731-2739.

Taori, K.; Matthew, S.; Rocca, J. R.; Paul, V. J.; Luesch, H., Lyngbyastatins 5–7, Potent Elastase Inhibitors from Floridian Marine Cyanobacteria, *Lyngbya* spp. *J. Nat. Prod.* **2007,** 70, 1593-1600.

Taori, K.; Paul, V. J.; Luesch, H., Kempopeptins A and B, Serine Protease Inhibitors with Different Selectivity Profiles from a Marine Cyanobacterium, *Lyngbya* sp. *J. Nat. Prod.* **2008,** 71, 1625-1629.

Tease, B. E.; Walker, R. W., Comparative composition of the sheath of the cyanobacterium *Gloeothece* ATCC 27152 cultuered with and without combined nitrogen. *J. Gen. Microbiol.* **1987**, 133, 3331-3339

Tillett, D.; Dittmann, E.; Erhard, M.; von Döhren, H.; Börner, T.; Neilan, B. A., Structural organization of microcystin biosynthesis in *Microcystis aeruginosa* PCC7806: an integrated peptide–polyketide synthetase system. *Chem. Biol.* **2000**, 7, 753-764.

Trimurtulu, G.; Ohtani, I.; Patterson, G. M. L.; Moore, R. E.; Corbett, T. H.; Valeriote, F. A.; Demchik, L., Total Structures of Cryptophycins, Potent Antitumor Depsipeptides from the Blue-Green Alga Nostoc sp. Strain GSV 224. *J. Am. Chem. Soc.* **1994**, 116, 4729-4737.

Van Wagoner, R. M.; Drummond, A. K.; Wright, J. L. C., Biogenetic Diversity of Cyanobacterial Metabolites. *Adv. Appl. Microbiol.* **2007**, 61, 89-217.

REFERENCES (continued)

Viaggiu, E.; Melchiorre, S.; Volpi, F.; Di Corcia, A.; Mancini, R.; Garibaldi, L.; Crichigno, G.; Bruno, M., Anatoxin-a toxin in the cyanobacterium Planktothrix rubescens from a fishing pond in northern Italy. *Environ. Toxicol.* **2004**, 19, 191-197.

Wehr, J.D.; Sheath, R.G., Freshwater algae of North America. Academic Press: San Diego **2003**, pp117-196.

Welker, M.; von Dohren, H., Cyanobacterial peptides - nature's own combinatorial biosynthesis. *FEMS Microbiol. Rev.* **2006**, 30, 530-563.

Williamson, R. T.; Márquez, B. L.; Gerwick, W. H.; Kövér, K. E., One- and two-dimensional gradient-selected HSQMBC NMR experiments for the efficient analysis of long-range heteronuclear coupling constants. *Magn. Reson. Chem.* **2000**, 38, 265-273.

Wilmotte, A.; Golubic, S., Morphological and genetic criteria in the taxonomy of Cyanophyta/Cyanobacteria. *Arch. Hydrobiol./Algol. Stud.* **1991,** 64, 1-24.

Wonnacott, S.; Gallagher, T., The Chemistry and Pharmacology of Anatoxin-a and Related Homotropanes with respect to Nicotinic Acetylcholine Receptors. *Mar. Drugs* **2006,** 4, 228-254.

Wood, S. A.; Rasmussen, J. P.; Holland, P. T.; Campbell, R.; Crowe, A. L. M., First report of the cyanotoxin anatoxin-A from Aphanizomenon issatschenkoi (Cyanobacteria) *J. Phycol.* **2007,** 43, 356-365.

Yamakoshi, H.; Ikarashi, F.; Minami, M.; Shibuya, M.; Sugahara, T.; Kanoh, N.; Ohori, H.; Shibata, H.; Iwabuchi, Y., Syntheses of naturally occurring cytotoxic [7.7]paracyclophanes, (-)-cyclindrocyclophane A and its enantiomer, and implications for biological activity. *Org. Biomol. Chem.* **2009**, 7, 3772-3781.

Yoshizawa, S.; Matsushima, R.; Watanabe, M. F.; Harada, K.-i.; Ichihara, A.; Carmichael, W. W.; Fujiki, H., Inhibition of protein phosphatases by microcystis and nodularin associated with hepatotoxicity. *J. Cancer Res. Clin.* **1990,** 116, 609-614.

Zafrir, E.; Carmeli, S., Micropeptins from an Israeli Fishpond Water Bloom of the Cyanobacterium *Microcystis* sp. *J. Nat. Prod.* **2009,** 73, 352-358.

APPENDICES

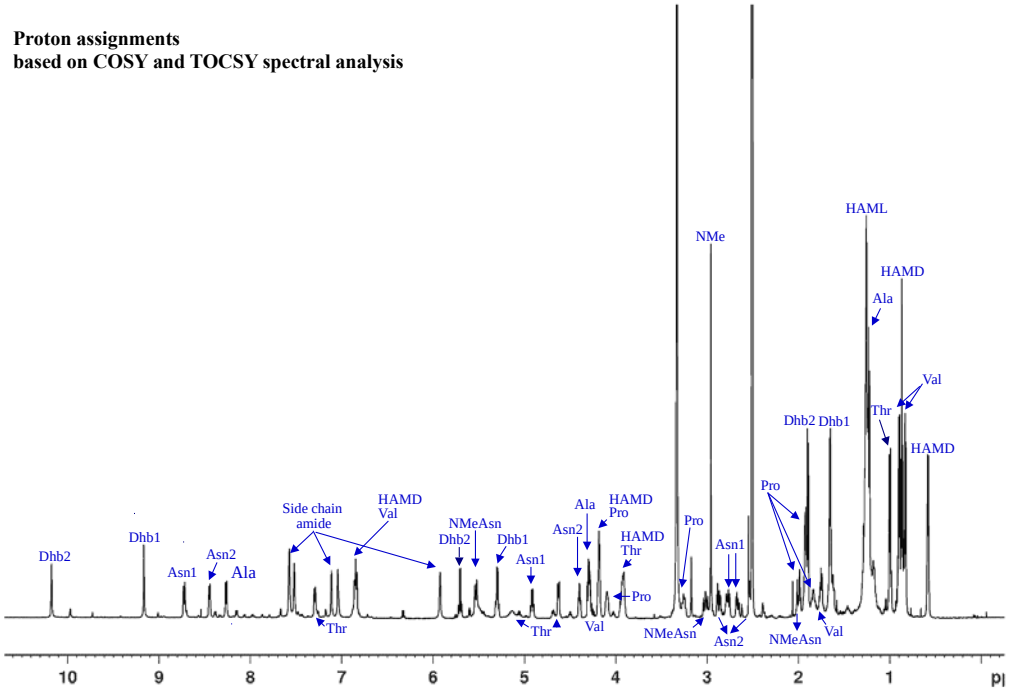

Figure S1. ^{1}H NMR spectrum of minutissamide A (**1**).

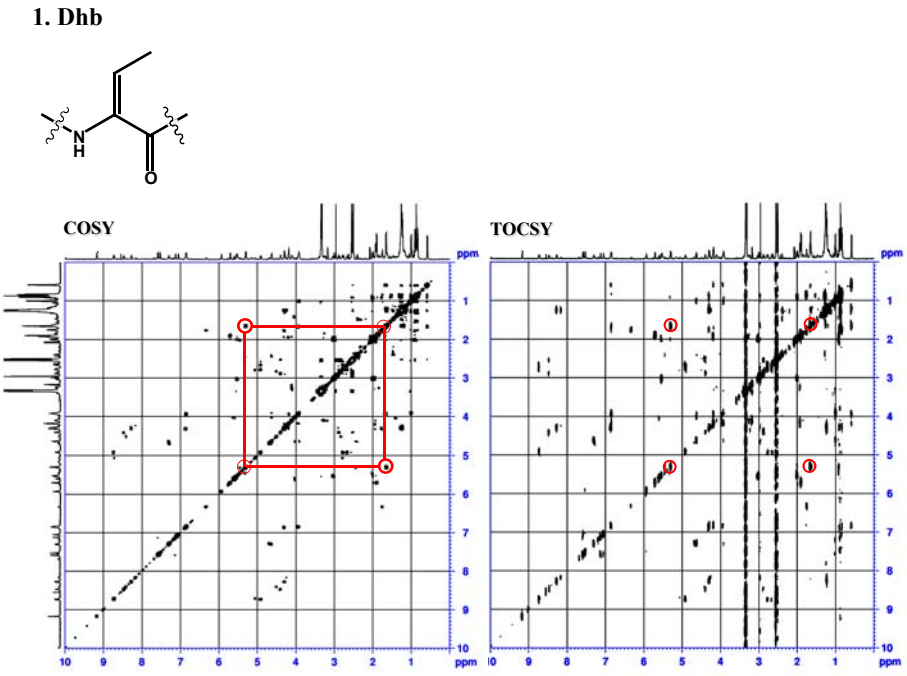

Figure S2. Spin system for Dhb assigned from the COSY and TOCSY spectra of **1**.

APPENDICES (continued)

2. Dhb

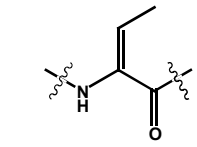

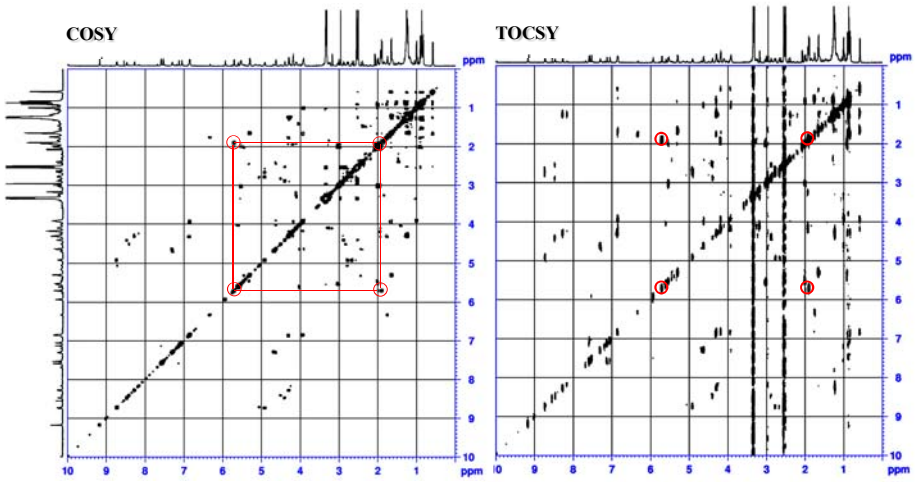

Figure S3. Spin system for Dhb assigned from the COSY and TOCSY spectra of **1**.

3. Asparagine

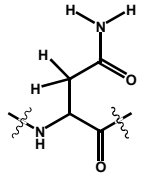

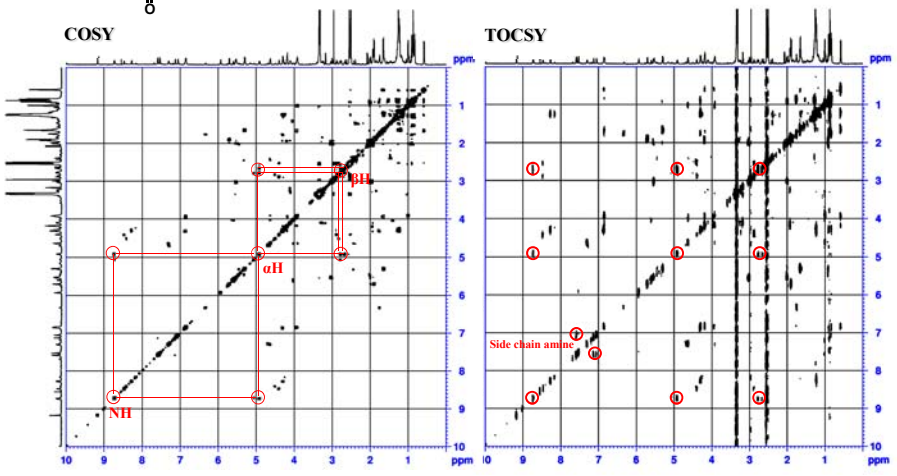

Figure S4. Spin system for Asn assigned from the COSY and TOCSY spectra of **1**.

APPENDICES (continued)

4. Asparagine

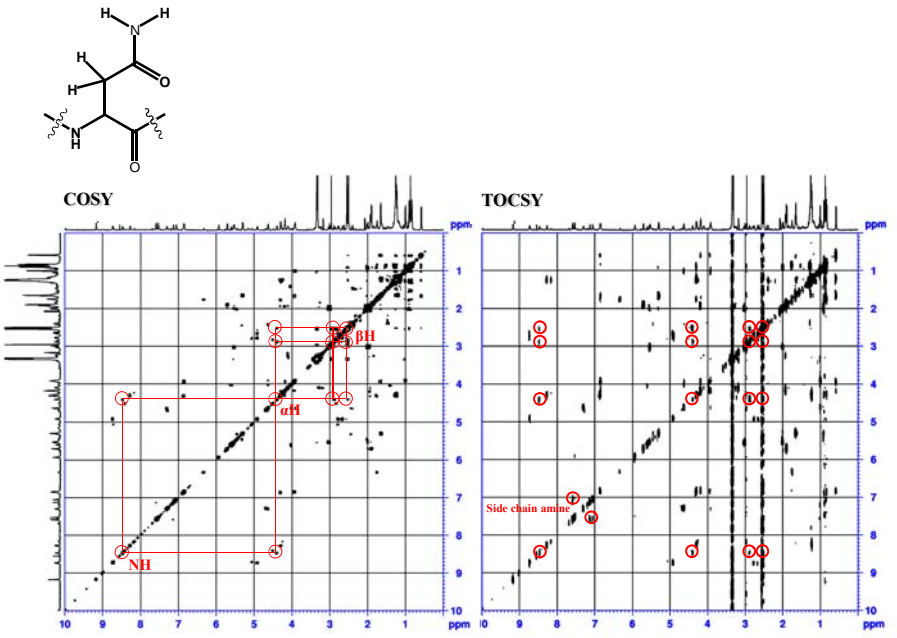

Figure S5. Spin system for Asn assigned from the COSY and TOCSY spectra of minutissamide A.

5. Alanine

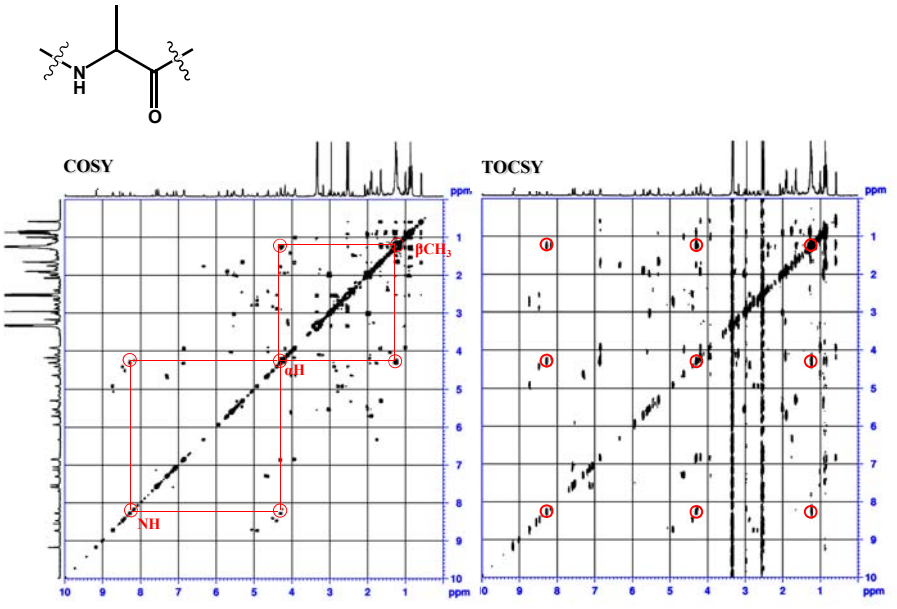

Figure S6. Spin system for Ala assigned from the COSY and TOCSY spectra of minutissamide A.

APPENDICES (continued)

6. Threonine

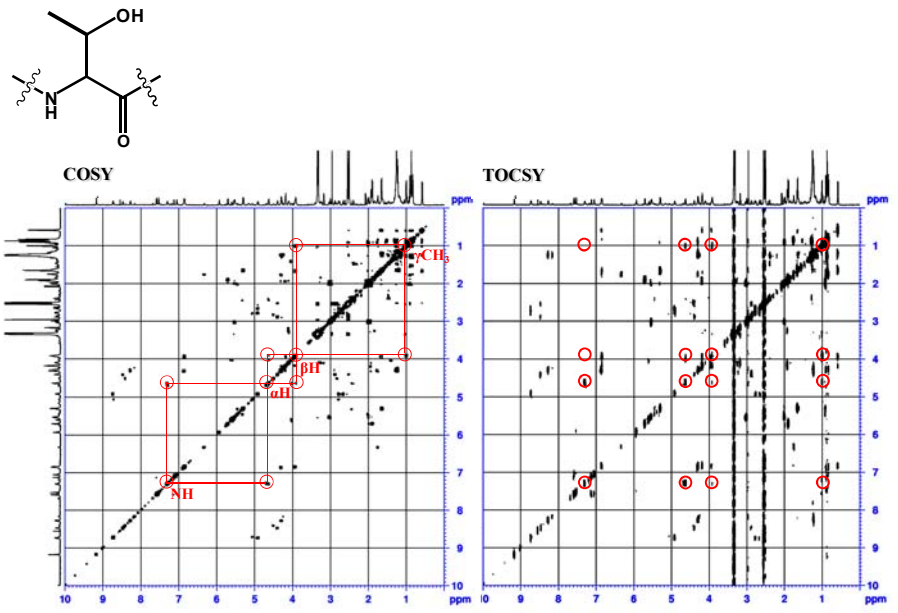

Figure S7. Spin system for Thr assigned from the COSY and TOCSY spectra of minutissamide A.

7. Proline

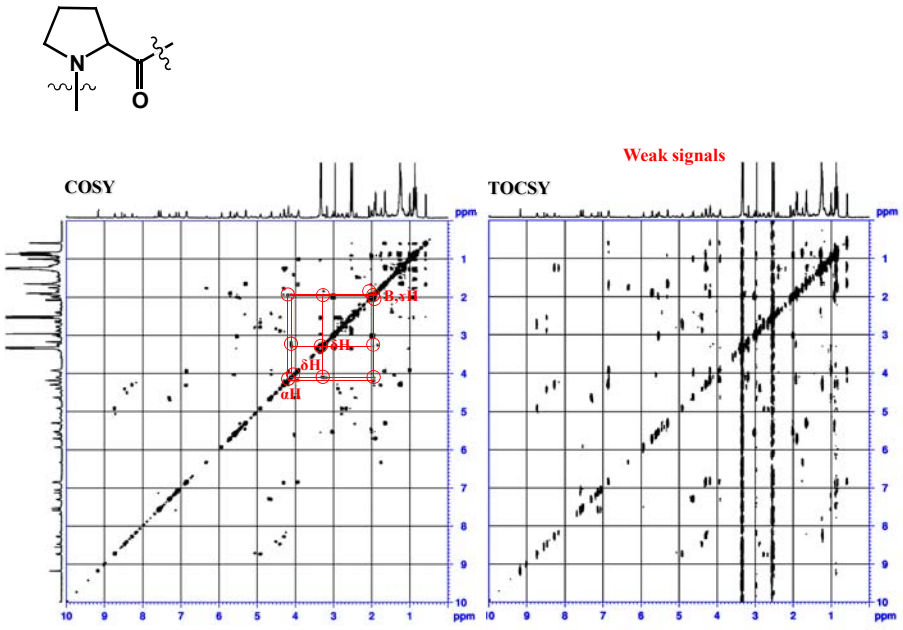

Figure S8. Spin system for Pro assigned from the COSY and TOCSY spectra of minutissamide A.

APPENDICES (continued)

8. N-methyl Asparagine

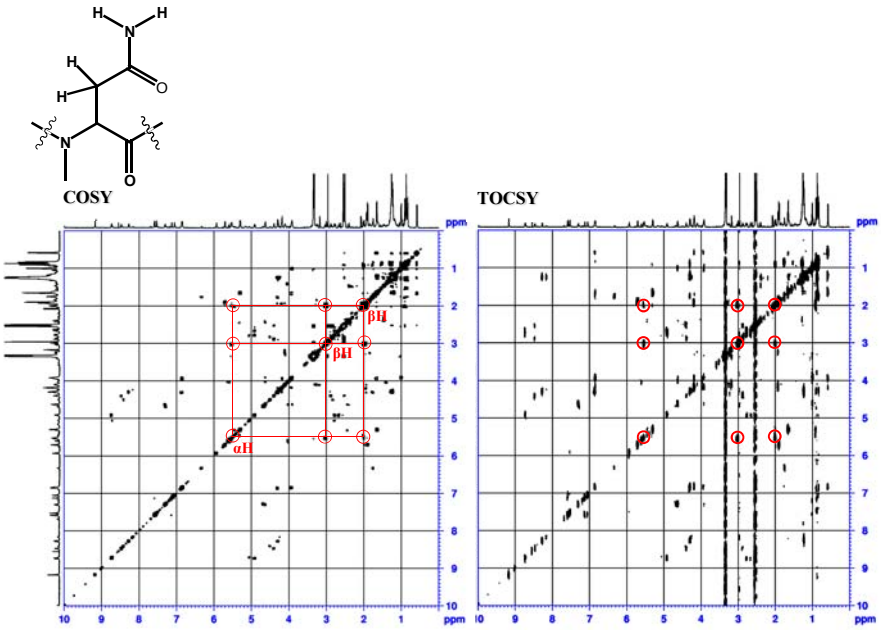

Figure S9. Spin system for *N*MeAsn assigned from the COSY and TOCSY spectra of minutissamide A.

9. Lipophilic side chain: HAMD

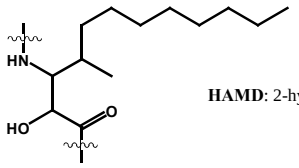

HAMD: 2-hydroxy-3-amino-4-methyldodecanoic acid

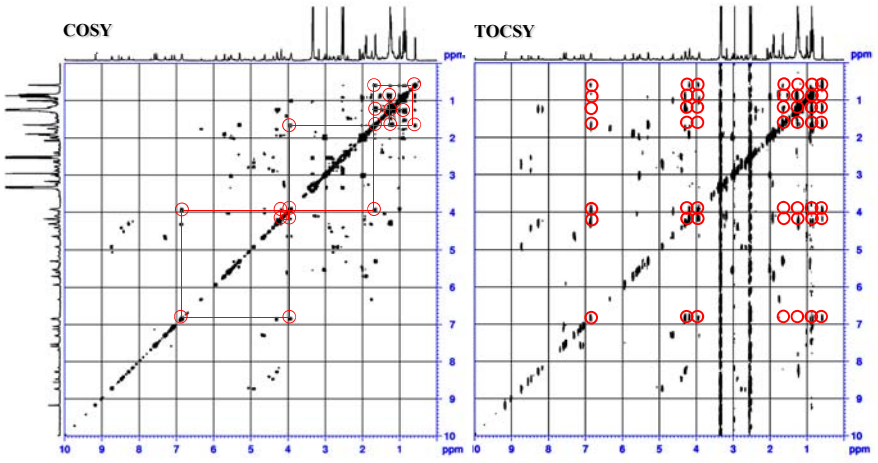

Figure S10. Spin system for HAMD assigned from the COSY and TOCSY spectra of minutissamide A.

APPENDICES (continued)

10. Valine

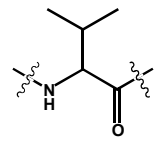

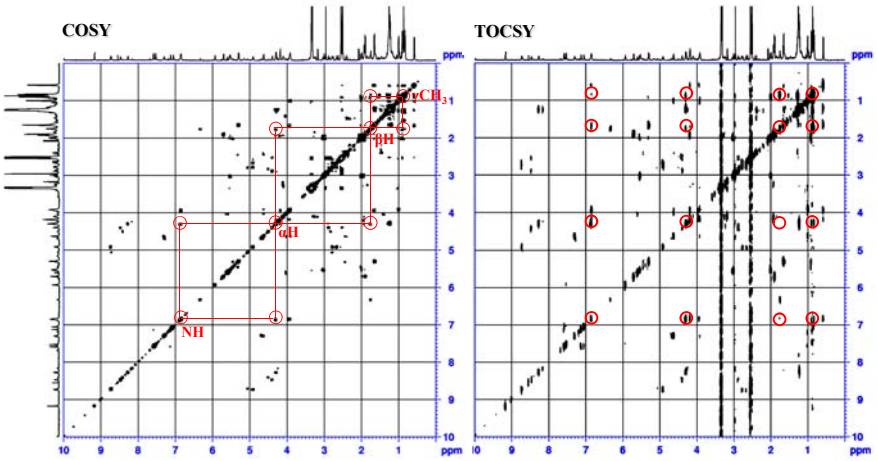

Figure S11. Spin system for Val assigned from the COSY and TOCSY spectra of minutissamide A.

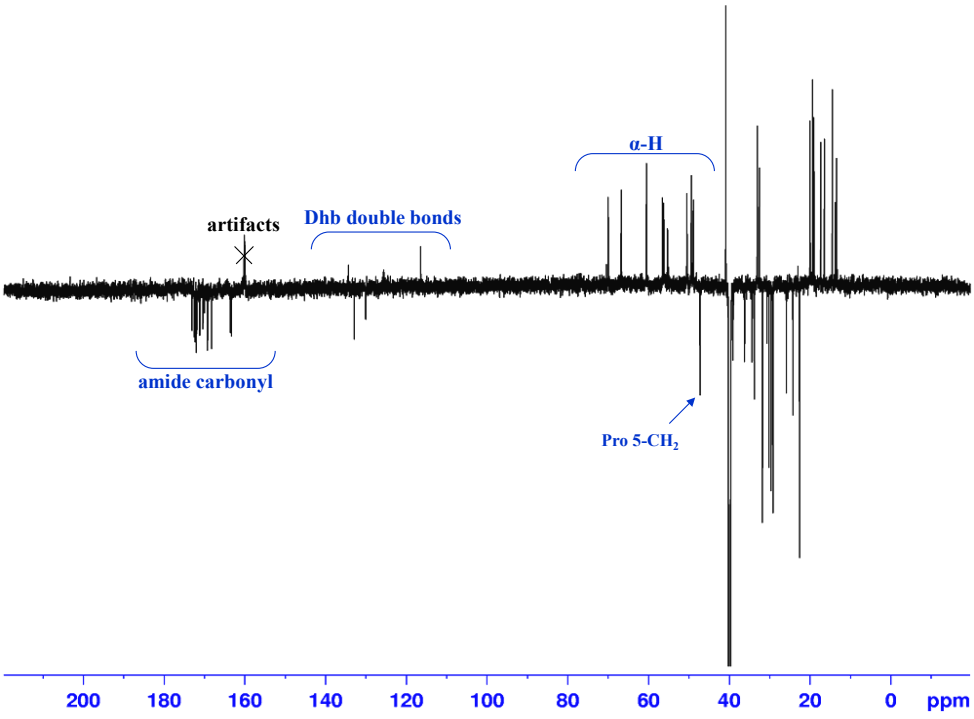

Figure S12. DEPT-Q spectrum (226 MHz, DMSO-d_6) of minutissamide A.

APPENDICES (continued)

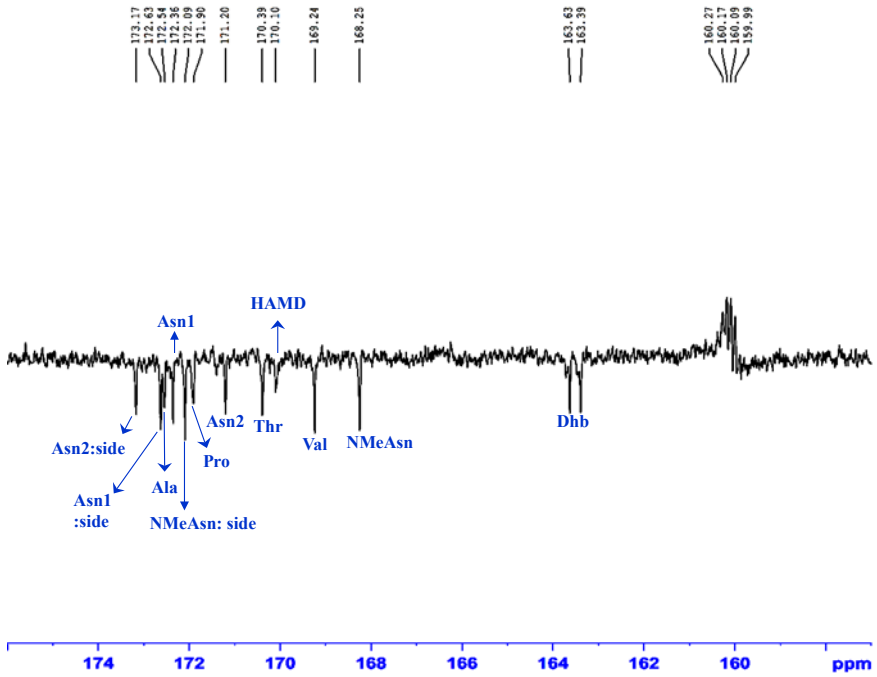

Figure S13. DEPT-Q spectrum (226 MHz, DMSO-d_6) in an amide carbonyl region of minutissamide A.

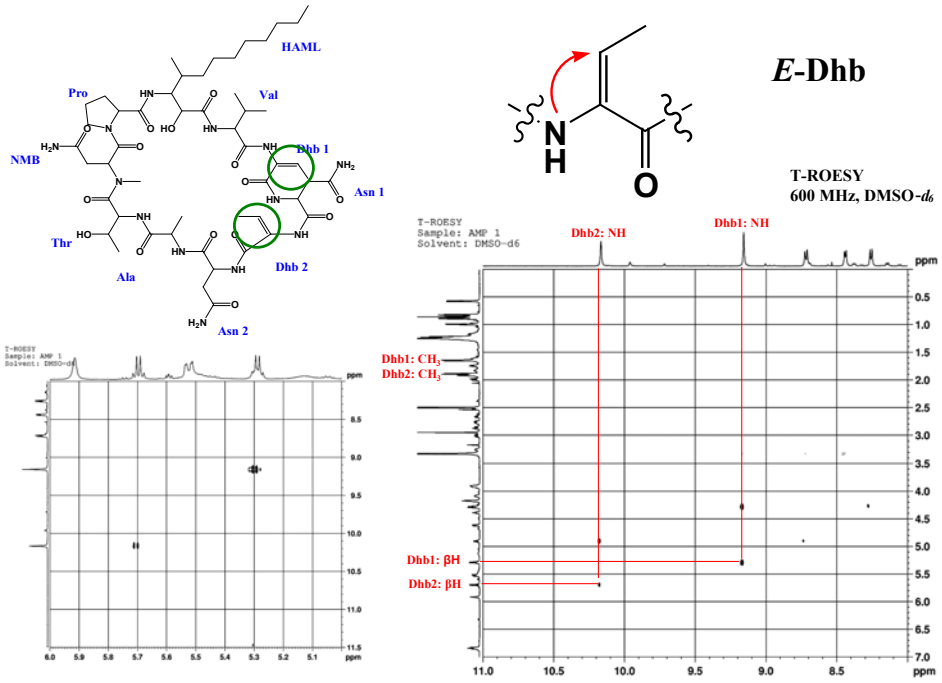

Figure S14. ROESY correlations used for the assignment of the geometric configurations of two Dhb residues in minutissamide A.

APPENDICES (continued)

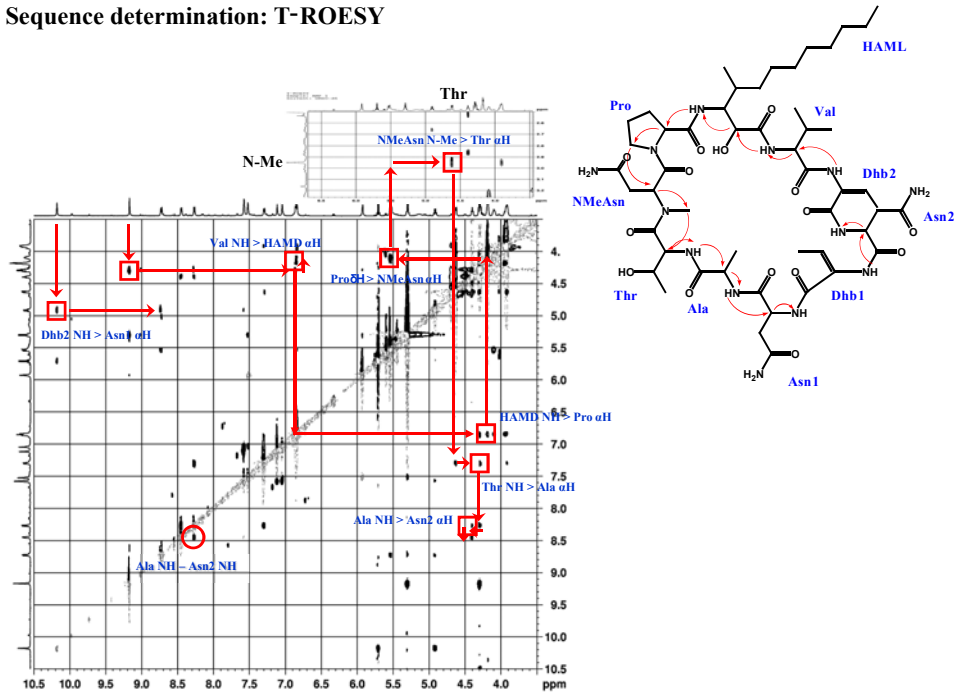

Figure S15. ROESY correlations used for the determination of the amino acid sequence of minutissamide A (HAML = Hamd).

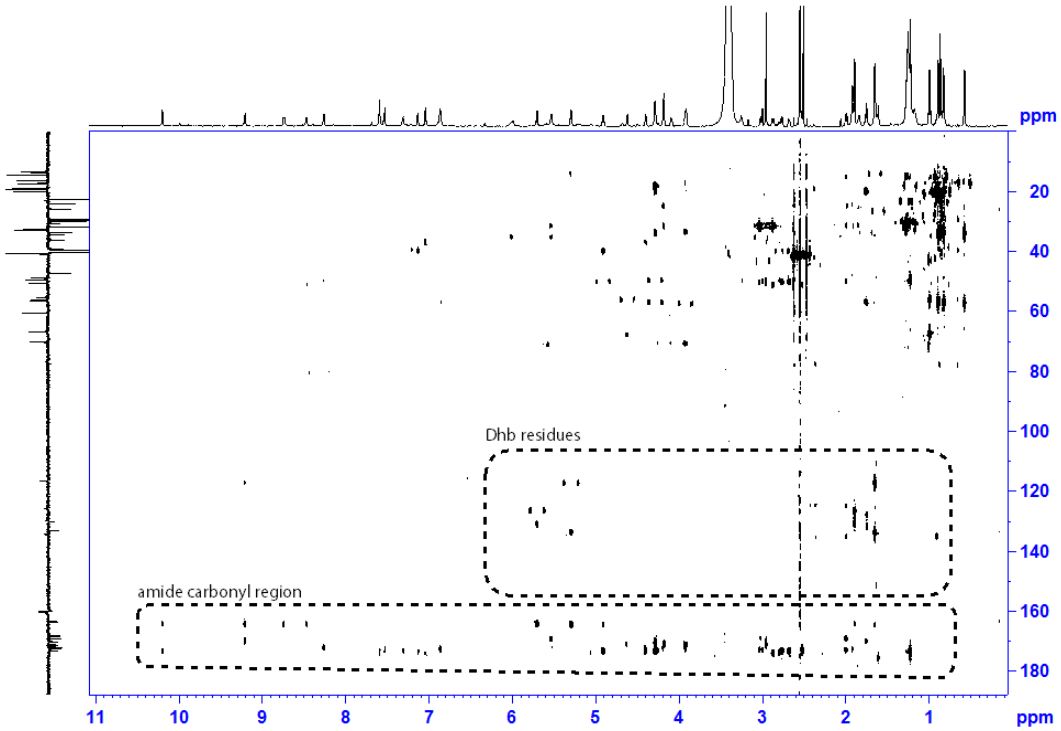

Figure S16. HMBC spectrum of minutissamide A.

APPENDICES (continued)

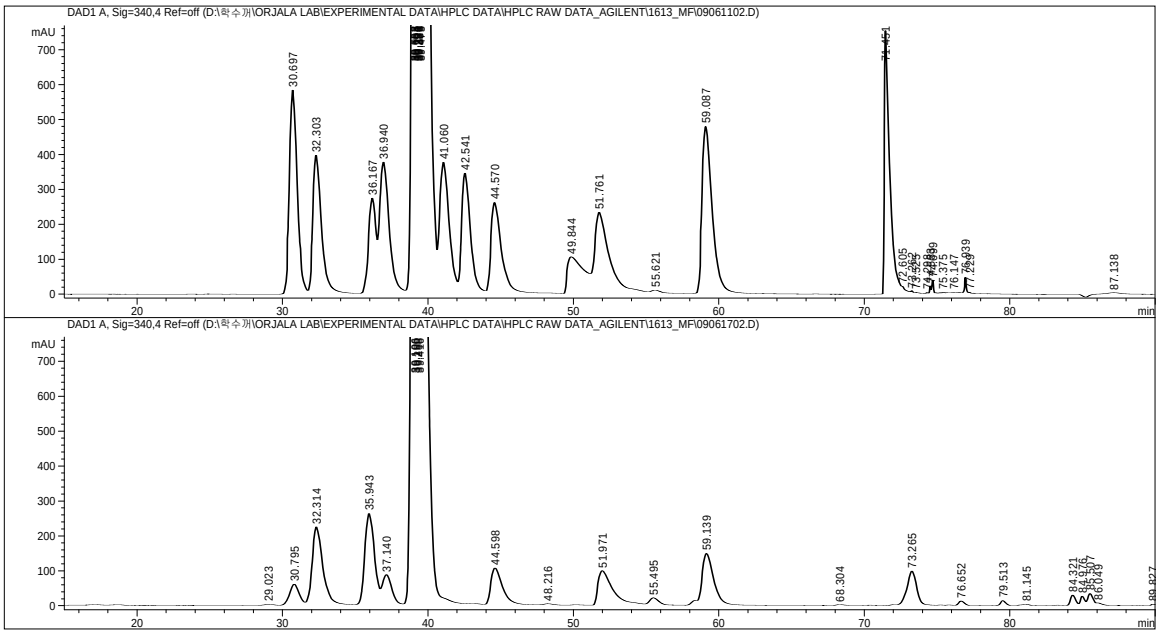

Upper: FDAA derivatives of standard amino acids, Bottom: FDAA derivatives of Acid hydrolysate of **1**

Amino acid	HPLC retention times; Marfey's derivatives of standard amino acids		HPLC retention times; Marfey's derivatives of Acid hydrolysate of **1**	Assignment
	L	D		
Alanine	41.1 min	51.8 min	52.0 min	D
Aspartate	32.3 min	36.9 min	32.3 min	L
N-methyl Aspartate	36.2 min	30.7 min	35.9 min	L
Proline	44.6 min	49.8 min	44.6 min	L
Threonine	30.7 min	42.5 min	30.8 min[a]	L
Valine	59.1 min	71.5 min	59.1 min	L

[a]Identified as L-Thr by LC-MS analysis

The peak at 37.1 min was not identified as D-Asp by LC-MS analysis

Figure S17. Marfey's analysis of minutissamide A for the absolute configurations of the amino acids

APPENDICES (continued)

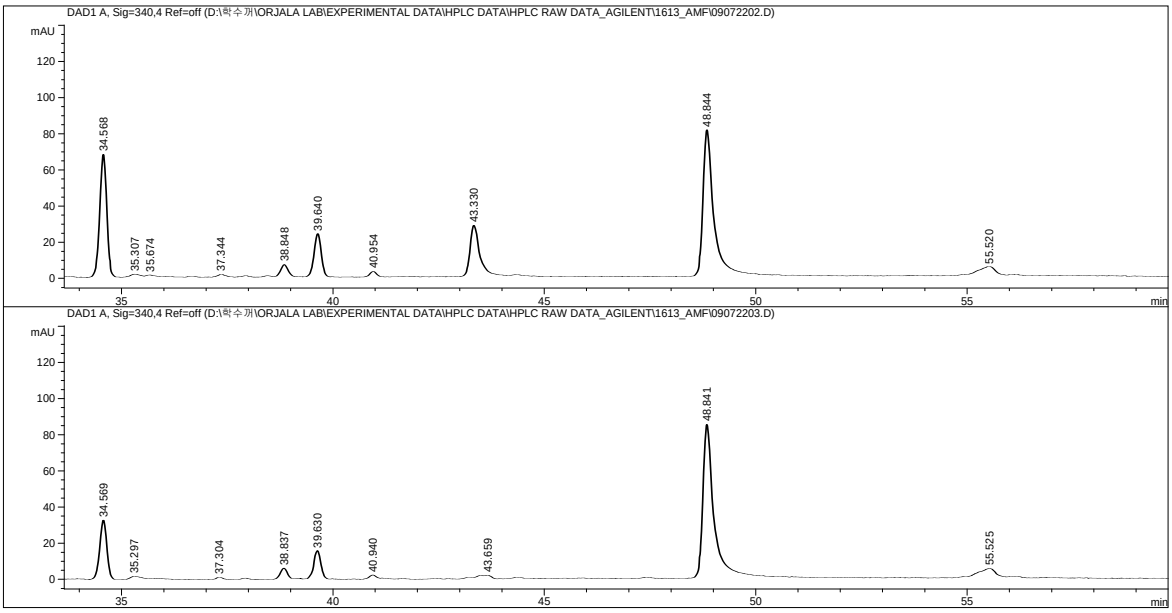

The peaks of FDLA derivatives of Hamd was assigned from LC-MS analysis

Derivatives	Retention times	Configurations
DL-FDLA derivatives of Hamd in **1**	43.3 min	S-L or R-D
	48.8 min	S-D or R-L
L-FDLA derivative of Hamd in **1**	48.8 min	**R-L**

Figure S18. Advanced Marfey's analysis of minutissamide A for the absolute configuration of the Hamd residue.

APPENDICES (continued)

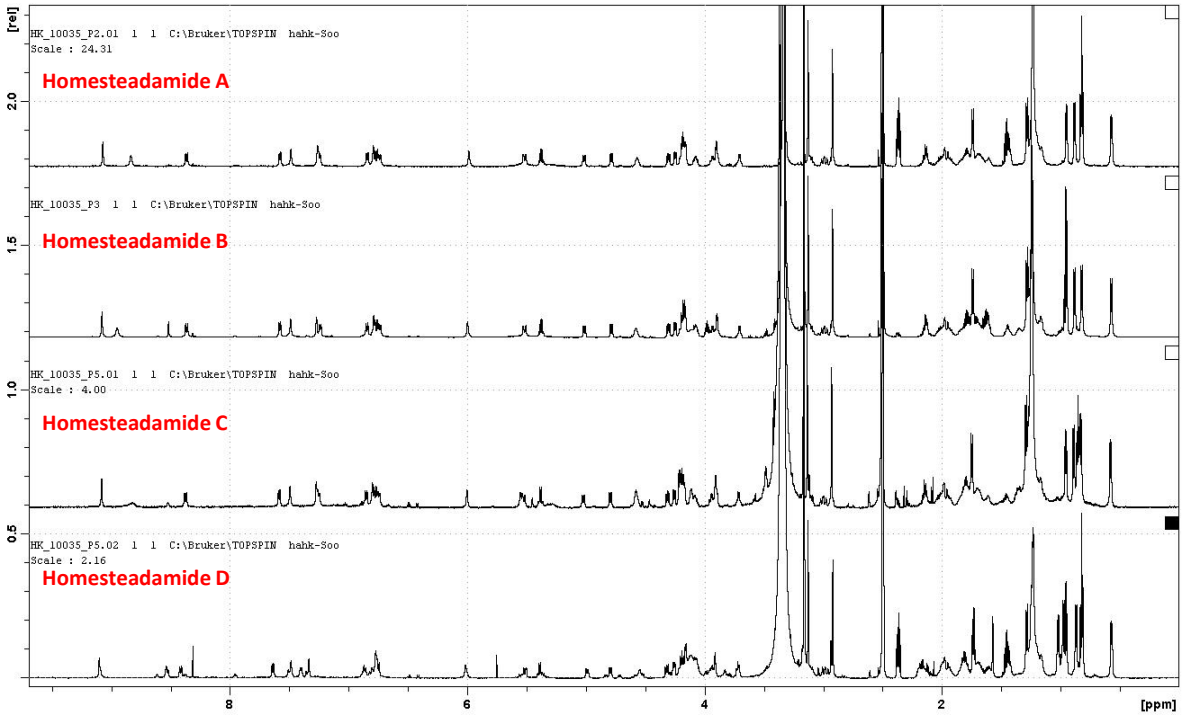

Figure S19. ^{1}H NMR spectra of homesteadamides A – D.

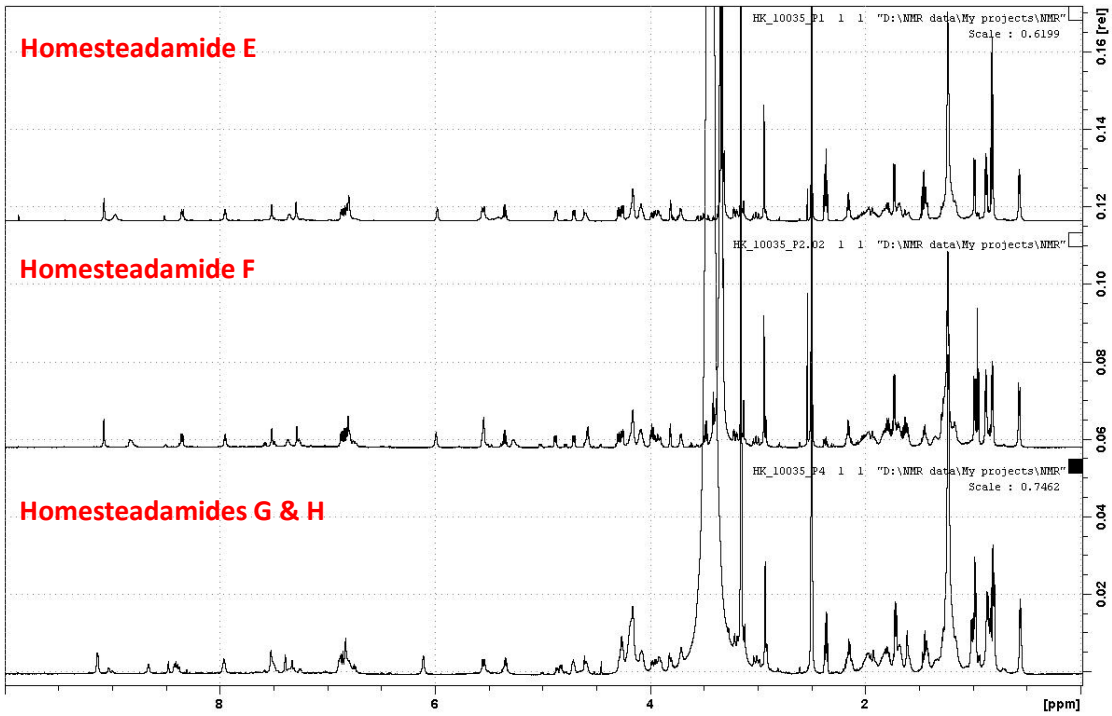

Figure S20. ^{1}H NMR spectra of homesteadamides E – H.

APPENDICES (continued)

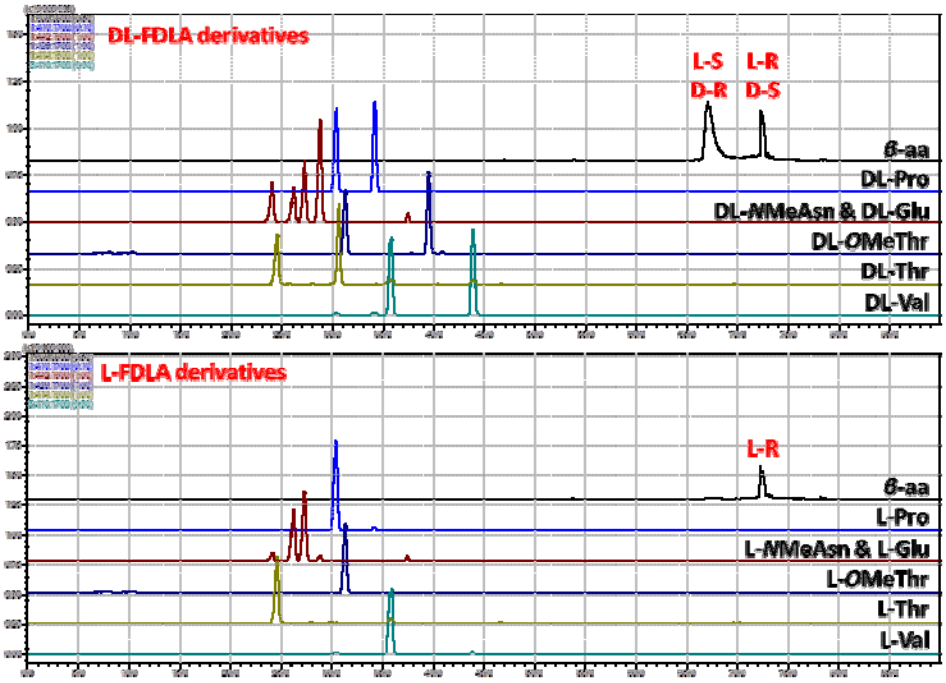

Amino acid	HPLC retention times of DL-FDLA derivative of acid hydrolysate of **1**		HPLC retention times of L-FDLA derivative of acid hydrolysate of **1**	Assignment
	L	D		
Hamoo	67.0 min (S)	72.4 min (R)	72.4 min	R
Pro	30.4 min	34.1 min	30.5 min	L
*N*MeAsn	26.3 min	24.0 min	26.3 min	L
Ala	30.9 min	35.4 min	35.6 min	D
Gln	27.2 min	28.7 min	27.4 min	L
Thr	24.5 min	30.6 min	24.7 min	L
Val	35.8 min	43.8 min	35.9 min	L

- L-FDLA derivative of Thr was further compared with L-FDLA derivatives of four Thr amino acid standards L-Thr, L-*allo*-Thr, D-Thr and D-*allo*-Thr, and corresponded with the retention time of L-Thr.

Figure S21. Advanced Marfey's analysis of homesteadamide A for the determination of amino acid configurations.

APPENDICES (continued)

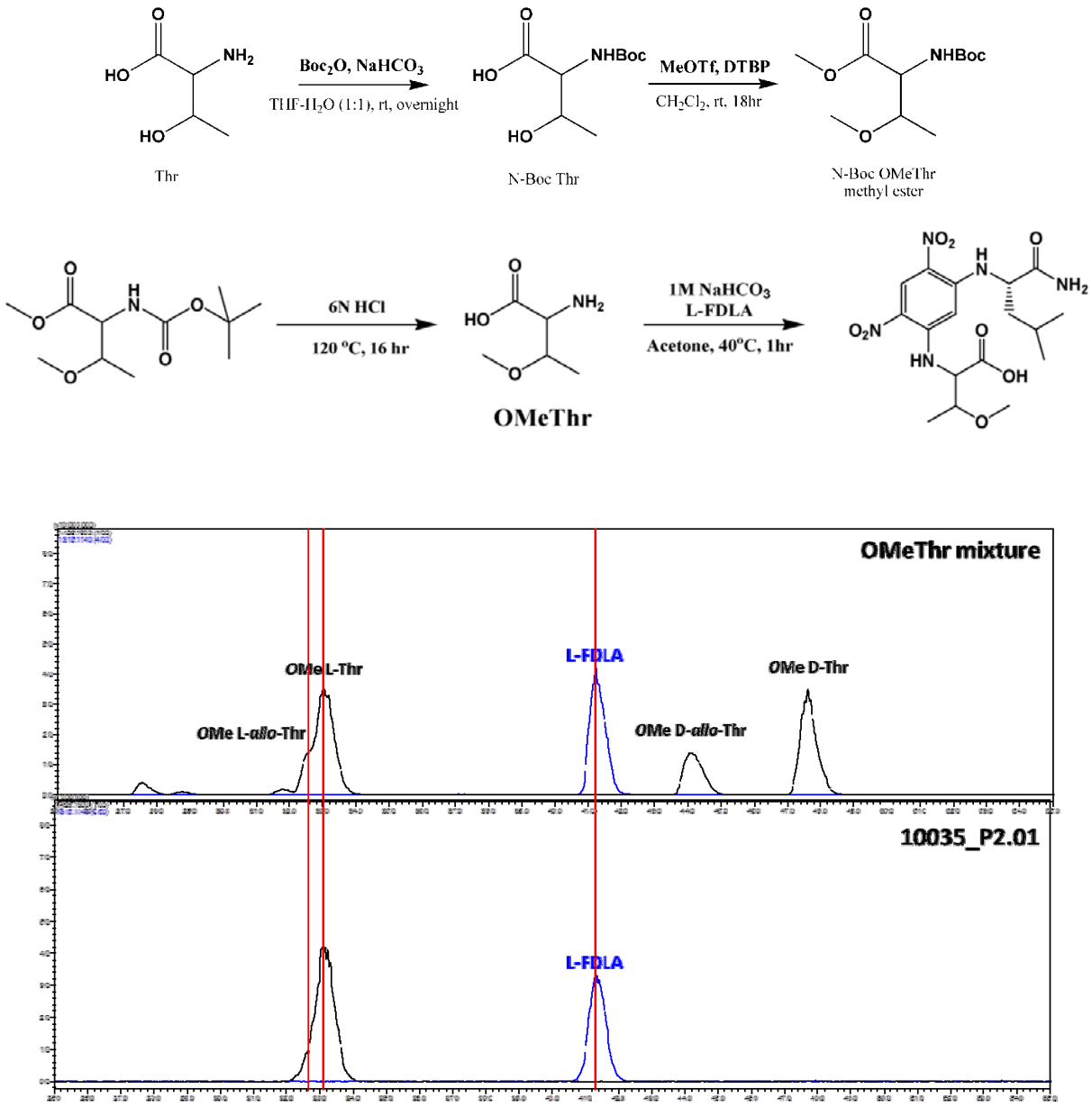

Figure S22. Synthesis of *O*MeThr standards and Marfey's analysis of the homesteadamides for the absolute configuration of *O*MeThr (10035_P2.01 = homesteadamide A).

APPENDICES (continued)

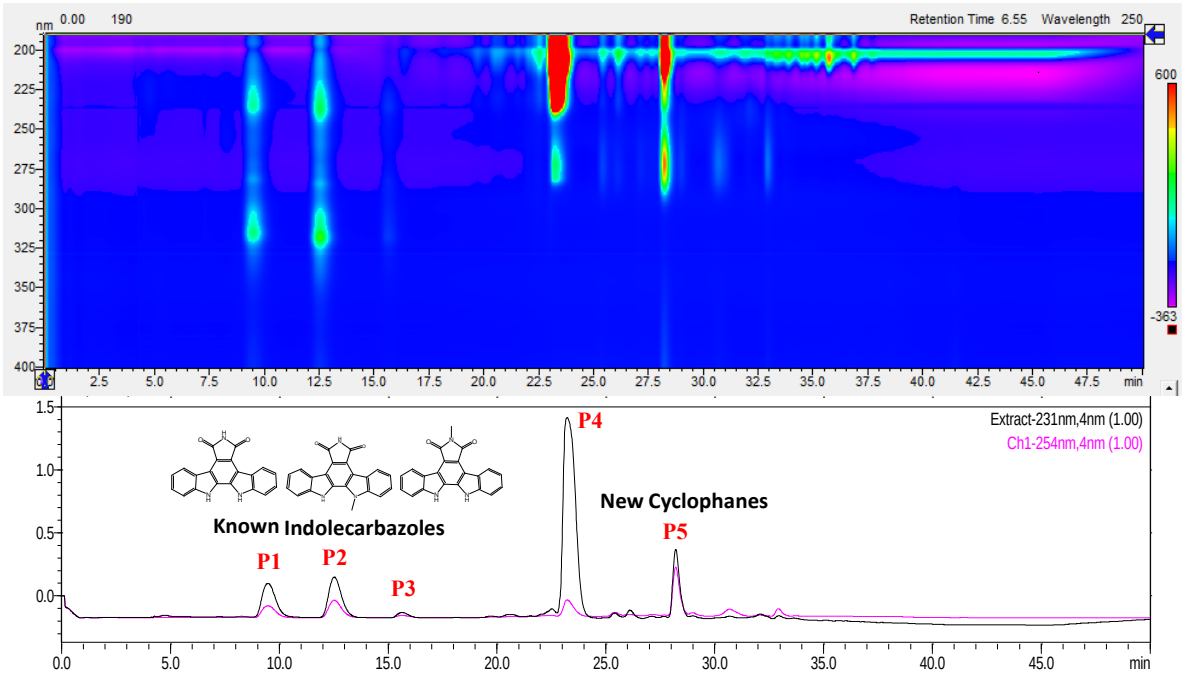

Figure S23. LC-MS analysis of cytotoxic fractions against HT-29 cancer cells from UIC 10062.

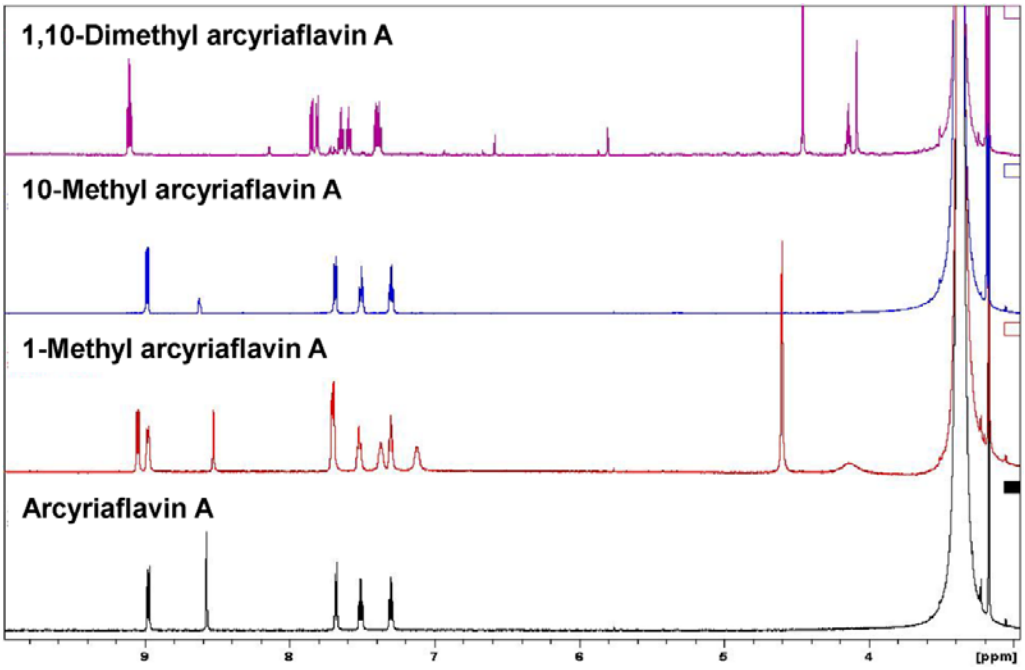

Figure S24. ^{1}H NMR spectra of known indolocarbazoles isolated from a *Nostoc* sp. (UIC 10062).

APPENDICES (continued)

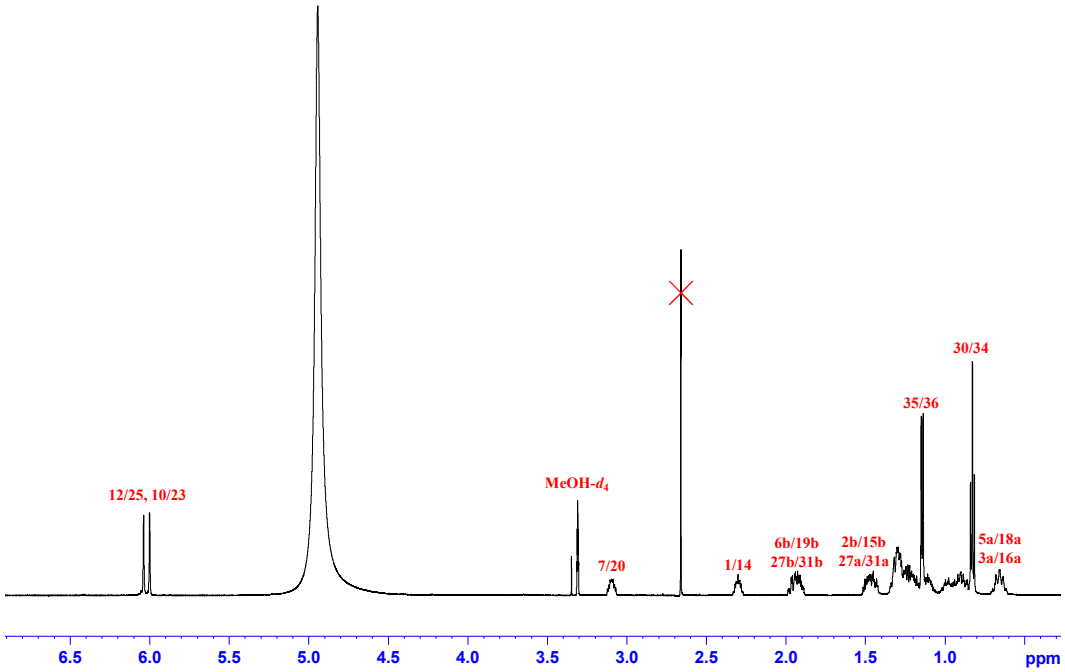

Figure S25. ^{1}H NMR spectrum (600 MHz, MeOH-d_4) of merocyclophane A.

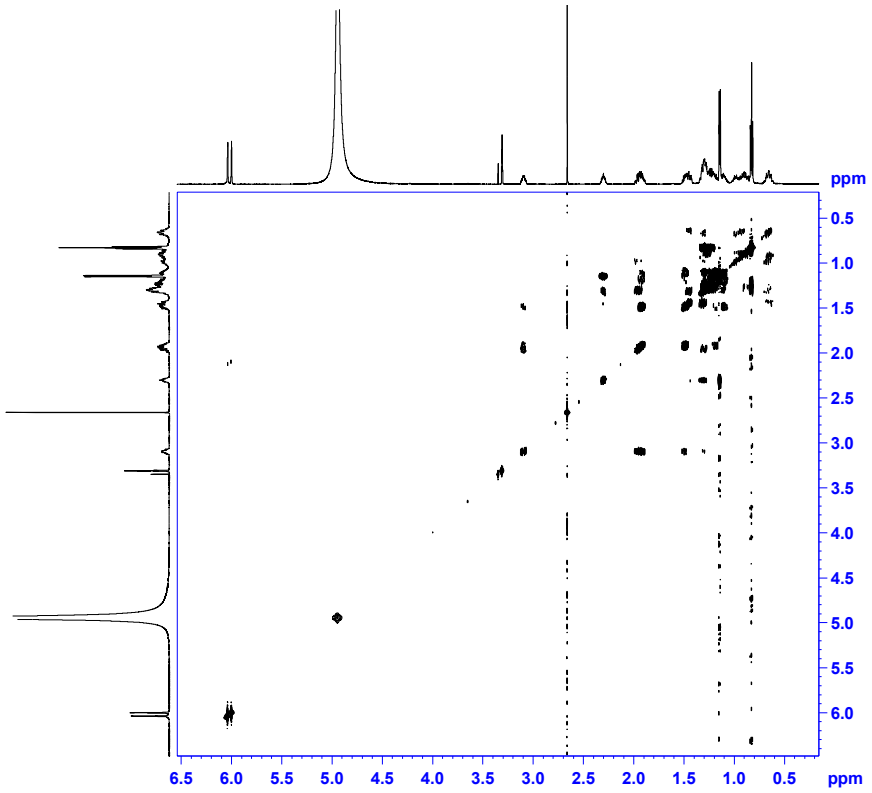

Figure S26. COSY spectrum (600 MHz, MeOH-d_4) of merocyclophane A.

APPENDICES (continued)

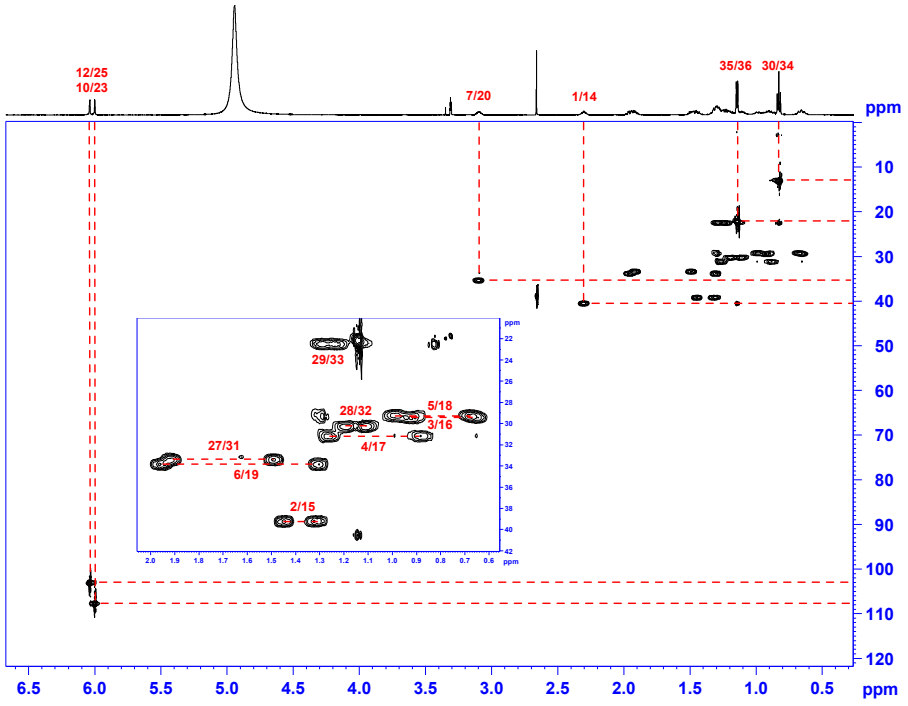

Figure S27. HSQC spectrum (600 MHz, MeOH-d_4) of merocyclophane A.

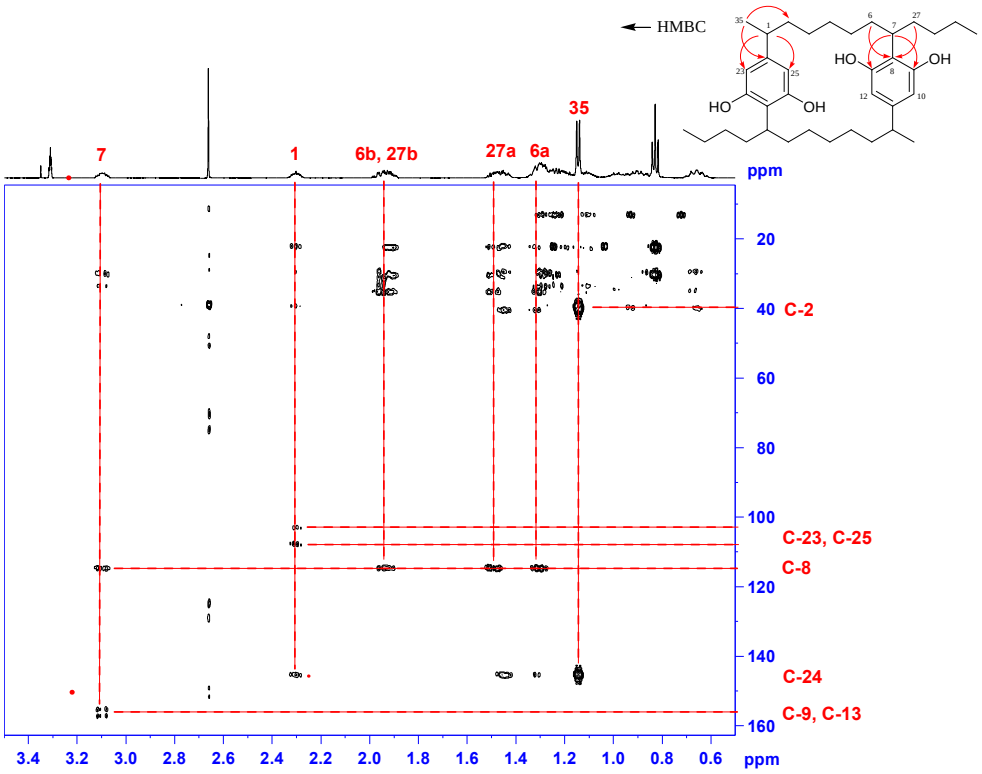

Figure S28. HMBC spectrum (600 MHz, MeOH-d_4) of merocyclophane A.

APPENDICES (continued)

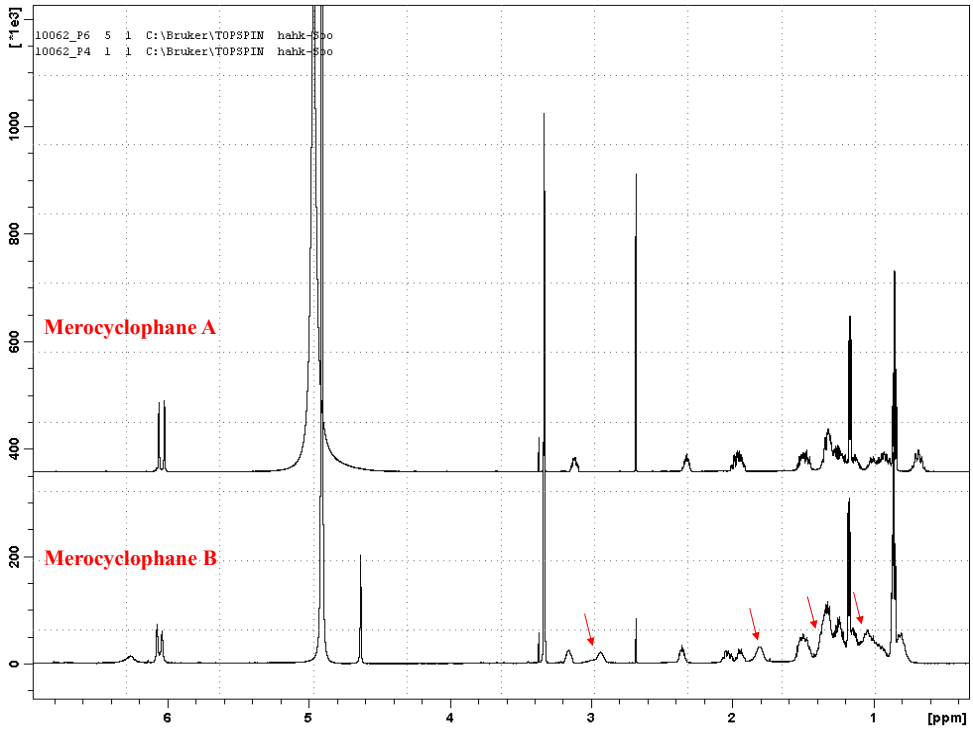

Figure S29. Comparison of ^{1}H NMR spectra between merocyclophanes A and B.

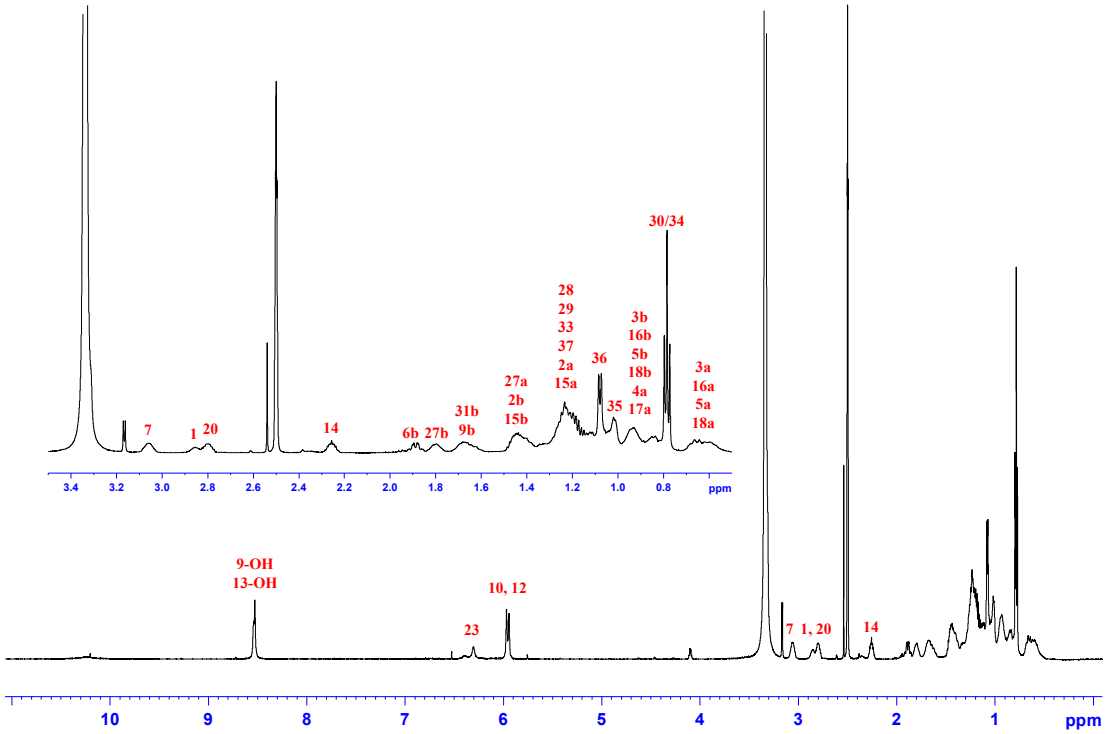

Figure S30. ^{1}H NMR spectrum (600 MHz, DMSO-d_6) of merocyclophane B.

APPENDICES (continued)

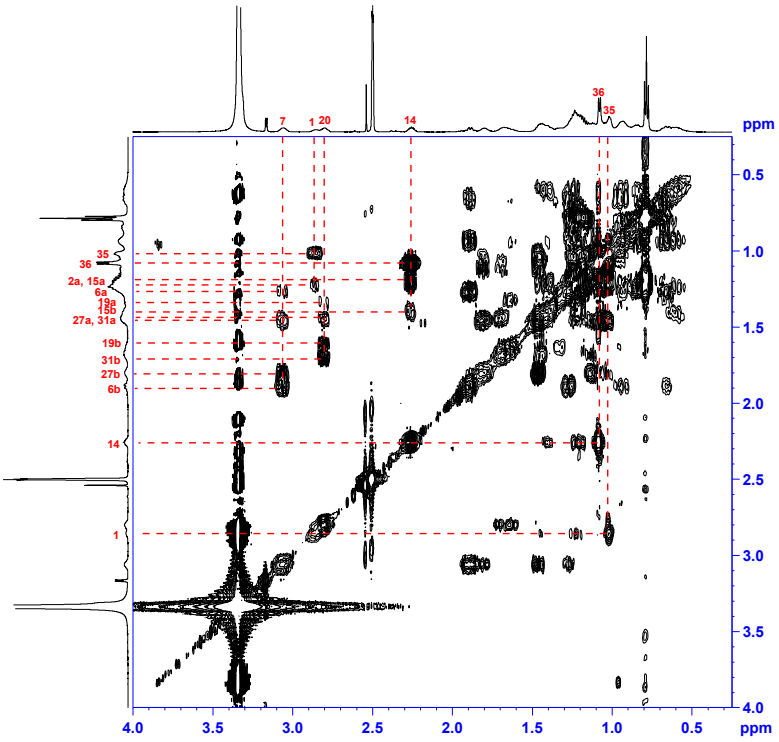

Figure S31. COSY spectrum (600 MHz, DMSO-d_6) of merocyclophane B.

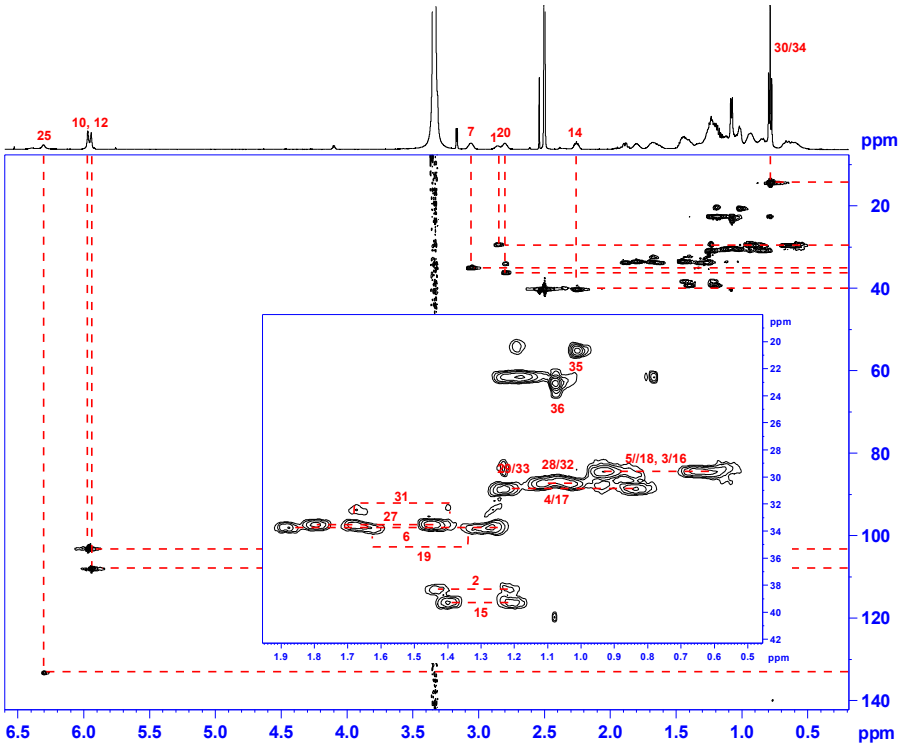

Figure S32. HSQC spectrum (600 MHz, DMSO-d_6) of merocyclophane B.

APPENDICES (continued)

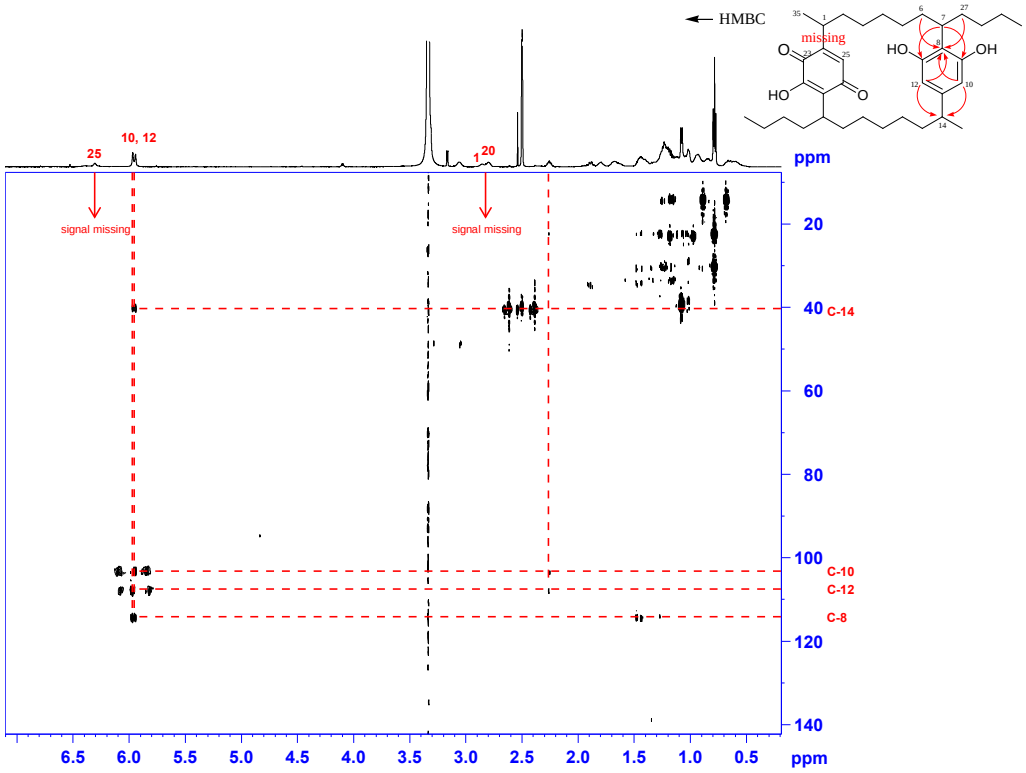

Figure S33. HMBC spectrum (600 MHz, DMSO-d_6) of merocyclophane B.

APPENDICES (continued)

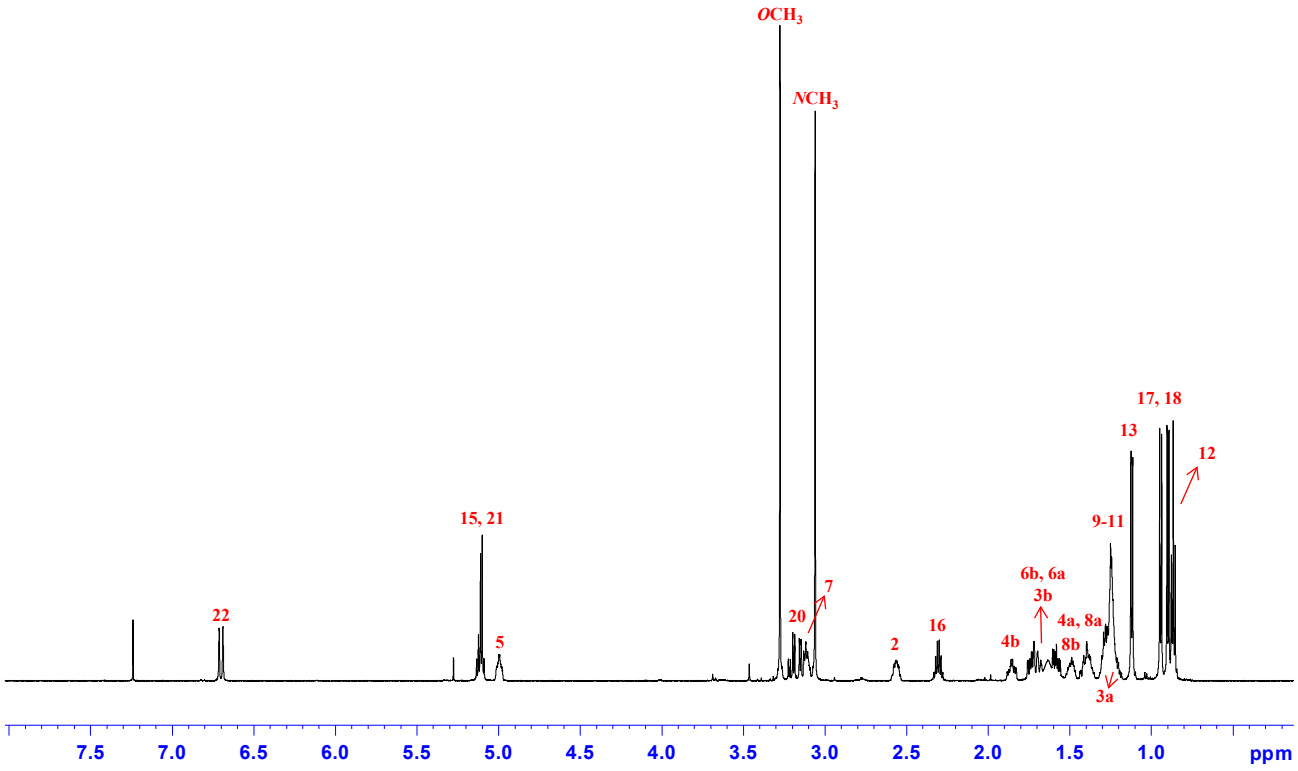

Figure S34. ^{1}H NMR spectrum (600 MHz, $CDCl_3$) of sanctolide A.

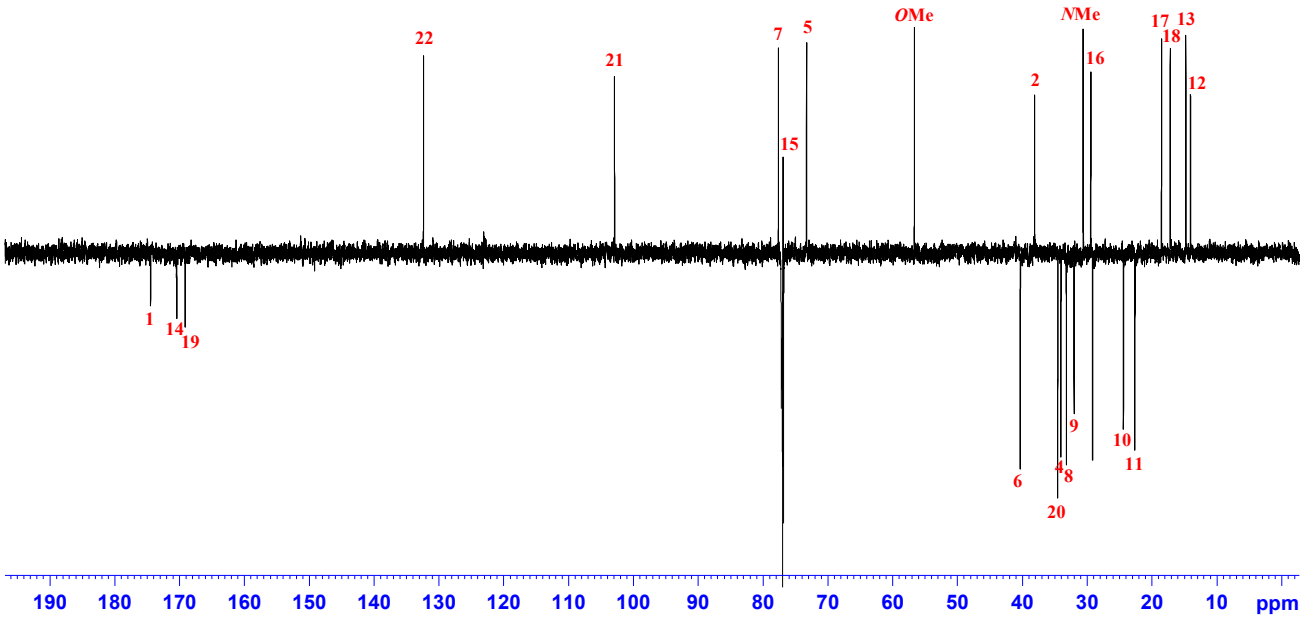

Figure S35. ^{13}C DEPT-Q NMR spectrum (226 MHz, $CDCl_3$) of sanctolide A.

APPENDICES (continued)

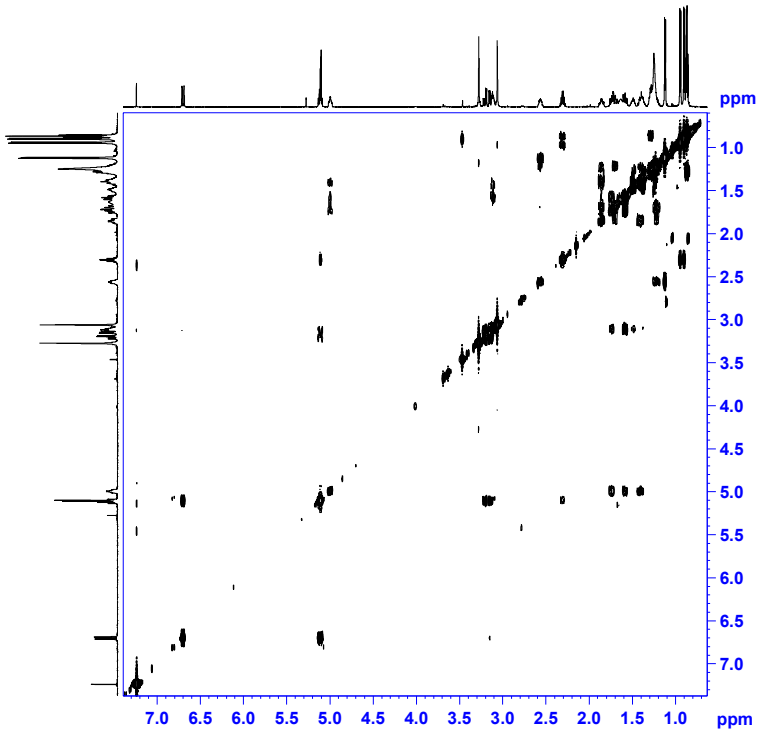

Figure S36. COSY spectrum (600 MHz, $CDCl_3$) of sanctolide A.

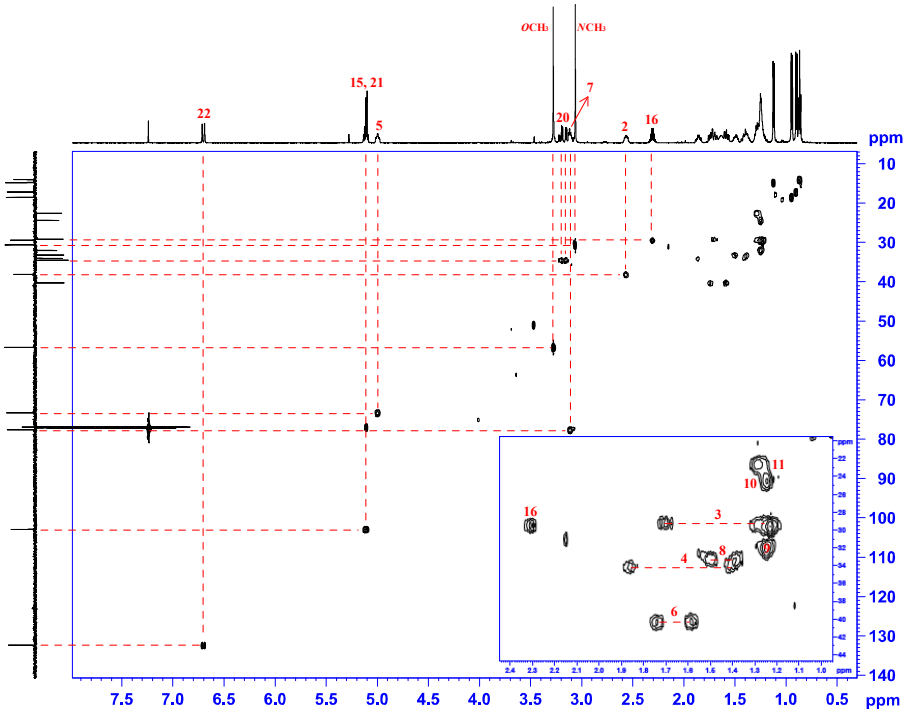

Figure S37. HSQC spectrum (600 MHz, $CDCl_3$) of sanctolide A.

APPENDICES (continued)

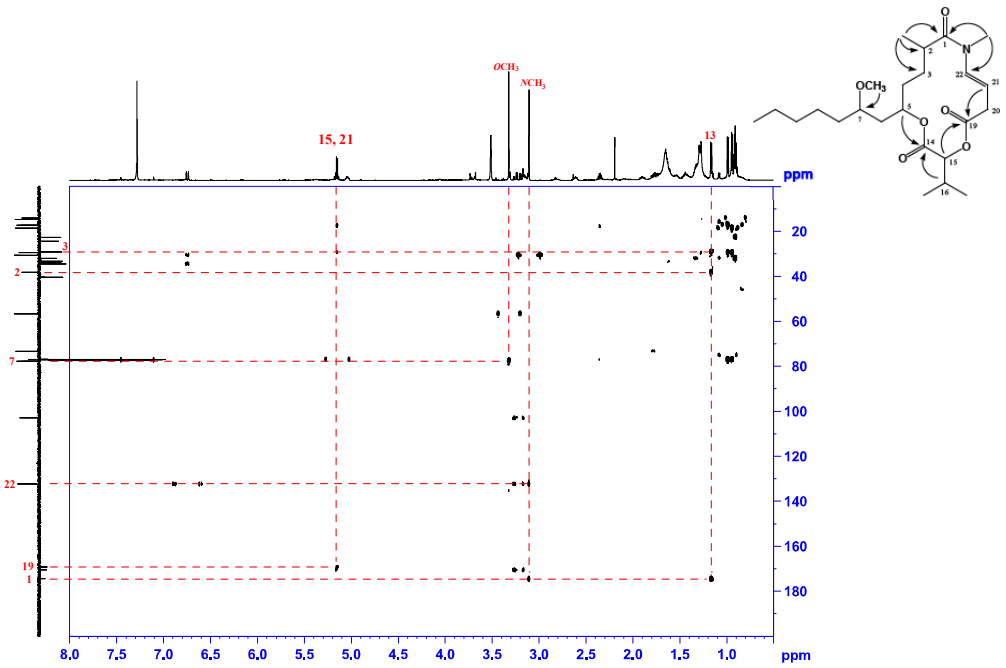

Figure S38. HMBC spectrum (600 MHz, $CDCl_3$) of sanctolide A.

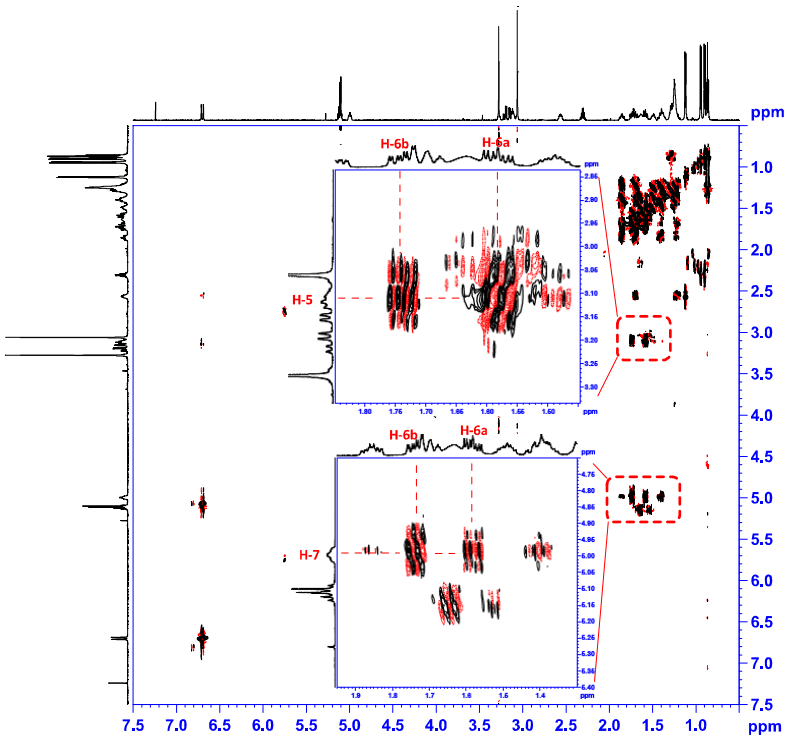

Figure S39. DQF-COSY spectrum (600 MHz, $CDCl_3$) of sanctolide A for *J*-based configurational analysis.

APPENDICES (continued)

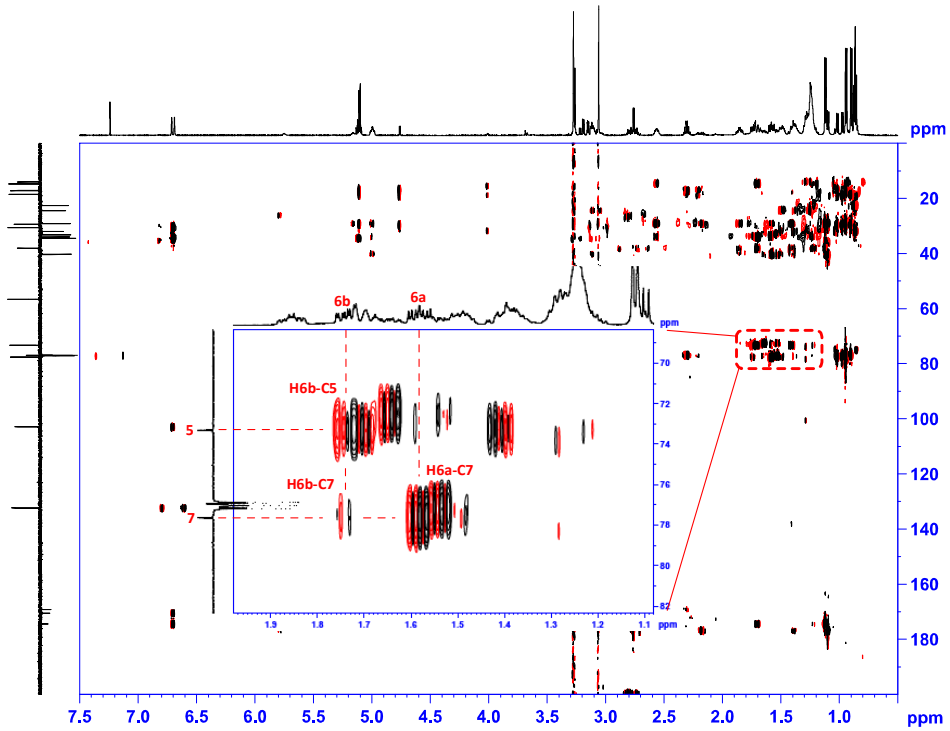

Figure S40. HSQMBC spectrum (600 MHz, $CDCl_3$) of sanctolide A for *J*-based configurational analysis.

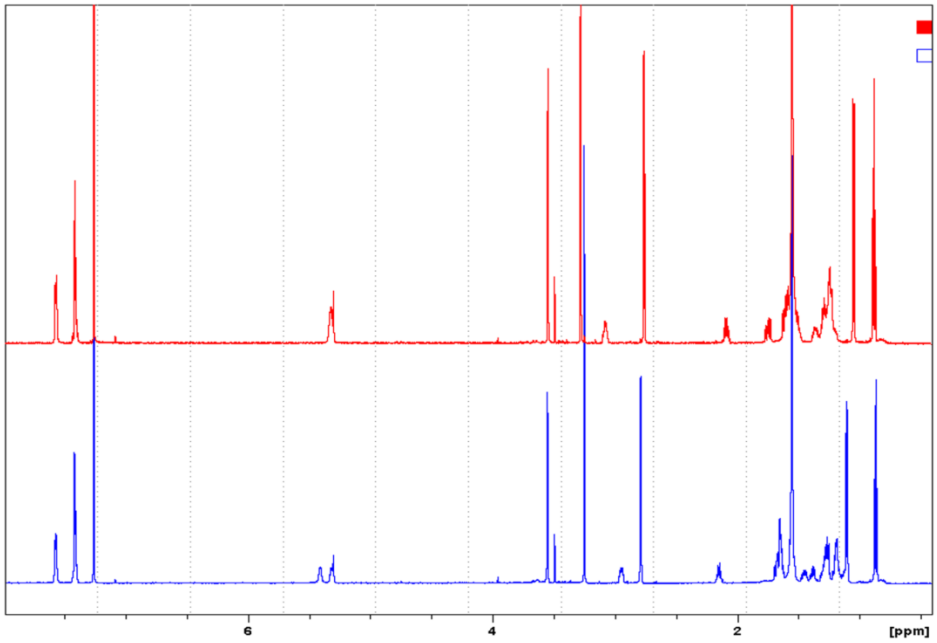

Figure S41. ^{1}H NMR spectra (600 MHz, $CDCl_3$) of **2S** and **2R** used for the determination of the absolute configuration of sancolide A. **Red**: (*S*)-MTPA ester (**2S**); **Blue**: (*R*)-MTPA ester (**2R**)

APPENDICES (continued)

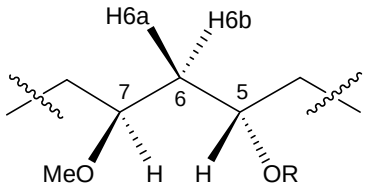

A: C5-C6

$^{3}J_{H5\text{-}H6a}$: 3.8 Hz (small)
$^{3}J_{H5\text{-}H6b}$: 8.1 Hz (large)
$^{2}J_{H6a\text{-}C5}$: 0 Hz (small)
$^{2}J_{H6b\text{-}C5}$: 6.7 Hz (large)
$^{3}J_{H5\text{-}C7}$: 4.1 Hz (medium)

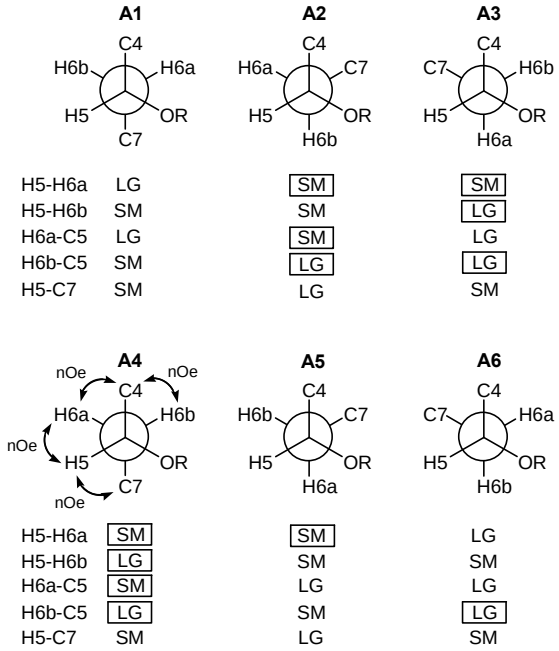

	A1	A2	A3
H5-H6a	LG	SM	SM
H5-H6b	SM	SM	LG
H6a-C5	LG	SM	LG
H6b-C5	SM	LG	LG
H5-C7	SM	LG	SM

	A4	A5	A6
H5-H6a	SM	SM	LG
H5-H6b	LG	SM	SM
H6a-C5	SM	LG	LG
H6b-C5	LG	SM	LG
H5-C7	SM	LG	SM

B: C6-C7

$^{3}J_{H6a\text{-}H7}$: 9.0 Hz (large)
$^{3}J_{H6b\text{-}H7}$: 2.9 Hz (small)
$^{2}J_{H6a\text{-}C7}$: 6.5 Hz (large)
$^{2}J_{H6b\text{-}C7}$: 0.7 Hz (small)

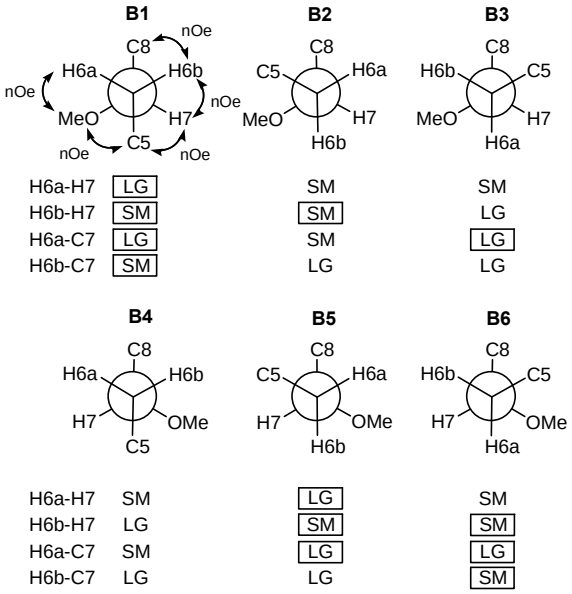

	B1	B2	B3
H6a-H7	LG	SM	SM
H6b-H7	SM	SM	LG
H6a-C7	LG	SM	LG
H6b-C7	SM	LG	LG

	B4	B5	B6
H6a-H7	SM	LG	SM
H6b-H7	LG	SM	SM
H6a-C7	SM	LG	LG
H6b-C7	LG	LG	SM

Figure S42. *J*-based configurational analysis for the relative configuration of the 1,3-methine system C5-C7 in sanctolide A: All the possible rotamer conformations are listed here.

APPENDICES (continued)

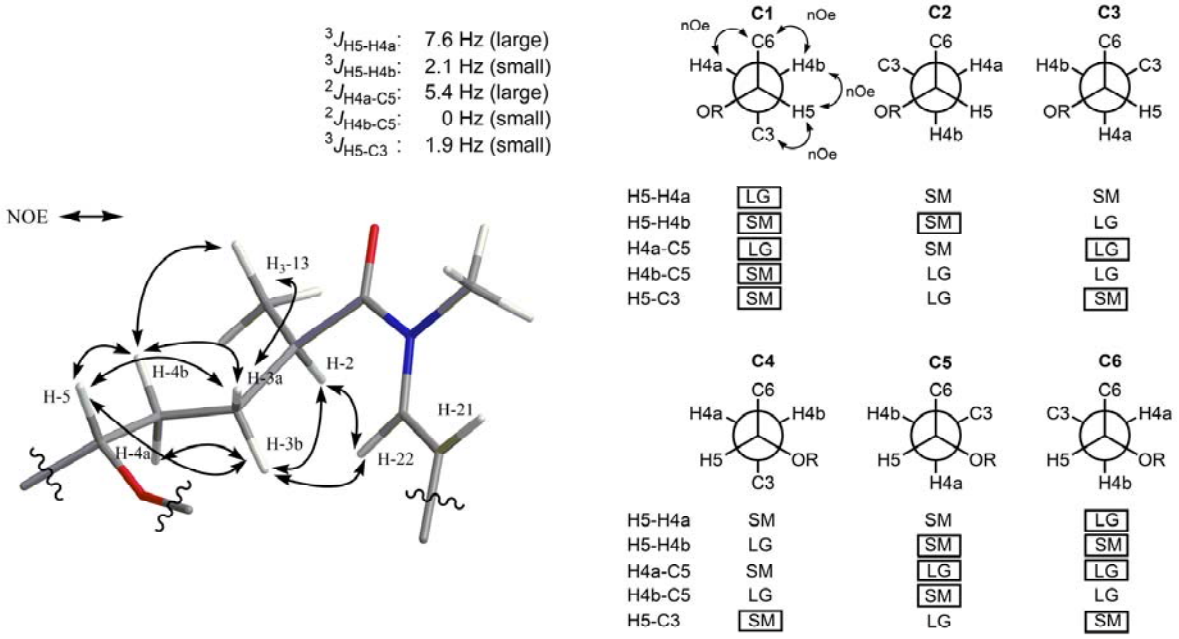

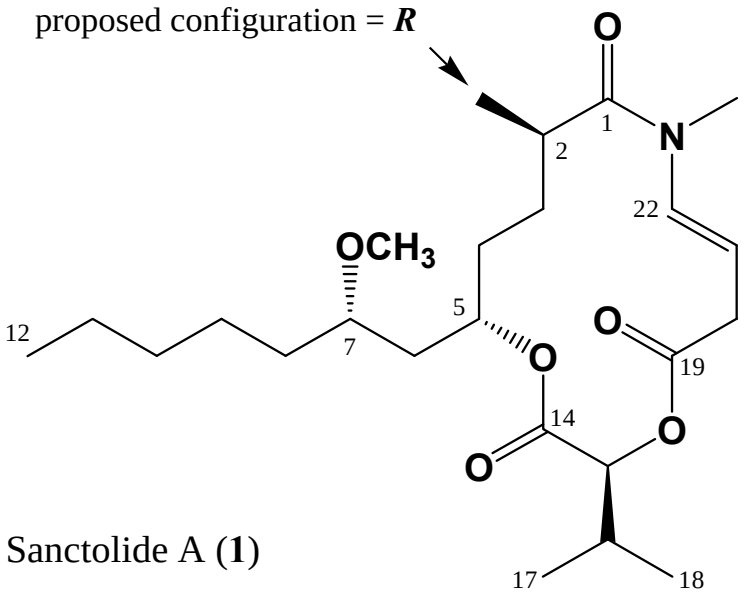

Figure S43. *J*-based configurational analysis for the relative configuration of the 1,4-methine system, C2-C5, in sanctolide A: All the possible rotamer conformations are listed here.

APPENDICES (continued)

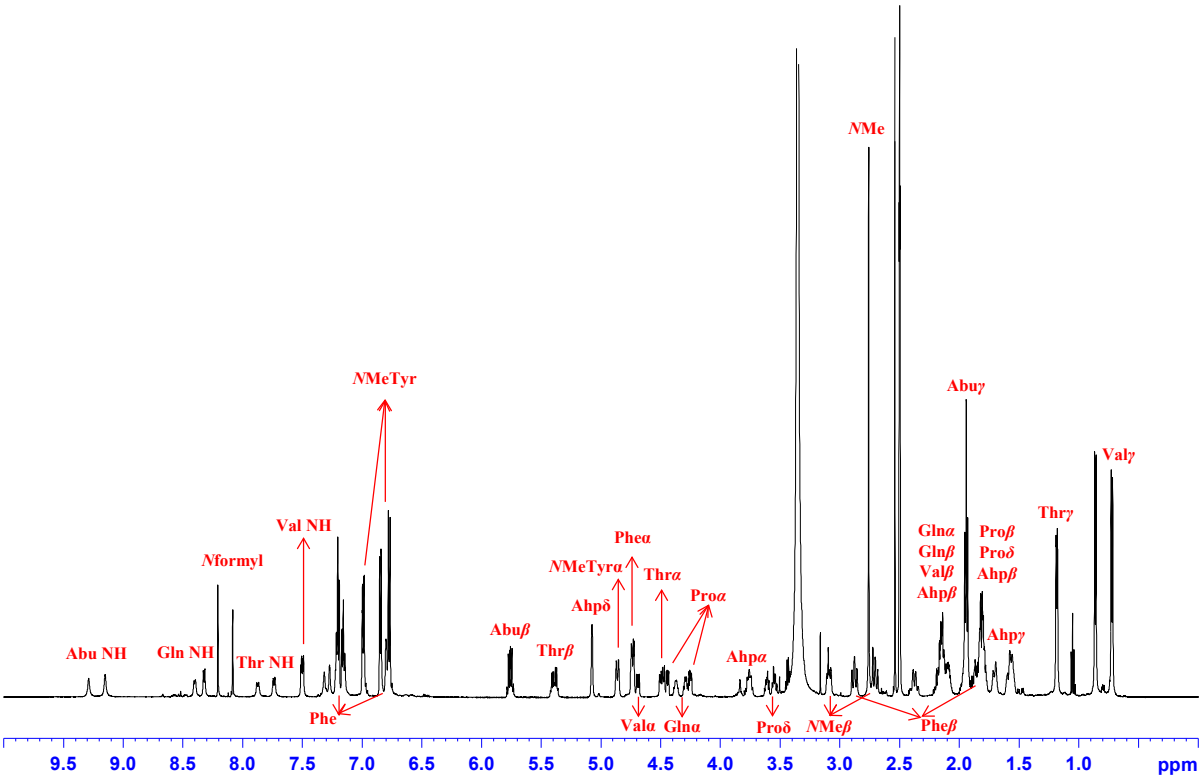

Figure S44. ^{1}H NMR spectrum (600 MHz, DMSO-d_6) of stigonemapeptin.

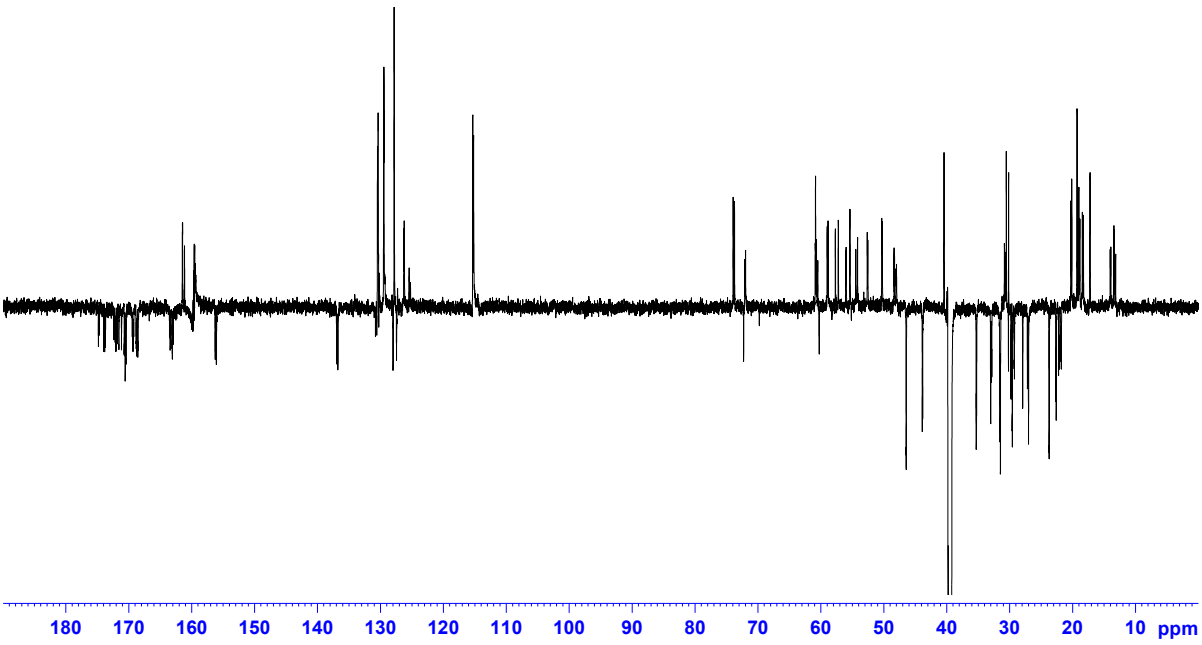

Figure S45. DEPT-Q spectrum (226 MHz, DMSO-d_6) of stigonemapeptin.

APPENDICES (continued)

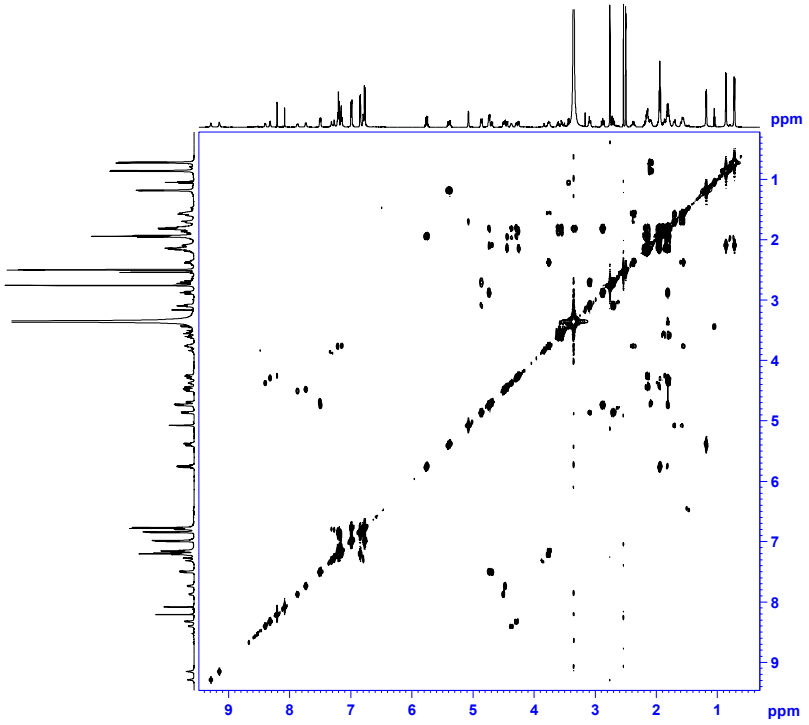

Figure S46. COSY spectrum (600 MHz, DMSO-d_6) of stigonemapeptin.

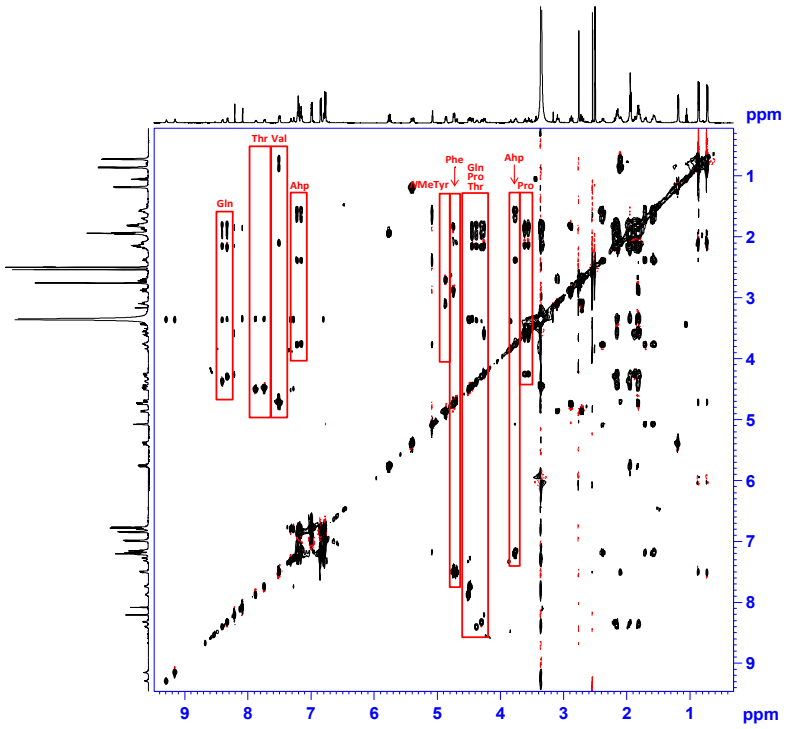

Figure S47. TOCSY spectrum (600 MHz, DMSO-d_6) of stigonemapeptin.

APPENDICES (continued)

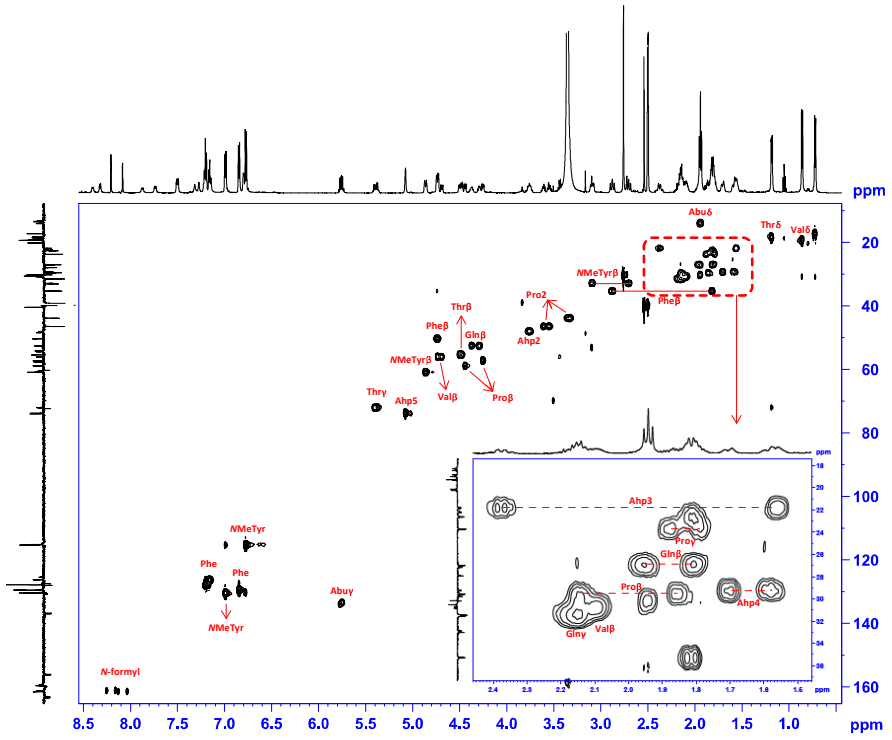

Figure S48. HSQC spectrum (600 MHz, DMSO-d_6) of stigonemapeptin.

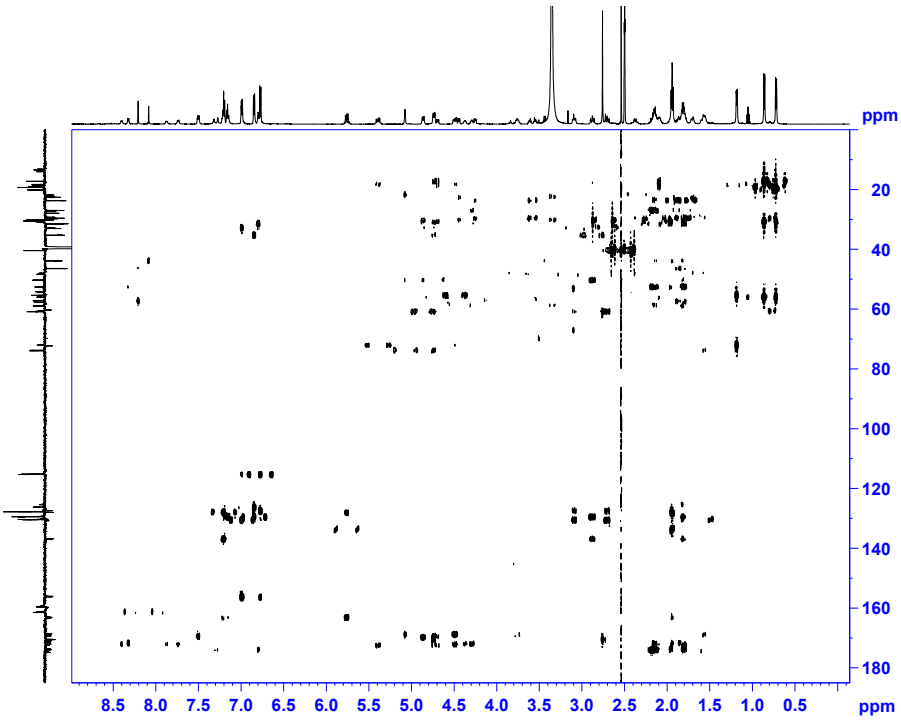

Figure S49. HMBC spectrum (600 MHz, DMSO-d_6) of stigonemapeptin.

APPENDICES (continued)

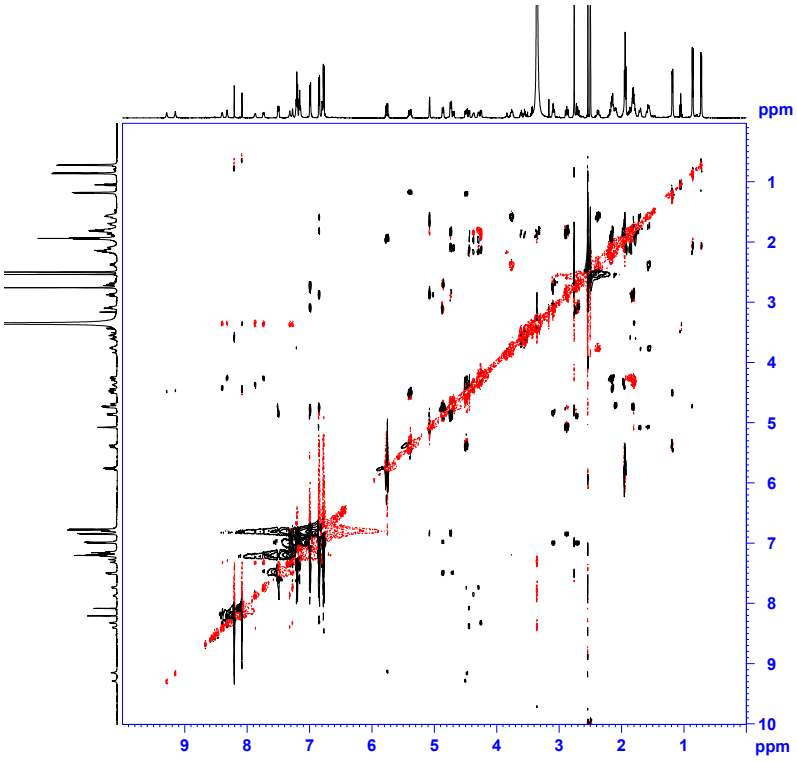

Figure S50. ROESY spectrum (600 MHz, DMSO-d_6) of stigonemapeptin.

VITA

NAME **Hahk-Soo Kang**

EDUCATION

University of Illinois at Chicago, USA (2008 – 2012)
Dept. of Medicinal Chemistry and Pharmacognosy, College of Pharmacy
Ph. D in Natural Products Chemistry (Advisor: Jimmy Orjala)

Chung-Ang University, South Korea (2003 – 2005)
MS in Biomaterial Chemistry

Chung-Ang University, South Korea (1998 – 2003)
BS in Biotechnology

PROFESSIONAL EXPERIENCE

Research Staff at KRIBB (Korea Research Institute of Bioscience and Biotechnology), South Korea (2005 – 2008)

TEACHING EXPERIENCE

Teaching Assistant (2008 – 2010)
Dept. of Medicinal chemistry and Pharmacognosy, College of Pharmacy, University of Illinois at Chicago, USA

Teaching Assistant (Spring, 2004)
Organic Chemistry LAB., Department of Biotechnology, Chung-Ang University, South Korea

AWARDS

The Kilmer Prize from American Society of Pharmacognosy & the American Pharmacists Association (Aug, 2011)

W.E. van Doren Scholar award from College of Pharmacy, University of Illinois at Chicago (Feb, 2011)

Poster Award from the Korean Society for Applied Biological Chemistry (Mar, 2006)

PUBLICATIONS

Kang, H. S.; Santarsiero, B. D.; Krunic, A.; Orjala, J. "Glycosylated Cylindrocyclophanes with Antiproliferative Activity against cancer cells from the Cultured Terrestrial Cyanobacterium *Nostoc* sp." Manuscript in Preparation.

Kang, H. S.; Sturdy, M.; Krunic, A.; Kim, H. J.; Shen, Q.; Swanson, S. M.; Orjala, J. "Homesteadamides A-H, antiproliferative cyclic lipodecapeptides from the cultured cyanobacterium Cf. *Anabaena* sp." Submitted to *Bioorg. Med. Chem.*

Kang, H. S.; Krunic, A.; Orjala, J. "Sanctolide A, a 14-Membered PK-NRP hybrid macrolide from the cultured cyanobacterium *Oscillatoria sancta*" *Tetrahedron Lett.* **2012**, 53, 3563-3567.

Kang, H. S.; Krunic, A.; Orjala, J. "Stigonemapeptin, an Ahp-containing Depsipeptide with Elastase Inhibitory Activity from the Bloom-forming Freshwater Cyanobacterium *Stigonema* sp." *J. Nat. Prod.* **2012**, 75, 807-811.

Kang, H. S.; Santarsiero, B. D.; Kim, H. J.; Krunic, A.; Shen, Q.; Swanson, S.

M.; Chai, H. B.; Kinghorn, A. D.; Orjala, J. "Merocyclophanes A and B, antiproliferative cyclophanes from the cultured terrestrial cyanobacterium *Nostoc* sp." *Phytochemistry* **2012**, 79, 109-115.

Kang, H. S.; Krunic, A.; Shen, Q.; Swanson, S. M.; Orjala, J. "Minutissamides A-D, Antiproliferative Cyclic Decapeptides from the Cultured Cyanobacterium *Anabaena minutissima*" *J. Nat. Prod.* **2011**, 74, 1597-1605.

Heo, S. J.; Ko, S. C.; Kang, S. M.; **Kang, H. S.**; Kim, J. P.; Kim, S. H.; Lee, K. W.; Cho, M. G.; Jeon, Y. J. "Cytoprotective effect of fucoxanthin isolated from brown algae *Sargassum siliquastrum* against H_2O_2-induced cell damage" *Eur. Food Res. Technol.* **2008**, 228, 145-151.

Kang, H. S.; Kim, K. R.; Jun, E. M.; Park, S. H.; Lee, T. S.; Suh, J. W.; Kim, J. P. "Cyathuscavins A, B, and C, new free radical scavengers with DNA protection activity from the Basidiomycete *Cyathus stercoreus*" *Bioorg. Med. Chem. Lett.* **2008**, 18, 4047-4050.

Kang, H. S.; Jun, E. M., Park, S. H.; Heo, S. J.; Yoo, I. D.; Kim, J. P. "Cyathusals A, B and C, New Antioxidants from the Fermented Mushroom *Cyathus Stercoreus*" *J. Nat. Prod.* **2007**, 70, 1043-1045.

POSTER PRESENTATIONS

Minutissamides A-D, Antiproliferative Cyclic Decapeptides from the Cultured Cyanobacterium *Anabaena minutissima*
Kang, H. S.; Krunic, A.; Shen, Q.; Swanson, S. M.; Orjala, J. 52nd Annual Meeting of American Society of Pharmacognosy, Paradise Point Resort, San Diego, California. July 30 – Aug 4, 2011

Stigonemapeptin, an Ahp-containing Depsipeptide from the Bloom-forming Freshwater Cyanobacterium *Stigonema* sp.
Kang, H. S.; Orjala, J. 52nd Annual Meeting of American Society of Pharmacognosy, Paradise Point Resort, San Diego, California. July 30 – Aug 4, 2011

Antiproliferative cyclophanes from the cultured freshwater cyanobacterium *Nostoc* sp.
Kang, H. S.; Sturdy, M.; Krunic, A.; Chai, H. B.; Kinghorn, A. D.; Orjala, J. 51st Annual Meeting of American Society of Pharmacognosy, St Petersburg Beach, Florida. July 10 – 14, 2010

PATENTS

Stereum ostrea extracts, separation method thereof and antiobesity composition comprising the same, Application No. 10-2008-0014619

Sargasols A, B and C, Novel compounds with antioxidant activity, their preparation method, and composition containing them, Application No. 10-2007-0015385